Thomas Sowoidnich

A study of retarding effects on cement and tricalcium silicate hydration induced by superplasticizers

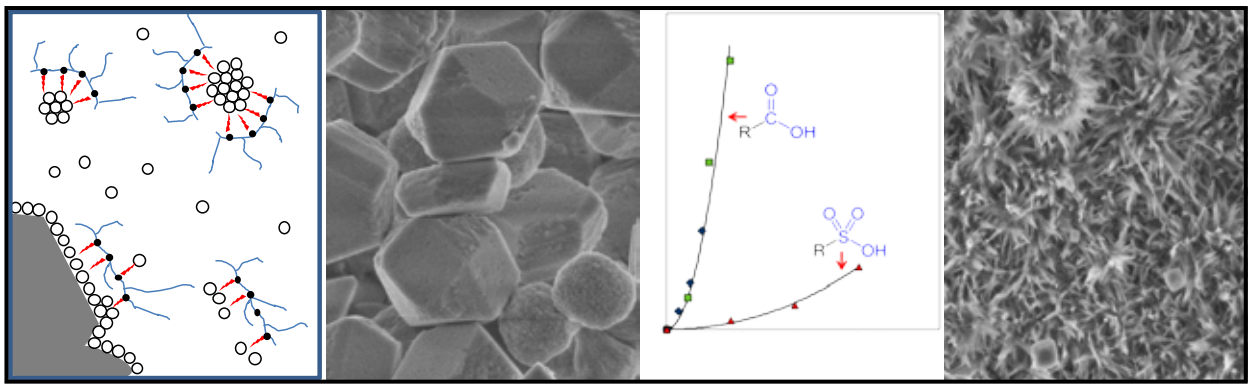

Bauhaus-Universität Weimar
2015

A study of retarding effects on cement and tricalcium silicate hydration induced by superplasticizers

DISSERTATION

zur Erlangung des akademischen Grades

DR. RER. NAT.

an der Fakultät Bauingenieurwesen
der Bauhaus-Universität Weimar

vorgelegt von

Thomas Sowoidnich

geboren am 30. Mai 1978 in Lutherstadt Eisleben.

Gutachter:
Prof. Dr.-Ing. Horst-Michael Ludwig (Mentor)
Prof. Dr. Denis Damidot
Prof. Dr. Robert J. Flatt

Tag der mündlichen Prüfung:
20.11.2015

ISBN: 978-3-00-052204-8

Herausgeber:
Bauhaus-Universität Weimar
F.A. Finger-Institut für Baustoffkunde
Professur Werkstoffe des Bauens
Direktor: Prof. Dr.-Ing. Horst-Michael Ludwig
Coudraystraße 11
99423 Weimar (Germany)

Danksagung

Diese Arbeit entstand im Zeitraum Oktober 2006 bis April 2014 am F.A. Finger-Institut für Baustoffkunde der Bauhaus-Universität Weimar während meines zweieinhalb jährigen Promotionsstipendiums der Graduiertenförderung des Freistaates Thüringen und anschließender Zeit als wissenschaftlicher Mitarbeiter.

Ich möchte mich bei all den Menschen ganz herzlich bedanken, die mich während der Bearbeitung meiner Arbeit unterstützt haben.

Mein besonderer Dank gilt Herrn Prof. em. Dr. habil. Jochen Stark dafür, dass er während seiner Zeit als Direktor des F.A. Finger-Institutes für Baustoffkunde mich als Doktorand aufgenommen und umfassend gefördert hat. Weiterhin gilt mein besonderer Dank meinem Mentor Prof. Dr. Horst-Michael Ludwig für die Übernahme der Betreuung, sein Vertrauen und seine hervorragende wissenschaftliche Unterstützung, die zielführenden Diskussionen und fachlichen Ratschläge. Insbesondere für die gewährte persönliche Freiheit bei der Bearbeitung des Themas möchte ich mich bedanken.

Meinen externen Gutachtern Herrn Prof. Dr. Denis Damidot und Herrn Prof. Dr. Robert J. Flatt möchte ich für das Interesse an meiner Arbeit, für die Erstellung der Gutachten sowie für die fachkundigen Diskussionen herzlich danken.

Während der Literaturstudie hat insbesondere die Biomineralisation mein Interesse geweckt, wobei die Diskussion mit Forschern dieser Disziplin meinem wissenschaftlichen Verständnis stark förderlich war. Vor diesem Hintergrund möchte ich mich ganz herzlich bei Herrn Prof. Dr. Helmut Cölfen (Universität Konstanz) für seine stets freundliche und konstruktive Unterstützung, die Messungen am MPI für Kolloid- und Grenzflächenforschung (Potsdam) und die zahlreichen Diskussionen zur nichtklassischen Kristallisationstheorie bedanken.

Darüber hinaus bin ich all meinen Kollegen zu Dank verpflichtet, insbesondere meinem Arbeitsgruppenleiter Herrn Dr. Möser für seine Ratschläge als auch Fr. Weickert und Fr. Bohne für die zahlreichen chemischen Analysen. Darüber hinaus möchte ich für die kollegiale Arbeitsatmosphäre und die freundschaftliche Zeit meiner gesamten Arbeitsgruppe herzlich danken, allen voran Dr. Christiane Rößler und Dr. habil. Frank Bellmann, die durch stete fachliche Diskussion und kritisches Lesen diese Arbeit sehr unterstützt haben. Weiterhin möchte ich den ehemaligen Studenten Albert Vogel, Stefan Hahn und Tim Rachowski für die Erstellung studentischer Arbeiten danken.

Meiner Familie und meinen Freunden möchte ich nicht zuletzt besonderen Dank für ihre Unterstützung in jeglicher Hinsicht und ihre Geduld aussprechen, wodurch sie wesentlich zum Erfolg der Arbeit beigetragen haben.

Weimar, den 20.03.2014 Thomas Sowoidnich

KURZFASSUNG

Fließmittel werden in Betonen verwendet, um deren Fließeigenschaften während der Verarbeitung zu verbessern und Wasser einzusparen. Beide Faktoren beeinflussen nicht nur den Frischbeton, sondern auch signifikant die Festbetoneigenschaften. Nachteilig wirken sich Fließmittel auf die Festigkeitsentwicklung aus, die z.T. sehr stark verzögert wird. Dies ist vor allem bei Bauteilen, die im Rahmen eines Vorfertigungsprozesses hergestellt werden, ein ökonomischer Nachteil. Die vorliegende Arbeit widmet sich den Ursachen für die Verzögerung der Portlandzementhydratation bei Verwendung von Fließmitteln. Um die komplexen Reaktionen, die während der Portlandzementhydratation auftreten, zu vereinfachen, betrachtet ein überwiegender Teil der Arbeit die Wechselwirkung Fließmittel-Tricalciumsilikat (Abk. Ca_3SiO_5 oder C_3S, Hauptbestandteil von Portlandzementklinker). Die Untersuchungen werden in drei Hauptteilen durchgeführt, wobei Methoden wie u.a. isotherme Wärmeflusskalorimetrie, elektrische Leitfähigkeit, Elektronenmikroskopie, ICP-OES, TOC als auch Analytische Ultrazentrifugation Anwendung finden.

Basierend auf der Wechselwirkung von Kationen mit anionischen Ladungsträgern von Polymeren wird die Interaktion von Calcium mit Fließmitteln im ersten Teil der Arbeit untersucht. Dabei kommt es überwiegend zur Komplexierung von Calciumionen durch die funktionellen Gruppen der Polymere (Carboxyl- bzw. Sulfonguppen), die in zementären Umgebungen sowohl gelöst in der wässrigen Phase als auch als Bestandteil von Partikelgrenzflächen vorhanden sind. Neben diesen Effekten kann auch gezeigt werden, dass Fließmittel die Bildung von nanoskaligen Partikeln hervorrufen, die infolge der sterischen Wirkung von Fließmitteln dispergiert in der wässrigen Phase vorliegen (Clusterbildung). Analog zu neuesten Erkenntnissen aus dem Bereich der Biomineralisation ist daher davon auszugehen, dass diese Nanopartikel durch Agglomeration das Kristallwachtsum beeinflussen.

Ausgehend von der Annahme, dass die Auflösungs- und/ oder Fällungskinetik durch die Wirkung von Fließmitteln behindert und damit für den Verzögerungseffekt der Fließmittel während der komplexen Hydratationsreaktion verantwortlich seien können, werden die zugrundeliegenden Vorgänge im zweiten Abschnitt getrennt voneinander untersucht. Es wird anhand von Lösungsuntersuchungen an C-S-H Phasen und Portlandit herausgestellt, dass die Komplexierung von gelösten Calciumionen durch funktionelle Gruppen der Polymere die Löslichkeit von Portlandit erhöht. Im Gegensatz führt die Komplexierung von Calciumionen in der wässrigen Phase zu einer Verringerung der Calciumionenkonzentration in der wässrigen Phase. Diese Effekte werden auf die unterschiedlich starke Adsorptionsneigung der Polymere an C-S-H-Phasen und Portlandit zurückgeführt. Es wird davon ausgegangen, dass die Adsorption aufgrund der größeren spezifischen Oberfläche stärker an den C-S-H-Phasen als am Portlandit auftritt. Demnach stellt sich dar, dass die Polymere erst nachdem die funktionellen Gruppen Calciumionen aus der wässrigen Phase komplexiert haben an den C-S-H-Phasen adsorbieren. Weiterhin kann gezeigt werden, dass die freie C_3S Auflösungsrate in Anwesenheit von Fließmitteln keinen direkten Zusammenhang zur Verzögerung erkennen lässt. Teilweise kommt es zu einer in Bezug zur Kontrollprobe ohne Fließmittel erhöhten sowie auch verringerten Auflösungsrate. Wird das

Komplexierungsvemögen der Fließmittel berücksichtigt, so kann durchaus eine verlangsamte freie Auflösungsrate ermittelt werden. Doch auch Calcit zeigt einen verzögernden Einfluss auf die freie C_3S Auflösung, obwohl es den Gesamtprozess der Hydratation signifikant beschleunigt. Somit kann die behinderte Auflösung als mögliche Ursache für die verzögernde Wirkung während der Zementhydratation weder bestätigt noch widerlegt werden. Dieser Punkt sollte in zukünftigen Arbeiten weiter untersucht werden. Im letzten Schritt dieses Untersuchungsabschnitts wird die reine Kristallisation von C-S-H-Phasen und Portlandit untersucht. Es stellt sich heraus, dass Fließmittel insbesondere durch die Wirkung der Komplexierung von Ionen in der wässrigen Phase sowohl die Induktionszeit verlängern als auch die Kristallwachstumsrate verändern. Dies allein kann aber nicht die komplette Verzögerungswirkung erklären. Ein wichtiger Verzögerungsfaktor ist die Adsorption der Polymere an Kristalloberflächen als auch eine fließmittelbedingte Dispergierung von nanoskaligen Einzelpartikeln, die deren Agglomeration zu Kristallen behindert.

Im letzten Hauptuntersuchungsabschnitt werden die gewonnenen Erkenntnisse auf die während der Zement- und Tricalciumsilikathydratation parallel ablaufenden Reaktionen analysiert. Dabei wird insbesondere die ionische Zusammensetzung der wässrigen Phase von C_3S Pasten und Suspensionen untersucht, um Hinweise für eine kinetische Hemmung der Hydratationsreaktion zu identifizieren. Zusammenfassend wird festgestellt, dass die Ursachen der verzögernden Wirkung von Fließmitteln auf die Hydratation von C_3S auf die starke Verzögerung der Kristallisation von Hydratphasen zurückzuführen ist. Dabei kommt den zwei Faktoren Komplexierung von Calciumionen an Oberflächen und Stabilisierung von nanoskaligen Partikeln eine zentrale Bedeutung zu. Diese Effekte können durch die Wirkung als Templat als auch durch Erhöhung der Löslichkeit infolge Komplexierung freier/gelöster Ionen teilkompensiert werden. Dass die Auflösungsreaktion durch die Anwesenheit von Fließmitteln behindert wird, kann nur indirekt anhand der Entwicklung von Ionenkonzentrationen festgestellt werden. Ob dieser Vorgang die Ursache oder die Folge des Lösungs-Fällungs-Mechanismus der Hydratation ist und damit die verzögernde Wirkung durch behinderte Auflösung des Edukts hervorgerufen wird, bleibt Gegenstand weiterer Untersuchungen.

Im Rahmen der Arbeit kann auch gezeigt werden, dass Fließmittel chemisch als Inhibitoren wirken indem sie den Frequenzfaktor verringern. Darüber hinaus wird erstmalig eine Methode entwickelt, die die Bestimmung der Ionenkonzentration in Pasten *in-situ* erlaubt. Mit deren Hilfe wird dargestellt, dass die Entwicklung der Ionenkonzentration als auch die allgemein verwendete Wärmefreisetzungsrate (Kalorimetrie) miteinander korrespondiert. Darüber hinaus erlaubt die entwickelte Methode die weitere Differenzierung der Accelerationsperiode in drei Stadien. Die Kristallisation von C-S-H-Phasen und Portlandit ist für den Beginn der Haupthydratationsperiode entscheidend.

ABSTRACT

Superplasticizers are utilized both to improve the fluidity during the placement and to reduce the water content of concretes. Both effects have also an impact on the properties of the hardened concrete. As a side effect the presence of superplasticizers affects the strength development of concretes that is strongly retarded. This may lead to an ecomomical drawback of the concrete manufacturing. The present work is aimed at gaining insights on the causes of the retarding effect of superplasticizers on the hydration of Portland cement. In order to simplify the complex interactions occurring during the hydration of Portland cement the majority of the work focuses on the interaction of superplasticizer and tricalcium silicate (Ca_3SiO_5 or C_3S, the main compound of Portland cement clinker). The tests are performed in three main parts accompanied by methods as for example isothermal conduction calorimetry, electrical conductivity, Electron Microscopy, ICP-OES, TOC, as well as Analytical Ultracentrifugation.

In the first main part and based on the interaction of cations and anionic charges of polymers, the interactions between calcium ions and superplasticizers are investigated. As a main effect calcium ions are complexed by the functional groups of the polymers (carboxy, sulfonic). Calcium ions may be both dissolved in the aqueous phase and a constitute of particle interfaces. Besides these effects it is furthermore shown that superplasticizers induce the formation of nanoscaled particles which are dispersed in the aqueous phase (cluster formation). Analogous to recent findings in the field of biomineralization, it is reasonable to assume that these nanoparticles influence the crystal growth by their assembly process.

Based on the assumption that superplasticizers hinder either or both dissolution and precipitation and by that retard the cement hydration, the impact on separate reactions is investigated. On experiments that address the solubility of C-S-H phases and portlandite, it is shown that complexation of calcium ions in the aqueous phase by functional groups of polymers increases the solubility of portlandite. Contrary, in case of C-S-H solubility the complexation of calcium ions in solution leads to decrease of the calcium ion concentration in the aqueous phase. These effects are explained by differences in adsorption of polymers on C-S-H phases and portlandite. It is proposed that adsorption is stronger on C-S-H phases compared to portlandite due to the increased specific surface area of C-S-H phases. Following that, it is claimed that before polymers are able to adsorb on C-S-H phases the functional groups must be screened by calcium ions in the aqueous phase. It is further shown that data regarding the impact of superplasticizers on the unconstrained dissolution rate of C_3S does not provide a clear relation to the overall retarding effect occurring during the hydration of C_3S. Both increased and decreased dissolution rate with respect to the reference sample are detected. If the complexation capability of the superplasticizers is considered then also a reduced dissolution rate of C_3S is determined. Despite the fact that the global hydration process is accelerated, the addition of calcite leads to a slower dissolution rate. Thus, a hindered unconstrained dissolution of C_3S as possibly cause for the retarding effect still remains open for discussion. In the last section of this part, the pure

crystallization of hydrate phases (C-S-H phases, portlandite) is fathomed. Results clearly show that superplasticizers prolong the induction time and modify the rate of crystal growth during pure crystallization in particular due to the complexation of ions in solution. But this effect is insufficient to account for the overall retarding effect. Further important factors are the blocking of crystal growth faces by adsorbed polymers and the dispersion of nanoscaled particles which hinders their agglomeration in order to build up crystals.

In the last main part of the work, the previously gathered results are utilized in order to investigate hydration kinetics. During hydration, dissolution and precipitation occur in parallel. Thereby, special attention is laid on the ion composition of the aqueous phase of C_3S pastes and suspensions in order to determine the rate limiting step. All in all it is concluded that the retarding effect of superplasticizers on the hydration of tricalcium silicate is based on the retardation of crystallization of hydrate phases (C-S-H phases and portlandite). Thereby, the two effects complexation of calcium ions on surfaces and stabilization of nanoscaled particles are of major importance. These mechanisms may partly be compensated by template performance and increase in solubility by complexation of ions in solution. The decreased dissolution rate of C_3S by the presence of superplasticizers during the in parallel occuring hydration process can only be assessed indirectly by means of the development of the ion concentrations in the aqueous phase (reaction path). Whether this observation is the cause or the consequence within the dissolution-precipitation process and therefore accounts for the retarding effect remains a topic for further investigations.

Besides these results it is shown that superplasticizers can be associated chemically with inhibitors because they reduce the frequency factor to end the induction period. Because the activation energy is widely unaffected it is shown that the basic reaction mechanism sustain. Furthermore, a method was developed which permits for the first time the determination of ion concentrations in the aqueous phase of C_3S pastes *in-situ*. It is shown that during the C_3S hydration the ion concentration in the aqueous phase is developed correspondingly to the heat release rate (calorimetry). The method permits the differentiation of the acceleration period in three stages. It is emphasized that crystallization of the product phases of C_3S hydration, namely C-S-H phases and portlandite, are responsible for the end of the induction period.

TABLE OF CONTENTS

LIST OF ABBREVIATIONS

Symbols	
a	Activity of species, size of polymer chain
A	Surface area
AP	Adsorption plateau
β	Saturation ratio, shape factor
c	Concentration
D	Diffusion coefficient
d	Dimension, diameter
ΔG°	Standard difference in free energy of the system
E	Energy
f	Function
f	Frequency, frictional coefficient
F	Force
θ	Wetting angle
ϕ	Factor dependent on wetting angle
γ	Activity coefficient, interfacial energy
h	Thickness/height
H	Hamaker constant
I	Ion strength
IAP	Ion activity product
k	Reaction rate
K	Equilibrium constant
κ^{-1}	Debye-length
λ	Interfacial energy
M	Molar mass
N	Number of monomers in the backbone
n	Nucleation, number of copolymer segments of the macromolecule
η	Viscosity
P	Number of monomers in the side chain
Ω, S	Saturation ratio
S	Surface occupied by polymer
Q	Reaction coefficient
r	Radius
ρ	Density
s	Sedimentation coefficient
SI	Saturation index
T	Absolute temperature
t	Time
u	Sedimentation velocity

V	Volume
υ	Molecular volume
ω	Specific molecule volume, angular velocity
z	Charge of polymer
ζ	Zeta-potential

Subscripts	
0	At beginning
-	Backward
+	Forward
a	Activation, surface
A	Adsorption
c	Centrifugation
cl	Crystal liquid interface
crit	Critical
cs	Crystal substrate interface
g	Growth
hom	Homogeneous
i	Kind of species
max	Maximum
n	Nucleus
P	Particle
r	Relaxation
s	Saturation
s	Solvent
SP	Solubility product
v	Volume

Constants	
R	Gas constant
e	Eulers number
k_B	Boltzmann constant
N_A	Avogadros number

cement and other notations	
C	CaO
S	SiO_2
H	H_2O
A	Al_2O_3
F	Fe_2O_3
$\bar{S}$	SO_3
N	Na_2O
K	K_2O
c	Cement

l/s	Liquid/solid mass ratio
SSA	Specific surface area
PCE	Polycarboxylate ester/ether
(M)PEG	(methoxy)polyethylenglycol

1 INTRODUCTION

Nowadays concrete is the most abundant building material used worldwide. It is expected that its usage will increase within the next decades[67]. As a composite material, concrete is built up mostly by aggregates glued by an inorganic binder. This binder is refered to as cement. The ability of shaping in nearly every desired fashion is a great advantage of concrete compared to other materials. During the course of hardening which involves chemical reactions it develops high strengths. By changing concrete's composition strength and other properties can be tailored to meet the desired needs. In order to enhance tensile strength mainly steel as reinforcement is used. Besides these relative simple principles for construction, the chemical mechanisms leading to strength development are not fully understood.

As other materials, also concrete is optimized in different manners, leading to specific applications, but also to higher sensitivity of the system. This is mainly enabled by the use of tailor-made substances added to the mixture, i.e. additives. One of the most important additives is the group of superplasticizers or high range water reducer. As implicated by the notation, the main contribution of these additives is the improvement of the fluidity and reduction of the water demand of the mixture. Based on the finding that the water/cement mass ratio dictates concrete properties (Féret 1892, Abrams 1919)[131] the first generation of these additives (plasticizers based on lignosulfonates) was introduced in order to increase the compressive strengths of concrete by lowering the water/cement ratio. With the use of plasticizers it was possible to produce a concrete with higher compressive strengths without the need to increase the cement content. Moreover, the increase in compressive strength is always connected with the increase in durability. However, with the plasticizers the limits for the mix design were low. It was the development of superplasticizers that opened new ways in improving compressive strength, durability and workability of concretes.[5] Since their introduction in concrete technology, the ramifications are revolutionary. Only by use of superplasticizers the placement of concrete can be fascilitated, architectural imaginations instantiated and water saved.

However, using superplasticizers is not always associated with advantages. As drawbacks of these additives incompatibilities with differenct cements and the retardation of cement hydration are handled. Latter manifests in prolonged setting times and lowered shuttering times, which is mainly an economical issue.[4]

Obviously, mechanisms leading to the setting of cement are subject of debate for several decades (e.g. [12, 86]). Up today, no consensus is found in the hydration kinetics of cement. Conversely, this process is mandatory in order to evaluate the origins of superplasticizer induced retardation of cement hydration.

The present work investigates the causes of the superplasticizer induced retardation of the cement hydration. Starting by an overview on the state-of-the-art of cement hydration including basic reactions, the impact of superplasticizers on cement hydration is investigated on cement model system tricalcium silicate because this clinker mineral accounts mostly for strength development and kinetics of hydration. Thereby, the impact of superplasticizers on individual reactions (dissolution, precipitation) is analysed. Finally,

results to basic principles of chemical reactions and to other fields of materials research are aspired showing that cement chemistry is in fact chemistry.

2 THEORETICAL BACKGROUND

2.1 General considerations

2.1.1 Thermodynamics and kinetics of chemical reactions

For interpreting and understanding cement hydration it is useful to outline the principles of reaction in general. In the following a brief overview on the principles of thermodynamics and kinetics is given. The interested reader is guided to the literature for more details and general considerations[8-9, 106].

The following general chemical reaction where educt phases A and B react to product phases C and D is considered.

$$aA + bB \underset{k_-}{\overset{k_+}{\rightleftharpoons}} cC + dD \tag{1}$$

This reaction will take place as long as a certain amount of educts transforms into product phases. Therefore it is not necessary that all educt phases are consumed. The extent of reaction is expressed as actual number of reacted phases related to total number of reacted phases ξ. After a certain time period equilibrium will be established between educts and products. Thermodynamics (time is no parameter) describes hereby only the states of reaction whereas kinetics deals with the fate of the reaction partners during the reaction period (time is a parameter). The driving force for this reaction is the difference in the Gibbs free energy of the system ΔG.

$$\Delta G = \Delta G^\circ + RT \log\left(\frac{a_C{}^c a_D{}^d}{a_A{}^a a_B{}^b}\right) \tag{2}$$

with ΔG° ... standard difference in free energy of the system

R ... molar gas constant ($R \sim 8.314\ J/(mol \cdot K)$)

T ... absolute temperature

$Q = \left(\frac{a_C{}^c a_D{}^d}{a_A{}^a a_B{}^b}\right)$ ... reaction coefficient expressed as activities of ion species in aqueous solution.

Ion activity a_i is defined by:

$$a_i = \gamma_i \cdot c_i \tag{3}$$

with γ_i ... activity coefficient of species i

c_i ... concentration of species i

According to equations (4) and (5) the driving force of the reaction is zero at equilibrium conditions.

$$\Delta G = 0 = \Delta G^\circ + RT \log\left(\frac{a_C{}^c a_D{}^d}{a_A{}^a a_B{}^b}\right) \tag{4}$$

$$\Delta G^{\circ} = -RT \log\left(\frac{a_C{}^c a_D{}^d}{a_A{}^a a_B{}^b}\right) = -RT \log\left(K_{SP}\right) \tag{5}$$

At equilibrium ($\Delta G=0$) the reaction coefficient Q is termed solubility product K_{SP} (see eq. (5)). Substitution of eq. (5) in eq. (2) gives equation (6).[9]

$$\Delta G = -RT \log\left(K_{SP}\right) + RT \log Q = RT \log\left(\frac{Q}{K_{SP}}\right) = RT \log\left(\frac{IAP}{K_{SP}}\right) \tag{6}$$

The term $\frac{IAP}{K_{SP}}$ is defined as saturation ratio Ω and $\log \frac{IAP}{K_{SP}}$ as saturation index SI of the system leading to equation (7).

$$\Delta G = RT \log\left(\Omega\right) = RT\left(SI\right) \tag{7}$$

This means that the driving force for a chemical reaction in aqueous solution is directly related to the state of saturation of the system with respect of the solid phase (product phase). Thereby the following cases are distinguished:

SI<0	...	System is undersaturated
SI=0	...	System is in its chemical equilibrium
SI>0	...	System is supersaturated.[105]

Because the reaction coefficient is associated with activities of the considered species, the effect of foreign and system inherent ions can be deduced. Thus, foreign ions vary the activity coefficient whereas inherent ions increase the concentration of the considered ions. Normally the presence of foreign ions increases the solubility of solids whereas the addition of system-inherent ions decreases the solubility of solids.

Considering the universe as a closed system and obeying the second law of thermodynamics everything is decreed to achieve the state of equilibrium by entropy maximization (“Big Chill”). Once at equilibrium the driving force for the system is zero (cf. eq. (4)). Therefore it is inevitable for a reaction to take place that there is disequilibrium between two distinctive states (e.g. chemical potential between educts and products). Once deviated from equilibrium the system responses (e.g. by chemical reaction, motion, radiation) to this change in order to reach equilibrium condition by the driving force. To highlight its importance the driving force can be considered as precondition for life on planets[109]. In this context it is discussed that life empowers the measure of disequilibrium on planet Earth to enforce the energetic difference and thus the driving force. After death the organism approaches equilibrium with its environment. These theories are subject of a long debate and lead to the emerging of the non-equilibrium thermodynamics.[101, 176]

As shown in section 2.1.1 the driving force for any reaction is the thermodynamic non-equilibrium. A reaction is therefore considered as a response of the system in order to achieve thermodynamic equilibrium. The pathway of the reaction and in particular the rate of reaction is subject of reaction kinetics.

For illustration purposes the general chemical reaction given in eq. (1) is considered again. The arrows symbolize the direction of the reaction as a result of a change in Gibbs free

energy based on the second law of thermodynamics. As shown in section 2.1.1 at $\Delta G<0$ the reaction will be favorably on the product site whereas at $\Delta G>0$ educts are predominantly formed. This corresponds to $SI<0$ and $SI>0$, respectively. Reactions proceed with particular rates signed by k_+ and k_- for the reaction forward and backward, respectively. Approaching equilibrium condition ($\Delta G=0$) the rates equalize, i.e. $k_+ = k_-$. This state at equal rates for forward and backward reaction is defined as principle of detailed balancing (PCB)[106]. Formation and decomposition of product phases are still observed, but the net reaction rate is zero. Since kinetics is caused by thermodynamic non-equilibrium it is obvious that besides factors from matter itself also the environment influences kinetics. Thus parameters govern the kinetics can be subdivided into inherent and environmental factors.

For interpreting reactions and finally aspects of the cement hydration it is reasonable to highlight one important point of the principles of thermodynamics and kinetics. If a system is in a non-equilibrium state, creating a driving force, thermodynamics is able to give a hint whether the reaction can proceed or not. But reaction kinetics governs the rate of reaction and therefore the time period for a reaction to take place. These periods can be in the range of ps (10^{-12} s) for molecular motion to Ps (10^{15} s) for plate tectonic dynamics[106]. Usually these reactions were recognized in daily grind as instantaneous or eternal (or never). Thus, progress in reaction is not always noticeable. Further examples are glassy materials, magmatic and metamorphic rock, metallic Al_2O_3 and even diamonds, which are at non-equilibrium under standard conditions. But the rate to reach the final stable state is very low and in practice not observable.

Classically, reaction kinetics is treated as temperature dependencies of reaction rates. This phenomenon was investigated in detail by Arrhenius (Nobel prize for chemistry 1903). It is assumed that a minimum energy (activation energy E_a) is needed for chemical reactions to take place. During chemical reactions particles collide and lead to the formation of reaction products. With the frequency factor A, gas constant R and temperature T the Arrhenius equation expresses the temperature dependency of the reaction rate constant k, see eq. (8).

$$k = A \cdot e^{-\frac{E_a}{RT}} \tag{8}$$

Only particle movements with a minimum energy result in chemical reaction. This is expressed in the exponent as the probability of collisions with minimum energy required. At infinite high temperatures the rate constant equals the frequency factor. The frequency factor exhibits the same unit as the rate constant.

As base for all reactions the concept of thermodynamics and kinetics will be addressed frequently in the sections of this work. Furthermore developed theories of more specific rules will be discussed and classified in this context.

2.1.2 The dissolution process of solids

Dissolution is the process of disintegration of solid materials and can be regarded as an inverse of a crystallization process[47]. Bonds between atoms have to be broken in order to destroy / dissolve the (crystal) structure. Concerning thermodynamics and especially its second law, matter is distributed in a foreign matter in order to gain entropy. Dissolution is thus associated with an increase in entropy, and every material (solute) exhibits a specific

solubility in other materials (solvent). For hydraulic materials the most important solvent is water. Following, the dissolution of solids in water as solvent and in particular the dissolution kinetics will be attended. This section will outline the kinetic description of dissolution and its multi parameter dependency.

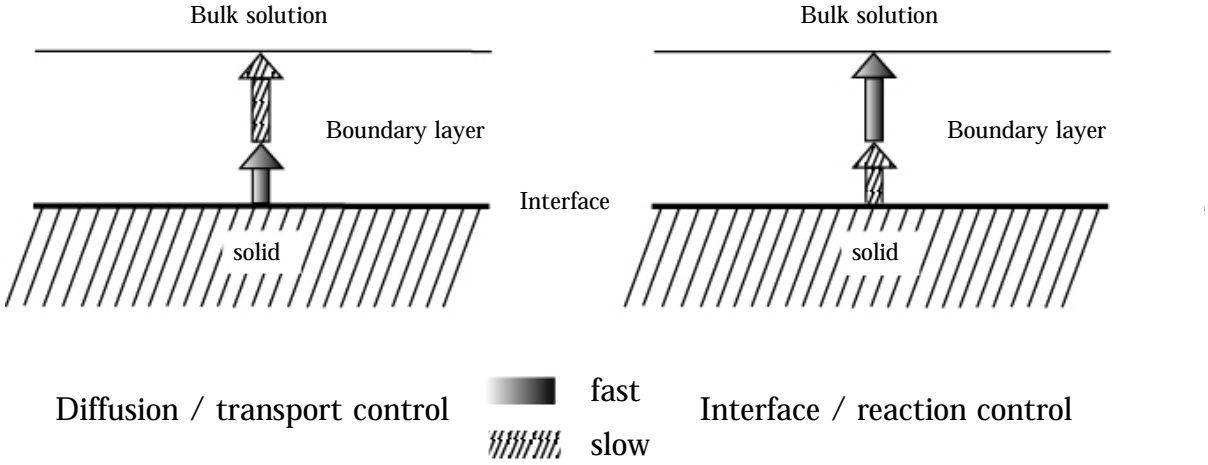

Fig. 2-1: Schematic representation of the dissolution modes. The slowest process dictates the overall reaction rate (adapted from[112]).

Formation and also dissolution of material in a solvent proceeds at the solute-solvent-interface. Interfaces can be assumed to be a disturbed part of the bulk and a discontinuum of the material because not all atomic units are uniformely bound to the underlying lattice. In dependence of the ambient matter different surface properties and effects are observed, e.g. surface tension and electrostatic repulsion / attraction of particles. In case of minerals dispersed in water the mineral-water-interface can be regarded as an electrode where electrostatic interactions occur between the mineral surface and ions. From this consideration different models as the electric-double-layer (Stern-Gouy-Chapman) or DLVO[a] theory were developed (see also section 2.1.4). Dissolution is linked to the transport of elementary units from the interface to the bulk solution. Within this scheme two different modes are distinguished, cf. Fig. 2-1. This differentiation is derived from differences in the reaction rate of both the interface and the transport to the bulk solution. Therefore the overall reaction rate is either more limited by diffusion or by interface reaction rate.

The basic atomic processes within the interface of dissolving a material in water are: (I) detachment of species (atoms, ions, molecules) from steps, edges or kinks, (II) moving of these species on the surface of the crystal, (III) detachment of the species from the surface, and (IV) transport of solvated species through the parent phase. Therefore steps I to II represent surface and III-IV transport controlled dissolution, respectively. With increasing reactivity of the material a gain in dominance of the transport processes are observed.[106, 187] Table 2-1 gives roughly a hint to categorize if either surface or transport processes control the solubility and dissolution rate of minerals.

[a] Denoted after the theory developers Derjaguin, Landau, Verwey, Overbeek

Thereby the dissolution of species from a kink position and from the surface is associated with the lowest and the highest energy demand, respectively. All other atomic positions are in between these stages. The reactivity of a material increases with increasing surface area due to the increased amount of reactive sites. The next sections deal with surface processes. After that, dissolution controlled by transport processes will be delineated.

Table 2-1: Solubility in water and mechanism of dissolution for different compositions[106].

Substance	Solubility	description	Substance	Solubility	description
Surface reaction control			Transport control		
$KAlSi_3O_8$	3×10^{-7}		AgCl	1×10^{-5}	
$NaAlSi_3O_8$	6×10^{-7}		$Ba(IO_3)_2$	8×10^{-4}	
$CaCO_3$	6×10^{-5}		$CaSO_4 \cdot 2H_2O$	5×10^{-3}	
$SrCO_3$	3×10^{-5}	Sparingly	$Na_2SO_4 \cdot 10H_2O$	2×10^{-1}	Readily
$BaSO_4$	1×10^{-5}	soluble	$MgSO_4 \cdot 7H_2O$	3×10^{0}	soluble
$SrSO_4$	9×10^{-4}		$Na_2CO_3 \cdot 10H_2O$	3×10^{0}	
Ag_2CrO_4	1×10^{-4}		KCl	4×10^{0}	
Opaline SiO_2	2×10^{-3}		NaCl	5×10^{0}	

2.1.2.1 Factors influencing solubility and dissolution rate in aqueous media

As demonstrated in section 2.1.1 kinetic studies are dependent on different parameters, which are inherent and environmental in nature. In particular, for dissolution of minerals these parameters can be divided as dependent on the (crystal) structure of the solute and on solution determining parameters. As common for all reactions the slowest step dictates the rate of the overall reaction. Thus, chemical reactions are either reaction (surface)-limited or diffusion (transport)-limited as demonstrated in section 2.1.2[106, 132]. A general relation of dissolution rate is given in eq. (9a)[76, 110, 175].

$$\text{Rate} = k_0 \cdot A(t) \cdot f(\Delta G) \qquad \text{geochemistry} \tag{9a}$$

$$\text{Rate} = \frac{D}{V \cdot h} \cdot A \cdot (c_S - c) \qquad \text{pharmacokinetics} \tag{9b}$$

In both cases the rate of dissolution depends on the surface area A as an inherent parameter. The environment governs the dissolution rate by means of driving force expressed as either degree of undersaturation ΔG (geochemistry) or difference between saturation concentration c_S and concentration of the solid in the bulk c (pharmacokinetics). Pharmacokinetic parameters D (diffusion coefficient), V (Volume of the medium), and h (thickness of the layer around the dissolving solid particle) addresses the dissolution of drug by transport due to diffusion into solution. In geochemistry mostly reaction-limited dissolution mechanisms are observed and thus only a rate constant k_0 is given. The following sections delineate the different parameters that control the dissolution in more detail. Before environmental parameters are discussed, the inherent parameters will be described.

2.1.2.1.1 Inherent parameters

A Interatomic forces

As mentioned before dissolution of a material requires a destruction of the interatomic bonds. Therefore the dissolution is governed by material parameters as type of atom and linkage. Predominantly the needed energy to disrupt interatomic linkage increases with increasing bonding force. For example covalent bonds in quartz (SiO_2) are stronger than the bonds in the ion crystal of halite (NaCl) which results in both higher solubility and dissolution rate of halite compared to quartz. In geochemistry it is known that silicates show very different stabilities against weathering[105]. Mostly, this originates from the stability of the SiO_4-tetrahedra linkage[171]. The stability increases with increasing degree of cross-linking, e.g. neso- <ino- <phyllo- <tectosilicate. Further the stability decreases with the substitution of Si by Al due to the increase of the oxygen distance in the tetrahedra, e.g. quartz> orthoklas> nephelin. Cross-linking cations stabilise the mineral with increasing specific charge and decreasing size. In summary the weathering stability of silicates increases in the sequence olivine <anorthite <pyroxene <amphibole <biotite <albite <muscovite ~ orthoclase <quartz.[171]

B Crystal structure

Dissolution of minerals varies in dependence of the crystal structure. Differences in atom coordination within the crystal structure results in different crystal planes. Because the interatomic forces vary, different crystal planes differ in their solubility and dissolution rate, cf. section 2.1.2. As a consequence the linkage of the functional groups and therefore the sites of reactivity are dependent on the crystal plane. The solubility decreases with increasing bonding of the functional groups.[187]

C Crystallographic defects

Another effect on dissolution rate on minerals are defects in the crystal structure. Defects can be associated with imperfections of atom assembly in crystals. Mostly observed defects are point and lattice defects.[100] It is reported that defects enhance the solubility of crystalline materials in aqueous solution[25, 30] (potassium perchlorate and quartz). Despite of these tests also no significant influence of defects on quartz dissolution were found[23]. The physical principle of defects and the link to environmental influences is handled in the following.

D Polymorphs and amorphs

A characteristic of crystalline materials is both short- and long-range order of the atoms. Polymorphs are crystals identical in chemical composition but different in crystal lattice and atom assembly. For example $CaCO_3$ occurs in nature as mineral vaterite, aragonite and calcite. These polymorphs show different bulk properties as mechanical strengths and solubility. Materials are called amorphous if the building units are assembled in short-range order similar to liquids. Again for $CaCO_3$, the existence of amorphous phases termed ACC (amorphous calcium carbonate) is postulated[33, 74, 116]. As mentioned before the stability against decomposition (solubility) depends on the bonds between the atoms in the material. Therefore different solubilities and dissolution rates of polymorphs and amorphous phases

are probable. Typically, variations in solubilities and dissolution rates of polymorphs are smaller than factor 10. In contrast this variation is typically several hundred times if amorphous material and its crystalline counterpart are compared.[81] This underlines the importance of the crystalline / amorphous state of matter which is also subject of section 2.1.3.3.

2.1.2.1.2 Environmental parameters

As mentioned before the solubility and the dissolution rate of a solute is dependent on both inherent and environmental parameters. The solvent has to break bonds of the solute and, simultaneously, the solvent atoms/molecules must be separated from each other by the solute molecules. From this issue two consequences for the dissolution arise. Firstly, an important role is assigned to the functional groups of both solvent and solute, i.e. non-polar (hydrophobic), polar (hydrophilic) and ionic. A general rule postulates that similar functional groups of solvent and solute lead to dissolution of the solute. Thus, non-polar solvents tend to dissolve non-polar and non ionized solutes, respectively. In this line, polar solvents tend to dissolve polar and ionized solutes. Secondly, the diffusion of solute molecules into the solvent determines the dissolution rate, cf. eq. (9b). The diffusion coefficient is directly proportional to the temperature and inversely proportional to the viscosity of the solvent.[132] Thus, an increase of the temperature increases the dissolution rate and an increase of the viscosity of the solvent leads to a decreased dissolution rate of the solute. However, in case of diffusion limited dissolution, the rate of dissolution can be altered by changing the thickness of the diffusion layer according to eq. (9). Hence, an increase of the dissolution rate due to increased relative solute-solvent movement can be achieved by intensive mix (agitation, ultrasound).

A Saturation state of the system

From eqs. (9a) and (9b) it is obvious that the rate of dissolution is directly proportional to the state of saturation of the system expressed by a ΔG function. This relationship is shown in Fig. 2-2 for the dissolution rate of albite ($NaAlSi_3O_8$). Also for other minerals an analogous dependency of the dissolution rate on saturation state of the system is observed.

Experimental data show that in dependence of undersaturation two distinctive mechanisms occur during the dissolution of minerals referred to as mechanisms I and II in Fig. 2-2. Their main boundaries are $\Delta G = 0$ and $\Delta G = -\infty$ which corresponds to equilibrium and infinitive dilution (undersaturation), respectively. At equilibrium the net rate (dissolution rate + precipitation rate) equals zero as deduced from the principle of detailed balancing (PCB). That means that finite dissolution and precipitation rate can be observed. At infinite degree of undersaturation minerals dissolve on highest rate which is independent on the degree of undersaturation (dissolution plateau, rate constant). According to the PCB theory this is due to the very slow precipitation rate of the mineral.

Near equilibrium the dissolution rate of minerals R is only dependent on the saturation state of the system[47]. Thereby the dissolution proceeds by step retreat which is associated with the detachment of atomic units on steps or kinks of the mineral surface. As demonstrated before, steps and kinks are these sites on the crystal surface which exhibit more energy than other sites. Changing ΔG from equilibrium ($\Delta G=0$) to higher degrees of

undersaturation ($\Delta G<0$) and *vice versa* involves a linear increase of the dissolution rate. At a certain value (ΔG_{crit}) the linear dependence between dissolution rate and saturation state of the system turns into an exponential dependence. This is caused by a change in the dissolution mechanism. The simple step retreat during mechanism I is taken over by dislocation control of the dissolution. This involves formation of etch pits on dislocations of the lattice. The critical state of undersaturation of the system ΔG^{d}_{crit} in Fig. 2-2 can be regarded as the energetic barrier which is needed to induce etch pit formation on the surface. Thereby the number of dislocations and the critical state of undersaturation for the change in dissolution mechanism are anticorrelated. Thus step retreat occurs on decreasing degrees of undersaturation. As a consequence the dissolution rate of minerals at dislocations is increased. It can be concluded that at same conditions a dislocated crystal structure dissolves faster than a more ordered due to etch pit opening. More information on calculations can be found elsewhere[47].

So far etch pit formation is attributed to defects in the lattice. But even on perfect flat surfaces etch pits can be formed and build vacancy islands *via* nucleation. In contrast to etch pit opening at dislocation the nucleation of vacancy islands is not only dependent on material parameters but also on the state of saturation of the system. The energy barrier for the nucleation of etch pits decreases with increasing undersaturation. On decreasing undersaturation of the system less etch pits are generated by nucleation of vacancy islands.

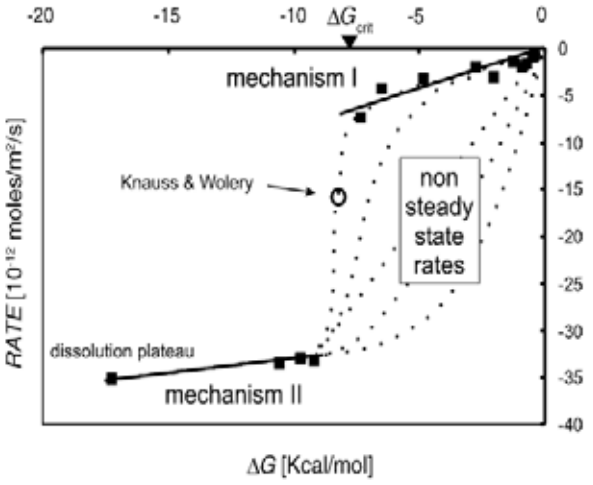

Fig. 2-2: Dissolution rate of albite ($NaAlSi_3O_8$) in dependence of the Free Energy of the system (adapted from[110]). See text for more information.

ΔG_{crit} can be affected by the dissolution history of the mineral. If the mineral is dissolved at higher degrees of undersaturation, more etch pits are formed (nucleation of vacancy islands). This leads to different dissolution rates at decreased degrees of undersaturation for virtual same materials as indicated in Fig. 2-2 (dotted lines)[110].

B Impurities, pH and other parameters

Altering the amount of charged species in the environment of the material leads to reaction on the interfacial surface. As a first consequence the surface will get electrical charged due to the adsorption of positively and negatively charged species. At certain value of adsorption of opposite charged species on the material surface, neutral surface charge can be achieved. This reflects a material parameter and is known as zero point charge (zpc)[106]. The most important species adsorbed on the surface of silicate minerals in presence of water are hydroxyl groups.

As a consequence of the attraction of charged ions on the material surface due to the simple electrical response, a subsequent reaction of the elementary species with the

adsorbate is provoked. This is associated with weakening or cracking of bonds between building units in the materials structure. Thus the surface charge influences the reactivity of the material which results in a catalyzing effect of charged species on the dissolution of minerals.[186]

Proton promoted dissolution

Proton promoted dissolution of minerals is characterized by breaking oxygen-bonds. This is attributed to a release of metal ions into solution and substitution of oxygen-metal-units by hydroxyl groups (surface protonation), see Fig. 2-3 (left hand) and eq. (10).[171]

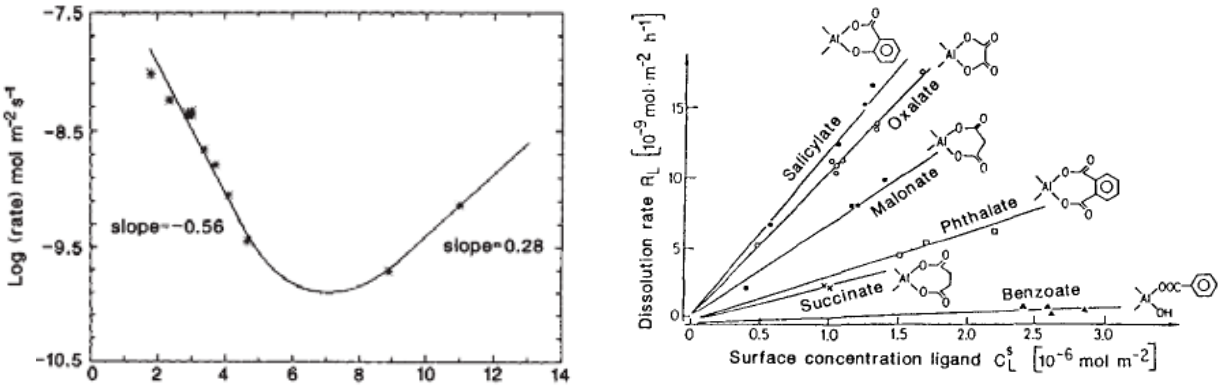

Fig. 2-3: (Left hand) Dissolution rate of olivine in dependence of pH (x-axis)[22] and (right hand) dissolution rate of δ-Al_2O_3 in dependence of type and concentration of added aliphatic ligands[185].

Commonly found metals for minerals are Fe, Al, Ca, Mg, K, Na. The bonds between silicon, carbon and phosphor (Si, C and P in eq. (10)) with oxygen are covalent and consequently a high stability is observed. An increase of H^+ leads to an increase of the surface protonation, and, thus, to an increased release of metal ions into solution. For example in dentistry it is known that higher amount of H^+ reduces the stability of dental enamel (hydroxylapatite) which leads to demineralisation of teeth (caries).[167]

$$\begin{aligned} -Si-O-M + H^+ &\rightarrow -Si-OH + M^+ \\ -C-O-M + H^+ &\rightarrow -C-OH^- + M^{++} \\ -P-O-M + H^+ &\rightarrow -P-OH^- + M^{++} \end{aligned} \qquad (10)$$

Hydroxyl and ligand promoted dissolution

Hydroxyl promoted dissolution (deprotonation) is associated with a separation of hydrogen from the surface to form water as shown in eq. (11).

$$-Si-OH + OH^- \rightarrow -Si-O^- + H_2O \qquad (11)$$

The hydroxyl groups can be replaced by organic ligands. Thus ligands can weaken the bonds in the material lattice by coordination and complexation of metal ions. With respect to dissolution of minerals, effective ligands are provided with more than 2 donor atoms in their functional groups and can form bi- or multidentate mononuclear surface chelates.

Examples are ethylenediaminetetraacedic acid (EDTA), F^-, di-carboxy acid (e.g. oxalate) and hydroxyl carboxylate[21]. Fig. 2-3 (right hand) shows the dissolution rate of δ-Al_2O_3 affected by different organic ligands. The dissolution rate of δ-Al_2O_3 is directly proportional to the concentration of these ligands on the surface.

Plants uses this effect for their metabolism by release of organic acids (oxalic, tartaric, malic and citric acid) to the environment which causes selective dissociation of minerals[171, 186]. Dissolution of dental enamel by organic ligands is a further example for this mechanism[167].

C Inhibition of mineral dissolution

It is known that cations are able to alter the mineral dissolution due to interaction with surface functional groups, e.g. Cr(III) inhibits hematite (α-Fe_2O_3) dissolution. Because of the higher mobility of hydroxyl groups, deprotonation of mineral surfaces may be observed at increased pH which promotes the dissolution as shown in eq. (11).[48, 187]

Inhibition of the dissolution may also be associated with a precipitation of a thin layer on the surface of the dissolving mineral (protective layer). This is mostly accompanied by an incongruent dissolution. Metals are known to form protective layer due to precipitation of corrosion products on the metal surface, e.g. for iron $Fe(OH)_2$, $FeCO_3$, Fe(II,III)(hydr)oxide. Aluminum reacts with water to form a corrosion layer. Common to these layers is that the corrosion progress is retarded. Also it is assumed that in transport controlled dissolution processes protective layers are formed.

2.1.2.2 Generalisation of dissolution rate theory

Lasaga's empirical equation summarizes the different influences on the rate of dissolution of minerals[106].

$$\text{Rate} = k_0 \cdot A_O \cdot e^{-\frac{E_a}{R \cdot T}} \cdot a_{H_+}^{nH^+} \cdot \prod_i a_i^{n_i} \cdot g(I) \cdot f(\Delta G_r) \qquad (12)$$

with

A_0	...	Specific surface area
$e^{-\frac{Ea}{RT}}$	...	activation energy of the process
$a_{H_+}^{nH^+} \cdot \prod_i a_i^{n_i}$	...	ion activity of the species in solution
$g(I)$	...	a function of the ion strength of the solution
$f(\Delta G_r)$	...	a function of the free energy of the system
k_0	...	rate constant of the reaction.

As can be deviated from section 2.1.2.1 equation (12) mainly focuses on environmental parameters. All inherent parameters were addressed in the rate constant k_0. It should be noted that this is a geochemical approach where only minerals with low solubility in water are handled. With increasing importance of diffusion-limited reactions as in pharmacokinetics k_0 should be substituted by a diffusion term, cf. equation (9b).

2.1.3 The precipitation process of solids

The formation of new phases from supersaturated media is subject of classical nucleation theory (CNT). In particular, mechanisms that lead to the formation of crystals from liquid phases are concerned. This topic is of interest for researchers for a long time period and was developed mainly by Gibbs, Volmer and Weber, Becker and Döring[128]. Therefore nucleation can be regarded as a first-order phase transformation. In general crystallization is subdivided into nucleation and crystal growth processes. During nucleation, stable nuclei are formed from atom clusters which grow during the second process. Moreover the mode of cluster formation is subdivided into primary nucleation (homogeneous and heterogeneous) and secondary nucleation. Homogeneous nucleation occurs in the absence of solid interfaces, whereas heterogeneous nucleation is observed in the presence of solid interfaces (e.g. foreign substances, walls). Secondary nucleation is observed by thermal and mechanical treatment of existing crystals[122]. In the present section the basic principles of nucleation and crystal growth are outlined which includes both thermodynamics and kinetics.

2.1.3.1 The nucleation process

2.1.3.1.1 Classical Nucleation Theory

Common for all reactions (cf. section 2.1.1), the driving force for a reaction is the difference in the Gibbs free energy of the system. In case of crystallization, as the process to form material, the system has to be supersaturated (saturation index > 0). This involves geometric dependencies because the separation of crystals from the solvent creates new interfaces. Eq. (13) addresses the change in Gibbs free energy of the system in dependence on the surface, volume and the driving force of reaction [adapted from 46, 128, 135].

$$\Delta G(d) = \beta_a \cdot d^2 \cdot \gamma_{cl} - \frac{\beta_v \cdot d^3}{\upsilon_m} \cdot k_B \cdot T \cdot \ln(S_a) \qquad (13)$$

with

β_a	...	Surface shape factor (sphere: $\beta_a = \pi$, cube $\beta_a = 6$)
d	...	Generalized particle dimension (sphere: diameter, cube: edge)
γ_{cl}	...	Interfacial energy between crystal and liquid
β_v	...	Volume shape factor (sphere $\beta_v = \frac{1}{6} \cdot \pi$, cube $\beta_v = 1$)
υ_m	...	Molecular volume of the formed crystal $\upsilon_m = \frac{M}{\rho \cdot N_A}$ (M-molar mass, ρ- density of the solid, Avogadro constant $N_A = 6.022 \cdot 10^{23}$ mol^{-1})
k_B	...	Boltzmann constant ($k_B = 1.3806488 \cdot 10^{-23}$ J/K)
T	...	Absolute temperature
S_a	...	Saturation ratio derived from ion activities

It is obvious that for both crystallization and for dissolution (cf. section 2.1.2) the main parameter and thus the driving force is the saturation ratio of the system. In case of crystallization, supersaturation induces the formation of crystals which are defined by their surface (β_a d^2) and volume (β_v d^3). In general for the precipitating nuclei, various shapes can be considered (β_a and β_v in (13)), for simplification often spheres are assumed. Because the interfacial energy attempts to decrease the surface area, the formation of nuclei is restricted and thus the term is positive in eq. (13). Contrary the volume of the precipitating phase leads to a decrease in Gibbs free energy of the system (negative sign). Thus the addition of the two terms shows a maximum at a certain dimension of the nuclei. Both the size of this critical nucleus (d_{crit}) and Gibbs free energy of formation can be calculated by setting the first derivative of eq. (13) with respect to the size equal zero ($\frac{\delta \Delta G(d)}{\delta d} = 0$).

$$d_{crit} = \frac{2 \cdot \beta_a \gamma_{cl} \cdot \nu_m}{3 \cdot \beta_v (k_B \cdot T) \cdot \ln S_a} \tag{14}$$

$$\Delta G_{max} = \frac{\gamma_{cl} \cdot \beta_a \cdot (d_{crit})^2}{3} \tag{15}$$

During the formation of the new phase the system has to overcome the barrier of activation energy for nucleation (ΔG_{max})[188]. Below this value the phase dissolves and no overall precipitation can be observed. In this case the phase is termed subnuclei[97] or embryo[106, 135]. If the supersaturation is high enough the precipitating phase with critical dimension is able to grow. This phase is called supernuclei[97] or nuclei[106, 135]. Further growth of these nuclei leads to a stabilization of the system since the Gibbs free energy of the system decreases.

From equation (14) can be inferred that the measure of the critical nuclei decreases with increasing saturation ratio. Thus also the energy barrier for the formation of the critical nuclei decreases with increasing supersaturation, cf. eq. (15).

If the size of the nuclei is expressed as the product of n atoms/molecules in a cluster with volume υ_m, the change in Gibbs free energy for nucleation can be calculated as a function of the number of atoms/molecules in the nucleus $\Delta G(n)$. Similar to the critical particle dimension (eq. (14)), setting the first derivative of this function equal zero ($\frac{\delta \Delta G(n)}{\delta n} = 0$), the number of atoms/molecules in the critical cluster can be calculated according to eq. (16) [adapted from 46, 135].

$$n_{crit} = \frac{8 \cdot (\beta_a)^3}{27 \cdot (\beta_v)^2} \cdot \frac{(\nu_m)^2 \cdot (\gamma_{cl})^3}{(k_B \cdot T)^3 \cdot \ln^3 S_a} \tag{16}$$

With decreasing supersaturation the crystallization is increasingly dominated by heterogeneous nucleation phenomenon. Heterogeneous nucleation can take place on similar or foreign substances and accelerates the overall crystallization process. Analogously to homogeneous nucleation, heterogeneous nucleation can be computed taken the different

interfacial energy between the precipitating phase and the substrate γ_{cs} into account. This leads to the critical Gibbs free energy of heterogeneous nucleation with the factor ϕ [128].

$$\Delta G_{crit}^{heterogeneous} = \phi \cdot \Delta G_{crit}^{hom\,ogeneous} \tag{17}$$

For heterogeneous nucleation, the wetting of the substrate by the precipitating phase dominates the interfacial energy. The wetting angle θ can be expressed as:

$$\cos\theta = \frac{\gamma_{sl} - \gamma_{cs}}{\gamma_{cl}} \tag{18}$$

Taking the wetting angle into account, the factor ϕ can be calculated.

$$\phi = \frac{(2 + \cos\theta) \cdot (1 - \cos\theta)^2}{4} \tag{19}$$

At wetting angle $\theta = 180°$ (spheroid droplet), the foreign surface is not affine to the precipitating crystal, consequently the Gibbs free energy of nucleation is the same for both homogeneous and heterogeneous nucleation ($\phi = 1$). Increasing affinity of the foreign and the precipitating surfaces decreases the Gibbs free energy of heterogeneous nucleation. Instantaneous nucleation is observed at $\theta = 0°$ (plane layer on surface). For this case the formation of the critical nuclei is not necessary, i.e. the solution is seeded with similar nuclei.

The nucleation rate J is referred to as the rate of formation of nuclei with critical size in a given volume and time (unit: $m^{-3}s^{-1}$). Because in literature different approaches describing single factors govern the nucleation rate are assumed, a clear picture is still not available. Nevertheless, for the first attempt the following equation gives a hint to main factors govern the nucleation rate.[97, 103, 122]

$$J_{hom} = \frac{dN_{crit}}{dt} = f \cdot A_{crit} \cdot n_{crit} \cdot z \tag{20}$$

with

f ... Frequency of attachment of monomers to the nucleus

A_{crit} ... Critical surface area of the nucleus

N_{crit} ... Number of critical nuclei in the volume, $N_{crit} = N_0 \cdot \exp\left(\frac{-\Delta G_{crit}}{k_B \cdot T}\right)$, Concentration of monomers in the solution $N_0 = \sqrt{K_{SP}} \cdot S \cdot N_A$

z ... Zeldovich factor compensates the removement of cluster with critical size from the bulk, $z = 2 \cdot \sqrt{\frac{\gamma_{cl}}{k_B \cdot T}} \cdot \upsilon_m \cdot \frac{1}{A_{crit}}$

Therefore the rate of homogeneous nucleation depends mainly on (i) the frequency of attachment of molecular units on the nuclei f and on (ii) the number of critical nuclei

formed due to the degree of supersaturation N_{crit}. Because for precipitation in solutions the monomers have to been transferred to the surface of the nuclei and across the solid/liquid interface, the attachment frequency is mainly diffusion controlled. This is the reversed step of dissolution after the breaking of bonds, cf. section 2.1.2. Therefore the attachment frequency f can be described as a function of the diffusion through solution. More details can be found elsewhere[103, 122].

In literature often a simple form is used [adapted from 46, 97, 128].

$$J(S)_{hom} = A1 \cdot \exp\left(-A2 \cdot \gamma^3 \cdot \frac{1}{\ln^2 S}\right) \tag{21}$$

With parameters A1 and A2 the main influence on the homogeneous nucleation rate in eq. (21) stems from the saturation state of the system S and interfacial energy.

Against the prediction from the CNT, where the nucleation occurs immediately once the supersaturation is achieved, often a time lag before the occurrence of nucleation is observed. This time is termed induction time t_{ind}. Mullin[128] separates the induction time into different parts.

$$t_{ind} = t_r + t_n + t_g \tag{22}$$

with

t_r ... Relaxation time to achieve quasi-steady-state distribution of cluster

t_n ... Time to form a stable nucleus

t_g ... Time needed for the crystal to grow to a detectable size

As given in eq. (22) the induction time depends on the ability to detect crystals/nuclei[97]. The induction time can be deduced from eq.(20) and eq. (21) by setting the number of critical nuclei equal to 1, cf. eq. (23).

$$\ln(t_{ind}) = A2 \cdot \gamma^3 \cdot \frac{1}{\ln^2 S} - \ln A1 \tag{23}$$

2.1.3.1.2 Non-classical Nucleation Theory

Although the classical nucleation theory (CNT) is suitable describing crystallization phenomena, it fails in certain points. Besides the need to establish a cluster shape, the CNT assumes that macroscopic properties, in particular interfacial energy and density, are equal in both macroscopic phase and critical nuclei. This is crucial, especially at low interfacial energies and high supersaturation values, which result in small nuclei containing

only few molecules, cf. eq. (16). Therefore this assumption is rather ambitious since the macroscopic crystal should be very distinctive in properties from that of a few molecules.

Recent experiments emphasize that prior to nucleation stable clusters are formed which are termed prenucleation clusters. According to this, the formation of critical nuclei as known from the classical picture of crystallization is not imperative. In the progress of crystallization the prenucleation cluster aggregates to larger crystals instead of the growth of critical nuclei, cf. Fig. 2-4. Because of this fundamental difference regarding the classical picture, this nucleation pathway is called Non-classical nucleation.[33] Also different tests give experimental evidences for the existence of prenucleation cluster in solutions, which are distinctive from simple ion pairs as well established inter-ionic arrangement.[73]

Non-classical nucleation theory explains many aspects of crystal growth phenomenon in

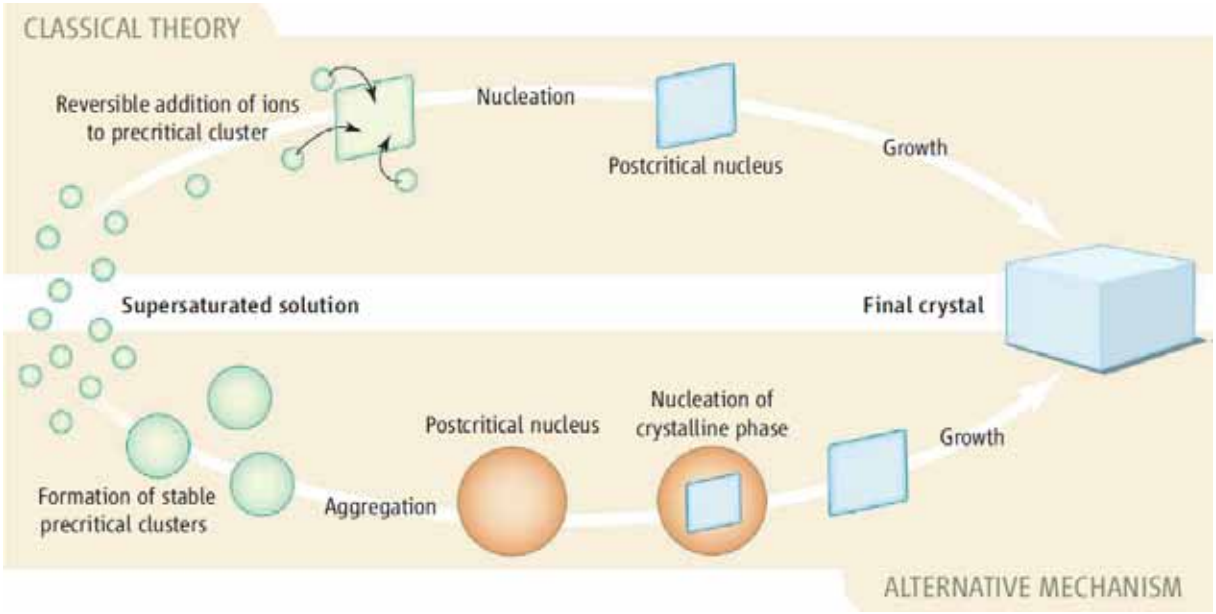

Fig. 2-4: Crystallization after the classical theory (top) with the formation of critical nuclei, which grow *via* ion attachment. The alternative theory (non-classical) describes the formation of prenucleation cluster instead of critical nuclei. Due to aggregation of these clusters the crystalline phase grows.[120]

particular. This strongly includes the morphology of biominerals, which is normally out of the scope of classical nucleation pictures. It was demonstrated that the aggregation process of the prenucleation cluster and thus the structure of the bulk material is controlled by the structure forming organism. This is mainly possible with the interaction of organic compounds and inorganic material, which leads to oriented attachment of prenucleation clusters and a soft-stiff composite bulk material. As a result, such crystals appear in X-ray or electron diffraction scattering experiments as single crystals[33] and show improved mechanical properties, i.e. higher tensile strengths.[201]

Recently, Picker[144] showed that C-S-H phases can be formed by the mechanism of non-classical crystallization, i.e. *via* particle mediated crystallization. He found out that tailor-made polymers are able to control the crystallization process, and C-S-H-polymer nanocomposites are formed with increased flexibility. Also the impact of different organic

polymers on the nucleation rate of C-S-H phases was reflected. It was demonstrated that polymers can both accelerate and decelerate the nucleation rate of C-S-H phases in dependence of their molecular structure. Dispite that the impact of these polymers on the more complex C_3S or even cement hydration was not addressed. Nevertheless this work opens new possibilities for cementitious materials.

2.1.3.2 The process of crystal growth

As stated in section 2.1.1, the overall reaction (crystallization) process is aimed to reduce the Gibbs free energy of the system. This energy is decreased in two distinctive processes. Firstly, stable nuclei are generated (nucleation) that grow during the second process (crystal growth). Thereby the particle size distribution of the precipitated crystals is influenced by their crystal growth. On decreasing crystal growth rates an increasing number of nuclei is formed to reduce the saturation state of the system. On the other hand, fast crystal growth processes lead to a small amount of large crystals. Kinetic studies are thus linked to determine the slowest step, since this process will control the overall crystallization rate. This section gives a short overview on the theories related to crystal growth.

In general two main steps in crystal growth are distinguished. Thereby the single steps are attributed as reverse process of crystal dissolution as shown in section 2.1.2 (p.25). The first step is the transport of monomer units due to diffusion or convection to the surface of the growing crystal. In the second step, these monomers are attached onto the surface of the crystals unit cell. Moving of these monomers on the surface and attachment of to steps, edges and kinks occurs in the further step. Therefore, the overall crystal growth process is limited either by transport of monomers to the surface (diffusion limited) or by the incorporation of these monomers into the crystal structure. It is reported that at low supersaturation mainly surface reactions whereas at high supersaturations mainly diffusion controls the crystal growth[97, 128, 188].

2.1.3.2.1 Integration controlled crystal growth

The first approach of crystal growth is suggested by Kossel, Stranski and Volmer, showing that monomers (molecules, atoms) were attached layer-by-layer on the surface of the growing crystal.[128, 188] Because the incorporation of these molecular units once they arrived the crystal surface occurs not instantaneously, a 2D diffusion is postulated which forms a layer of 1 nm thickness, whereby the moieties move on the surface to integrate on a high attractive centre of the crystal, i.e. dislocations as kinks and edges. Therefore the growth rate should increase with increasing defect density of the crystal. But the observation of defect healing induced by crystal growth contradicts the theory, since measured growth rates are higher than predicted by the model. Once, the layer is completed, a new nucleation centre is necessary in the crystal growth progress. Besides growth on edges, a first assumption states that active centers are built in analogy to heterogeneous nucleation on the surface of the crystal. Accordingly, the mono-nuclear model states that the single nucleus on the crystal surface grows until the layer is completed (Burton and Cabrera, Nielsen).[128] In the poly-nuclear model these nuclei stay in their size and the surface coverage is controlled by their number. The birth and spread model combines these two

modes (Hillig, Nielsen)[46, 128]. With respect to the saturation state of the system, nucleation on active centers requires a critical supersaturation (cf. eq. (15) and (17)). Therefore no crystal growth should occur on low degrees of supersaturation, which contradicts experimental data and thus limits this theory. Burton, Cabrera and Frank solved this problem, as they assumed that growth takes place on screw dislocations of the crystal (BCF model)[188]. Therefore only low degrees of supersaturation are needed for the crystal growth. Fig. 2-5 illustrates the layer growth mechanism in summary.

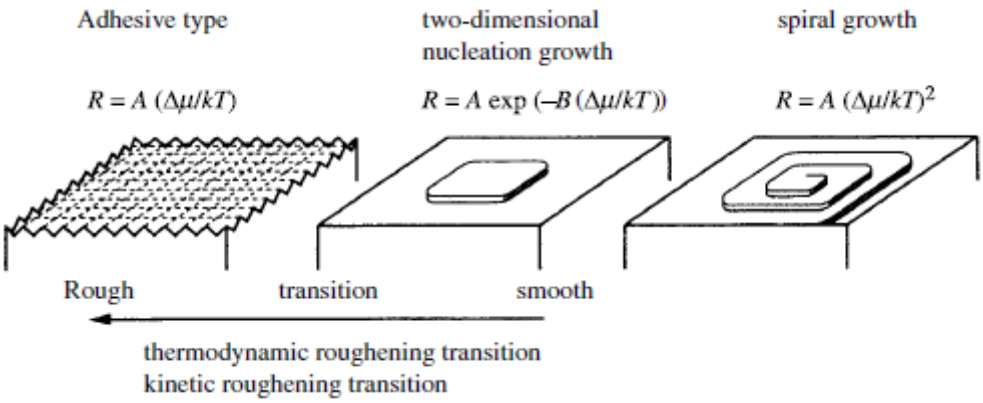

Fig. 2-5: Growth mode mechanisms in dependence of the surface roughness.[188] The rates R are expressed dependent on the driving force Δ(μ/(kT)) with A and B as constants. In direction of the arrow the supersaturation increases.

2.1.3.2.2 Diffusion controlled crystal growth

During crystal growth monomer units are occluded in the crystal lattice. Thereby the number of these moieties which are transported to the crystal interface can be rate limiting. This case is termed diffusion controlled crystal growth[106] and is especially observed in fast growing crystals, which are mostly highly soluble.[205] One first hint for the diffusion control is the concentration of ions/monomers in the surrounding of the crystals interface. If the surface grows fast, concentration gradients occur on the interface of the crystal to the mother liquior, and the crystal growth is controlled by the rate of transport of building units to the surface of the crystal. Thus, diffusion controlled reactions can be modified by altering the diffusion coefficient of the mother liquior by decreasing the viscosity or increase the rate of mass transfer, i.e. due to increasing stirring rate.

2.1.3.2.3 Morphology of crystals

Since the degree of supersaturation dictates the growth kinetics of crystals, also the crystal morphology is controlled by the driving force. As mentioned before, high supersaturation causes surface nucleation of the crystals, which results in a roughening. Further increase in supersaturation leads to the formation of needles and whiskers. At decreasing supersaturations, the growth mode changes until only growth on screw dislocations (spiral) is observed, cf. Fig. 2-6.

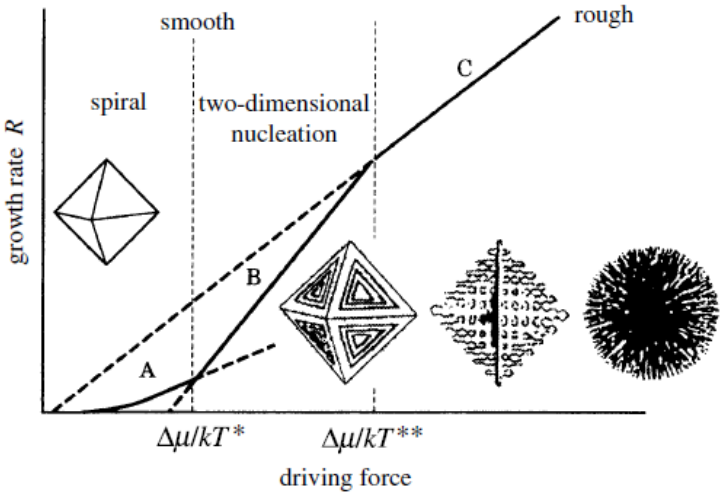

Fig. 2-6: Schematic picture of the change in crystal habit dependent on the driving force of the system. This picture also shows the areas of the different modes of crystal growth.[188]

An experimental proof of the proposed models on crystal growth is given as AFM images[205] in Fig. 2-7. Here, the growth of calcite (a) and canavaline (b) is initiated at low (small pictures) and high supersaturations (large pictures). This observation reflects the scheme in Fig. 2-6 and shows that due to modification of the supersaturation both *Habitus* and *Tracht* of the crystals are altered.

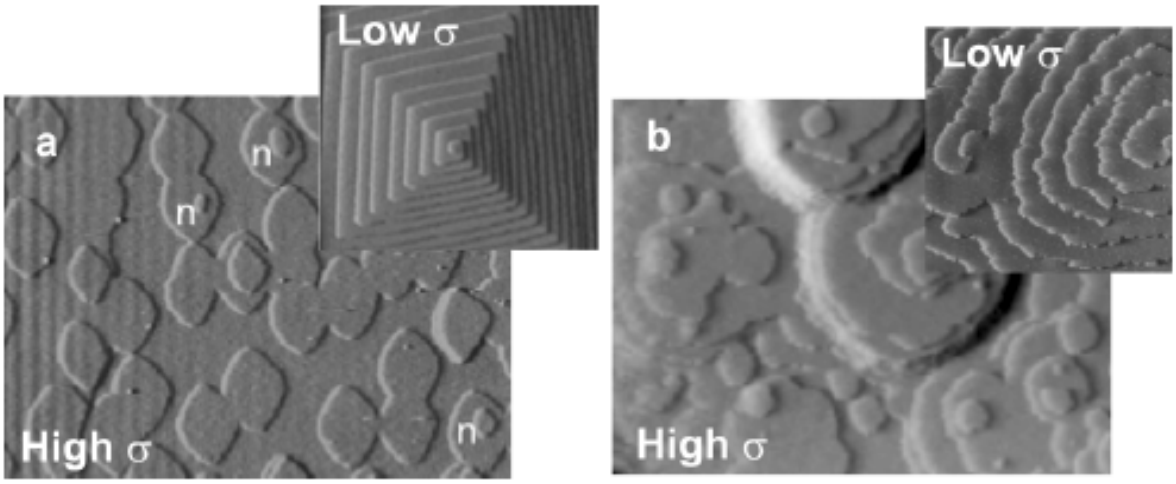

Fig. 2-7: AFM images[205] of a) calcite and b) canavaline growing in dependence of the degree of supersaturation σ (high and low). Island-on-island growth is indicated by the letter n.

Habitus and *Tracht* are the result of the growth processes of crystal faces, which are strongly dependent on the crystal lattice. The interfacial energy of the faces determines the growth rate of certain faces. Thereby the growth rate increases with interfacial energy. The overall energy of all faces tends to a minimum (Gibbs). Accordingly, Wulff's theorem states that faces with the lowest interfacial energy are present in the *Habitus* and *Tracht* of crystals, when equilibrium conditions are achieved. Therefore changes in *Habitus* or even in *Tracht* are the result of reducing the growth rate of certain faces of the crystal. Because

crystal faces are reactive sites in the crystal, substances in the environment as foreign ions and organic polymers are able to modify or even block the growth of the faces. This can lead to modification in *Habitus* and *Tracht*.

2.1.3.2.4 Influence of organic polymers on inorganic material crystallization

Likewise in dissolution processes, the presence of organic polymers is able to alter crystallization of inorganic materials. This issue is especially addressed in biomineralization[200], where it is known that nature controls mechanical[11], optical[6] and surface related properties, e.g. crystal shape, of materials built by invertebrates, vertebrates and plants[33].

2.1.3.3 Progress of crystallization

Ostwald (Nobel Prize in chemistry 1909) investigated the products formed during the crystallization process. In numerous cases he found that less stable polymorphs are built in the first, and the most stable polymorphs in the final state of crystallization.[128] Besides thermodynamic consideration, kinetic parameters are also important in the description of general crystallization processes. This is especially relevant for polymorph formation, where the crystal is similar in the chemical composition but differs in the arrangement of the atoms and thus in the crystal lattice. The different lattices manifest in turn in, e.g., different stabilities, solubility and melting points. Polymorphs are also handled in section 2.1.2.1. Kinetically controlled crystallization can be differentiated from thermodynamically controlled crystallization mainly by the barriers of energy activation for the nucleation, growth, and phase transformation. Especially in biomineralization the formation of certain polymorphs was found. Nature is able to control each reaction step during the Ostwalds step rule. Thereby the crystallization starts with the formation of an amorphous phase, which is transformed into crystalline phases at the end of the crystallization process.[33] Also the amorphous phase can be stabilized for long time periods. A schematic illustration of the concept of the Ostwald step rule is given in Fig. 2-8.

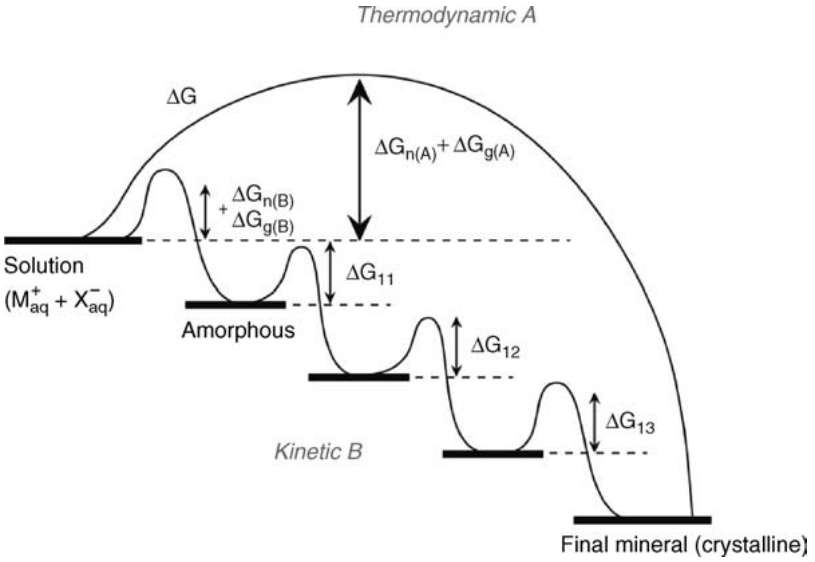

Fig. 2-8: Crystallization pathway under thermodynamic (A) and kinetic control (B) which is known as Ostwald step rule. The main difference is the measure of the activation energy to form the amorph or the polymorph.[33]

In biomineralization the formation of the amorphous phase plays a crucial role in the overall crystallization process. For calcium carbonate as very important mineral in nature, two amorphous phases are distinguished, namely ACCI and ACCII.[73] In sequence of kinetic crystallization pathway, vaterite, aragonite and finally the most stable calcite are known. Biominerals show significant amounts of amorphous phases besides less stable crystalline phases (e.g. aragonite). In cement research the precipitation of a precursor phase for Calcium-Silicate-Hydrate (C-S-H, see section 2.2.2) is postulated during C_3S hydration[18].

2.1.4 Forces between particle surfaces

Particles exhibit electrical charges on their surfaces which causes surfaces forces. These are determined by the outermost atoms or molecules of the material and the surrounding medium. The magnitude of these forces is mainly dependent on the distance away from the surface. The sign of the surface forces are either attractive or repulsive in dependence of their origin.

2.1.4.1 Van der Waals forces

Ubiquitously, van der Waals forces are present between surfaces and intervening medium. This force arises from atomic and molecular dipoles interacting with each other. At intimate contact of the surfaces (distance =0) the force is referred to as adhesion force.[145] It is obvious that the composition of the surface impacts the magnitude of the van der Waals force. This relation is expressed by the Hamaker constant H. Values of the Hamaker constant for ettringite and C_3S are calculated to H=0.055 J and H=1.6 J, respectively[53]. In comparison weaker attractive van der Waals forces than in cement paste should be observed for $BaTiO_3$ particles[206] with $H \approx 8 \cdot 10^{-20}\,J$. Mostly, van der Waals forces are attractive, but for dissimilar materials this may also be repulsive. Furthermore, the magnitude of the van der Waals force can be altered by the particle size (surface area). But changes in pH and the presence of surfactant or other polymers do not affect the van der Waals force.[90]

2.1.4.2 Double layer forces

The interaction of solid surfaces with a polar medium (e.g. water) causes adsorption or desorption of surface species with magnitudes determined by the specific solubility product of the mineral, cf. section 2.1.1. As a consequence, the surface is electrical charged referred to as Nernst potential. In case of C-S-H particles in high alkaline solution (pH>10), SiO^- groups are the dominant surface species, and the surface is predominantly negatively charged.[93] The neutralization of the surface charging is evoked by adsorption of oppositely charged species (counterions) from the surrounding solution, and the known Helmholtz or Stern layer is established. Accordingly, C-S-H particles are surrounded by Ca ion species[93, 104]. Ions from solution adsorb on the Stern layer and develop a diffuse ion cloud around the particle with the characteristic thickness κ^{-1}, denoted as Debye-length. This layer is referred to as the electric double layer (EDL) or diffuse layer. In contrast to the Stern layer, the EDL constitutes mobile ions and thus the diffuse layer may be sheared off on a slipping plane if the particle is exposed to electrical fields. The electrical potential on the slipping plane is referred to as ζ –potential. Latter is a measure for the stability of a

suspension against coagulation and flocculation. With increasing absolute ζ –potential this stability increases. An overlap of different electric double layer of similar charged particles causes a repulsive force.

Due to changes in pH and the type and quantity of the electrolyte in suspension (ion strength) the magnitude of the ζ -potential and the Debye-length can be modified. Furthermore, the size of the particle will affect the magnitude of the inter-particle force induced by the electric double layer.[90, 145]

Whereas van der Waals forces are unaffected by species in the surrounding solution, the diffuse double layer is also susceptible to the presence of surfactants and polymers. The interaction of these polymers with the surface determines the resulting inter-particle force. This interaction is determined by the polymer concentration and molecular structure, i.e. polymer conformation on the interface. Superplasticizers influence the electrical potential due to the interaction of the functional groups with the ions of the Stern layer. Thereby, the electrical potential (measured as ζ –potential) is changed and thus the tendency to flocculation is reduced.[3, 147, 199]

2.1.4.3 Steric and electrosteric forces

Polymers can cause repulsive forces on surfaces after adsorption. In the simplest case they act as lubricants. Polymers with grafted side chains cause steric forces, which lead to a dispersion force on the particle surface. Polycarboxylate ether based superplasticizers contain two functions. On the one hand, the carboxy groups on the main chain alter the electrical double layer potential. On the other hand, the grafted side chains lead to steric repulsion forces between the particles.[53, 199, 207] Thus, the mode of dispersion is based on both steric and electrostatic dispersion, called electrosteric.[90] It is generally accepted that the main contribution to the dispersion in cement pastes is caused by the steric repulsion.

The magnitude of the steric performance depends on type, molecular architecture, concentration, degree of adsorption of the polymer, and on the other hand on the susceptibilities of the electrical double layer (pH, ion strength, material).

2.1.4.4 Net surface forces

The interplay of the different surface forces described above determines the resulting surface force and thus the tendency of the particles to disperse, coagulate or flocculate. Within the DLVO theory, van der Waals and electrical double layer forces are combined. Mostly the van der Waals force acts attractive, whereas the electrical double layer force is repulsive. The net interaction force is the sum of these two terms, but can also be extended to other forces, e.g. the steric force. In dependence of the distance from the particle surface and the magnitude of the force, the interaction of particle surfaces in aqueous solutions are differentiated in strongly attractive, long-range repulsive, and weakly attractive. A scheme of the three different particle interactions is given in Fig. 2-9.

Fig. 2-9 a) represents only van der Waals attractive forces. This case is observed at the isoelectric point (ζ=0, zero point charge) of the material, thus no electrical double layer force occurs. The van der Waals force is of short range order. In Fig. 2-9 b) is shown that at short distances the attractive van der Waals force is dominant, which is overwhelmed by

repulsive forces at larger distances. This can be the result of electrical double layer forces and/or steric forces. Short range repulsion forces can be overlapped by attractive van der Waals forces, see Fig. 2-9 c). As a consequence, the particles are weakly attractive coordinated at larger distances, but the adhesion is prohibited at low distances. The short range repulsion forces can be the result of structural forces, e.g. hydration forces.

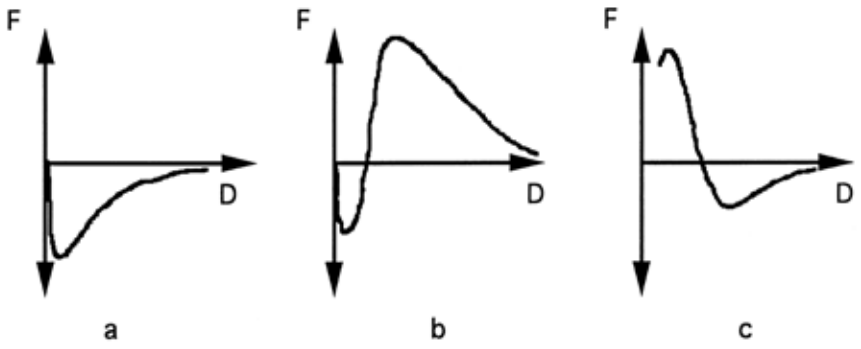

Fig. 2-9: Surface-surface interactions indicated by inter-particle force F and distance between the particles D. a) strongly attractive due to van der Waals forces, b) strongly repulsive, and c) weakly attractive. Negative forces correspond to attraction.[90]

2.1.4.5 Bridging forces

Bridging forces can on the one hand be caused by polymers, which adsorb on surfaces of different particles. These polymers are often referred to as flocculants[77, 111]. On the other hand, chemical reactions can result in mineral bridges[33]. As a consequence particles are connected with each other. In cement paste this behaviour is known for example from the fast precipitation of the hydration products of the clinker mineral C_3A, which interacts with both the solved sulphate and potassium content in the aqueous phase. In the absence of sulphate, larger agglomerates of calciumaluminate hydrate (C-A-H, e.g. C_4AH_{13}) crystals precipitate which are able to form a rigid network[181]. As a result, the cement paste loses its workability ('flash set'). This is avoided due to the addition of water soluble sulphate (set regulator). In this case small crystals of ettringite ($C_3A \cdot 3CaSO_4 \cdot 32H_2O$) form a network on the C_3A surface.[181] Similar to C-A-H phases, potassium reacts with calcium and sulphate to syngenite ($K_2SO_4 \cdot CaSO_4 \cdot H_2O$). The formation of this mineral may due to its elongated habitus lead to stiffening of the cement paste[165]. Furthermore at high calcium and sulphate concentration in the aqueous phase, gypsum precipitates ('false set') and similar to syngenite and C_4AH_{13} inter-particle forces are overlapped by bridging forces.

2.2 Material specific considerations

2.2.1 Portland cement and superplasticizers

2.2.1.1 Portland cement

Ordinary Portland cement (OPC) is a mixture of Portland cement clinker and set regulator. Also calcium carbonate can be intermixed (up to 5 %). As shown by a polished section in Fig. 2-10 OPC clinker contains different phases. The main compound of OPC are calcium silicate minerals. Alite (tricalcium silicate Ca_3SiO_5, C_3S in cement notation, see list of abbreviations) with up to 4 % substituted foreign oxides is the main compound of OPC clinker. Other OPC clinker compounds are belite (dicalcium silicate (Ca_2SiO_4, C_2S) with foreign oxides), tricalcium aluminate (C_3A) and calciumaluminate ferrite ($C_4Al_xFe_{1-x}$, with $0<x<0.7$) with a constitution in OPC clinker of 15 to 30 %, 5 to 10 % and 5 to 15 %, respectively.[195] In contact with water each phase reacts to hydrate phases. The reaction mechanism is governed by educt dissolution and product precipitation as described by Le Chatelier[107].

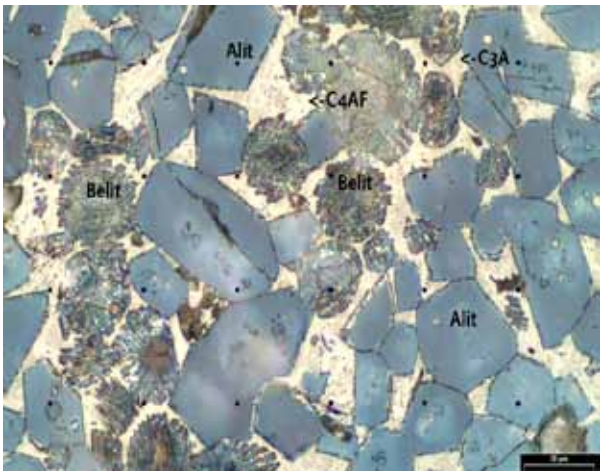

Fig. 2-10: Light microscopy image of a polished section of a PC clinker[177].

Due to the variable nature of the educts a wide variation of products as hydrate phases are observed. With a percentage of 50 to 70 % in OPC clinker, alite dictates many properties of cements and concretes.[195] For example the hydration kinetics of Portland cement is largely governed by alite. Furthermore the formation of C-S-H phases as alite and belite products is responsible for the strength development of cements[195].

2.2.1.2 Superplasticizer

2.2.1.2.1 History

Since materials are used, improving of its properties on specific needs was conducted. Examples can be found in the building materials between Euphrat and Tigris and later on during the period of the ancient Romans in Europe[3, 180]. Thus, also about 90 % of the concretes produced in Germany today contain admixtures and thereof are 75 % plasticizer and superplasticizer, respectively[210]. The history of modern (super)plasticizers began in the 1930s in the USA. On the one hand it is believed that the benefits to use these substances as dispersing agent were discovered for carbon particles in concrete, which were used to visualize the central lane of highways. For this purpose a sodium salt of polynaphthalene sulfonate[b] from the painting industry was used. Later on the much cheaper product lignosulfonate was found to act liquefying.[3, 180] On the other hand as first plasticizer or

[b] Correct notation: sulfonated salts of polycondensates of naphthalene and formaldehyde

water reducer lignosulfonates are handled[153]. Nevertheless, combinations of polynaphthalene sulfonates and lignosulfonates were further developed to increase the vantages of the two groups. Though for decades lignosulfonates were predominantly used, the need for higher liquefaction of concrete mixtures led to the rediscovering of the naphthalene sulfonates in Japan in the 1960s. Simultaneously, polymelamine sulfonate[c] as a performant superplasticizer was developed in Germany.[3, 52, 180] Further steps toward in developing superplasticizers was made in Japan with the formulation of polycarboxylate based superplasticizer. This new group was patented 1981 by the company Nippon Shokubei and used since the middle of the 1980 in Japan.[153] Up today within the polycarboxylates four subgroups are distinguished.[80] With an increasing importance as concrete admixture, polycarboxylates exhibit a temporary market share in Germany of about 45 %[210].

2.2.1.2.2 Composition of superplasticizer

Superplasticizers differ in their molecular architecture, which includes molecular units and design. Because of the huge variability only the most common superplasticizers, Naphthalene sulfonate formaldehyde (NSF) and polycarboxylate (PC), which were also used in this work, are outlined.

Fig. 2-11 shows the chemical structures of both Naphthalene sulfonate and polycarboxylate based superplasticizers.

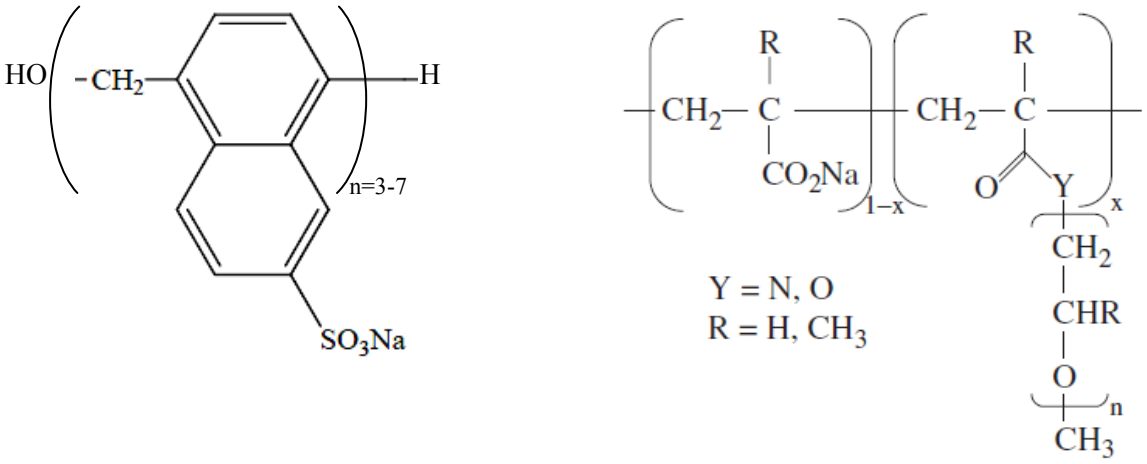

Fig. 2-11: Chemical structure of polynaphthalene sulfonate[153] (left hand) and polycarboxylate[75] based superplasticizers (right hand).

Naphthalene sulfonates constitute chains of naphthalene rings with sulfonic acid groups as functional units. A repetition of 3-7 monomer units are used as superplasticizer.[153] In contrast, polycarboxylates are, because of the grafted side chains, comb or brush like polymers[72]. As a consequence of the multi component composition, latter group of polymer can be designed with a huge variability. In general, polycarboxylates have a fewer number of functional groups and contain a higher number of monomeric units than naphthalene sulfonates, which results in typical molecular weights of 20.000-150.000 Da and 500-20.000 Da for PCE and NSF, respectively[153].

[c] Correct notation: sulfonated salts of polycondensates of melamine and formaldehyde

Polycarboxylates can be varied in terms of number and ratio of the building units and in the nature of the monomers. The backbone is typically build of acrylic acid, but can also contain additional monomers of maleic acid[80]. The side chains are polyethylene glycol (PEG) monomers, which are terminated mostly by a methoxy group (CH_3). Therefore they are described as methoxy polyethylenglycol (MPEG). But also a hydroxy group (OH) as termination for the PEG is described in the literature. In this case a hydroxy polyethylenglycol (HPEG) is build.[150] The grafting of side chains is based either on ester, ether, amid, or imid linkage. The functional groups responsible for adsorption are sulfonic acid (SO_3^-) and carboxy acid (COO^-) in case of NSF and PCE, respectively. Table 2-2 shows a possible classification of these admixtures and summarizes the main differences between the subgroups of the polycarboxylates.

Table 2-2: Summary of plasticizer and superplasticizer properties (adapted from [80, 153]).

Group	Admixture		Special features
Plasticizer/ water reducer	Lignosulfonate		Mostly used admixture, moderate liquefaction
Superplasticizer/ high range water reducer	Polycondensate	Polynaphthalene sulfonate	Lower slump loss, higher retardation, ready-mix-concrete
		Polymelamine sulfonate	Higher slump loss, lower retardation, precast concrete
	Polycarboxylate	Generation 1	Ester side chain linkage, more effective than polycondensates and lignosulfonates
		Generation 2	Ether side chain linkage, increased stability at higher temperatures
		Generation 3	Amide- and Imide side chain linkage
		Generation 4	Carboxy groups in backbone, side chains based on amidoamine and PEO
	Small molecules		Similar structure units as polycarboxylates, but low degree of polymerisation, high level of adsorption

2.2.1.2.3 Size and conformation on surfaces

The knowledge of the polymers size and their conformation in solution and on surfaces is useful to understand the interaction of superplasticizers with cement. Usually, naphthalene sulfonates are described as simple chains with functional groups. The polycarboxylate based superplasticizers are illustrated as comb or brush like polymers due to the grafted side chains as demonstrated above. For the carbon chain containing 3 atoms the length is given to 0.251 nm at maximum. Seven units of side chains of polyethylene glycol (PEG) measures

$d_{(CH2\text{-}CH2\text{-}O)7}$=1.95 nm. Thus, a polycarboxylate comb shaped polymer with 25 units of PEG and 70 units of acrylic acid and copolymer of methyl polyethylene glycol methacrylate scales 20 nm x 7 nm at maximum stretch.[140]

By contrast, the conformation and size of polymers in aqueous solution is dependent on the amount of units N and P, which build the backbone and the side chains in a polymer segment n, respectively. With increasing number of monomers in the backbone and low number of side chains, i.e. low side chain density, the backbone behaves like a decorated chain, see DC in Fig. 2-12. With increasing number of monomers in the side chains P, i.e. with increasing side chain length, the backbone loses a part of its flexibility and becomes more and more stretched, cf. flexible backbone worm FBW in Fig. 2-12. Furthermore, if the number of units in the backbone decreases in polymers with increased number of side chain units P, the overall conformation of the comb molecule is more like a star with stretched backbone, cf. stretched backbone worm SBW, stretched backbone star SBS, and flexible backbone star FBS in Fig. 2-12.[72]

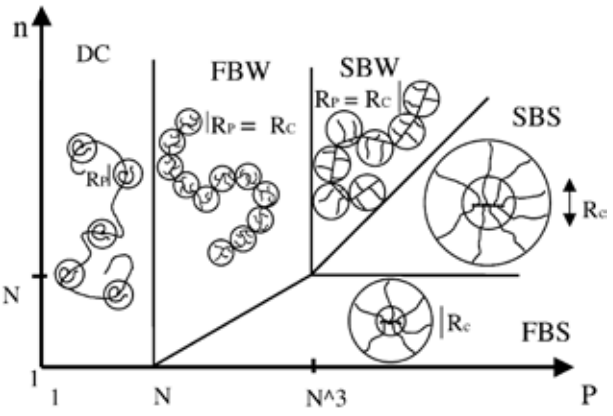

Fig. 2-12: Scheme of the conformation of comb shaped polymers in aqueous solutions. The abbreviations are given in the text.[72]

The conformation of polycarboxylate superplasticizer in solution is mainly considered as flexible backbone worm regime[84], cf. Fig. 2-12, but can change with different molecular architectures. The hydrodynamic radii of different polycarboxylates are determined by means of dynamic light scattering to 4.4-10.1 nm, which was shown to be independent on pH and ion strength in the range between $8<pH<12.8$ and $3x10^{-2}<I<4x10^{-1}$, respectively.[84] The polymer can be subdivided with respect to their ability to gyrate in spherical blobs, cf. R_P and R_C spheres in Fig. 2-12.

The polymers conformation after adsorption on surfaces is not well known, but it is assumed that the backbone is slightly extended[52, 84]. The blobs of spheres in the model mentioned above reduces to hemispheres after adsorption[56, 75].

The (poly)acrylic acid is insoluble in water and thus the polymer precipitate. This precipitation in water can be hindered by two ways. Firstly, due to the dissociation of the polymers carboxy groups ($pH>10$)[206] and secondly, by the grafting of water soluble polymer segments, i.e. side chains of PEG, on the backbone[75]. It should be noted that the screening of the carboxy groups by ions like calcium, which is termed complexation, can cause a precipitation of the (poly)acrylic acid in the absence of grafted side chains even at high pH[99]. In literature, different coordinated complexes of carboxy groups with calcium are known[84, 98, 151]. The calcium complexation is handled in later sections in more detail.

2.2.2 Hydration of Portland cement as dissolution-precipitation process

Since OPC is used, numerous studies were needed to understand the mechanisms govern the cement hydration. Up today there are still debates relating to particular aspects of

hydration. Especially the origin of the induction period is of interest for both academic and product research over decades. Le Chatelier[107] was one of the first researchers who recognized the cement hydration as a dissolution-precipitation-process. This mechanism is the base for hydration of hydraulic binders (e.g. OPC) and non hydraulic binders (e.g. gypsum). Because the products are mostly hydrate phases water acts as both solvent and reaction partner. As a characteristic for dissolution-precipitation mechanisms both educts and products are solid phases. Products are formed *via* precipitation due to the dissolution of educts. Using C_3S hydration as model for cement hydration, the dissolution-precipitation process can be described by equation (24)[71].

$$C_3S + (3 - x + n)\,H \rightleftarrows C_xSH_n - (3 - x)\,CH \quad [\Delta H = -121\ kJ\,mol^{-1}] \tag{24}$$

As demonstrated in section 2.1.1 in general, the driving force for this reaction is caused by the thermodynamic non-equilibrium of C_3S in presence of water. This driving force emerges in two distinctive modalities as expected for a dissolution-precipitation process. First the anhydrous solid educt phase, e.g. C_3S, dissolves in the solvent (SI<0 with respect to C_3S) and second hydrous solid product phases precipitate (SI>0 for hydrate phases). Thereby the precipitation of product phases is dependent on the dissolution of educt phase(s). One product in eq. (24) are C-S-H phases with various compositions as indicated by the variables x and n in eq. (24). Because C-S-H phases contain viewer amounts of calcium than released during the C_3S dissolution, portlandite ($Ca(OH)_2$, CH) as a secondary product phase precipitates. The overall reaction enthalpy is the sum of exothermic C_3S dissolution (-132 kJ mol^{-1}), endothermic C-S-H and exothermic CH precipitation (+25 kJ mol^{-1} and -16 kJ mol^{-1}, respectively)[40]. The value given in eq. (24) is estimated for x=1.7 and n=2.7.[71]

A kinetically limited reaction can be shown for the reaction of cements with water and in particular in the dissolution of clinker compounds, depicted in Fig. 2-10. A thermodynamic measure of the dissolution is the solubility. The time needed and the way to achieve the solubility is governed by kinetics. For the dissolution of clinker components it is necessarily that the surface is accessible to water. Aluminate (C_3A) mostly known as the clinker phase with the highest reactivity dissolves very fast in contact with water. But this can be limited when other phases, particularly alite, encloses aluminate. After alite has dissolved, the surface of the enclosed aluminate is accessible to water and its reaction can proceed further. Because of this kinetic inhibition the aluminate is only partly transformed after a few minutes. From the polished section of an OPC clinker in Fig. 2-10 this situation can be deduced. With respect to the OPC clinker example, the aluminate hydration can be regarded as kinetically limited by the surrounded alite phase. Therefore the aluminate reaction is associated with the alite hydration, and concerning OPC clinker experiments, a mixture of these pure phases shows a completely different reaction pathway. This becomes more important since alite shows a period of low activity during its hydration –the induction (or dormant) period- which secondary affects all enclosed clinker phases. As a consequence alite dictates not only the nature of hydration product due to its role as main

constituent in OPC clinker as mentioned before. Also the kinetics of OPC hydration is dominated by alite. This underlines the importance of alite in hydration process.

The reaction given in eq. (24) is associated with stages different in their rates. Because the reaction is highly exothermic, monitoring of the heat release rate enables to distinguish different reaction stages. Also the composition of the ion concentration in the aqueous phase gives valuable information about the reaction. Fig. 2-13 shows schematically the different stages of hydration.

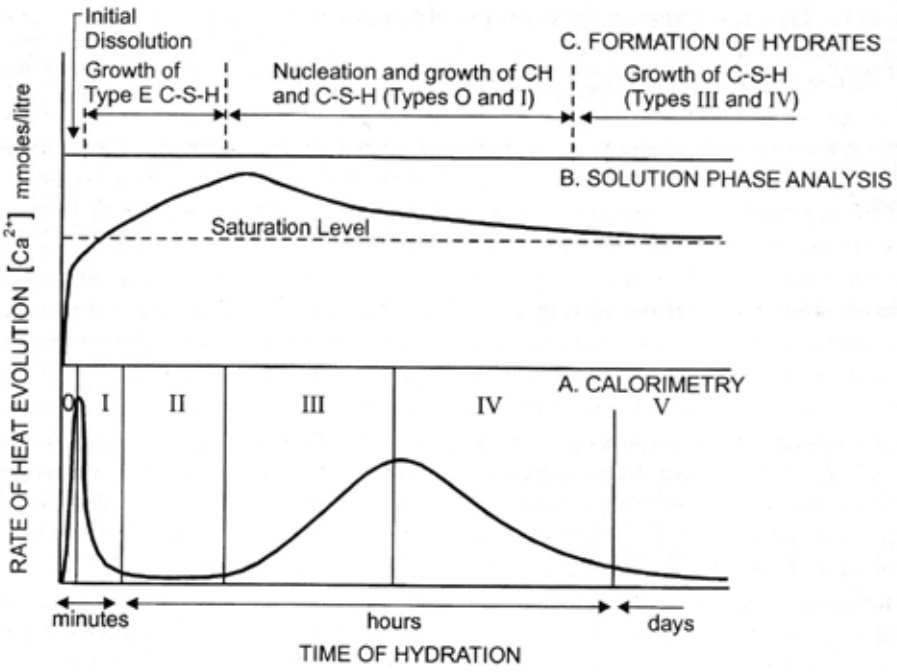

Fig. 2-13: Stages of Ca_3SiO_5 hydration revealed by A) rate of heat release (bottom), B) evolution of Ca^{2+} in the aqueous phase of the paste (middle) and C) associated sequence of hydrate formation.[71]

The reaction commences with an initial dissolution of the anhydrous C_3S (stage 0). Here, the dissolution is congruent, because the stoichiometry of dissolved ions equals the composition of the educt phase. Eq. (25) gives the general expression of congruent dissolution[28].

$$Ca_3SiO_5 + 3H_2O \rightarrow 3Ca^{2+}(aq) + H_2SiO_4^{2-}(aq) + 4OH^- \quad [\Delta H = -138\ kJ\,mol^{-1}] \tag{25}$$

Stage I is the first deceleration period in the hydration progress and is associated with a decline in reaction rate and thus the dissolution reaction in stage 0 is stopped. The period of low reactivity, the induction period, begins with stage I and ends typically after 1-3 hours in stage II. During this period, the material is plastic and workable. The main reaction is observed during stage III (acceleration period) and stage IV (second deceleration period). Within these periods the setting and hardening of the cement and C_3S paste due to growth of hydration products occur. Stage IV and V are associated with a steady decline in reaction rate mainly due to diffusive processes on the surface of the hydrating material.[71]

Whereas superplasticizer increase the duration of the induction period, and thus act as a retarding admixture, it is necessary to know the origin of the induction period. This will lead to ideas on the origin of the retardation induced by superplasticizer. Thus an understanding of stages 0-III is needed, since the fate of later hydration and the properties of the products are governed by the early hydration. The next section outlines the published theories regarding the causes of the induction period.

2.2.3 Portland cement pastes during the period of workability

In this section, the time period of workability of cement pastes is emphasized in order to classify the action of superplasticizers. In the first part (sections 2.2.3.1 and 2.2.3.2), the cement paste is described with respect to the forces between particles and the hydration reaction during the stage of workability. Because this stage coincides with the induction (or dormant) period in cement hydration, theories on the origin of the induction period are stressed in detail. The second part of this section shows the influence of superplasticizer on inter-particle forces and induction period.

2.2.3.1 Inter-particle forces

Portland cement pastes are a mixture of cement clinker and set regulator dispersed in water. The particle diameters measure between 0.1 µm and 100 µm. During hydration, different forces are observed between these particles. The different clinker compounds bear different Nernst potentials on their surfaces because of their atomic composition. Furthermore these clinker compounds feature different reactivity with water. Thus, different electric double layer are formed, which consequently lead to different ζ-potentials for alite, belite, aluminate and ferrite. It should be emphasized that both sign and absolute value of the ζ-potential are strongly related to the ion composition, ion strength (including pH) of the aqueous phase and the particle size of the solid, cf. section 2.1.4. Thus, reasonable values for cement pastes are only obtained in aqueous phase of cement pastes.

Zingg *et al.*[214] investigated C_3S/C-S-H and ettringite in synthetic pore solution with respect to the zeta potential and found values negative and positive in sign, respectively. Thus, cement suspensions tend to agglomerate due to attractive forces between cement clinker compounds. The same conclusion were drawn from Yoshioka *et al.*[208] and Ferrari *et al.*[49]. Furthermore Bellotto and Faini observed in dynamic mode rheology experiments that cement particles form structures of attracting particles, which rebuild if destroyed.[19-20] As a result, cement paste acquires a cohesive force, which for example enables the workability under water without the separation of compounds. The occurrence of cohesive forces indicates that repulsive forces between particles are less pronounced and inter-particle forces are mainly attractive. Consequently, cements reach the zero point charge (zpc) at pH values above pH≈12.4[84]. As stated before, measurements of the zeta potential must increase in absolute value at pH different from the zero point charge (zpc), because the van der Waals forces are compensated by electric double layer forces. The reduction in pH may thus result in strong repulsive behavior and forces a decrease in cohesion and finally the cement paste to decompose.

The classical DLVO theory was extended to highly charged particles in high ion bearing solutions. For this purpose C-S-H particles were investigated. It was found that cohesive

forces in between the particles exert due to ion-ion correlations on different surfaces more strongly than van der Waals forces. Both, C-S-H phases and C_3S exhibit a high surface charge density due to the deprotonation of surface silanol groups, which lead to high demand on counter ions for charge compensation. In systems with high surface charge densities, as C-S-H, this counter balance lead to attractive forces between particles and thus to the cohesion of cement pastes. With the ion-ion correlation the occurrence of attractive forces between similar charged surfaces can be explained.[92-93, 104, 141] In later stages during hydration, both number and size of C-S-H phases increase. As a consequence, the stiffnes of cement pastes increases. Finally, the compressive strength development of cement and C_3S pastes is correlated with the formation of C-S-H phases[127, 181]. According to the findings on the origin of cohesion of cement pastes outlined before, this may be the result of inter-particle forces between growing C-S-H phases.

2.2.3.2 Reactivity – an overview on the causes of the induction period

Numerous studies are aimed to the origin of the induction period in cement hydration. Accordingly, a huge number of proposed models were developed. But until now, none of them is fully accepted and some details are still under debate. In this context, the model of Gartner and Gaidis[69] is the most frequently used.

It is widely accepted that tricalcium silicate is responsible for the induction period in cement hydration. This induces secondary a delayed reaction of other clinker compounds as mentioned in section 2.2.2. Table 2-3 summarizes the basic principles of these different theories including causes of both onset and termination of the induction period. Currently for the origin of the induction period in C_3S hydration, three main theories are mostly discussed and are presented in the following subsections. But before the ion concentrations during C_3S hydration are handled.

2.2.3.2.1 Ion concentrations during C_3S hydration

The aqueous phase of hydrating tricalcium silicate is extensively investigated. Left hand graph of Fig. 2-14 shows Ca-SiO_2 phase diagram obtained in the aqueous phase of C_3S hydrated under suspension conditions[12-13, 40].

C_3S hydration commences with a congruent dissolution which end is associated with a decrease in silicate ion at nearly constant Ca ion concentration (curve PQ in Fig. 2-14 left hand). It was pointed out[13, 15] that contrary to hydration of β-C_2S the drop of silicon is a characteristic of C_3S hydration. Thus, before C_3S solubility is reached the precipitation of a certain type of C-S-H phase occurs. The region of instantaneous C-S-H precipitation is limited by a distinct curve (curve I in Fig. 2-14 (left hand)) which is obtained by variation of the calcium ion concentration in the starting solution. After the first C-S-H precipitation period (drop from curve I) the ion composition follows the kinetic path (or associated path) until in point C portlandite precipitates. Equilibrium conditions are obtained for ion concentrations corresponding those of point F. First attempts are made (cited by Taylor[195]), but Barret and Bertrandie[12-13, 15] and also Damidot and Nonat[40-41] found that the hydration of C_3S is always on the kinetic path independently of the experimental conditions. Jennings[86] and Gartner and Jennings[70] summarized appropriate data obtained in numerous studies, see Fig. 2-14 (right hand). They concluded that in dependence of the experimental

design two distinctive curves can be drawn. Thereby the presence of C_3S causes significant variations in ion compositions, which describes a line above (curve B in Fig. 2-14 (right hand)) the solubility of stable C-S-H(s) phases (curve A in Fig. 2-14 (right hand)). The kinetic path was separated in two distinctive steps leading to different types of C-S-H phases (in Fig. 2-14 SI and SII, respectively). These are formed below and above a calcium ion concentration in the aqueous phase of approx. 20 mmol/l and grow mainly parallel and perpendicular to the C_3S surface, respectively[64-65, 136]. ^{29}Si NMR experiments showed that C-S-H(SI) and C-S-H(SII) differ mainly in the Ca/Si ratio of 1.0-1.5 and >1.7, respectively.[44]

Table 2-3: Hypothesis related to the cause of the induction period and its termination[28, 69, 71, 174]

Onset	Brief description
Protective layer	Formation of a metastable layer around C_3S grains, which slows down dissolution.[18, 69-70, 89, 96, 138, 183]
Boundary layer of superficially hydroxylated C_3S	Superficial protonation of the C_3S surface (C_3S_{sh}) leads to a less soluble educt and thus to a reduced dissolution rate.[15-16]
Dissolution controlled C_3S hydration	The rate of C_3S dissolution is controlled by the ion composition and crystallographic defect density of C_3S. During the induction period increased Ca^{2+} and OH^- concentrations in combination with low defect density cause low dissolution rates.[94, 174]
Electric double layer	Electric double layer on the C_3S surface is formed due to incongruent C_3S dissolution leading to a Si rich surface. The Ca^{2+} ion adsorption on this Si rich surface leads to positive surface charge hindering further dissolution.[28, 71]
Crystallographic defects	Density of lattice effects is related to the length of the induction period.[50-51, 94]
Aluminum induced induction period	Presence of aluminum in the aqueous phase induces the onset of the induction period due to precipitation of C-A-S-H phases.[17, 66]
Termination	**Brief description**
Rupture of protective layer	Osmotic pressure leads to a destruction of the protective layer.[71]
Formation of C-S-H	The formation of stable C-S-H in the expense of metastable C-S-H phases formed during the induction period leads to a loss of protective properties.[86, 183]
Growth of C-S-H	Growth rate of C-S-H phases already precipitated during the induction period increases exponential which causes a rapid C_3S dissolution.[64-65]
Formation of Portlandite	The precipitation of Portlandite determines the rate of the overall reaction, since Si ions are consumed by C-S-H precipitation and thus the poisoning of reactive sites for Portlandite precipitation ends.[192, 209]

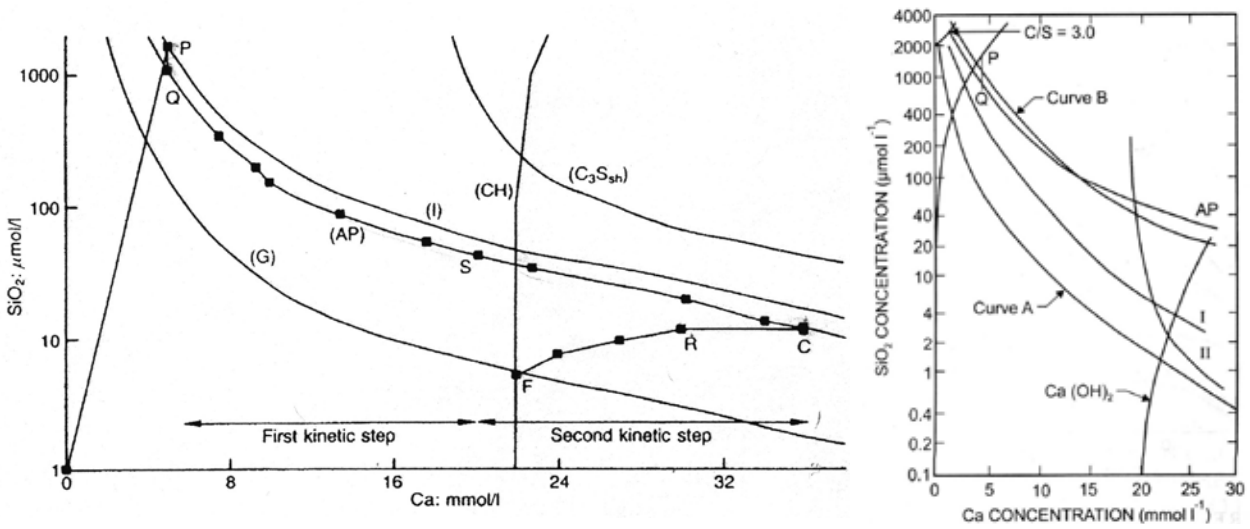

Fig. 2-14: Ca - SiO_2 diagram of the aqueous phase during the tricalcium silicate hydration. Left hand: Kinetic path describing characteristic points in the Ca-SiO_2 diagram for the C_3S hydration[40]. Right hand: general considerations by Gartner and Jennings. Associated path (AP), C-S-H solubility curves (G) of types (SI), (SII), (m), and (s) (I, II, B, and A respectively).[71]

Whereas the positions of the curves in Fig. 2-14 are widely accepted[12, 87], the main debate is related to their interpretation, in particular to the origin of the kinetic path. Common to these theories is that the C_3S solubility is restricted, although calculations[18, 182] demonstrate a high solubility. Barret and Bertrandie[12] postulated the formation of low quantity of C-S-H and subsequent rate balance between superficially hydroxylated C_3S_{sh} dissolution and C-S-H precipitation resulting to ion concentrations in the aqueous phase determined by the kinetic path. On the other hand, Gartner and Jennings[70] correlated curve B (kinetic path) thermodynamically as solubility of metastable C-S-H (C-S-H(m)) precipitated on C_3S surface instead. These interpretations are up today controversially discussed.

2.2.3.2.2 Restricted C_3S solubility due to formation of a protective layer

The oldest theory claims the formation of a first product on the C_3S surface, which is protective against C_3S dissolution. The end of the induction period is associated with the destruction or increased permeability of this phase. This can be the result of ageing or phase transformation. Since the first appearance in 1962[96], the theory is nowadays frequently used. Because of its protective character, this theory is referred hereafter to as protective layer theory.

Whilst the direct observation of the protective layer is still a challenge for instrumental methods, several data were published in order to characterize the reaction on the surface of tricalcium silicate. Techniques (list is not exhaustive) are for example, Nuclear Magnetic Resonance spectroscopy (NMR)[44, 158, 160, 163], Electron Microscopy (TEM, SEM)[31, 121, 160, 178], Nuclear Resonance Reaction Analysis (NRRA)[173], Quasi-Elastic Neutron Scattering (QUENS)[59], Secondary Neutron Mass Spectroscopy (SNMS)[35, 138], and X-Ray Photoelectron Spectroscopy (XPS)[159]. It is postulated that the protective layer reaches thicknesses of a few nanometres[69-71, 87-88, 198]. Furthermore it is reported that the surface contains hydrated monomeric silicon tetrahedra, which is significantly distinct from later stable C-S-H phases (C-S-H phases contain polymeric silicate chains).[18, 163] But a direct evidence by means of

EM or AFM is still inexistent. Latter and the missing explanation how such a surface phase is transformed into the stable C-S-H phases are weak points of the protective layer theory.

2.2.3.2.3 Theories postulating low inherent solubility of C_3S

A Formation of low soluble superficially hydroxylated C_3S

The second theory explicitly excludes the formation of a protective layer on the C_3S surface. Barret and Menetrier postulated that after congruent dissolution the surface of C_3S becomes protonated (cf. section 2.1.2.1.2, p.31) which they proposed as 'superficially hydroxylated layer' (C_3S_{sh}).[16] This was also stated by Trettin[197]. Therefore C_3S_{sh} exhibits lower solubility than C_3S but higher than C-S-H. The low difference in the solubility leads to a low driving force and thus to low reaction rate. Later Damidot *et al.*[40-41] and Garrault and Nonat[64-65, 137] extended this model and they assumed in accordance to Barret and Bertrandie[12-13] that the associated (kinetic) path is the result of the rate balance between dissolution of C_3S_{sh} and precipitation of stable C-S-H(s), see curve AP in Fig. 2-14. It was shown that both the number of C-S-H nuclei and their growth govern the overall hydration process of C_3S[64-65]. The degree of hydration increases with the number of nuclei precipitated on the C_3S surface, cf. Fig. 2-15 (left hand). Furthermore it is emphasized that growth mode and growth rate depends on the calcium ion concentration in solution. Accordingly, C-S-H growth is separated into parallel and perpendicular to the C_3S surface occurring at low and high calcium ion concentrations, respectively. Thereby in saturated lime solution, the parallel growth rate approaching the perpendicular growth rate with $4 \cdot 10^{-11}$ m/s and $1.8 \cdot 10^{-11}$ m/s, respectively.[64-65] With decreasing $Ca(OH)_2$ concentrations, the parallel growth rate increasingly surpasses the perpendicular growth rate, see Fig. 2-15 (right hand).

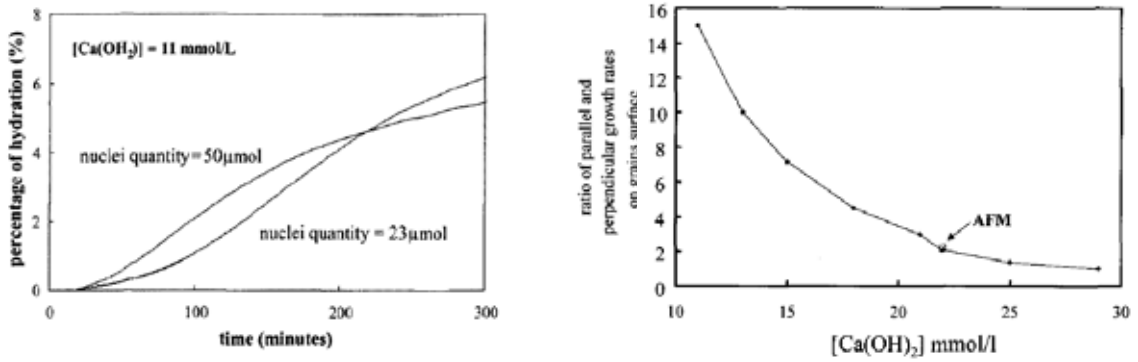

Fig. 2-15: Left hand: Influence of the initial quantity of C-S-H nuclei on the percentage of hydration against time in 11 mmol/l $Ca(OH)_2$ solution at l/s ratio of 50.[64] Right hand: Dependency of the ratio between parallel and perpendicular growth mode of C-S-H on the $Ca(OH)_2$ concentration in the solution. The model was compared to AFM measurement.[64]

Once the C-S-H nuclei are formed, the nucleation and growth theory predicts their growth fairly well. However, it was discussed if a rate balance between dissolution and precipitation can exist during the hydration of C_3S. In this context it is unclear why the amount of the initially precipitating C-S-H is limited although C_3S exhibits a high solubility[18, 182]. Therefore, the theory of limited solubility of C_3S was originally based on the concept of superficially hydroxylated C_3S_{sh}. Later[174] on the concept of the slow dissolution step hypothesis, see next subsection.

Slow dissolution step hypothesis

Alternatively to the formation of a protective layer and the concept of superficially hydroxylated C_3S, the dissolution theory of low-solubility minerals (cf. section 2.1.2) was adapted to C_3S hydration in order to explain the origin of the low C_3S solubility and thus the onset of the induction period. It is based on the observation that the C_3S dissolution rate is strongly dependent on the Gibbs free energy of the system (ion concentration of the solution).[37-39, 63-64, 133-134] Furthermore, as it is shown in Fig. 2-2 (p.30), the dissolution of low-solubility minerals like albite, proceeds on different mechanisms in dependence of the degree of undersaturation. High degrees of undersaturation induce dissolution on etch pits, which is the fastest mechanism. It is proposed that the alite dissolution rate increases with increasing defect density on its surface. This is supported by the works of Fierens and Verhaegen[51] and Odler and Schüppstuhl[139], who observed a dependency of the length of the induction period on cooling regime during the C_3S synthesis. Also an annealing of alite, which may cause a reduction of the defect density and leading to increased lengths of the induction period, is in line with this theory.[94] The influence of the degree of undersaturation on etch pit formation was investigated by means of SEM. Experiments at high degree of undersaturation (e.g. in water) markedly induces etch pit formation on alite surfaces, cf. Fig. 2-16a. Lower degrees of undersaturation in contrast, as it is observed in experiments with saturated lime solutions, show smooth surfaces with no etch pits, see Fig. 2-16b.

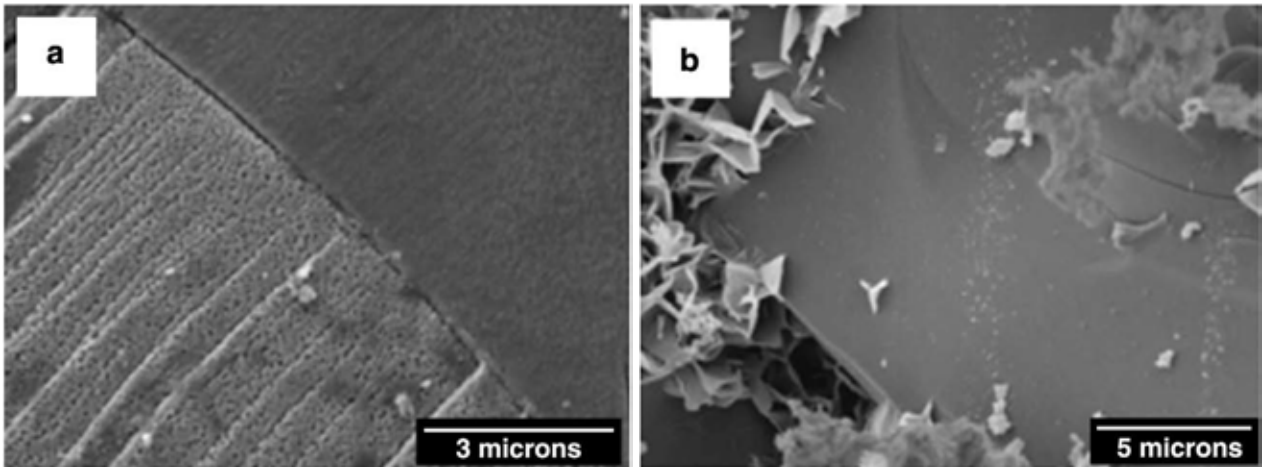

Fig. 2-16: Alite surface after 2 minutes dissolution in a) water and b) saturated lime solution.[94] High degree of undersaturation (left hand) causes formation of etch pits whereas smooth surfaces are observed at low degree undersaturation (right hand).

The accumulation of dissolved ions, above all calcium and hydroxide, into the solution causes a fast decrease in undersaturation. According to Juilland *et al.* the driving force is quickly insufficient for etch pit opening and the dissolution proceeds by means of slow step retreat mechanism.[94] This is believed to cause the induction period[134] and is illustrated in Fig. 2-17.

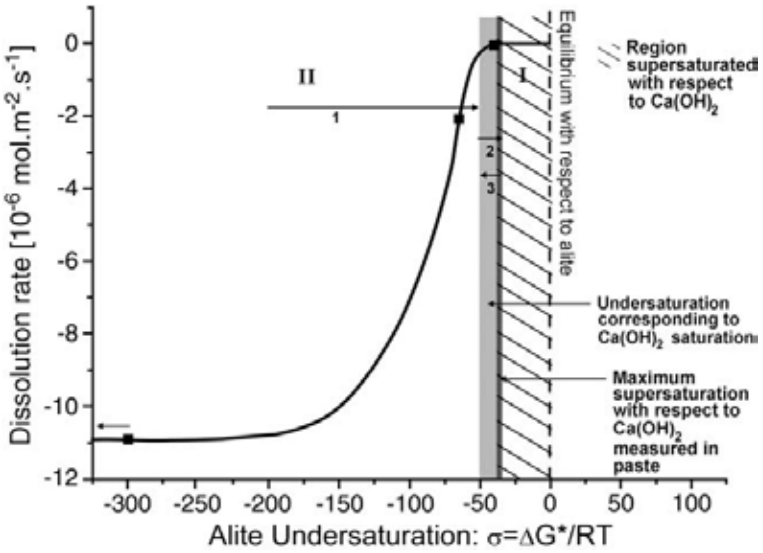

Fig. 2-17: Proposed mechanism of dissolution controlled alite hydration with dependency on the saturation state of the system. With decreasing degree of undersaturation (high $Ca(OH)_2$ concentration) etch pit opening vanishes (zone II) and causes low dissolution rates occurring *via* step retreat (zone I). High $Ca(OH)_2$ concentrations are observed during the induction period of alite pastes.[94]

Although the dissolution driven induction period omits the formation of a severely identifiable protective layer, several points were discussed. Gartner[68] questioned the application of this theory from low-solubility minerals to moderately soluble substances like alite in the context of high degrees of undersaturation. Furthermore he pointed out that after the period of pure dissolution the ion composition remains on the curve of C-S-H-(m) (kinetic path[12-13, 40]), see Fig. 2-14. Thus the onset of the acceleration period subsequent to the induction period seems not to be compatible to the dissolution theory. Makar *et al.*[115] also discussed the model and stated coincide with Gartner[68] that rather a barrier layer is formed than the pure dissolution mechanism is responsible for the onset of the induction period. This conclusions were drawn from extensive SEM study showing etch pits mainly at the end of the induction period in presence or absence of an accelerator.

B Aluminum induced dormant period

Recently, Begarin *et al.*[17] underlined the impact of aluminum on the hydration kinetics of C_3S. It was demonstrated during experiments on diluted and continuously stirred C_3S suspensions starting in water at l/s ratio of 250 that the conductivity plateau was prolonged due to presence of aluminum. Furthermore it could be shown that calcium and silicon concentrations are lowered when aluminum was present because of precipitation of C-A-S-H phases. These phases are shown to prolong the induction period in more extent than C-S-H phases does. Therefore it is concluded that aluminum induces formation of C-A-S-H phases which are unable to serve as nuclei for C-S-H phases. But on the other hand it is reported that aluminum doped C_3S shows increased reactivity with respect to the pure C_3S[184]. It should be further emphasized that the experiments by Begarin et al.[17] were performed at l/s ratio of 250 in water as starting solution. Thus, it is questionable that the first electrical conductivity plateau during suspension hydration corresponds to the induction period under paste conditions.

2.2.3.3 Causes of the re-acceleration of hydration

According to the definition mostly related to the rate of heat release during paste hydration of C_3S, the induction period ends at the transition to stage III in Fig. 2-13. Thus the rapid C_3S dissolution and C-S-H precipitation marks the onset of the main hydration period. As shown in Table 2-3 different theories were developed in order to explain the termination of the induction period.

The first theory is based on the observation of relatively high degree of supersaturation with respect to portlandite, before its precipitation occurs. It was assumed that the presence of silicon in the solution permits the crystallization of CH ('silica poisoning'). In other studies it was observed that in dependence of the l/s ratio, portlandite precipitation may be shifted to different stages of the hydration.[40-41] Thus, the precipitation of portlandite as sole onset of the acceleration period is excluded, since also addition of portlandite may act retarding.[69]

Further theories are related to the formation or not of a protective layer on the C_3S surface. It was postulated that if a protective layer exist, osmotic pressures can cause a rupture of the layer to reinitiate the C_3S dissolution.[71] But more recently it is postulated that the growth of C-S-H(s) governs the onset of the acceleration period.[64, 69-71] This is supported by the fact that the addition of calcium carbonate, silicon dioxide (SiO_2) or even synthetic C-S-H phases accelerate the hydration, mainly due to the precipitation of stable C-S-H on surfaces different from C_3S.[69] Thus, also the amount of C-S-H(s) precipitated during stage 0-II has a strong influence on the onset of the acceleration period independent on the existence or not of a protective surface layer.

2.2.3.4 Impact of superplasticizers on Portland cement pastes

Since the development of plasticizers and superplasticizers numerous studies were performed in order to characterize different aspects of the interaction of these admixtures with cement and cement components. Because of the intension to use these admixtures, the focus was laid mainly on the liquefying action and on the compatibility to different cements. Furthermore, different kinds of molecular architectures were investigated in order to find optimal parameters for a broad superplasticizer application. Contrary, little attention was paid on the origin of the retardation which is observed in combination with the use of superplasticizer. This section gives an overview on the influences of superplasticizer on the hydration of Portland cement with special attention to the retardation.

The liquefying action of superplasticizer in cement suspension is based on the adsorption of the polymer functional groups on the solid surfaces and the establishment or increasing of repulsive forces between cement particles. Moreover, the repulsive force can be enhanced by grafting deformable non reactive side chains on the backbone to exert steric forces. Accordingly to basic concepts of inter-particle forces in section 2.1.4, it was found that the interaction of superplasticizer with cements is dependent on:

- Composition of the cement clinker
- Composition of the aqueous phase of the cement paste (e.g. concentration of SO_4^{2-})
- Molecular architecture of the polymer (size, functional groups on the backbone, acid/copolymer ratio (side chain density) and side chain length)

These basic properties influences main aspects of the interaction of superplasticizer with cement, namely adsorption, impact on inter-particle forces, and retardation of cement hydration, which are presented in the next subsections.

2.2.3.4.1 Adsorption

Firstly, the surface characteristics of the cement clinker compounds determine the adsorption of superplasticizer. It is assumed that hydrating cement clinker possesses mainly negative charges on the Nernst layer. Accordingly, the polymer can only adsorb with its negative charge (e.g. COO^- groups) on the Stern layer or within the slipping plane of cement particles which are positively charged (mainly due to Ca^{2+}-counterions). Furthermore several studies showed that superplasticizer interact strongly with the clinker mineral C_3A[208, 213] or more precisely with its hydration products. There is a direct correlation between C_3A content and superplasticizer dosage to achieve equal workability, e.g. slump flow. Zingg *et al.*[214] postulated that superplasticizer may adsorb directly on the Nernst layer of ettringite instead of the Stern layer[3, 125]. Also the intercalation, i.e. a***b***sorption, of superplasticizer resulting in the formation of organo mineral phases is discussed[52, 54, 75, 148]. Both theories are able to explain the lower dosage needed to reach same workability at delayed addition of superplasticizer to the mixture. By contrast, the interaction of superplasticizer with the clinker minerals C_3S and C_2S is contentious, which is mainly attributed to both the divergences in reported zeta potentials, which are between -5 mV and +10 mV[208, 214] and the huge impact on C_3A hydration.

Secondly. the composition of the aqueous phase influences the adsorption *via* ion strength and type of contained ions. Because of the high reactivity of C_3A at the beginning of hydration, superplasticizers adsorb preferentially on this clinker mineral as mentioned before. Contemporary, sulphate ions show a strong interaction with C_3A and the hydration product ettringite. Therefore superplasticizer and SO_4^{2-} compete to adsorb on C_3A and hydration products thereof[3, 52, 54, 91, 125, 168, 203]. If ettringite is solely investigated, this interaction is independent on the calcium ion concentration and pH of the aqueous phase, since the zeta potential of ettringite is mainly dependent on the concentration of SO_4^{2-} [119]. Because of difficulties arising due to the reactivity with water and thus possible chemical reactions may dominate inter-particle forces, e.g. bridging mineral forces as described in 2.1.4.5, the interaction of superplasticizers were studied on model systems. Therefore calcite, quartz, muscovite, silicon nitride, and MgO were used[49]. The latter is chosen because of its similar zero point charge (zpc) close to the surface properties on cement[84]. Again, the adsorption of Ca^{2+} on the MgO surface in high alkaline environment leads to an increase of the zeta potential to more positive values. On the other hand, the addition of sulphate ions reduces the zeta potential. These experiments reveal that superplasticizer adsorption is favoured in presence of Ca^{2+} and hindered when ions of SO_4^{2-} are present.

Besides the effect of SO_4^{2-} and Ca^{2+}, the inter particle forces are altered due to ion strength of the aqueous phase[142]. Houst and coworkers[83] calculated the Debye length ($1/\kappa$) of the double layer (cf. section 2.1.4.2), which decreases with increasing ion strength. This is in accordance to the findings of Yamada *et al.*, where increasing ionic strength decreases the dispersion force of superplasticizer.[203]

Besides the composition of the solid and the surrounding aqueous phase, thirdly the polymer's molecular architecture has a further impact on the adsorption process. It is known that the adsorption decreases when side chains are grafted on the polymer backbone. Therefore naphthalene sulfonate based superplasticizer reach a higher degree of adsorption than grafted superplasticizer on carboxylate ether base. Accordingly, the length and the number of side chains on the backbone (side chain density) alter the adsorption. Shorter side chains and low side chain density increase the ability of adsorption. Furthermore, the dimension and thus the molecular weight and type of functional group of the polymer affect adsorption.[3, 52, 91, 125, 149, 153, 202, 204, 213]

The adsorption phenomenon is investigated by Plank *et al.* with a thermodynamic approach, i.e. with respect to the Gibbs free energy of adsorption[152]. The steps electrostatic attraction and the release of ions on the mineral surfaces during the adsorption process are related to as enthalpic (H) and entropic (S) contribution to the Gibbs-Helmholtz equation ($\Delta G = \Delta H - T \cdot \Delta S$). It was shown that these thermodynamic parameters are strongly dependent on the ion composition of the aqueous phase, on the polymer characteristics (molecular weight, type of anchor groups), and on the adsorption degree. As the concentration of Ca^{2+} in the aqueous phase increases, the heat of adsorption (ΔH) decreases. This is the result of Ca complexation by the polymer. Consequently, the degree of adsorption and thus electrostatic attraction forces are reduced, but in this case the entropy is increased. Increasing anionic charge density of the polymer favours adsorption due to increase of the enthalpic contribution to the Gibbs free energy. In presence of polymers with longer side chains and thus decreasing anionic charge density, the adsorption is mainly driven by entropic phenomenon. With increasing degrees of adsorption the overall process becomes more and more endothermic. Further polymer adsorption approaches a plateau. In summery it was stated that adsorption processes are mainly associated with a gain in entropy.

2.2.3.4.2 Impact on inter-particle forces

The adsorption of superplasticizers on the Stern layer of cement compounds or their hydrate phases influences inevitable the forces between particles. This phenomenon is described as reducing in zeta potential and increase of the repulsion between particles.[130] As a consequence, the particles are dispersed in the suspension and agglomerates of cement particles are destroyed.

The greatest influence on the inter-particle force is attributed to the clinker mineral C_3A and its hydrate product phases. It is observed that in the presence of superplasticizers at early hydration time, ettringite crystals are dispersed in the cement matrix instead of fixed on surfaces as in the case of the absence of superplasticizer.[212] This phenomenon was also

observed for portlandite at later hydration periods.[165] Conversely, the impact on C-S-H inter-particle forces is not well investigated.

Polymer may impact solely the electric double layer force or furthermore in a combined way electrosteric forces, cf. section 2.1.4.3. It was found that naphthalene sulfonate based superplasticizers are assigned to the first group, whereas grafting of side chains lead to the second mechanism.[199, 207] Thereby, the magnitude of the repulsive force depends on the adsorption capability and the nature and length of the side chains[99]. Latter is discussed controversially. Winnefeld *et al.*[202] found in cement pastes that the side chain length is of minor importance for the rheological properties (yield stress, plastic viscosity) and the main influence stems from the acid/ copolymer ratio (side chain density). Both yield stress and plastic viscosity decreases with decreasing acid/ copolymer ratio and therefore also the mortar spread diameter is enhanced. This was also observed by Zingg *et al.*[213]. Contrary, Yamada *et al.*[204] reported that the fluidity increases with increasing acid/ copolymer ratio and smaller backbone length, which is supported by Ran *et al.*[157]. Also it is observed than the type of anchor group determines the performance as plasticizer. Therefore and with respect to carboxy groups, sulfonic groups permit an improved flowability[204].

In summary it can be concluded that the impact of superplasticizer on the inter-particle forces mainly depends on their adsorption ability. The repulsive forces can be increased by side chains grafted on the polymer backbone. However, this can cause a lower adsorption degree. Thus at certain side chain length and density on the backbone an optimal superplasticzer performance may exist.

2.2.3.4.3 Impact on the reactivity of cement

Superplasticizer based on naphthalene sulfonate and polycarboxylate induces a change in hydration kinetics of cement and cement compounds. More precisely, the setting times are retarded in presence of superplasticizer. It was demonstrated that the setting retardation is caused by the prolonged duration of the induction period. Because the clinker mineral alite is responsible for the occurance of the induction period, the prolonging of this period can be considered as an interaction of this cement compound with superplasticizer. Thus, in the following the influences of superplasticizer on the hydration of tricalcium silicate are mainly given.

Compared to the numerous studies of the interactions of superplasticizer and cement, only little attention was laid on the pure C_3S superplasticizer interaction. Cement paste experiments reveal that up to 3 days the degree of hydration is significantly lowered in presence of superplasticizer. Thus it was concluded that the dissolution of C_3S is hindered[108]. By contrast, Kirby and Lewis[99] found that superplasticizer enhance the dissolution of C_3S, which is attributed to Ca complexation (see section 2.2.1.2) by not adsorbed superplasticizer, which is also supported by Jansen *et al.*[85]. In fact, carboxy groups are able to complex Ca ions from solution[151]. A decrease in Ca concentration is linked to a decrease in degree of supersaturation (cf. section 2.1.3) with respect to C-S-H phases. Thus, according to section 2.1.3 the precipitation of C-S-H phases takes place at a lower rate. However, Lothenbach *et al.*[108] concluded from their experiments on Portland cement pastes, where no significant increased calcium ion concentrations were measured,

that the complexation of calcium ions is not responsible for the retardation of hydration. Also hints are given that superplasticizer can modify the crystal growth mechanism of C-S-H phases[91]. Furthermore, superplasticizer may stabilize the bilayer of counterions[125-126] or may form a semi permeable membrane around cement grains[123, 213]. Thus, the dissolution and consequently the release of ions into solution are hindered. Ridi *et al.* reported an increased activation energy for the nucleation and growth stage of C_3S hydration (acceleration period) in presence of superplasticizer. Also the morphology of the C-S-H phases is affected.[161] Nicoleau[133] and Pourchet *et al.*[155] investigated the dissolution rate of C_3S in solutions containing various concentrations of $Ca(OH)_2$. It was found that the dissolution rate was decreased with increasing concentration of calcium hydroxide concentration. Thus it was concluded by latter and other researchers[108, 202, 213] that superplasticizers retard the C_3S hydration by means of a hindered C_3S dissolution. This was supported by the observation of faster C-S-H precipitation than C_3S dissolution during the induction period[133, 155]. At the end of the induction period, the superplasticizer containing sample showed an increased silicon concentration in the aqueous phase, which is in contrast to the reference sample without superplasticizer. Although this phenomenon is not well understood, the observation may be a hint on the promoted dissolution rate in presence of superplasticizer during the acceleration period.

Yamada *et al.*[204], Nicoleau[133], and Pourchet *et al.*[155] found that the retardation is related to the concentration of functional groups of the polymer. Winnefeld *et al.*[202] performed a study with a systematic variation of the molecular architecture of superplasticizer. They are in accordance with the finding of other authors[204, 213] that increasing acid/copolymer ratio and shorter side chains prolong the duration of the induction period in Portland cement.

In brief, a clear picture on the causes of the prolonged induction period in presence of superplasticizer is not available. Main discussed reasons are a) hindered C_3S dissolution, b) complexation of Ca ions due to the polymers functional groups, and c) a changed crystal nucleation and growth period. Finding of the causes of retardation of cement hydration is even more difficult, since the causes of the onset of the induction period is still under debate. Superplasticizer should impact on this stage of cement hydration, which also reflects the dispersability.

2.2.4 Aims of the study

The examination of the literature reveals that several points in the superplasticizer cement interaction are well studied. But a lack in understanding the influences of superplasticizer on the early hydration of cements is obvious. More precisely, the origin of the superplasticizer induced retardation of the cement hydration, which features a prolonged induction period, is still under debate. This fact is furthermore complicated, since several theories on the origin of the induction period in cement hydration, or even C_3S hydration, diverge.

The present work is dedicated to improve the understanding of the interaction between superplasticizers and cements with respect to the hydration kinetics. Therefore, it is investigated in **three different parts a)** what the principal modes of action of superplasticizers are, how these mechanisms influence **b)** separate reactions and finally **c)**

the in parallel occurring reactions during C_3S hydration. Assuming that tricalcium silicate is mainly responsible for strength development and hydration kinetics of Portland cement, the main part of the study is aimed to investigate the causes of the retardation of the C_3S hydration induced by superplasticizers. Thereby, the impact of the polymer architecture of superplasticizers on the magnitude of retardation on cement and C_3S hydration is fathomed. By means of electrical conductivity on both C_3S pastes and suspensions and the composition of the aqueous phase the retarding effect is handled in more detail. Finally, the interactions between superplasticizers and C_3S are summarized in a model.

3 MATERIALS AND METHODS

3.1 Materials

This section gives an overview on the used materials and methods. The performance of the experiments with their specific parameters regarding materials and methods are described in detail in the corresponding parts. As a general aspect the temperature was adjusted to 23°C with a variation of ±2K if not otherwise stated.

3.1.1 Superplasticizers

Throughout the experimental work the influence of superplasticizers on hydration is investigated. Therefore, superplasticizers with different molecular architectures were synthesized by radical polymerization (Bozzetto S.P.A., Italy). The copolymers (side chains) are poly(ethylene glycol) units (PEG) with molecular weights of 1000 and 5000 g/mol which corresponds to a repeating of 23 and 114 PEG units, respectively. Also one naphthalene sulfonate based superplasticizer was tested. Table 3-1 shows the molecular properties of the used superplasticizers. Thereby the values for the acid/ copolymer ratio (determined by mass of constituents) and the number of monomers (backbone, side chain) are given for the situation before the synthesis. Molecular weigth was determined by Gel Permeation Chromatography (GPC) in the same apparatus (and calibration) for all superplasticizers. In order to obtain pH neutral solutions the polymers are titrated with NaOH to pH=7.0. Therefore the addition of SPs is associated with introducing Na^+ ions into the system, which is reflected by the right row of Table 3-1. In experiments these superplasticizers are dosed in different concentrations whereas the given numbers refer to the dry mass of superplasticizers with respect to C_3S and is given in mass percent (m.-%).

Table 3-1: Properties of the used superplasticizer solutions.

SP	Backbone	Copolymer (ester grafting)	Molar Acid/ Copolym.	Molecular weight macro-molecule [g/mol]	Polydis-persity index	Na^+ content per g SP [mmol/l]	Polymer content [m.-%]
PCE1	Methacrylic acid	MPEG 1000	2.9	10,930	5.3	21.7±0.6	40.2
PCE2	Methacrylic acid	MPEG 5000	7.2	20,800	2.7	14.4±0.5	40.0
PNFS	Naphthalene sulfonate	-	-	17,900	12	45.8±1.3	41.8

As represented in Fig. 3-1 (left hand) and according to Gay and Raphaël[72] individual macromolecules of comb copolymers can be described by three structural parameters, namely n (repeating units), N (monomers in the backbone) and P (monomers in side chains). These structural parameters are given in Table 3-2.

Table 3-2: Structural parameters of the used PCEs.

SP	N	n	P
PCE1	3.9	8.2	23
PCE2	11.8	2.7	114

The structure of the PCEs used in the present work is classified in the phase diagram for comb homopolymer according to Gay and Raphaël[72], see right hand scheme of Fig. 3-1 (for abbreviations see Fig. 2-12 (p.48)). Therefore PCE1 is associated with a flexible backbone worm (FBW) conformation, whereas PCE2 is located at the border between FBW and FBS and will be regarded as a flexible backbone star (FBS).

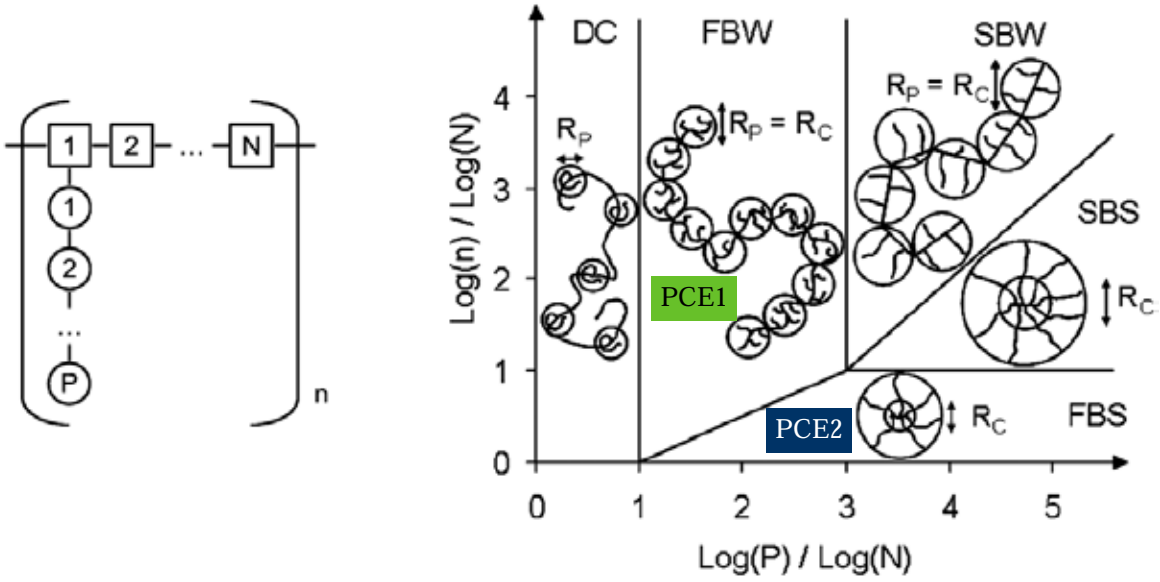

Fig. 3-1: Schematic drawing of comb copolymers (left hand) and PCE conformations (right hand) according to the phase diagram for comb homopolymers after Gay and Raphaël (taken from Marchon et al.[117]).

3.1.2 Tricalcium silicate (C_3S)

During the experiments different synthetic charges of triclinic C_3S were used. These charges were synthesized by burning at least three times a mixture of calcium carbonate ($CaCO_3$, Merck, p.a.) and amorphous silica (SiO_2, Merck, p.a.) at 1823 K (1550 °C) (free lime content of C_3S: <0.2 m.-%). C_3S was ground to a specific surface area ranging between 4960 and 8467 cm^2/g (BET) and an average particle diameter of approx. 9 µm (LS Coulter 230). The chemical analysis can be found in the appendix (Table A-1).

3.1.3 Calcite

Calcite as precipitated calcium carbonate (Precarb 100, Schaefer) was used. This calcite had a BET specific surface area of 8.92 m^2/g and an average particle diameter of 1.8 µm.

3.1.4 Calcium hydroxide

Calcium hydroxide ($Ca(OH)_2$) was used from Merck (Germany) to prepare solutions for various experiments. The calcium hydroxide was dissolved in expense of solubility in CO_2 free water under N_2 atmosphere (glove box). After 30 min the suspensions was filtered through 0.45 µm filter.

3.2 Methods

3.2.1 Charge titration of superplasticizers

Charge titration experiments were performed in an automatic titrator (Mütek PCD 03, Germany) according to the protocol given by Plank and Sachsenhauser[151]. Electrical current caused by counter-ions, which are removed by vertical oscillation of a plunger from the superplasticizer sample, was measured. Titration of a cationic polymer (diallyl dimethylammonium chloride (polydadmac), c=0.001 mol/l) to a superplasticizer solution was performed until the zero point charge was reached. The amount of added polydadmac refers to the number of anionic charges of the macromolecule.

3.2.2 Isothermal conduction calorimetry

Heat release during the hydration was measured with isothermal calorimeter operating at 25°C. Therefore the ToniCal Trio device from Tonitechnik (Germany) was used. The device measures the differences of the electrical current induced by temperature development of a sample to an inert material (cement stone) possessing similar heat capacity (differential calorimetric analysis, DCA).

From the total heat released during the C_3S hydration the degree of hydration is determined. For this purpose, the complete C_3S hydration, which corresponds to a degree of hydration of 1, is associated with a heat release[71] of 121 kJ/mol, cf. eq. (24).

3.2.3 Simultaneous TG/DSC (STD)

For DSC/TG measurements STD Q600 (TA Instruments) was used at heating rate of 10 K/min in platinum crucible under constant flow of N_2 in the chamber. The amount of portlandite was determined by measuring the mass loss in the range of approx. 400-460°C.

3.2.4 Scanning Electron Microscopy (SEM)

Experiments by Scanning Electron Microscopy (SEM) were carried out with an Environmental SEM (ESEM, XL 30, FEI) equipped with a field emission gun (FEG). Images were recorded from secondary electrons (SE) at approx. 10 mbar / 80 % humidity at the sample surface at various acceleration voltages. Additional tests were performed by using a Nova NanoSEM 230 (FEI) equipped with a FEG. Detection of SE at very low acceleration voltages was permitted by the use of a through lense detector.

3.2.5 Ion concentration of aqueous solutions

3.2.5.1 Electrical conductivity

Dissolved ions in aqueous solution are moveable under an electric current, which measure is proportional to the ion valence, concentration and mobility (activity). Thus, measurement of electric conductivity gives information of the ion composition in aqueous solution. In this work InLab 731 (Mettler-Toledo) electrode in combination with measuring units were used.

3.2.5.2 Spectroscopic determination of ion concentrations

Ion concentrations were measured by Ion Coupled Plasma – Optical Emission Spectroscopy ICP-OES (Horiba ActivaM, Jobin Yvon). Thereby the aqueous solution is applied to Argon

plasma. Elements in the aqueous sample are then induced to emit characteristic radiation in the UV/VIS spectra. Both the intensity and the wavelength of this radiation are proportional to the concentration and type of element in the sample, respectively. A calibration of the spectrometer before the measurements with known concentrations permits the calculation of specific ion concentrations from intensities (software ACTIVAnalyst 5.4.2). Wavelengths were 317.933 nm (Ca<750 mg/l), 373.690 nm (Ca>750 mg/l), 251.611 nm (Si), 589.592 nm (Na) and 181.972 nm (S).

3.2.5.3 Potentiometric determination of ion concentrations

Potentiometry as an electrochemical method relates electrical currents between two electrodes (metal-liquid interfaces), which are an ion selective electrode (ISE) and a reference electrode (RE), to ion concentrations in aqueous solution. By means of a milli-volt meter the difference in electric current between these electrodes is recorded. Thereby the reference electrode provides a stable electrical current whereas the current of the ISE depends on the ion concentration of the ions which concentration/activity is aimed to be determined. Both electrodes are in contact to the measuring solution in order to complete the electrical circuit.

RE contains a silver wire coated with silver chloride immersed in potassium chloride solution saturated with respect to silver chloride. The ISE is composed of a selective membrane which is sensitive with respect to measuring ions. Materials for the membrane are made of glass (pH electrode), solids and PVC containing a carrier for specific ions (e.g. calcium selective electrode). This membrane separates the measuring solution from the inner standard solution. The inner solution is equipped as the reference electrode and the charge transfer is compensated by the electrode.

Based on the Nernst equation, cf. eq. (26), the differences of the electrical currents are directly related to the ion activity (concentration).

$$E = E^0 + \frac{R \cdot T}{z \cdot F} \ln(a_i) \tag{26}$$

With E^0 as standard electric potential of the reference electrode, R as universal gas constant, T is absolute temperature, z is the valence of the ion or number of electrons transferred, F the Faraday constant and a_i the activity of the ions which are measured. Thus, increasing the ion activity by a factor of 10 causes an increase in measured electrode potential of $\ln 10 \cdot \frac{8.314\ \mathrm{J/(K \cdot mol)} \cdot 298\ \mathrm{K}}{z \cdot 96485\ \mathrm{C/mol}} = \frac{59.16\ \mathrm{mV}}{z}$ at 25 °C room temperature. This value is referred to as electrode slope. Practically, the electrode slopes are determined *via* calibration before the measurements. It should be emphasized that also ions different from the analyte may cause an electrical current (interferences).[9]

3.2.5.4 pH

PH was measured by a glass electrode (A7780, Schott Instruments). Calibration was performed at 25 °C room temperature using two commercial standards (pH=7, pH=10) and one self made standard using saturated $Ca(OH)_2$ solution (pH=12.45).

3.2.5.5 Total organic carbon (TOC)

TOC content in solution was determined by combustion and subsequent CO_2 detection by IR spectroscopy (liquiTOC, Elementar, Germany). Thererfore, the liquid sample was treated with H_3PO_4 in order to remove CO_2 included in inorganic compounds (e.g. $CaCO_3$). Then the remaining organic carbon was oxidized to CO_2 which emerges from the solution and is detected by means of IR spectroscopy. The accuracy of the adsorption values was ±4.9 % determined on 3 identical samples.

3.2.5.6 Ion activity

Ion activities were calculated from ion concentrations by software PREEQC Interactive (version 2.15.0.2697) with phreeqc and pitzer database.

3.2.6 Analytical Ultracentrifugation (AUC)

Analytical Ultracentrifugation (AUC) permits the observation of particle sedimentation during the centrifugal experiment by measuring optical properties of the liquid. The method was developed by Svedberg (Nobel prize in chemistry 1926) and acquires the determination of different properties, e.g. particle size and molecular weight of particles suspended in a solvent. A detailed description can be found elsewhere[190-191].

The sedimentation coefficient s is defined as proportional factor between sedimentation velocity and centrifugal field strength, cf. eq. (27). After the inventor of the ultracentrifuge the unit of s is named Svedberg (S), with 1 $S=10^{-13}$s.

$$s \equiv \frac{u}{\omega^2 r} = \frac{V_P \cdot (\rho_P - \rho_S)}{f} \tag{27}$$

with

u	...	Sedimentation velocity
ω^2, r	...	Angular velocity, radial position of the particle
ρ_i, V_i	...	Density, volume of particle and solvent (indices p and s, respectively)
f	...	Frictional coefficient

A direct measure of an analytical centrifuge experiment is the sedimentation velocity (u) of particles. Thus the sedimentation coefficient (s) can be calculated, cf. eq. (28). Utilizing both the Stokes equation and the Stokes-Einstein equation with viscosity of the solvent μ_S the calculation of particle diameter d_P is permitted. [154, 190-191]

$$d_P = \sqrt{\frac{18 \cdot \eta_S \cdot s}{\rho_P - \rho_S}} \tag{28}$$

4 RESULTS AND DISCUSSION

4.1 Calcium complexation and cluster formation as principal modes of action of superplasticizers

4.1.1 Aim

The present chapter is aimed to elucidate general interactions between structural units of macromolecules used as superplasticizers with ions and particles as sketched in Fig. 4-1.

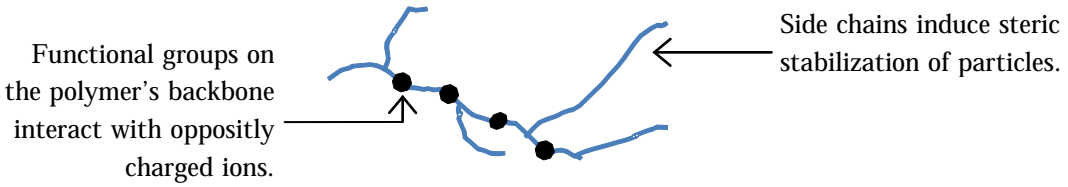

Fig. 4-1: Schematic of polymer's structure features that excerts interaction with ions and particles.

As described in section 2.2.3.4 (p.58) functional groups of the polymers of superplasticizers are able to complex ions due to their anionic charge and the pH environment in cement pastes. In cementitious systems, mainly calcium is bound by SPs. Because grafting of side chains at the polymer causes dispersion of particles, the interaction between calcium and functional groups of macromolecules is expected in both cases: on surfaces and in solution. In contrast to the mode of action of the functional groups of superplasticizers, complexation of ions on surfaces is well studied (described as adsorption, see section 2.2.3.4, p.58). In the present chapter the interaction between calcium ions and functional groups of polymers is therefore divided into two parts: complexation of calcium ions on surfaces (section 4.1.2) and complexation of calcium ions in aqueous solution (section 4.1.3). Finally it is investigated if complexation of calcium ions in solution induces formation of clusters as a result of growth of simple ion complexes. Thus, this part is attributed to the effect of cluster formation frequently discussed in the field of biomineralization (2.1.3, p.33).

4.1.2 Complexation of calcium ions on surfaces – adsorption

In the present section the complexation of calcium ions on surfaces (adsorption) is investigated. This behavior is tested in a vast number of experiments presented in literature. Nevertheless, a low number of researches are related to the adsorption of SPs on C_3S surfaces, which is thus an issue for the present experiments.

4.1.2.1 Experimental setup

4.1.2.1.1 Materials

Additionally to experiments with tricalcium silicate the testing is started by using OPC (CEM I 42.5R with Na_2O^{eq} of 0.94). The specific surface area was 4620 cm^2/g (Blaine method) and 15,878 cm^2/g (BET). The chemical composition, particle size distribution as well the mineralogical composition (QXRD) is summarized in the appendix (Tables A-2 and A3, Fig. A-1).

To investigate specific points in more detail, the number of different PCEs shown in Table 3-1 is expanded exclusively for present investigations. Details on the chemical structure of

these SPs are given in Table 4-1. Accordingly to PCE1 and PCE2 the numbers are gathered in the same way as described in section 3.1.1 (p.67).

Table 4-1: Properties of additional superplasticizer solutions for cement testings.

SP	Backbone	Copolymer (ester grafting)	N[a]	n[a]	P[a]	Molecular weight macromolecule [g/mol]	Polymer content [m.-%]	Polymer confor-mation[a]
PCE3	Methacrylic acid	MPEG	4.6	9.0	23	12,600	40.0	FBW
PCE4	Methacrylic acid	MPEG	5.3	14.9	23	21,720	40.0	FBW
PCE5	Methacrylic acid	MPEG	11.8	2.7	114	16,200	40.0	FBS

[a] according to Gay and Raphaël[72].

4.1.2.1.2 Experiments

Before the complexation of calcium ions on surfaces (adsorption) by superplasticizers was recorded the numbers of functional groups are determined. This permits the correlation of complexation of calcium with number of anionic groups. Taking the chemical structure given in Table 3-1 into account the number of functional groups of the macromolecule can be calculated. These values are proven experimentally by using the particle charge detector (PCD) described in section 3.2.1 (p.69).

Superplasticizer adsorption was determined by measuring Total Organic Carbon (TOC, see section 3.2.5.5, p.71) content in the aqueous phase of pastes before and after 10 min of hydration (depletion method). The liquid/solid ratio of C_3S pastes was adjusted to 0.5 and in case of cement to 0.5 and 0.37, respectively. Standard deviation of random errors was determined for one SP on 5 different samples. Measurements of all other samples were performed in duplicate.

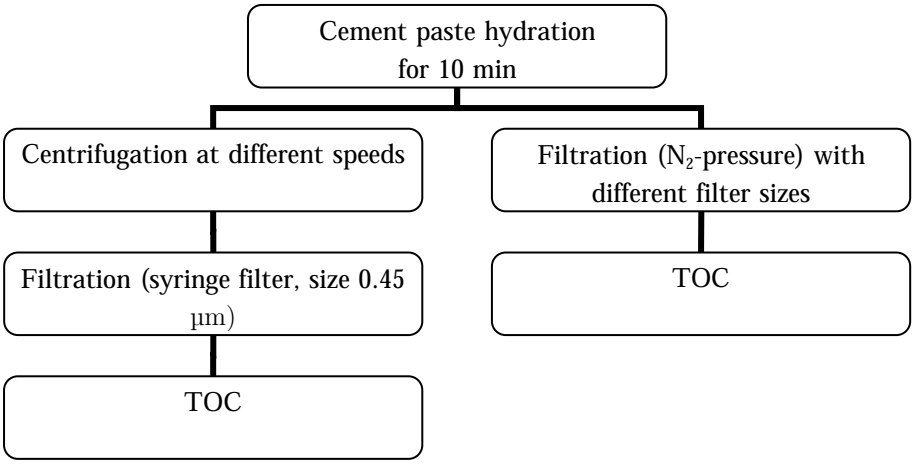

Fig. 4-2: Scheme of the investigation on the impact of sample preparation on adsorption values.

Cement pastes were treated with different sample preparations (centrifugation and filtration) varying in field and duration of centrifugation and pore size of the filter as

sketched in Fig. 4-2. In case of solely filtering (right hand chart of Fig. 4-2), the paste was treated with a N_2 pressure of 5 bar in a pressure filtration device (Sartorius 16249, V_{max}=0.2 l, Watman filter with diameter of 47 mm and filter sizes of 0.1 µm (NC10) and 0.45 µm (ME25), respectively). The extraction of the aqueous phase of C_3S pastes was done accordingly to the left hand chart of Fig. 4-2 by centrifuging pastes for 5 min at centrifugation field of 15,500 g. Additionally, a centrifugation field of 30,000 g and 57,000 g was utilized. In all cases the supernatant was filtered through 0.45 µm syringe filter.

The obtained aqueous phase was additionally treated with H_3PO_4 in order to expel inorganic carbon before TOC was measured, cf. chapter 3.2.5.

4.1.2.2 Results and discussion

4.1.2.2.1 Determination of the number of anionic groups of the polymers

The anionic charge of the polymers was determined by means of both calculation using data (Table 3-1, Table 4-1) and titration experiments. Results are presented in Table 4-2.

Table 4-2: Calculated and measured numbers of anionic groups per gram of polymer solution (polymer content according to 2nd right row of Table 3-1 and Table 4-1).

SP	Anionic groups [mmol/g]	
	Calculated	Measured
PCE1	2.32	2.70 ± 0.05
PCE2	1.28	2.21 ± 0.13
PCE3	2.58	2.11 ± 0.01
PCE4	2.95	1.94 ± 0.01
PCE5	1.80	1.39 ± 0.01
PNFS	7.03	7.87 ± 0.03

It can be seen that the ranking of the total number of functional groups is equal for both approaches. This is also reflected by the Na^+ content of the superplasticizer solution which stems from the adjustment to neutral pH (see Table 3-1). Moreover, the comparison between calculation and measurement shows similar values (except of PCE2 and PCE4 which is discussed in the next subsection). It should be noted that calculation was performed taking into account the average polymer structure. During polymer synthesis, however, always a distribution of polymer structures is obtained (polydispersity, see Table 3-1). Thus, it can be stated that PCD measurements give reasonable data for the used superplasticizers. As expected and in accordance to others[151], the anionic charge density of PNFS exceeds that of PCE. Moreover, within the PCE group PCE1 exhibits an increased anionic charge at equal dosage with respect to PCE2 as a result of its chemical structure.

4.1.2.2.2 Experimental parameters that influence adsorption values

Before the adsorption of superplasticizers on C_3S surfaces is handled, we examine parameters that influence the experimental results. These are shown in Fig. 4-3 using OPC at w/c ratios of 0.37 and 0.5, respectively.

As revealed by results in Fig. 4-3 increasing centrifugal field in the range between 15,000g and 57,000g leads to decreasing measured TOC value in the aqueous phase and thus increased degree of adsorption from 20 to 28 % for w/c ratio of 0.5. In case of w/c ratio of

0.37, this effect is only visible as trend in Fig. 4-3 because of the increased standard deviation. If samples with w/c of 0.37 are centrifuged at 57,000g for 30 min a stronger adsorption with respect to the 5 min treatment at the same centrifugation field is observed. But samples with w/c of 0.5 show no differences in adsorption when centrifugation duration is prolonged (5 and 30 min). However, variation in duration of centrifugation results in decreased and increased values of adsorption for w/c ratio of 0.5 and 0.37, respectively.

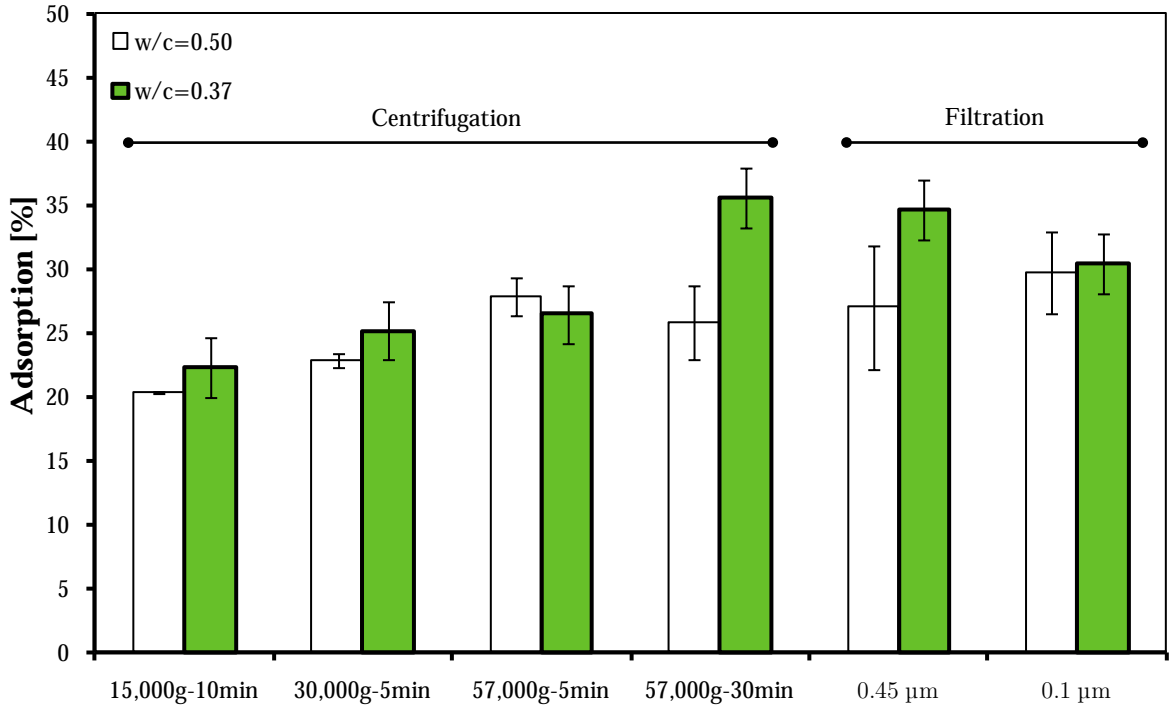

Fig. 4-3: Impact of the sample preparation (centrifugation and filtration) on the determined adsorption degrees (depletion method) of PCE1 on cement hydrated for 10 min at different w/c ratios and constant SP-dosage (0.25 m.-% bwoc). It can be seen that increasing centrifugal field leads to increasing values of adsorption. Pore size of filters has only minor impact on the determined adsorption and is comparable to centrifugation at 30,000g.

During solely filtering of the cement paste (right hand chart of Fig. 4-2) it is generally observed that a lower amount of solution compared to centrifugation can be extracted. Results of the adsorption measurements show no clear trend at various pore sizes of the filter when standard deviation is considered. Obviously, filtering leads to similar results compared to centrifuging at higher speeds.

These results demonstrate that sample preparation is critical for adsorption measurements, predominantly for lower w/c ratios. The investigated PCE1 is regarded as very good dispersing agent among the investigated SPs. But SPs with even higher dispersing ability may gain the dependency of the adsorption value on sample preparation protocol.

4.1.2.2.3 Complexation of calcium ions on tricalcium silicate surfaces (adsorption) by superplasticizers

Investiagtions on polymer adsorption is frequently performed by TOC measurement in the aqueous phase before and after the addition of the solid. Thereby the variation of the superplasticizer dosage (adsorption isotherms) gives valuable insights into the adsorption mechanism. As known from literature[84], adsorption isotherms are plotted as adsorbed

amount of polymers against dosed amount. Typically, an adsorption curve contains a linear increasing part at lower polymer dosages where the surface becomes covered by the polymer. Thereby, an increased adsorption affinity of superplasticizers on a certain surface is associated with an increasing slope. Further increase in SP dosage induces often adsorption saturation and, as a consequence, a plateau in the curve is obtained. This plateau is associated with the dosage of polymer needed to saturate the surface, i.e. SP doses beyond this threshold are not adsorbed by the surface in this adsorption layer. In this work however, further dosages beyond this plateau lead to increasing adsorption of polymers on surfaces again. This may be the result of surface aggregation and can also be associated with micelle formation, provided the micelles do not pass through the filter used. In Table A- 4 the raw data is given. Fig. 4-4 shows the adsorption isotherms of SPs on tricalcium silicate.

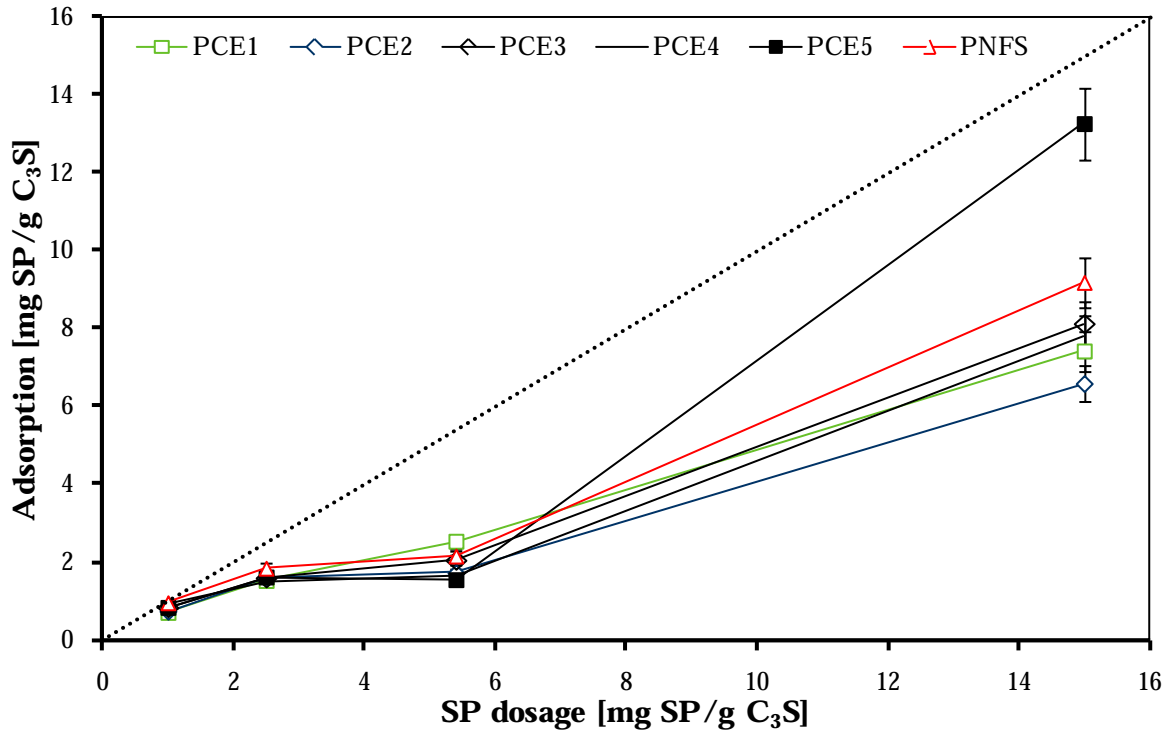

Fig. 4-4: Superplasticizer adsorption isotherms recorded after 10 min of C_3S hydration at l/s ratio of 0.5. At increased SP dosage a plateau is observed which corresponds to saturation of the surface. Further increase in SP adsorption shows increased adsorption values that may result from surface aggregation or micelle formation. Dotted line indicates complete adsorption.

In order to examine the PCE adsorption data shown in Fig. 4-4 the approach of polymer adsorption reported by Marchon et al.[117] (which in turn is based on the scaling law approach originally published by Gay and Raphaël[72]) is utilized. The reasonable assumption is that the driving force for adsorption is electrostatic, i.e. interaction between functional groups of the polymer with opposite charged ions on surfaces (mainly calcium in case of cementitious materials). In a first step the adsorption plateau after the linear increasing adsorption is investigated. According to Flatt et al.[55], the occupied surface by a macromolecule S can be expressed as:

$$S = \frac{\pi}{\sqrt{2}} a_N a_P \left(2\sqrt{2}(1-2\chi)\frac{a_P}{a_N} \right)^{\frac{2}{5}} P^{\frac{9}{10}} N^{\frac{3}{10}} n \qquad (29)$$

Thereby parameters N, P and n describe the chemical structure of the polymer (section 3.1.1 (p.67)), a_N the backbone monomer size, a_P the side-chain monomer size and χ the Flory parameter. For calculations values of a_N=0.25 nm, a_P=0.36 nm and $\chi = 0.37$ (for PEO) were used. A detailed description of the theory is given elsewhere[55, 75]. With the molecular weight of the polymer $M_{Polymer}$ and Avogadro's number N_A the theoretical adsorption plateau AP^{theor} can be calculated by

$$AP^{theor} = (N_A \cdot S)^{-1} \qquad (30)$$

In Fig. 4-5 the measured adsorption plateau is plotted against the predicted (eq.(30)).

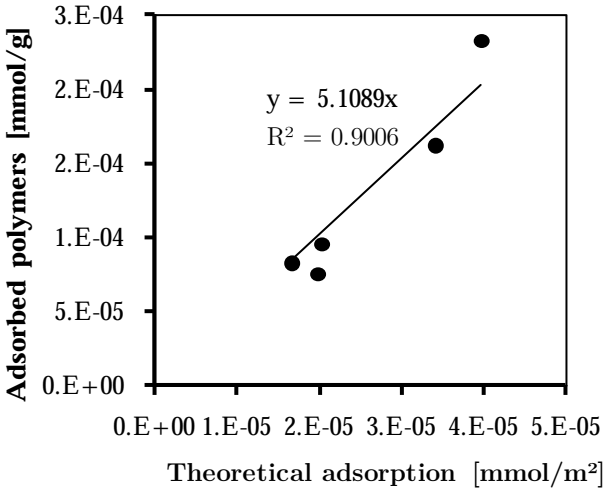

Fig. 4-5: Measured and calculated adsorption plateau. Measurements indicate about 5 times higher adsorption as predicted.

It can be seen that all polymers can be related on a linear function with a slope of ~5.1. Thereby the slope corresponds to the specific surface area of C_3S at the period of sampling (10 min hydration). Taking the initial specific (BET) surface area of ~0.8 m^2/g into account the calculated value indicates that the surface area is increased by a factor of 6.4. That result is propably wrong since the surface area is increases within 10 min of hydration (and during the induction period) from ~0.8 m^2/g to ~1.3 $m^2/$, i.e. by a factor of 1.6. The causes of this effect can be speculated differently. It may be caused by the fact that whether the model needs to be extended although it was demonstrated by experiments on C-S-H[55] that the model is applicable for this solid. A further cause of this behaviour may be the aggregation of polymers in micells. This effect is seen to be responsible for the strong increase of the polymer adsorption after the plateau. Finally the CaO content of the C_3S (0.2 m.-%) may influence the adsorption by an increased release of calcium into the aqueous phase. By that, stronger adsorption of polymers may occur. Combining the results it can be stated that more work is needed to clearify the adsorption characterisitics of PCEs on C_3S surface. This includes in particular gathering more data points. Nevertheless, the results show that the scaling law approach from polymer science is capable to qualitatively account for the adsorption plateau.

The linear region before the adsorption plateau is reached is investigated next. Under the assumptions of an adsorbed conformation following eq. (30), a reversible adsorption equilibrium and an adsorption energy dominated by electrostatic interactions, a first

principle derivation of an adsorption equilibrium constant $K_{A,1}$ has been proposed[55, 117] and leads to equation (31)

$$K_{A,1} = (N-1)^2 \, z^2 \, P^{-\frac{9}{5}} \, N^{-\frac{3}{5}} \, n^{-1} \tag{31}$$

with z as the anionic charges of a functional group. Alternatively, there may also be an impact of the effective charge of the polymer. This can be assessed by following equations

$$z_{eff} = \frac{z_{meas}}{z_{calc}} \tag{32}$$

with the calculated charge z_{calc} and the measured charge of the polymer z_{meas} (determined by means of charge titration with Polydadmac, section 3.2.1 (p.69). Taking the effective charge of the polymer into account we can define an effective adsorption equilibrium constant according to equation (33):

$$K_{A,1,eff} = K_{A,1} \cdot z_{eff}^{\,2} \tag{33}$$

The affinity of polymers for adsorption on surfaces can be assessed by plotting adsorbed amounts against not adsorbed fractions of the dosed polymers (Langmuir adsorption isotherm), see Fig. 4-6.

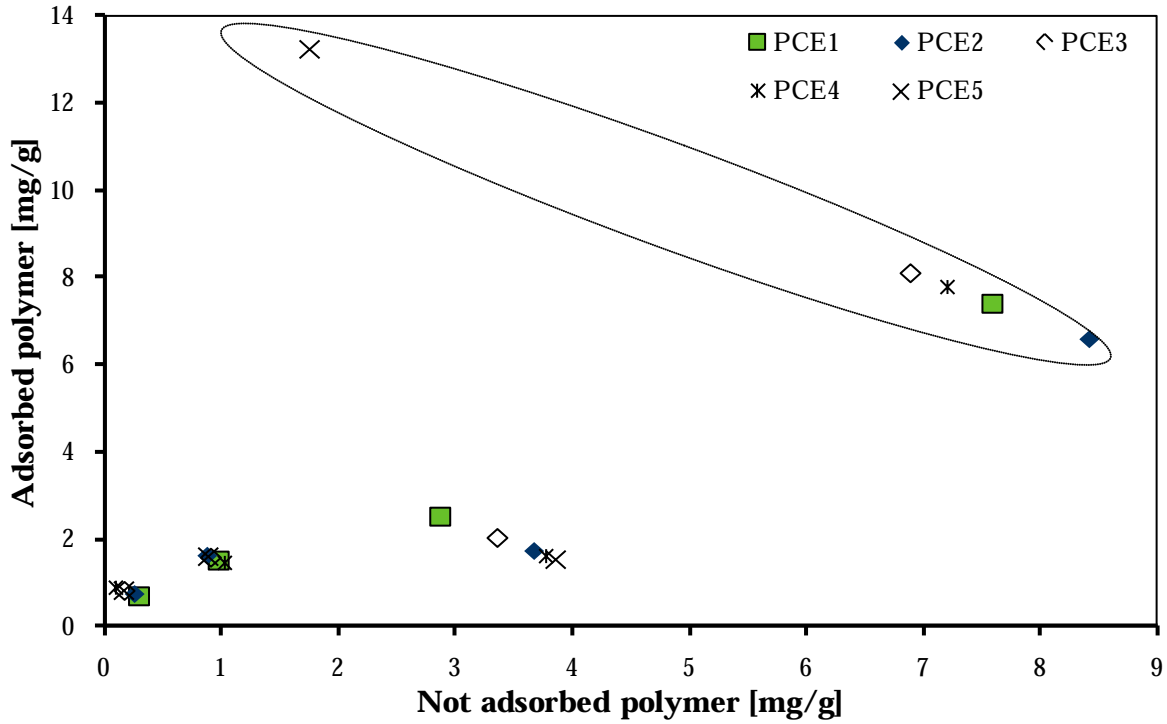

Fig. 4-6: Adsorbed and not adsorbed fraction of dosed polymers (Langmuir adsorption isotherm). Highest polymer dosage is highlighted by an ellipse.

From Fig. 4-6 it can be deduced that the fraction of not adsorbed polymer increases with increasing dosage. At highest polymer dosage (ellipse in Fig. 4-6) and especially for PCE5

the adsorption is strongest. This behaviour may be caused by micelle formation as stated before. The region before the plateau in each data series can be used in order to investigate the driving force of adsorption. For this the data is examined in two different ways. On the one hand (scenario A) it is *a priori* claimed (based on the scaling law approach) that adsorption of polymers is never complete, i.e there is a finite number of initially dosed polymers that is not adsorbed (adsorption-desorption equilibrium). In this case the linear fit is forced to go through the origin of the graph. On the other hand (scenario B) complete adsorption of polymers on surfaces at low dosages is allowed up to a certain dosage. Here the offset can be referred to as critical fraction of the polymer that is either completely adsorbed or precipitated. For scenarios A and B the data is fitted linearly using the first two data points. In Fig. 4-7 these fits are shown exemplarily for PCE1. All other fits are given in the appendix (Fig. A- 2).

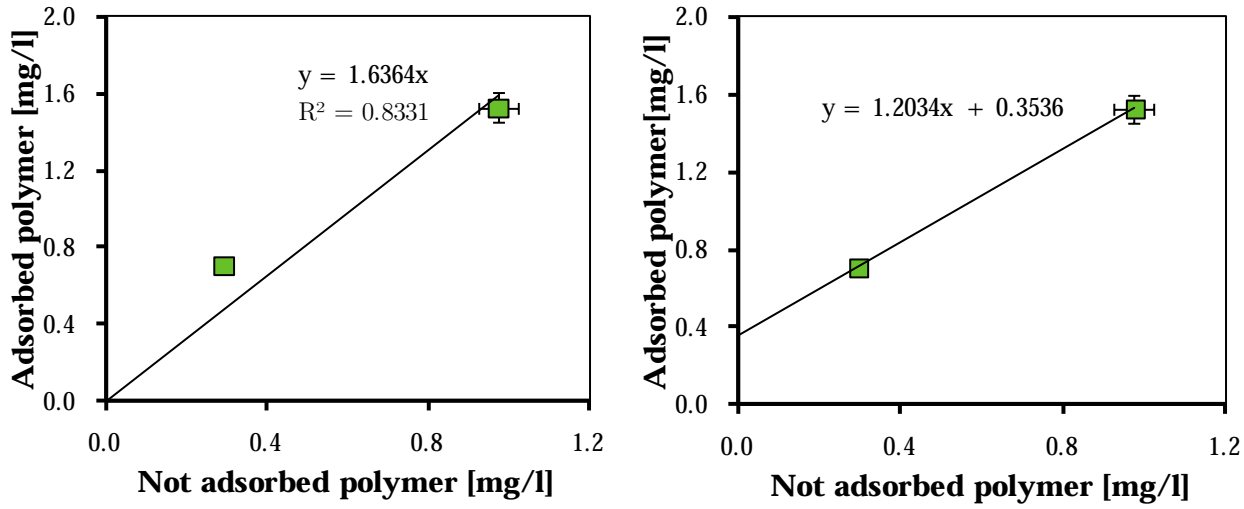

Fig. 4-7: First two points of the relation between adsorbed and not adsorbed fraction of polymers with two different data examinations (line forced to go through origin (left hand) and with an offset (right hand)). Error bars indicate an uncertainity of 5%.

Based on these two possible data treatments the slopes of these curves are correlated to adsorption equilibrium constants. It turns out that in case of assuming incomplete adsorption (scenario A) a better fit is obtained for $K_{A,1}$ than for $K_{A,1,effective}$. In contrast, if a fraction of polymer is allowed to completely adsorb (scenario B) the effective adsorption equilibrium constant $K_{A,1,effective}$ is preferentially chosen. In Fig. 4-9 the slopes from different data analysis approaches (scenarios A and B) are plotted against the adsorption equilibrium constants ($K_{A,1}$ and $K_{A,1,effective}$).

On the regression (linear, power law) shown in Fig. 4-9 it can be seen that the slope of the Langmuir adsorption isotherm and both adsorption equilibrium constants are related. However, both approaches have their limitations. These are in case of forcing the linear fit through the origin (scenario A) that PCE2 is not related to the other polymers. Therefore, this polymer is not included in the linar regression in Fig. 4-9. In order to include PCE2 in the regression the slope between adsorbed and not adsorbed amount of this polymer was determined by using 4 instead of 2 data points (filled symbol turns into the open symbol as indicated by an arrow in Fig. 4-9 (left hand)). By this a good fit is obtained. The second

limitation is if the linear regression is allowed to show an offset (scenario B) then the effective adsorption equilibrium constant (not the theoretical adsorption equilibrium constant) show a good correlation. The reasons for this behaviour are unknown, but in this case all polymers follow this relationship. Moreover, for scenarios A and B both a linear (solid lines in Fig. 4-9) and a power (broken lines in Fig. 4-9 (right hand)) regression can be used.

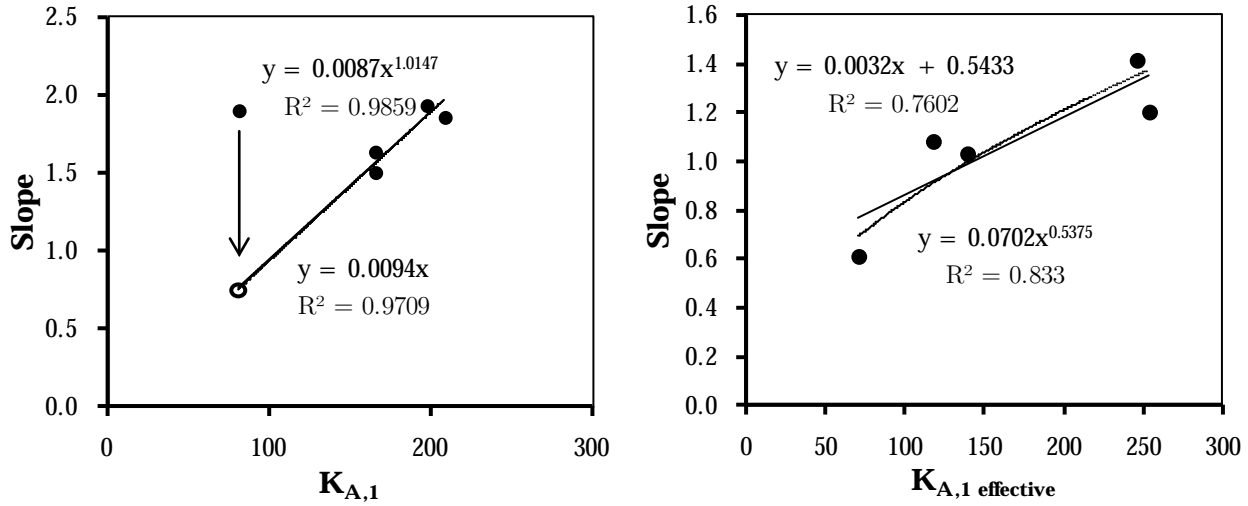

Fig. 4-9: Slope computed from the relation between adsorbed and not adsorbed fraction of the dosed polymers plotted against the adsorption (left hand) and effective adsorption equilibrium constant. It should be noted that for $K_{A,1}$ the slope was forced to go through the origin (scenario A) whereas for $K_{A,1,effective}$ the regression was allowed to show an offset (scenario B). For scenarios A and B the slope and (effective) adsorption equilibrium constant correlate directly both with a power law (broken lines) and linearly (solid lines).

Nevertheless, under consideration of these limitations Fig. 4-9 strongly suggests that the driving force for adsorption can be expressed by an adsorption equilibrium constant that relates to molecular structure in terms of electrostatic interactions and surface occupied by the adsorbed molecules[55, 75, 117]. With this in hand it can be stated that stronger adsorption is observed for polymers with increasing $K_{A,1}$ and/or $K_{A,1,effective}$. In other words, adsorption can be linked to polymer architecture. Further experimental data should be gathered in order to validate or invalidate this statement.

In Fig. 4-8 the offset which is referred to as the fraction of polymer that is initially completely adsorbed on the C_3S surface (scenario B) is correlated with the number of monomers in the backbone (N) and in the side chains (P), respectively, expressed as N^2/P.

On the linear fit in Fig. 4-8 it can be seen that with increasing N^2/P the offset

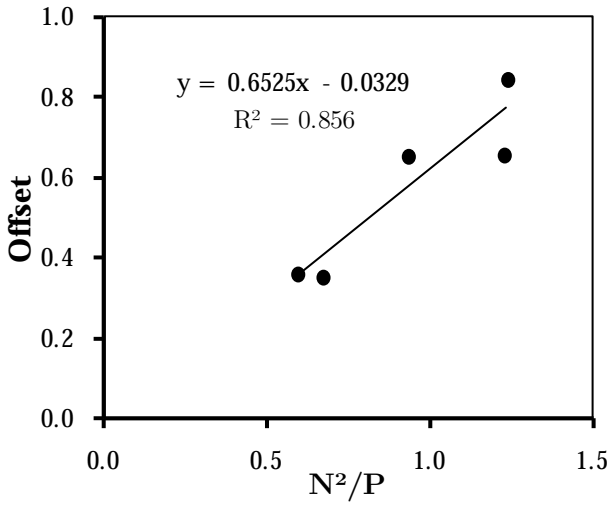

Fig. 4-8: Offset of the linear fit between adorbed and not adsorbed fraction of dosed polymers as a function of N^2/P.

increases. This indicates that the fraction of completely adsorbed polymers increases for polymers with increasing density of anionic charges in the backbone and decreasing length of the side chains. The relation between N^2 and P was introduced by Zimmermann et al.[211] and Flatt et al.[57] in order to account for the sulphate sensitivity of PCEs (expressed there as P/N^2). Again as for the examination of the slope more work is needed to verify or invalidate one of the two data interpretation approaches (scenarios A and B). An essential question is to determine how the molecular structure affects adsorption. These results suggest that it is possible to determine such relation, but they also indicate possible limitations of the existing approaches. Moreover, it is important to understand whether precipiation or aggregation processes take place and how these may affect data interpretation. For this, adsorption isotherms with large number of data points but also solubility tests would be needed.

4.1.2.3 Summary

The gathered data confirms that SP adsorption on tricalcium silicate is very strong, especially during adsorption of the first polymer layer. In accordance to findings by others[29, 82] sulfonate groups interact more strongly with calcium compared to carboxy groups at low doses. In case of the PCEs adsorption can be related to polymer architecture. For this, two approaches are proposed each of them with their limitations. On the one hand a chemical equilibrium between the surface and the solution from the very beginning of adsorption is assumed (scenario A). This situation leads to an extended linear regime, starting from the origin, if the number of surface charge sites occupied by the polymer is low[117].

The other proposed approach assumed that an initial fraction of the polymer is fully adsorbed and that nothing remains in solution. This fraction could potentially also be precipitated or adsorbed onto specific surface. While the reasons are not kown, the implication of such a situation is that adsorption data would be fit with a line not passing through the origin (scenario B). For both a good correlation to the experimental data is obtained. Because of fundamental differences of the approaches (scenarios A and B) further work is needed to clearify the laws that drive adsorption. The plateau after the linear increasing part of the adsorption isotherm was investigated. Results show that this plateau can be related to the surface occupied by a macromolecule which however is mainly affected by the polymer architecture. If this value is high then a lower amount of polymers is adsorbed at the adsorption plateau. Also here more work is needed. This includes also attempts to resolve complex experimental issues that appear to surround the measurements of adsorption isotherms on C_3S.

For example it could be shown that sample preparation is of major importance in determining different adsorption degrees, see Fig. 4-3. This shows that comparison of adsorption degrees reported by different authors may be difficult and can lead to misinterpretations.

4.1.3 Complexation of calcium ions in the aqueous solution

Results on complexation of calcium ions on surfaces (adsorption) suggest that the main structural parameters of the macromolecule for adsorption are the type and number of anionic groups of the polymer. Because complexation of ions is not restricted only to occur

on surfaces, in the following the interaction of the anionic groups of the polymers with ions dissolved in solution is investigated. Thus, the interaction between not adsorbed polymers and calcium ions is investigated.

4.1.3.1 Experimental setup

In order to determine the amount of calcium bound in Ca-superplasticizer complexes in aqueous solution, the calcium ion binding capability of superplasticizers was determined. Therefore the free calcium activity in solution was measured by means of Ion Selective Electrode (ISE, Mettler Toledo (perfectION)). Because the electrode potential is related to the calcium activity, see section 3.2.5.3 (p.70), and thus to the ion strength of the solution, latter has to kept constant for robust measurements. This is achieved by addition of 2 ml of Ion Strength Adjustor (ISA, 4M KCl) to 100 ml of sample solution *ex-situ*.

Superplasticizer was added in intervals of 0.5 ml to 50 ml to a 0.1 M $CaCl_2$ solution. After the addition of SPs the system needs several seconds for stabilization. Therefore electric potential was recorded subsequently to this period. The Ca binding capacity by superplasticizers was calculated as function of superplasticizer dosage, initially. Thereby, the dilution of the solution due to the water content of the superplasticizers was taken into account. In a second step calcium complexation capacity was related to the number of functional groups of the macromolecule determined previously.

4.1.3.2 Results and discussion

Fig. 4-10 shows the Ca complexation capability of superplasticizers in 0.1M $CaCl_2$ solution as function of SP dosage. For comparison the dosage is related to dry mass of SP per volume solution. Because measurements at increased pH values leads to damages upon the electrode, in a first step only pH neutral solution ($CaCl_2$) was used although approx. 80% of the functional groups are dissociated in this pH region[206]. Thus, results obtained in $CaCl_2$ solution may lead to slight underestimations regarding calcium complexation capability in cementitious systems.

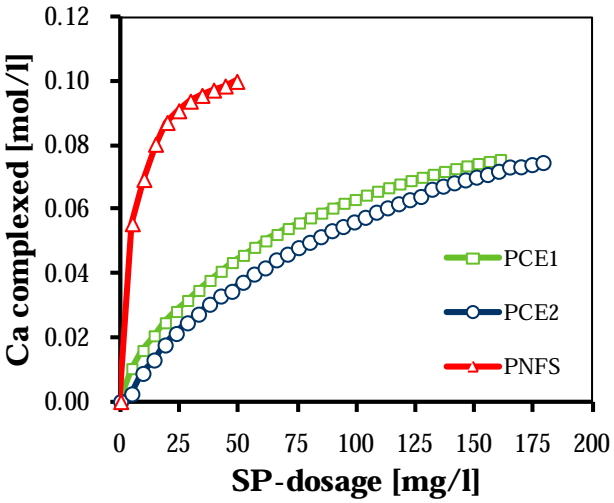

Fig. 4-10: Ca complexation capability of SPs as function of SP-dosage in 0.1 M $CaCl_2$ solution. It can be seen that PNFS exhibits the largest charge quantity and therefore complex more Ca ions compared to PCEs.

In Fig. 4-10 it can be seen that both PCE show similar complexation capability. But PCE1 (squares in Fig. 4-10) tends to complex more Ca from solution than PCE2 (circles in Fig. 4-10). Moreover, superplasticizer based on naphthalene sulfonate shows stronger tendencies for Ca complexation than PCEs (triangles in Fig. 4-10). Starting from 0.1 M $CaCl_2$ solution, at a dosage of 50 mg/l PNFS complex all Ca ions in the aqueous solution.

Among different parameters regarding the chemical structure of the macromolecules (e.g. type and number of anionic group, side chain length and grafting, molecular mass) it is investigated which polymer parameter is mostly responsible for the different complexation behaviors. Therefore and in accordance to complexation of calcium ions on surfaces (adsorption) shown in section 4.1.2 (p.75), in the next step Ca complexation data is related to the number of functional groups of the macromolecule. Thereby, both calculated and measured numbers of anionic charges given in Table 4-2 are used. Results are shown in Fig. 4-11.

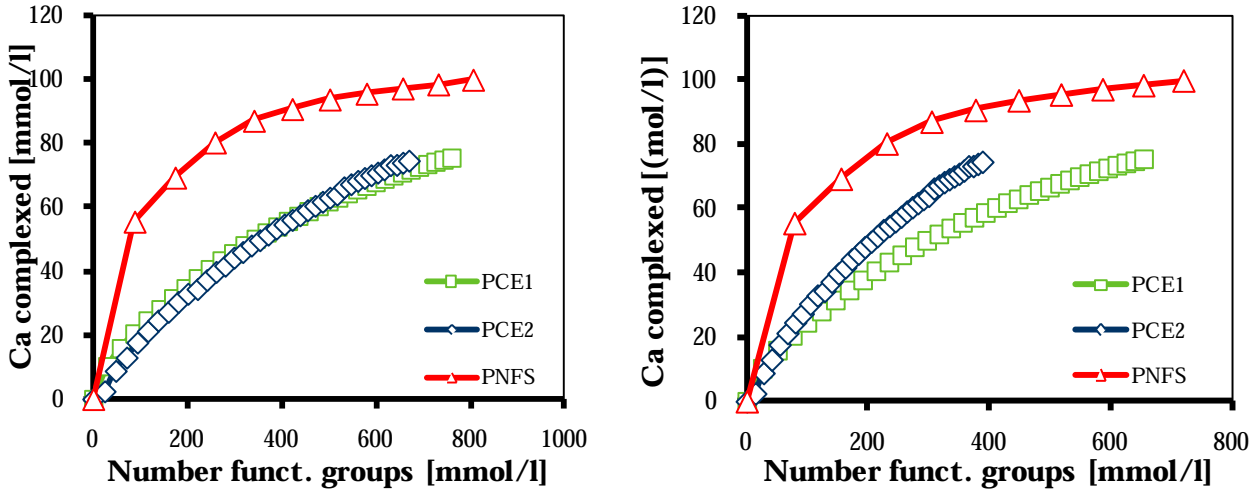

Fig. 4-11: Ca complexation capability of SPs in 0.1 M $CaCl_2$ solution as function of number of functional groups (measurement (left hand), calculation (right hand)) of the macromolecule. The graphs reveal that Ca complexation is driven by both type and number of functional groups of the polymer. Moreover, the measurements give better correlation at increasing SP-dosages compared to the calculations.

As evidenced by Fig. 4-11, the Ca ion complexation is mostly related to the absolute number of anionic groups of the polymers. Thereby differences between calculation and measurement are observed at increased SP-dosages. Furthermore it is revealed that the type of functional group has a strong impact on the interaction with calcium ions. Therefore, Ca ions show more affinity to sulfonic groups of PNFS compared to carboxy groups of PCEs.

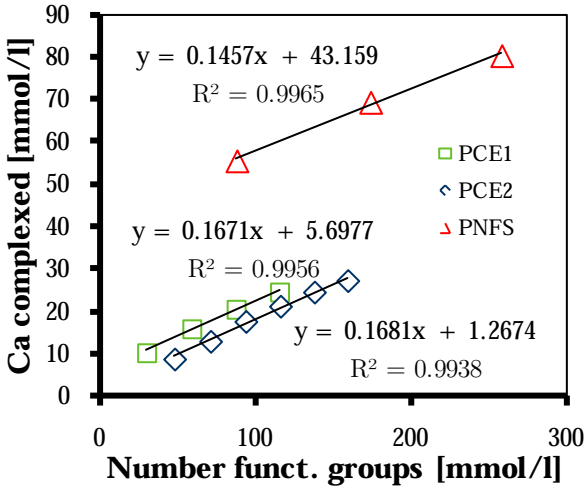

Fig. 4-12: Calcium ion complexation of polymers in dependence on the number of added functional groups for SPs during titration experiments in 0.1M $CaCl_2$ solution (see section 4.1.3 (p.84)).

The first 3 to 6 points of Fig. 4-11 were linearly fitted, see Fig. 4-12. Slopes are approx. 0.17, 0.17 and 0.15 for PCE1, PCE2 and PNFS, respectively. These data indicate that in case of PCEs roughly every sixth functional group complexes one calcium ion when a positively charged complex (see eq. (34)) is considered. In case of PNFS the number of sulfonic groups per calcium is 4.

Discussion of the differences between calculated and measured number of functional groups in case of PCEs is more speculative. At this point it is rather reasonable to account the calcium complexation predominantly to the type of functional groups although side chain length may be also important which may explain the differences in Ca complexation at increased SP-dosages in Fig. 4-11 (right hand).

In the following, data is used in order to calculate complexation constants between calcium ions and anionic groups according to the following expressions:

$$\begin{aligned} Ca^{2+} + 2L^{-} &\Leftrightarrow (2LCa)^{0} \\ Ca^{2+} + L^{-} &\Leftrightarrow (LCa)^{+} \end{aligned} \tag{34}$$

$$\begin{aligned} K_{C,0} &= \frac{\gamma_0[Ca \cdot L]}{\gamma_2[Ca^{2+}] \cdot \gamma_1{}^2[L^{-}]^2} \\ K_{C,+} &= \frac{\gamma_1[(Ca \cdot L)^{+}]}{\gamma_2[Ca^{2+}] \cdot \gamma_1[L^{-}]} \end{aligned} \tag{35}$$

Thereby the complexation at low SP dosages (first four points in Fig. 4-11 omitting point zero) is fitted linearly. For dosed anionic groups (referred to as ligand L) values of 0.05, 0.05 and 0.1 mol/l for PCE1, PCE2 and PNFS were used, respectively, in order to calculate calcium complexation values. Ion activity coefficients (γ_1, γ_2) were determined using software PHREEQC (pitzer.dat) considering Ca, Cl, anionic groups, Na (added with SP) in 4M KCl solution (ion strength adjustor). Using these calculations the complexation constants based on eq. (35) for neutral ($K_{C,0}$) and positively charged ($K_{C,+}$) calcium-polymer-complexes are determined. Results are given in Table 4-3.

Table 4-3: Calcium-polymer-complexation constants in $CaCl_2$ solution according to eq. (35) at (23±2)°C.

Superplasticizer	Log $K_{C,0}$	Log $K_{C,+}$
PCE1	-0.7	0.48
PCE2	-0.7	0.48
PNFS	-1.2	0.48

Calculations shown in Table 4-3 demonstrate that the considered complexes differ in their constants. Therefore, the value of the complexation constant for neutral complexes ($K_{C,0}$) is decreased with respect to positively charged complexes ($K_{C,+}$). This indicates that with respect to the positively charged complexes the number of calcium ions paired in neutral calcium-polymer-complexes is lower. Considering the complexation constants in neutral complexes it is obvious that sulfonic groups complex a lower amount of calcium compared to carboxy groups. Positively charged complexes show no effect on the type of functional group. The comparison of calculated complexation constants in the present work with published data reveals similar values. For example constants of log K=4.0 and log K=1.2 for Ca-acetate (monocarboxy acid) complexes are reported[45] for neutral and positively charged complexes, respectively. To the best of the author's knowledge no values are

reported for sulfonic groups. All in all it is concluded that calculations according to eq. (35) allow a quantitative determination of complexation capability.

For following experiments the Ca complexation capability of superplasticizers is important. Because the complexation is not linearly related to SP-dosage and the number of functional groups, respectively, the data is fitted by mathematical functions. These functions are given in Table 4-4 and can be used to assess the Ca complexation capability of the used SPs.

Table 4-4: Ca complexation capability in mol/l of selected SPs related to (i) dry mass of SP and (ii) to SP solutions (approx. 40 m.-% dry mass, Table 3-1) with units of mg/l solution and ml/l solution, respectively.

Super-plasticizer	Ca complexation capability Related to dry mass of SP	Related to SP solution (approx. 40 m.-% dry)
PCE1	$Ca^{compl.} = 0.10673 * SP/(67.80269 + SP)$	$Ca^{compl.} = 0.10673 * SP/(140.55285 + SP)$
PCE2	$Ca^{compl.} = 0.12669 * SP/(255.92347 + SP)$	$Ca^{compl.} = 0.12669 * SP/(122.8426 + SP)$
PNFS	$Ca^{compl.} = 0.11009 * SP/(10.47598 + SP)$	$Ca^{compl.} = 0.11009 * SP/(5.25745 + SP)$

4.1.3.3 Summary

As documented in literature, anionic charges of polymers are able to complex cations[6, 151]. The complexation of calcium ions dissolved in solution by anionic groups of SPs was determined in the present work by measuring Ca ion activity by means of Ca selective electrode. Results show, Ca complexation capability increases with increasing anionic charge of the polymer. But also the type of functional groups affects the Ca complexation capability in dependence on dosage. In comparison to carboxy groups a stronger tendency for Ca complexation was found at low dosages for the sulfonic groups which turn over at high polymer dosage. This effect is reflected by calculations of complexation constants. Moreover, data confirm findings from adsorption measurements (section 4.1.2 (p.75)).

4.1.4 Cluster formation in the aqueous phase of tricalcium silicate pastes

As a result of interaction of anionic groups of the macromolecule and calcium ions, Ca-polymer complexes are detected on surfaces and in solution. In the next experimental step it is investigated if such complexes can also be found during tricalcium silicate paste hydration. Furthermore it is focused on determining if Ca-polymer complexes show growth to larger aggregates during the course of hydration.

4.1.4.1 Experimental setup

The composition of the aqueous phase in presence of one selected superplasticizer (PCE1) was investigated by means of Analytical Ultracentrifugation (AUC), see section 3.2.6 (p.71). For this a C_3S paste was centrifuged and filtered (0.45 µm) after 10 min of hydration at 15,000g (gravitational acceleration, g=9.81 m/s^2). The aqueous phase of the C_3S paste was subsequently investigated by means of AUC. Thereby the particle sedimentation induced by a high centrifugal field is measured as time dependent change of the particles location, i.e. sedimentation velocity. From that, the particle diameter can be

calculated using equations given in section 3.2.6. The AUC experiments were performed with a Beckman-Coulter, Optima XL-A/XL-I ultracentrifuge with self made 12 mm 2.5° titanium center-pieces at Max Planck Institute for Colloids and Interfaces (Potsdam, Germany). Particle sedimentation due to the centrifugal field was measured with Rayleigh interference optics at 25°C at 48,000 and 260,000g, respectively. The obtained sedimentation coefficients distribution c(s) were diffusion corrected using the software Sedfit by Schuck[172] and their intensities were normalized. Uncorrected sedimentation coefficient distributions are given as g(s).

4.1.4.2 Results and discussion

4.1.4.2.1 Centrifugation at 48,000g

In a first step sedimentation coefficient distribution (g(s)) for PCE1 containing aqueous phase of C_3S pastes was determined at a centrifugal field of 48,000g, cf. Fig. 4-13.

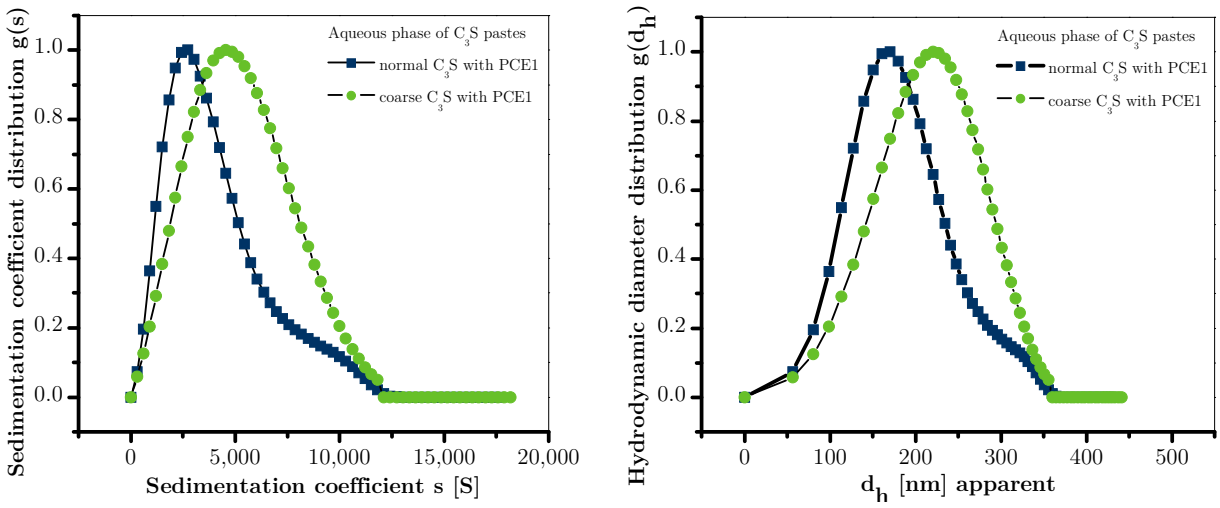

Fig. 4-13: Sedimentation coefficient distribution (left hand) and calculated particle size distribution (right hand) of particles detected at centrifugal field of 48,000g in the aqueous phase of C_3S pastes after 10 min hydration. Measured density of particles: 1.147 g/cm³. In both cases (normal and coarse (>5µm in diameter) C_3S) similar particle sizes are observed as products of C_3S hydration.

In the aqueous phase of SP containing C_3S paste sedimentation coefficient distribution (g(s)) of sedimenting particles was detected. In the absence of SP no particle sedimentation was observed in the aqueous phase of C_3S paste. Thus it can be assumed that in the absence of SP either small particles are not existent or strongly agglomerated. In addition to normally ground C_3S powders also C_3S with a particle size >5 µm was used for AUC experiments. This was necessary in order to distinguish, whether the sedimenting particles in the aqueous phase are newly formed, i.e. C-S-H phases or dispersed C_3S particles. Results of AUC measurements on the aqueous phase of C_3S >5 µm containing SP are also shown in Fig. 4-13 (left hand). Obviously and analogously to normal ground C_3S also in the >5 µm C_3S paste sedimentation of particles is observed if SP is present.

SEM-SE imaging (Fig. 4-14) and EDX analysis (insert of Fig. 4-14) were applied to characterize the sedimented particles. By means of SEM experiments the size of particles can be approximated to a range of 100 - 300 nm. Before the size distribution of particles in

the aqueous phase of C_3S pastes by AUC data utilizing eq.(28) can be performed, the density of particles must be determined. This was done by measuring the density of particles with DMA5000 (Anton Paar, Germany) according to the following protocol. In DMA5000 the density of the aqueous phase of C_3S was measured in different dilutions with deionized water. In parallel the aqueous samples were dried at 105°C in order to determine the solid content. Extrapolation of the regression between density and solid content to dilution equal zero was performed in order to determine the density of the sedimenting particles. According to this procedure the particle density measures 1.147 g/cm^3. Based on this, sedimentation coefficient distribution is expressed as particle size distribution shown in Fig. 4-13 (right hand). It can be seen that an approximatly similar particle size distribution is obtained when calculation from AUC measurements (eq.(28)) and SEM analysis are compared. This is further proven by comparing normal and >5 μm C_3S pastes (Fig. 4-13 (right hand)). As a result it is confirmed that the sedimented particles are newly formed hydration products.

Chemical analysis by means of SEM-EDX shown in the inset of Fig. 4-14 reveal the presence of calcium, silicon, oxygen and carbon as the constituents of the sedimented particles. The amount of oxygen detected indicates that the particles contain water and or hydroxyl ions. Drying of the sample has been carried out under nitrogen gas atmosphere to inhibit carbonation. Thus it is assumed that the major amount of detected carbon is of organic origin, i.e. this indicates that superplasticizer is present in the centrifuged residue. Therefore it is concluded that the sedimented particles contain polymer included or adsorbed in/on C-S-H particles (i.e. C-S-H polymer clusters).

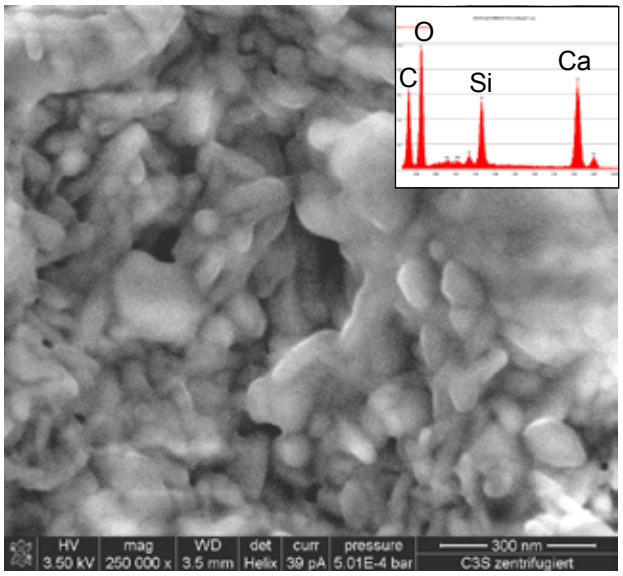

Fig. 4-14: SEM-SE image of particles formed in the aqueous phase of SP containing C_3S pastes. The inset shows the EDX spectra of these particles. The ratio of (Ca+Si)/O reveals the presence of hydrated Ca-Si phases and the high content of C indicates organic polymer (SP).

Quantification of the carbon/silica ratio of the sample by means of EDX is conducted in order to calculate a number of adsorbed/absorbed polymers on/in C-S-H-phases. Results give a carbon/silica of 3.4. With this and using 1.10 g/cm^3 and 1.8 g/cm^3 as polymer and C-S-H density (lowest value from literature[7, 24]), respectively, then the theoretical particle density is computed to 1.22 g/cm^3. This value is slightly higher than measured by means of DMA5000 and may reflect that C-S-H phases exhibit lower density in the beginning of precipiation as assumed.

4.1.4.2.2 Centrifugation at 260,000g

In the next experimental step the centrifugal field was increased to 260,000g in order to detect nanosized particles[34]. The smaller sedimentation coefficients confirm that compared

to a centrifugal field of 48,000g smaller particles are present in the aqueous phase, cf. Fig. 4-15.

Similar to the observations at 48,000g sedimenting particles were only detected in the SP containing sample. The aqueous solution of >5 µm C_3S-SP paste showed identical sedimentation velocities as that of the normal C_3S-SP paste. In order to evaluate whether these sedimenting particles are calcium-polymer complexes or C-S-H - polymer clusters also a pure SP solution and SP solution containing $CaCl_2$ (similar calcium concentration as measured in the C_3S paste, i.e. 21 mM) were centrifuged. Results are also displayed in Fig. 4-15 (left hand).

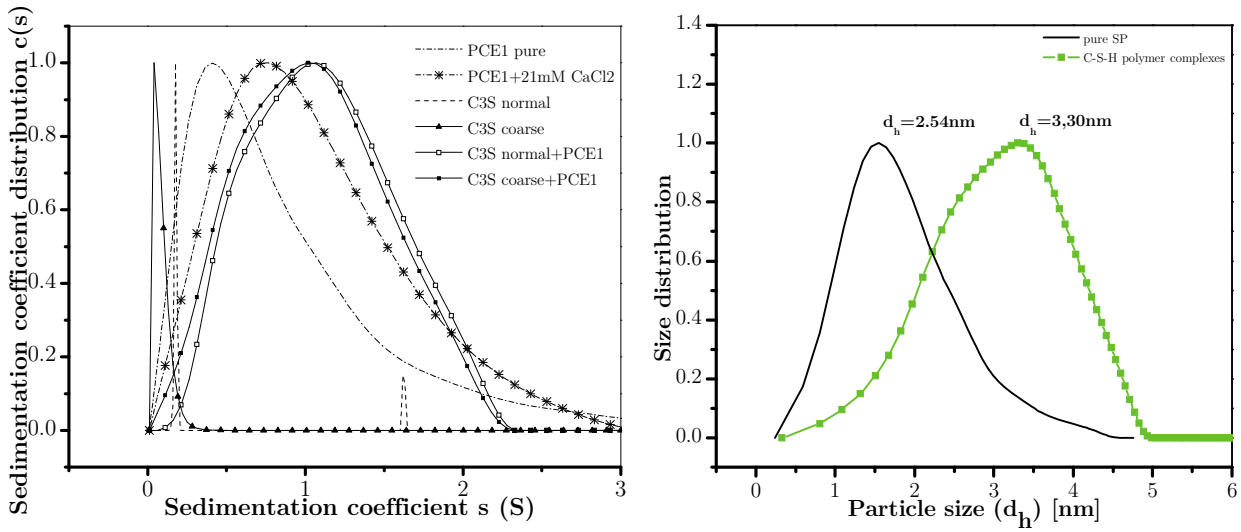

Fig. 4-15: (left hand) Sedimentation coefficient distribution c(s) (diffusion corrected) of pure PCE1, PCE1 with 21mM $CaCl_2$ and particles detected in the aqueous phase of C_3S pastes after 10 min hydration at centrifugal field of 260,000g. (right hand) calculated particle size distribution of pure SP and particles in the aqueous phase of C_3S pastes. Assumed density of polymer: 1.10 g/cm³, Measured density of C-S-H-polymer clusters: 1.147 g/cm³. This figure shows that nanoscaled C-S-H-polymer clusters are detected in the aqueous phase of C_3S paste in presence of superplasticizer.

Clearly, the addition of $CaCl_2$ to the SP solution leads to both an increase of the sedimentation velocity and to a broadening of the sedimentation coefficient distribution. The increased sedimentation coefficients indicate that complexes between SP and calcium are formed. Comparing the sedimentation velocity distribution of the calcium - SP complexes and the aqueous phase of C_3S pastes containing SP it becomes obvious that particles in the aqueous phase of the paste are sedimenting significantly faster. This can be taken again as clear indication that the sedimenting particles in the aqueous phase of C_3S – SP suspension are clusters of calcium, hydrogen, polymer and silicon. Fig. 4-15 (right hand) shows the particle size distribution of the pure PCE1 in comparison to the particles formed in the aqueous phase of C_3S-SP paste. For the calculation densities of 1.1 g/cm³ and 1.147 g/cm³ for pure PCE1 and particles in the aqueous phase of C_3S pastes were used. Whereas pure PCE1 exhibits a mean particle size of 2.5 nm, C-S-H particles formed in the aqueous phase of C_3S pastes with PCE1 measure 3.4 nm in diameter. This shows the broad distribution of latter particles ranging from approx. 3 nm to 350 nm, cf. Fig. 4-13 to Fig. 4-15.

4.1.4.3 Summary

The examinations of the aqueous phase of C_3S paste 10 min after hydration by means of AUC reveal the formation of C-S-H phases in the presence of superplasticizer. Without SP no particles were detected. This finding is supported by SEM-EDX showing C-S-H phases with increased carbon content with similar particle sizes as determined by AUC. According to literature[12-13, 40, 70, 86] first C-S-H phases precipitate during C_3S hydration in the beginning of hydration. Thus it is concluded, superplasticizers disperse C-S-H phases in the aqueous phase and crystallization is no longer restricted to surfaces.

Increased centrifugal fields (260,000g) showed that even nanoscaled C-S-H-polymer phases, i.e. C-S-H-polymer clusters, are formed. Compared to pure calcium-SP complexes, C-S-H-polymer clusters are larger. The sizes of C-S-H-polymer clusters were calculated by means of eq. (28). Therefore the density of those particles was determined by DMA5000 to be 1.147 g/cm^3 which is smaller to reported values for mature C-S-H phases in the range of 1.8[24] and 2.604[7] g/cm^3. It is reported that the density of pre-nucleation clusters of amorphous calcium carbonate[74] measures 1.47 g/cm^3. Compared to calcite (2.71 g/cm^3) the density of ACC clusters is strongly decreased in this system. Hence, the determined low density of first C-S-H phases compared to mature C-S-H phases is reasonable since these phases are dispersed by superplasticizers.

Finally it is concluded that superplasticizers induce not only formation of simple calcium-polymer complexes as demonstrated in section 4.1.3 (p.84), but also C-S-H-polymer clusters. If these clusters aggregate then this results in a broad particle size distribution. Otherwise it is also possible that a fraction of these clusters remain dispersed in the aqueous phase.

4.1.5 Concluding remarks

Experiments of the present chapter were designed to elucidate the basic modes of actions of superplasticizers during C_3S hydration. It was found that superplasticizers complex calcium ions *via* electrostatic interaction by their anionic groups. These Ca ions can be both a constituent of surfaces and dissolved in aqueous media. Moreover, it is shown that Ca ion complexes dispersed in aqueous solution can be grow to larger aggregates than simple ion complexes, i.e. clusters.

4.2 Influence of superplasticizers on separate dissolution and precipitation processes occurring during C_3S hydration

4.2.1 Aim

In the previous section it was shown that superplasticizers complex Ca ions both on surfaces (adsorption) and in solution due to electrostatic interaction between anionic groups and calcium ions. Moreover, it was demonstrated that due to performance of superplasticizers clusters are formed in the aqueous phase of C_3S pastes. In the following the impact of these effects on separate dissolution and precipitation processes is fathomed. Thus, the basic mechanisms of cement hydration are investigated independently from each other. In chapter 4.2.3 a general view on the influence of superplasticizer on the solubility of C-S-H and portlandite will be taken. Afterwards, chapter 4.2.4 will deal with the kinetics of C_3S dissolution. Finally in section 4.2.5 the impact of superplasticizers on pure crystallization of C-S-H phases and portlandite will be investigated. Thereby, special attention is paid on parameters describing polymer's molecular architecture.

4.2.2 Synthesis of C-S-H phases

In order to investigate the impact of superplasticizers on the dissolution behavior of tricalcium silicate's hydration products, C-S-H phases were synthesized. The methodology and characteristics of the synthesized C-S-H phases is described in the following.

4.2.2.1 Experimental setup

Freshly burned CaO and SiO_2 were added (glovebox, N_2 atmosphere) to water in acid cup bottles. The C/S (molar) ratio was adjusted to 1.4. Subsequently, the bottle was tightly sealed and transferred out of the glovebox. After 28 days of reaction at moderate shaking the bottle was transferred back into the glovebox. Then the suspension was filtered (0.45 µm filter, Watman ME 25). For characterization by XRD and wet chemical analysis the C-S-H phases were washed with 2-propanol, filtered (0.45 µm) and dried at 40 °C. XRD experiments were carried out using a Siemens D5000 diffractometer operating with copper radiation at 40 kV and 40 mA. The scanning was performed at a step width of 0.03° 2Θ over an angular range from 4 to 70° 2Θ with 5 s counting time per step. For chemical analysis the mass loss after heating of C-S-H phases was determined and the solid was analyzed by means of ICP-OES.

4.2.2.2 Results and discussion

Chemical analysis of C-S-H phases reveals that the sample comprises of 31.9 m.-% CaO and 24.5 m.-% SiO_2 (and 0.05 m.-% Na_2O). Thus, the molar Ca/Si is 1.4. Additionally, the mass losses were determined to 30.7 and 12.9 at 105°C and 950°C, respectively. XRD measurements shown in Fig. 4-16 document that only traces of additional phases are formed, i.e. calcite, vaterite, portlandite. Hence, the synthesis protocol leads to pure C-S-H phases.

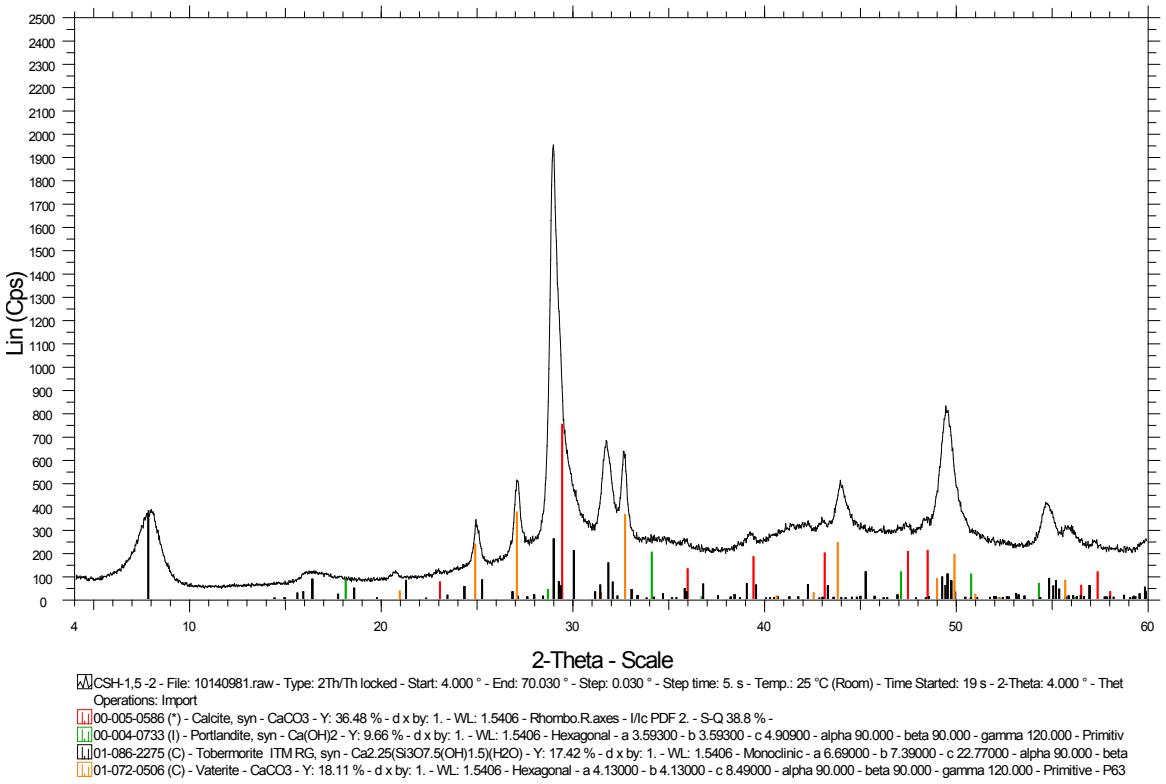

Fig. 4-16: XRD analysis on synthetic C-S-H phases (black line) showing that pure C-S-H phases with minor traces of additional phases is formed.

4.2.2.3 Summary

In the present section the synthesis and characteristics of synthetic C-S-H phases is handled. Therefore CaO and SiO_2 were added to water under N_2 atmosphere. By means of wet chemical analysis and XRD it was revealed that pure C-S-H phases can be obtained by the used approach.

4.2.3 Solubility of C-S-H phases and portlandite

The solubility of C-S-H phases and portlandite in presence of superplasticizers is investigated in order to characterize whether or not superplasticizers have an impact on solubility of hydrate phases obtained during hydration of C_3S. Therefore superplasticizers presented in Table 3-1 are utilized. Whereas portlandite was purchased, C-S-H phases are synthesized previously to the experiments, see section 4.2.2 (p.93). In a first step the solubility of C-S-H phases and portlandite is investigated. Then the impact of superplasticizers on solubility of these hydrate phases is tested.

4.2.3.1 Experimental setup

C-S-H phases (synthesis described in section 4.2.2, p.93) were mixed with water and calcium hydroxide solutions (different concentrations), respectively, in presence or not of SPs (Table 3-1, various concentrations) for 14 days.

Portlandite (Merck, pure) was solely mixed with water and SPs for 20 hours. Both suspensions were shaken in sealed containers at temperatures of 23°C and 20°C in case of

C-S-H phases and portlandite, respectively. That the solutions were always supersaturated with respect to the solids was ensured by working at l/s ratios of 70 (C-S-H phases) and 80 (portlandite). Thus, in case of complexation of ions, solids can release additional ions into solution contrary to the Ca complexation measurements conducted in section 4.1.3 (p.84). Experiments were stopped by separating a fraction of the suspensions which was then filtered (0.22 µm syringe filter (Carl Roth)). Subsequently, the filtered solutions were acidified for stabilization purposes. Finally all solutions were analyzed by means of ICP-OES. Final concentrations were corrected by the dilution induced by acidifying.

4.2.3.2 Results and discussion

4.2.3.2.1 Solubility of C-S-H phases

A Reference without superplasticizers

In the present study the solubility of C-S-H phases is investigated. Therefore, various starting solutions different in their calcium ion concentration were adjusted. Results are shown in Fig. 4-17.

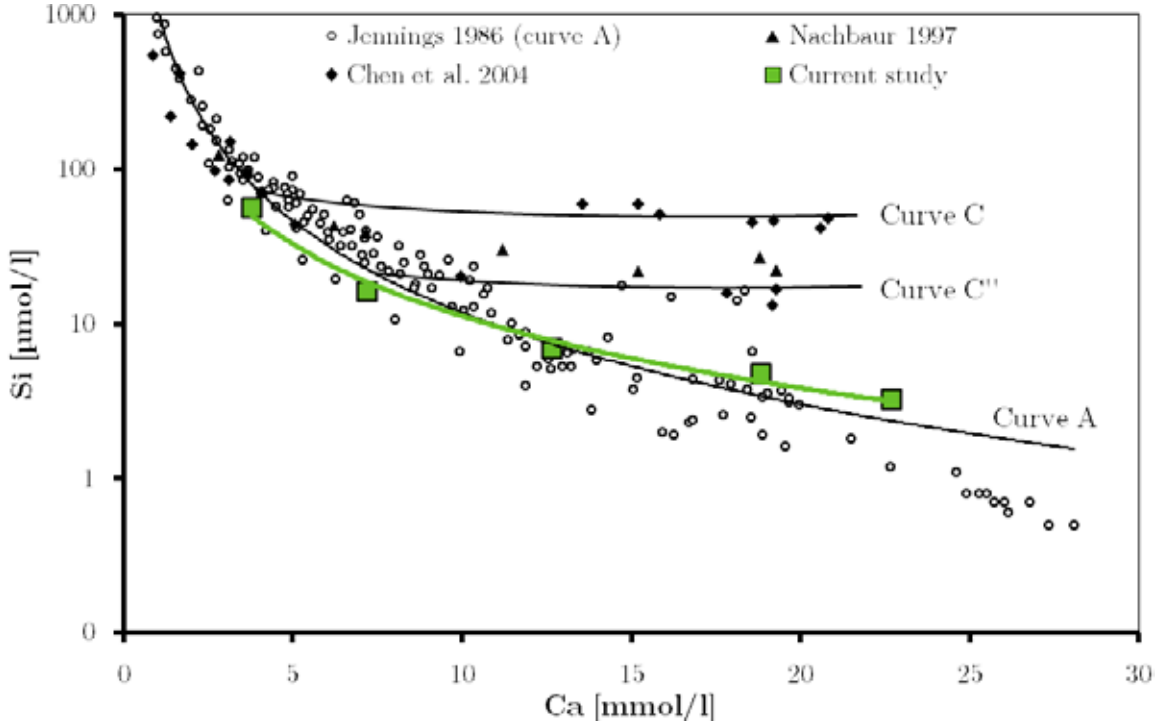

Fig. 4-17: Solubility of C-S-H phases synthesized in the present study (green filled squares) in comparison to published data. Curve A is drawn by Jennings[86], curve C and C'' by Chen et al.[32]. Data from Nachbaur[129] can be shown to fall on curve C''. The dissolution of C-S-H phases synthesized in the present study can widely be described by curve A.

In literature different solubilities of C-S-H phases are reported mainly due to the variable chemical composition of C-S-H phases studied. Barret and Bertrandie[15] refered data from Greenberg et al.[79] and Greenberg and Chang[78] to solubility of C-S-H phases termed 'curve (G)'. Based on data from Fuji and Kondo[61], Brown et al.[26], Halstead and Lawrence 1960, Barret and Bertrandie[16], Suzuki et al.[189], Flint and Wells[58], Roller and Ervin[164] and Taylor[194], Jennings[86] published a slight different solubility curve termed 'curve A', see Fig. 4-17. Later Chen et al.[32] postulated that additionally curve C, C' and C'' can be drawn.

Thereby curve C'' is based on data from Chen et al.[32] obtained by double decomposition experiments and additionally from Roller and Ervin[164] and Greenberg and Chang[78]. It can be demonstrated in Fig. 4-17 that data from Nachbaur[129] (mix of CaO and SiO_2 with water) surprisingly fall also on curve C''. In addition, curve C published by Chen et al.[32] is obtained by C-S-H formed by hydrating C_3S.

From the way of synthesis one would expect that the solubility of the C-S-H phases used in the present study should fall on curve C''. But it is shown by Fig. 4-17 that the solubility of C-S-H phases synthesized in the present study can be widely described by 'curve A'.

B Impact of superplasticizers on dissolution of C-S-H phases

General impact of superplasticizers

Data of the dissolution of C-S-H phases in presence of superplasticizers is documented in Table A- 5. Based on this the Ca-Si relationship is plotted in Fig. 4-18 for PCE1, PCE2 and PNFS. Abbreviations a,b and c refer to low, middle and high SP-dosages, respectively. Exact values are given in Table A- 5.

As demonstrated in Fig. 4-18 the addition of superplasticizers to C-S-H phases leads to an increase of the silicate ion concentrations in the aqueous phase. Generally PCE based superplasticizers shows a stronger effect on silicate ion concentration compared to PNFS. Furthermore, this effect is stronger at low calcium ion concentrations and increasing SP dosage for PCE1 and PNFS. In contrast at low dosage of PCE2 (series a) an increase in silicate ion concentration at increased Ca ion concentrations is observed. When PCE2 dosage is increased (series b and c) this effect vanishes. PNFS shows only at high dosages (series c)

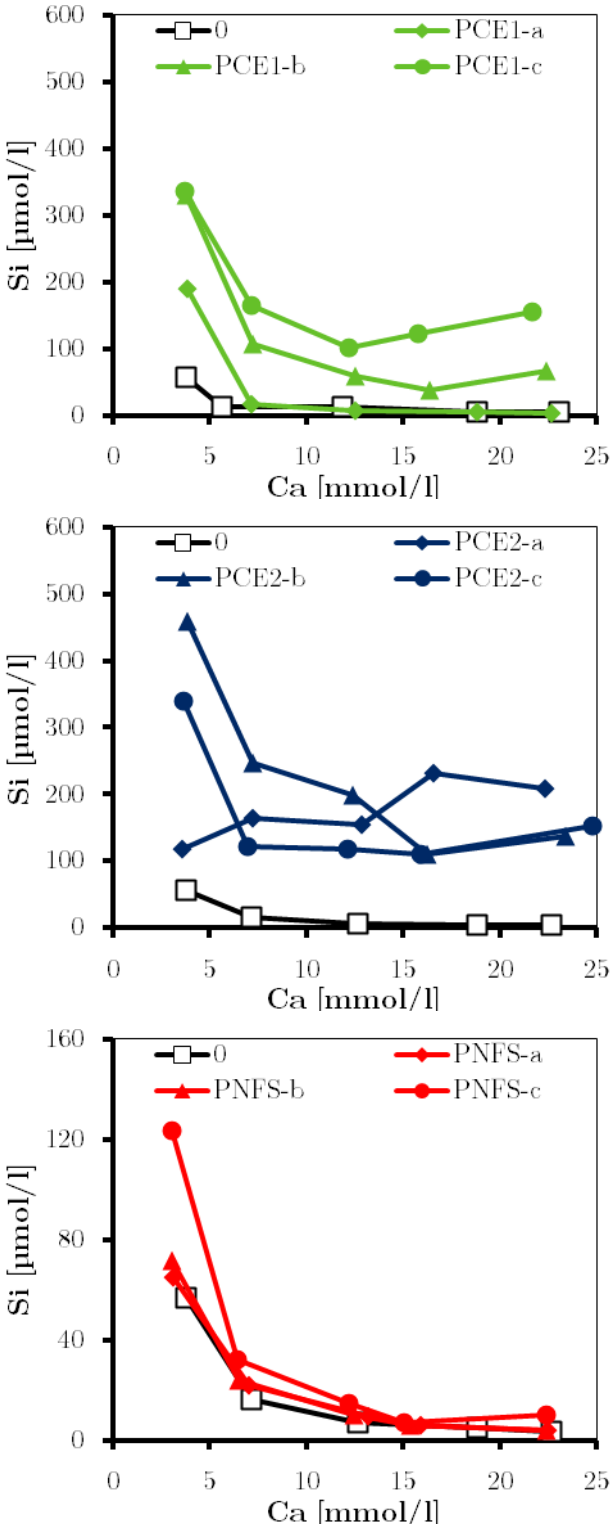

Fig. 4-18: Impact of superplasticizers (PCE1 (top), PCE2 (middle), PNFS (bottom)) at various dosages (a-low, b-middle, c-high, see Table A- 5) on Ca and Si concentrations in the aqueous phase of dissolving C-S-H. It can be seen that at low Ca concentration a larger amount of Si is released by C-S-H phases when SPs are present.

remarkable effects on C-S-H solubility. One can speculate on the role of the side chains in this respect. It is possible that the grafting of side chains results in increased dissolution of silicate ions since it was shown in chapter 4.1 (p.75) that sulfonic groups complex calcium ions to a larger extent compared to carboxy groups. But a clear statement can not be made since both polymer groups (PCE, PNFS) are too different in their molecular structure. All in all it can be concluded that the presence of superplasticizer induces changes in the ion concentrations of dissolving C-S-H phases.

In the following the increase in silicon and decrease in calcium concentration in the presence of superplasticizers is investigated in more detail. In particular the presence of foreign ions in solution (section 2.1.1 (p.23), sodium in case of the used SPs) and the interaction of anionic groups of polymers with calcium can result in changes in ion concentrations.

Role of sodium and calcium ion complexation capability on solubility of C-S-H phases

The addition of superplasticizers is associated with additions of sodium. For the investigated superplasticizers the sodium content is given in Table 3-1. As mentioned in chapter 2.1.1 (p.23) the presence of foreign ions can alter the activity of ions and thus increase the solubility of minerals by this mechanism. Furthermore, foreign ions can exert interactions with single ions that contribute to the solubility product of mineral phases. In case of C-S-H this is observed with OH^- ions that interact with Ca^{2+} released by C-S-H phases and sodium added with SPs. Therefore, the observed effect of increased silicate ion concentration in the aqueous phase may be related to the presence of sodium in solution. In order to test this hypothesis a C-S-H phase with distinct chemical composition is postulated. For this, the model according to Fuji and Kondo[60] is used for C-S-H phases that exhibit Ca/Si molar ratio of 1.4. Based on that we can propose the following chemical composition:

$$(0.833 + x)\,Ca(OH)_2\ SiO_2\ 0.917H_2O \tag{36}$$

By means of thermodynamic data of Babuskin et al.[10] the free enthalpy of formation of C-S-H phases with Ca/Si of 1.4 can be computed to -2361.9 kJ/mol. In the next step the solubility product of this C-S-H phase can be calculated in accordance to the following equation.

$$1.4(Ca(OH)_2\ SiO_2\ 0.917H_2O + 0.083H_2O \Leftrightarrow 1.4Ca^{2+} + H_3SiO_4^- + 1.8OH^- \tag{37}$$

For this reaction ΔG_r is determined to 72.04 kJ/mol. Finally, eq. (6) can be used to compute the solubility product, i.e. log K_{SP}=-12.62.

Taking eq. (37) and K_{SP} into account the impact of sodium on silicate ion concentration can be evaluated. These calculations were performed with PHREEQC[143] (phreeqc.dat) software for a sodium concentration of 5 mmol/l which slightly exceeds the maximum measured value (Table A- 5) at a constant pH of 12.09 (pH slightly decreases with the addition of SPs as documented in Table A- 5). Results are shown in Table 4-5.

Values in Table 4-5 indicate that the addition of 5 mmol/l sodium to the aqueous phase of dissolving C-S-H would lead to an increase in silicate ion concentration of 5%. The comparison to measured values reveal that in case of water as starting solution (series 1) silicate ion concentration increases in the range between 15 and 814 %. This demonstrates that solely the impact of sodium is to low to account for the strong increase in silicate ion concentration.

Table 4-5: Influence of sodium addition on the silicate ion concentration during dissolution of C-S-H phases for a hypothetic C-S-H composition (eq. (37)).

Na ion concentration [mmol/l]	Silicate ion concentration [µmol/l]	$Si^{without\ Na}/Si^{with\ Na}$
0.0	12.1	1.05
5.0	12.7	

Therefore and most probably, the presence of the polymers is mostly responsible for the increase in solubility of C-S-H phases and not sodium. In this respect, a clear relationship between added number of functional groups and variation in silicate ion concentration in the aqueous phase was not found. However, it is most probable that the increased silicate ion concentrations are caused by artifacts. This issue is discussed in more detail in forthcoming section 4.3.3 (p.141). Similarly to the experiments presented in the present section it is shown in section 4.3.3 that C-S-H phases formed during C_3S hydration surpasses the filter and increases ion concentrations due to dissolution prior to ICP-OES measurements. Taken this effect into account then an increase in silicate ion concentration of 500 µmol/l causes theoretically an increase of calcium ion concentration of 0.7 mmol/l (if molar Ca/Si of 1.4 is used for calculation). Because of lower sensitivity of the ICP-OES measurements at high Ca ion concentrations this artifact is more pronounced when silicate ion concentrations are considered since the sensitivity for silicon is much higher in lower concentrations.

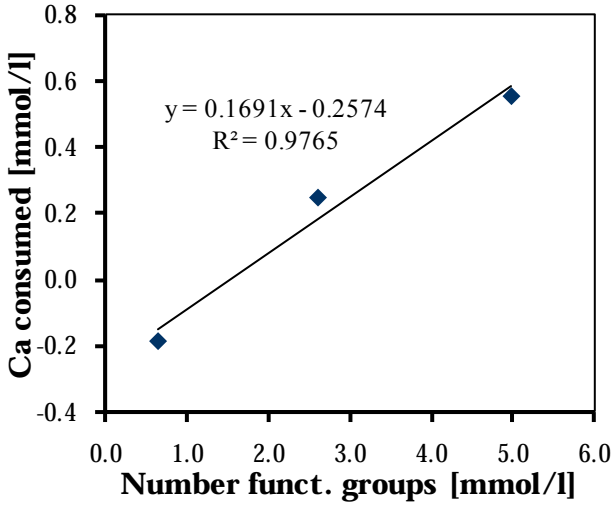

Fig. 4-19: Calcium ion consumption by polymers in dependence on the number of added functional groups for PCE2 during dissolution of C-S-H (series 3).

Besides silicon also calcium concentrations in the aqueous phase of dissolving C-S-H phases are varied in the presence of SPs. Fig. 4-19 demonstrates exemplarly on PCE2 (series 3) that with added number of functional groups the calcium ion concentration decreases. This indicates that the aforementioned artifacts (presence of sodium, insufficient filtering) are overcompensated by the polymers. Here we want to focus on the role of the complexation capability of polymer's functional groups on decreased calcium ion concentrations. To account for this effect the solubility data is examined in terms of slope of the linear fit (Ca consumed vs. number of functional groups). Results are presented in Table 4-6.

Table 4-6: Slope (R^2 in parentheses) of linearly fit between consumed Ca and number of functional groups [mmol/l] during dissolution of C-S-H in different calcium concentrations of the starting solution (series 1-5).

Series	Ca^{2+} in aq. phase of the reference sample	Slope (R^2)		
		PCE1	PCE2	PNFS
1	3.8	0.0216	-	0.0062
		(0.9744)	(0.0019)	(0.7015)
2	7.2	0.0352	0.0668	0.0282
		(0.9543)	(0.7936)	(0.8621)
3	12.7	0.0558	0.1691	0.0448
		(0.9096)	(0.9765)	(0.8853)
4	18.8	0.0928	0.1829	0.0462
		(0.8069)	(0.9957)	(0.9925)
5	22.7	-	-0.5912	0.0021
		(0.0027)	(0.9286)	(0.8573)

Because of the limited data set only trends can be inferred. Slopes of the curves with very low correlation coefficient are excluded in Table 4-6. Nevertheless, by omitting series 5 (which obviously show no correlations to all other series) it is documented that the slope of the linear curve increases with increasing calcium ion concentration in the aqueous phase. This is observed for all tested superplasticizers and can mathematically expressed by

$$\frac{dCa}{dL} = -k \cdot Ca \tag{38}$$

With dCa the decrease of the calcium ion concentration in the aqueous phase, L the ligand concentration and the slope k. Integration of eq. (38) leads to

$$\begin{aligned} d\ln(Ca) &= -k \cdot dL \\ Ca &= Ca_0 \cdot e^{-k \cdot L} \end{aligned} \tag{39}$$

with Ca_0 the calcium ion concentration of the starting solution.

The comparison of the polymers reveals that PCE2 shows the highest slopes followed by PCE1. The increase of the slope leads to conclude that the affinity between functional groups and calcium ions increases. Whereas the pH of the aqueous phase increases with calcium ion concentration of the starting solution (see Table A- 5) this may be the result of increased dissociation of functional groups of the polymers which was also discussed in section 4.1.3.2 and shown by others[206]. Thus, it is concluded that compared to PCE1 PCE2 is more effective at removing calcium ions per unit charge of the polymer. This may be caused by the fact that PCE2 needs more calcium ions for adsorption.

Similar values for the corresponding slope during complexation experiments in $CaCl_2$ solution (section 4.1.3, p.84) were found in case of PCE2. This indicates that PCE2 shows similar behavior in C-S-H dissolution experiments and in complexation tests with $CaCl_2$. But this effect is much weaker for PCE1 and PNFS which reach only about 54 % and 34 %

of the slopes in $CaCl_2$ experiments, respectively. This observation leads to conclude that either a fraction of polymers is adsorbed on the C-S-H surface or the ability for calcium complexation by polymer's functional groups during C-S-H dissolution is dependent on a further structural parameter of PCEs. This may be the presence and length of grafted side chains. This hypothesis is supported by values shown in Table 4-6 which reveal that highest slopes are found for PCE2 followed by PCE1 in all tests. In accordance, PNFS without side chains shows lowest slopes.

4.2.3.2.2 Solubility of portlandite

A Reference without superplasticizers

Compared to C-S-H phases the dissolution of portlandite is less complex. The calcium ion concentration of the reference without superplasticizer was determined to 20.1±0.4 mmol/l at a pH of 12.47 and 20°C.

B Impact of superplasticizers on solubility of portlandite

Results of the experiments on dissolution of portlandite in the presence of superplastcizers in dependence on the number of functional groups added with the polymers are shown in Fig. 4-20.

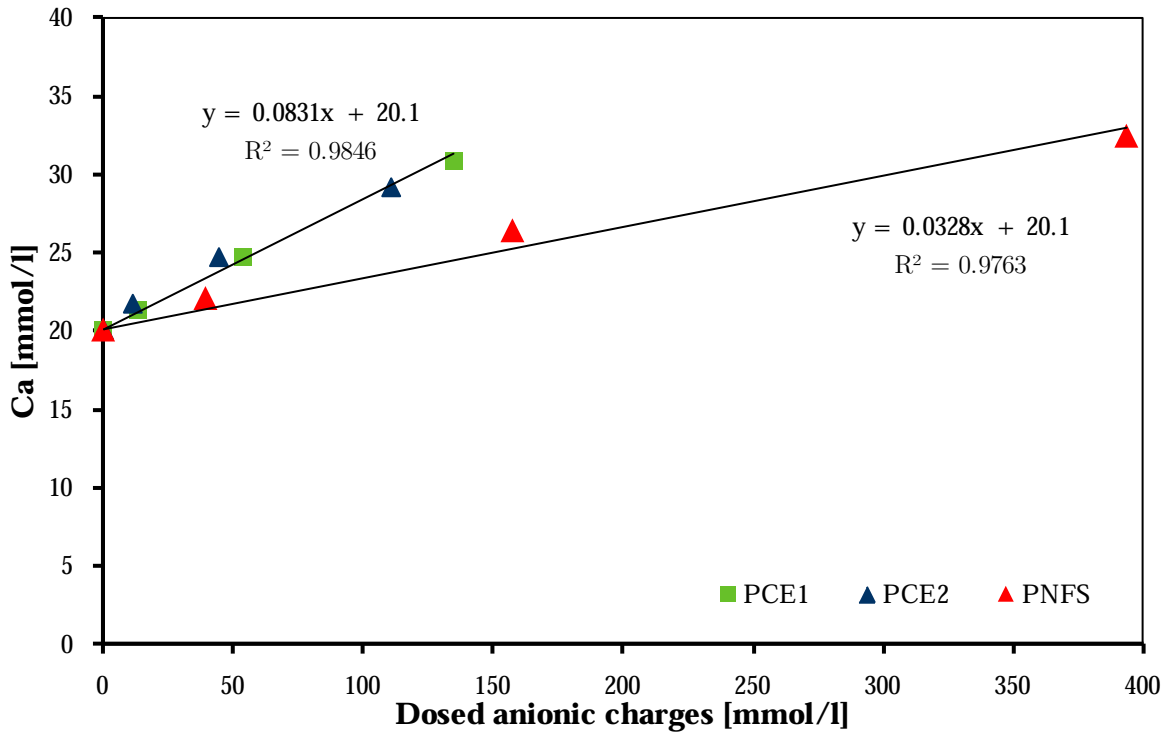

Fig. 4-20: Impact of superplasticizers on the Ca ion concentration during portlandite dissolution determined by shaking supersaturated solutions containing solid portlandite. It is observed that superplasticizer enhance the solubility of portlandite with stronger impact of PCEs than PNFS.

As shown in Fig. 4-20 the addition of superplasticizers leads to an increase in calcium ion concentration in dependence on type and dosage of superplasticizer. This is in contrast to experiments regarding dissolution of C-S-H and complexation tests in $CaCl_2$ where in both cases a decrease in calcium ion concentration was measured. It may be surprising why in

case of portlandite the presence of polymers increase calcium ion concentration and not in the other cases. Obviously, in $CaCl_2$ solution calcium ions are screened by the functional groups and no additional source is present that impacts ion concentrations. In case of C-S-H phases and portlandite the change in calcium ion concentration in the aqueous phase may be explained by adsorption of polymers. It is reasonable to assume that polymers need to complex calcium from solution in order to be able to adsorb on C-S-H phases. As a result calcium ion concentrations decrease in C-S-H solubility experiments. In contrast, portlandite seems to compensate the calcium ion complexation predominantly by additional release of calcium ions into solution. Accordingly, the adsorption of polymers on portlandite may be weaker compared to C-S-H. This, however, can be explained by the surface area which is larger for C-S-H phases as compared to portlandite.

With respect to the role of polymer architecture this interpretation can be extended. As indicated by the linear fits in Fig. 4-20 the impact of superplasticizers on solubility of portlandite can be related to the type of functional group of the polymers. Comparing the slopes it is revealed that carboxy groups cause release of calcium ions in more extent as compared to sulfonic groups. This is in accordance to findings deduced from C-S-H solubility experiments (cf. Table 4-6) and in experiments addressing complexation of calcium in $CaCl_2$ solutions (section 4.1.3 (p.84)). There it was shown that only at very low polymer dosages the ability to complex calcium ions is stronger for sulfonic groups compared to carboxy groups (cf. Fig. 4-11 and Fig. 4-12). At higher dosages this relation turns over.

In the following only changes in calcium ion concentration are considered without taken into account if these are reduced or increased compared to the reference. From the slopes in Fig. 4-20 it can be deduced that in case of portlandite lower calcium ion concentrations are screened by polymer's functional groups as compared to C-S-H phases. Hence, 12 carboxy groups are needed to release 1 additional calcium ion from the portlandite crystal. This number is 30 in case of sulfonic groups. Therefore it can be concluded that the impact of superplasticizers on the solubility of C-S-H phases is by factor 2 stronger compared to portlandite. Again this may be the result of different degree of adsorption of polymers, and thus different amounts of non-adsorbed polymers in the aqueous phase that changes calcium ion concentration in solution.

C Determination of complexation constants

The increase in calcium ion concentration during portlandite dissolution in presence of superplasticizers can be expressed by complexation constants introduced in eq. (35) for neutral ($K_{C,0}$) and positively charged complexes ($K_{C,+}$). Therefore, data given in Table 4-7 is plotted linearly (increase in calcium ion concentration as a function of dosed functional groups going through the origin) in order to compute the slopes for each SP. The slope values are 0.081 (R^2=0.9983), 0.0866 (R^2=0.9691) and 0.0328 (R^2=0.9758) for PCE1, PCE2 and PNFS, respectively. With these slopes the complexation constants were determined using ion activity coefficients (γ_1, γ_2) calculated by means of the software PHREEQC[143] (phreeqc.dat). In the right rows of Table 4-7 the values of the complexation constants are given.

Table 4-7: Increase in Ca ion concentration during portlandite (Ca=20.1±0.4 mmol/l) solubility experiments in dependence on the SP dosage and corresponding complexation constants (according to eq. (35)).

Superplasticizer	Dosage		Ca [mmol/l]	Log $K_{C,0}$	Log $K_{C,+}$
	SP [g/l]	Functional groups (ligand) [mmol/l]			
PCE1	0.5	13.5	21.3±0.7		
	2	53.9	24.7±0.6	-1.2	0.3
	5	134.8	30.9±2.1		
PCE2	0.5	11.0	21.8±0.1		
	2	44.2	24.8±1.0	-1.2	0.3
	5	110.4	29.2±1.8		
PNFS	0.5	39.4	22.1±1.1		
	2	157.4	26.4±0.2	-1.7	0.4
	5	393.6	32.5±0.3		

It can be seen in Table 4-7 that PCEs show similar complexation constants which is expected from Fig. 4-20 (PCE1 and PCE2 fall on a same linear function). Thereby the values of the complexation constants for neutral complexes for PCEs are higher as compared to the PNFS. This indicates that within these complexes calcium ions are screened in more extend by carboxy then by sulfonic groups. However, in the positively charged complexes calcium is screened by both functional groups in equal numbers. Also the values of the complexation constants for positively charged complexes are higher as compared to the neutral complexes. Compared to the complexation constants determined in $CaCl_2$ solution the values of the corresponding constants determined during portlandite solubility experiments are lower, cf. Table 4-3 and Table 4-7. For example the neutral complexation constants for carboxy groups are -1.2 and -0.7 determined in the experiments with portlandite and $CaCl_2$ solution, respectively. This difference may be the consequence of polymer adsorption on portlandite which further supports the discussion of adsorption of polymers on C-S-H phases and portlandite during solubility testing. Following that, the differences in complexation constants during portlandite experiments between sulfonic and carboxy groups may be the result of two effects. Either adsorption of PNFS is stronger than adsorption of PCEs and/or PNFS needs less calcium ions to be able to adsorb. Thus, the not adsorbed polymers seem to increase solubility.

From literature data it can be deduced that the solely impact of sodium on solubility of portlandite is too low to account for the observed values. For example[196] the presence of 50mM NaCl causes an increase of portlandite solubility of 8% which is significant lower than the measured increase in solubility in presence of SPs exhibiting lower amounts of sodium.

4.2.3.3 Summary

In the present section the solubility of C-S-H phases (prepared in section 4.2.2 (p.93)) and portlandite in presence of superplasticizers was investigated. Data reveal that superplasticizers induce changes in concentrations of ions in the aqueous phase of dissolving C-S-H phases and portlandite. These changes are based on interactions between polymer's functional groups and calcium ions with minor impact of sodium ions introduced with the polymers. Thereby carboxy groups show stronger affinity to calcium as compared to sulfonic groups. The mechanism of changes in ion concentration was discussed in the light of adsorption of polymers on C-S-H phases and portlandite. In this respect it was discussed that during solubility experiments polymers may complex calcium ions from solution before they can adsorb. Thereby the adsorption is much stronger on C-S-H phases as compared to portlandite which may be the result of the larger surface area of C-S-H. This data interpretation was supported by computing complexation constants. Because compared to the corresponding constants determined in $CaCl_2$ solution (where no adsorption occurs) it was shown that a lower number of calcium ions is complexed during the experiments on portlandite solubility. Increased silicate ion concentrations during dissolution of C-S-H phases are discussed in terms of artifacts during sample preparation. It is finally postulated that the presence of superplasticizers leads to an increased solubility of both C-S-H phases and portlandite by not-adsorbed superplasticizers in dependence of the added number of functional groups.

4.2.4 Unconstrained dissolution rate of tricalcium silicate

Results in section 4.2.3 (p.94) showed that superplasticizers have an impact on solubility of hydrate phases that are formed during hydration of tricalcium silicate the main constituent of OPC clinker. The present section is aimed at investigating if the dissolution rate of tricalcium silicate is affected by superplasticizers. This permits discussion whether or not retardation of C_3S hydration is caused by hindered dissolution of tricalcium silicate.

4.2.4.1 Experimental setup

Unconstrained dissolution of C_3S was investigated *ex-situ* in highly diluted suspensions (batch) in order to stem the precipitation of C-S-H phases on the C_3S surface. Therefore an interaction of dissolution and precipitation of hydrates can be excluded and a pure C_3S dissolution is obtained. Accordingly, liquid/solid ratios of up to 2000 were chosen. For each experiment the volume of the solution was 400 ml. The experiments were performed at 25 °C in glass beaker (800 ml, diameter=95 mm) in N_2 atmosphere (glove box) in order to prevent carbonatization. The suspensions were stirred with a stir bar coated with Teflon at

constant stirring rate of 600 rpm. Starting solutions were either doubly deionized water or saturated calcium hydroxide solution. Both were washed with nitrogen to remove carbon dioxide. Superplasticizer was added to the starting solutions before the C_3S. Subsequently the experiment was started with the addition of C_3S to the solution. After appropriate time periods, samples of approx. 6 ml were withdrawn using syringes equipped with syringe filter (0.22 µm). Subsequently, the solution was acidified with approximately 0.2 ml of a 5M HNO_3 in order to prevent precipitation of product phases. After the measurement with ICP-OES the concentration was corrected due to the dilution induced by the acidification. Using software (Origin v8.0773, OriginLab cooperation, USA) the silicon concentrations versus time were fitted with an exponential equation, i.e. mathematical fit, cf. Fig. 4-21. Dissolution rates were calculated from the first derivative of these functions. Subsequently these derivatives were normalized to the initial C_3S BET surface area. In this calculation the decrease in absolute C_3S surface area during the dissolution was mathematically approximated. As can be seen in Fig. 4-21, the dissolution rate descends with time.

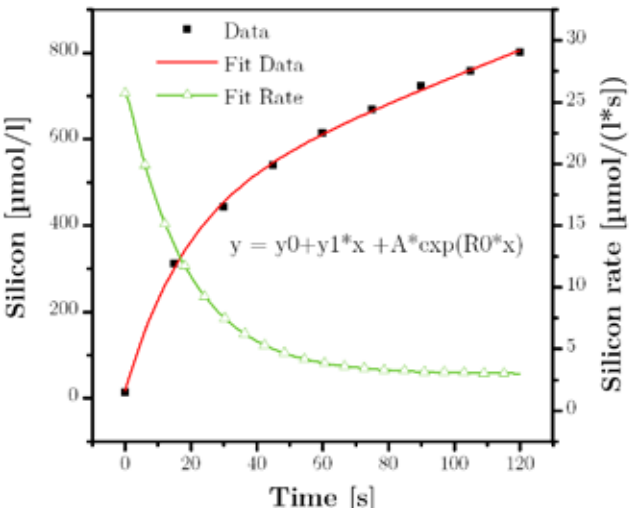

Fig. 4-21: Typical evolution with time of silicon during the C_3S dissolution at high l/s ratio (l/s=2000). Squares and line represent data and data fit, respectively. Right hand axis shows the first derivative (silicon rate) of the fit (triangles).

4.2.4.2 Results and discussion

4.2.4.2.1 Impact of environmental parameters

A Liquid to solid ratio

Fig. 4-22 shows the calculated C_3S dissolution rate in dependence of time (left hand) and Ca concentration of the solution (right hand) for different l/s ratios. All data from measured ion concentrations are listed in Table A-6 to Table A-11 in the appendix.

The unconstrained dissolution rate of C_3S in water as starting solution decreases in dependence of time and l/s ratio (Fig. 4-22). At l/s ratio of 500, 1000 and 2000 the unconstrained dissolution rate of C_3S in the beginning of the experiments measures 76±25, 97±26 and 85±5 µmol/(sm²), respectively. Taking the standard deviation into account, C_3S dissolves unconstrained in water at a mean maximum rate of 86 µmol/(sm²), which represents the rate constants for C_3S dissolution, cf. eq. (9) and (12). Whereas unconstrained dissolution rates of C_3S at l/s of 500 and 1000 differ only slightly over time, at l/s=2000 increased unconstrained dissolution rates of C_3S especially at t>20 s are measured.

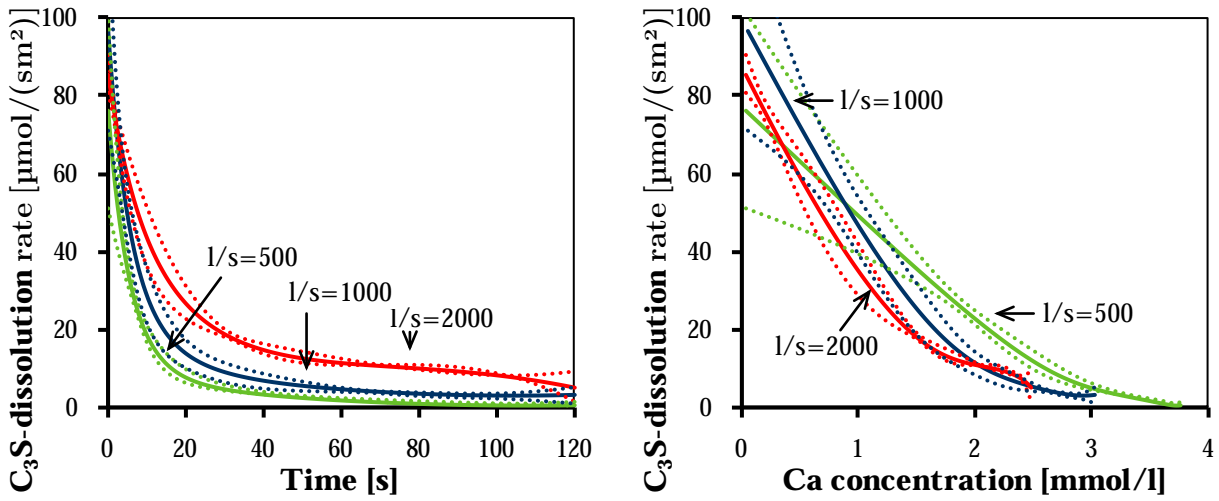

Fig. 4-22: C_3S-dissolution rate in dependence of time (left hand) and evolving Ca concentration of the solvent (right hand). Standard deviation indicated by dotted lines was determined on 4 (l/s=500) and 3 (l/s=1000 and 2000) different samples. It is shown that C_3S dissolution rate decreases with time and decreasing l/s ratio. This observation can in first approximation be related to the Ca ion concentration in the aqueous solution.

Right hand graphic of Fig. 4-22 shows the unconstrained dissolution rate of C_3S in dependence of evolving Ca ion concentration of the aqueous phase. In general, unconstrained dissolution rate of C_3S decreases with increasing Ca ion concentration of the aqueous phase. If Ca ion concentration exceeds 2.5 mmol/l the dissolution rate measures only 1 to 5 µmol/(sm²). Moreover when standard deviations are considered, impact of l/s ratio can be explained by the Ca ion concentration in aqueous solution. Because the dissolution rate is restricted to Ca ion concentration of the aqueous phase, C_3S has to dissolve for longer time periods to reach certain Ca concentrations in the aqueous phase when the l/s ratio increases. For example after 80 s of dissolution the Ca ion concentration in the aqueous phase measures 3.6, 2.7 and 2.1 mmol/l for l/s of 500, 1000 and 2000, respectively. For these l/s ratios the dissolution rates measures 1.2, 3.4 and 10.1 µmol/(sm²), respectively. In summary, the l/s ratio directly impacts the deceleration (slope of the rate vs. time curve). Thus, with increasing l/s ratio the increased dissolution rates at the beginning of the experiment decrease more slowly. Moreover, the C_3S dissolution rate is significantly reduced when Ca ion concentration increases from 0 to 2.5 mmol/l in the aqueous phase but only slightly if Ca concentration is increased above 2.5 mmol/l, see Fig. 4-22 (right hand).

B Ca ion concentration in the starting solution

Table 4-8 shows the rate constants for unconstrained dissolution of C_3S in dependence of the calcium concentration of the starting solution at l/s ratio of 1000.

The unconstrained C_3S dissolution rate of 97±26 µmol/(sm²) in water is reduced to 0.7±0.25 µmol/(sm²) in presence of approx. 22 mmol/l Ca in the starting solution. This demonstrates furthermore the strong influence of Ca on the dissolution rate of C_3S.

Table 4-8: Influence of calcium ion concentration of the starting solution of unconstrained dissolution rate of tricalcium silicate.

Ca ion concentration [mmol/l]	C_3S dissolution rate [µmol/(sm²)]]
0.0	97±26
22.0	0.7±0.25

Results of the present work are in accordance to previous findings[47, 106, 110] outlined in detail in section 2.1.2 (p.25). Whereas inherent parameters (e.g. particle size, specific surface area) were kept constant in this study, the impact of environmental parameters on C_3S dissolution rate was demonstrated. Accordingly, during dissolution of C_3S the l/s ratio and the presence of superplasticizers were varied. It was shown that according to general findings[47, 106, 110], the presence of Ca (as inherent ion in the solute) decreases the dissolution rate of C_3S. Starting in water, C_3S dissolves on increased rate. This is in accordance to general findings outlined in chapter 2.1.2 and results by Pourchet *et al.*[155] and Nicoleau and Nicoleau *et al.*[133-134].

4.2.4.2.2 Influence of superplasticizers on C_3S dissolution rate

Because the standard deviation for unconstrained dissolution rate of C_3S was lowest at l/s ratio of 2000, the impact of superplasticizer on the C_3S dissolution rate was investigated at this ratio. Fig. 4-23 shows the impact of superplasticizer dosage on the C_3S dissolution rate in water as starting solution. Here, only PCE1 was investigated.

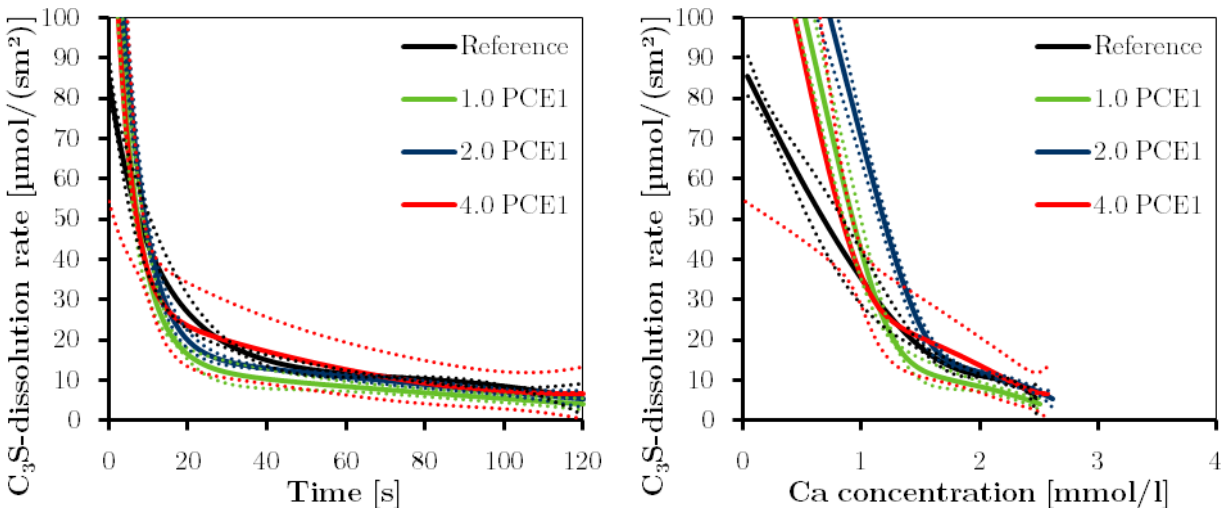

Fig. 4-23: Influence of PCE1 dosage (given in legend as g_{SP}/g_{C3S}) on unconstrained dissolution rate of C_3S in dependence of time (left hand) and evolving Ca ion concentration in the aqueous phase (right hand) for l/s ratio of 2000. Confidence intervals determined on 3 different samples are given using ± 1 sigma and are indicated by dotted lines. No clear impact of superplasticizer dosage on unconstrained C_3S dissolution rate is observed.

Results in Fig. 4-23 (left hand) show no significant variation in the C_3S dissolution rate with time when superplasticizer dosage is increased. But as a general feature the standard deviation increases when SPs are added. Similar results are gathered for the impact of the evolving calcium ion concentration on the C_3S dissolution rate in presence of various

dosages of superplasticizer PCE1, cf. Fig. 4-23 (right hand). But here a slight increase in dissolution rate is observed. This may be related to the complexation of calcium ions in solution which seems to promote dissolution rate as discussed before.

The impact of the molecular architecture of different superplasticizers on the rate of unconstrained dissolution of C_3S is shown in Fig. 4-24 for dissolution starting in water and SP dosage of 4.0 g_{SP}/g_{C3S}.

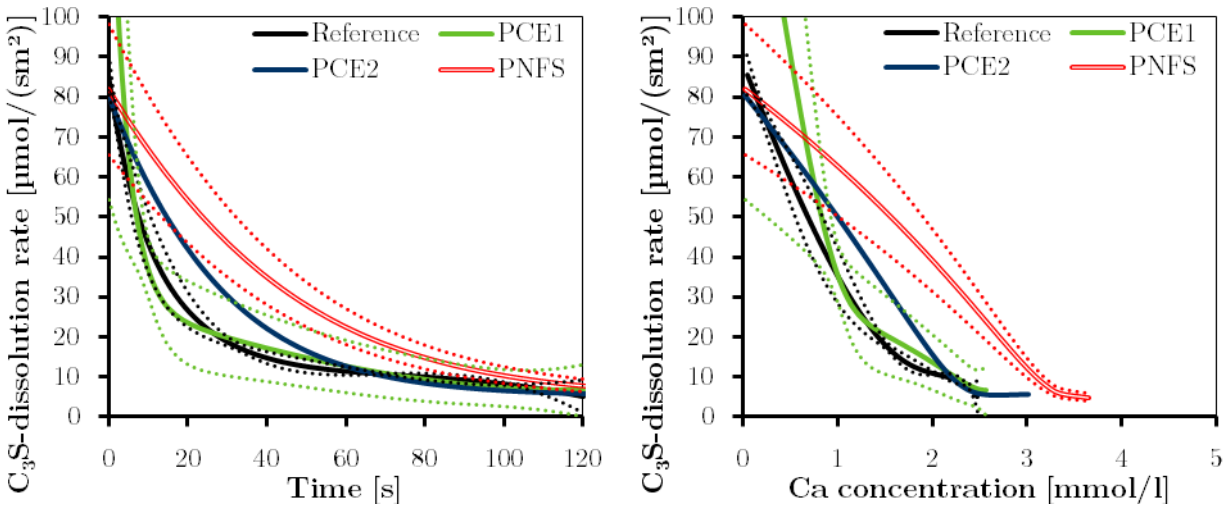

Fig. 4-24: Influence of superplasticizer addition on unconstrained dissolution rate of C_3S in dependence of time (left hand) and evolving Ca concentration of the aqueous phase (right hand) for experiments in water and 4.0 g_{SP}/g_{C3S} SPs as starting solution. Confidence intervals determined on 3 different samples are given using ± 1 sigma and are indicated by dotted lines. Variations in polymer architecture have a minor impact on C_3S dissolution rate.

Left hand graph of Fig. 4-24 shows the decreasing C_3S dissolution rate with time, which is affected by the presence of superplasticizer. For clearness the standard deviation is only shown for two superplasticizers, but under its consideration no significant difference between all samples can be found, especially at the beginning and the end of the experimental run. In this interim section of the experiment PNFS causes increased dissolution rate compared to PCEs. Here the increased calcium complexation capability determined in section 4.1.3 (p.84) may account for this behavior. But generally, a clear dependence of molecular architecture and dissolution rate is not deduceable. Only a strong influence of the evolving Ca ion concentration of the aqueous phase on unconstrained dissolution rate of C_3S was furthermore found, cf. right hand graph of Fig. 4-24.

Results of C_3S dissolution in the presence of superplasticizer and saturated calcium hydroxide solution are depicted in Fig. 4-25.

Results in Fig. 4-25 (left hand) show once again that C_3S dissolves unconstrained at a lower rate if saturated $Ca(OH)_2$ solution is the starting solution. During 120 seconds the rate decreases not linearly from 1 µmol/(sm²) to 0.08 µmol/(sm²) for the reference. In contrast, if superplasticizers are present the unconstrained dissolution rate of C_3S decreases linearly with time for PNFS based superplasticizer. Despite of that, PCE based superplasticizers induce a constant unconstrained dissolution rate with time in saturated calcium hydroxide solution. But at later time periods (i.e. increased Ca ion concentration) superplasticizers induce higher unconstrained dissolution rates of C_3S with respect to the reference. The

influence of the evolving Ca ion concentration in the aqueous phase on the unconstrained dissolution rate of C_3S is shown in Fig. 4-25 (right hand). Independent on the superplasticizer addition, similar ranges of the C_3S dissolution rate (0.2 to 1.0 µmol/(sm²)) at Ca concentrations of approx. 21 mmol/l were determined. Thus, clear evidence neither on hindered nor on promoted dissolution rate in presence of superplasticizer can be deduced from the experimental data derived from $Ca(OH)_2$ solution as starting solution.

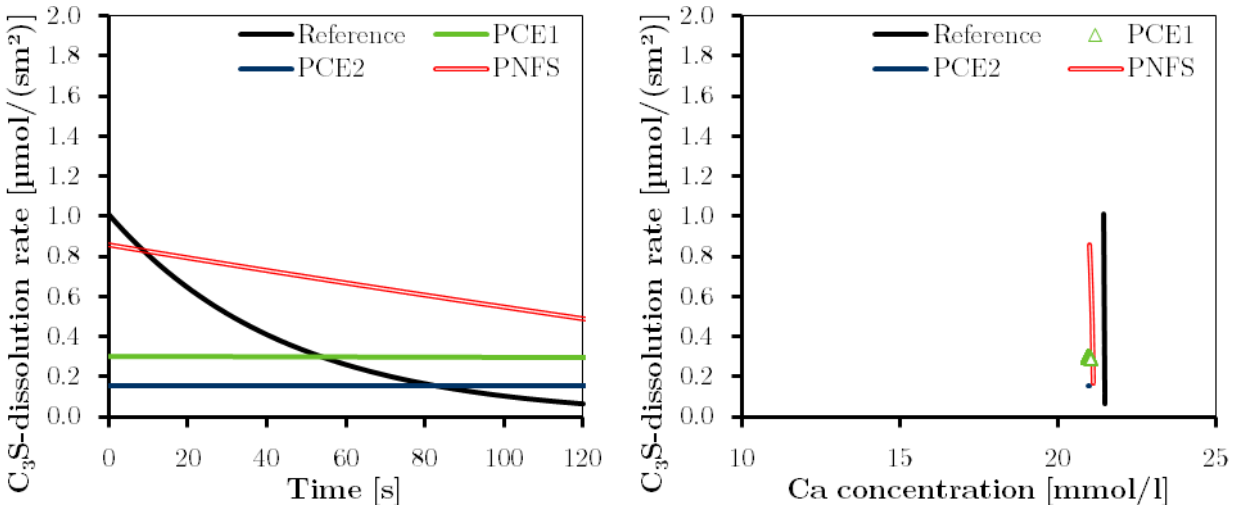

Fig. 4-25: Influence of superplasticizer addition (4.0 g_{SP}/g_{C3S}) on unconstrained dissolution rate of C_3S in dependence of time (left hand) and evolving Ca concentration of the aqueous phase (right hand) started in saturated calcium hydroxide solution. No clear effect of SPs on unconstrained dissolution rate of C_3S in saturated $Ca(OH)_2$ solution is observed.

Table 4-9 compares maximum dissolution rates of C_3S measured in the present work with published values. Furthermore, the impact of the starting solution is given.

Table 4-9: Maximum C_3S dissolution rate [µmol/(sm²)] in different starting solutions.

SP	SP conc. [g_{SP}/g_{C3S}]	Max. rate in water (l/s ratio)		Max. rate in saturated $Ca(OH)_2$ solution (l/s ratio)		Author
-	0	14	(5000)	-		Gartner *et al.* [71]
-	0	120	(50000, 10000)	0.68	(10000)	Nicoleau[134]
-	0	60	(>100000)	0.2	(250)	Nicoleau[133]
				0.25	(500)	
-	0	11	(0.5)	0.05	(0.5)	Damidot *et al.*[37]
-	0	76	(500)	-		Present work
-	0	97	(1000)	0.7	(1000)	Present work
-	0	85	(2000)	-		Present work
PCE1	1	164	(2000)	-		Present work
PCE1	2	175	(2000)	-		Present work
PCE1	4	160	(2000)	0.3	(2000)	Present work
PCE2	4	80	(2000)	0.2	(2000)	Present work
PNFS	4	82	(2000)	0.9	(2000)	Present work

Results in saturated $Ca(OH)_2$ solution are generally 1-2 orders of magnitude reduced compared to dissolution in water. The scatter of data by various studies shown in Table 4-9 indicate that experimental setup is critical point. Moreover the fitting parameters of raw data in order to calculate dissolution rate may also influence the value of dissolution rate. Rates given by Nicoleau[133-134] are in same order of magnitude as in the present work. But values for experiments in saturated calcium hydroxide solution show by factor of ~2 higher values between those given by Nicoleau[133] and present values. Recently published values from Nicoleau[134], however, are similar to those measured in the present study. Distinctively lower values are reported by Gartner *et al.*[71] and Damidot *et al.*[37] for both water and saturated $Ca(OH)_2$ solution as starting solution. The comparison of results shows that discussion on dissolution needs a clear distinction on the environmental conditions. Nevertheless comparison of all results reveals a striking influence of Ca ion concentration (ion activity product) on the dissolution process of C_3S as predicted by the dissolution theory outlined in section 2.1.2 (p.25).

As stated in section 2.1.1 (p.23), the dissolution rate of minerals is dependent on the degree of undersaturation of the system. To account for this behavior in the following the ion concentrations in aqueous solution are expressed as ion activity product (IAP) for the following reaction:

$$Ca_3SiO_5 \rightarrow 3Ca^{2+} + H_4SiO_4 + 6OH^- \qquad (40)$$

According to eq. (40) in Fig. 4-26 the dissolution rate of C_3S is plotted in dependence of the IAP. The data is extended to the impact of calcite ($17.8\ m^2_{calcite}/g_{C3S}$) at similar l/s ratio of 2000. Furthermore, published data from Nicoleau et al.[134] is also examined.

As expected from theory, the dissolution rate of C_3S decreases with increasing IAP. As shown in Fig. 4-24, PCE1 leads to increased dissolution rate of C_3S compared to the reference at low IAP. This is similar to findings for dissolution of earth minerals by plants[171, 186] and hydroxyl apatite in human teeth[167]. As already stated by Kirby and Lewis[99] and Pourchet *et al.*[155] and analogous to solubility of C-S-H phases and portlandite (section 4.2.3 (p.94)), the calcium complexation capability of not adsorbed polymers may be responsible for this behavior. Because of their high dosage it is expected that the majority of the superplasticizers is not adsorbed on C_3S. Analytically, this complexation should result in increased C/S molar ratios in the aqueous phase. In fact, especially at the beginning of the experiment increased values for C/S are measured for PCE2 and PNFS, but not for PCE1 (remains at 3.0), see Table A- 9 and Table A- 10 in the appendix. If we assume that no polymer is adsorbed on C_3S then, under consideration of the calcium complexation capability determined in section 4.1.3 (p.84), a lower IAP is calculated (dotted lines in Fig. 4-24). This result means that at similar IAP the dissolution rate is reduced. By that we see that PCE1 reduces the C_3S dissolution rate also at high IAP. More clearly are the cases of PCE2 and PNFS. Both reduce the C_3S dissolution rate very strongly. Interestingly also the presence of calcite reduces the dissolution rate of C_3S.

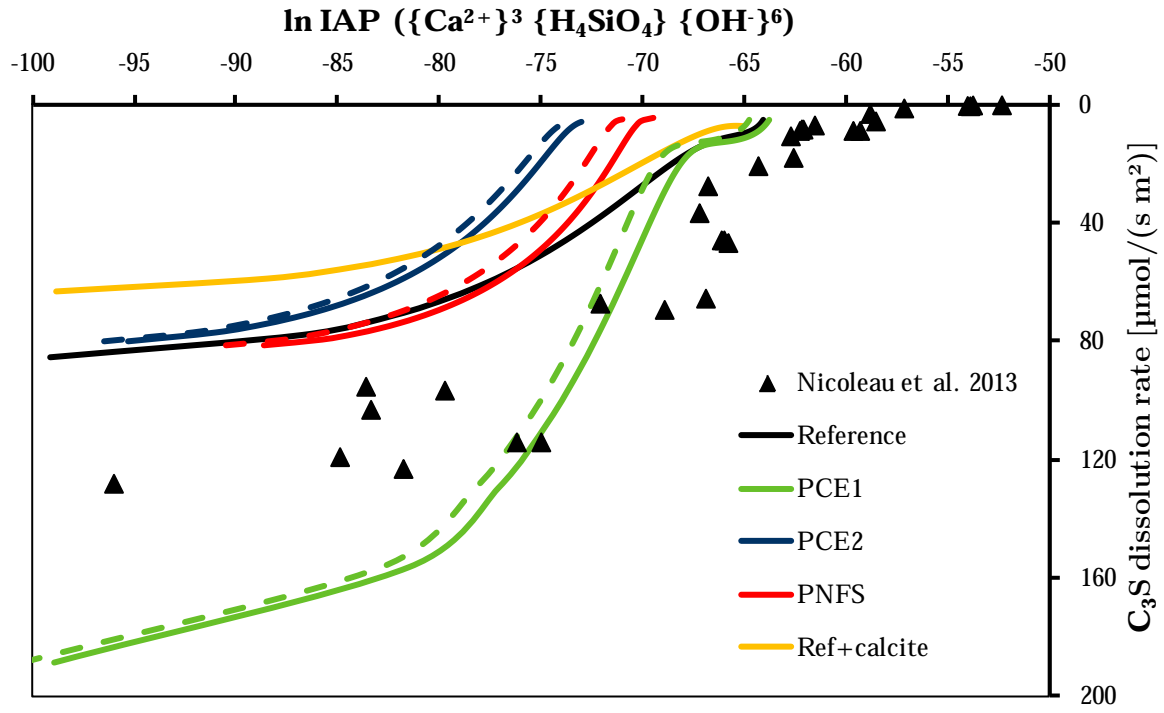

Fig. 4-26: C_3S dissolution rate vs. IAP (eq.(40)) in the presence or not of SPs ($4 g_{SP}/g_{C3S}$) and calcite ($17.8\ m^2/g_{C3S}$). Triangles refers to Nicoleau *et al.*[134], dotted lines indicate IAP resulting after Ca complexation by the SPs (leads to reduced dissolution rates at equal IAP). At increasing IAP decreased dissolution rate of C_3S is determined. PCE1 increases the rate at low IAP, and induces approx. similar rates as reference at increased IAP. Other SPs show similar dissolution rates as reference at low IAP, but lower rates at increasing IAP. Calcite reduces the C_3S dissolution rate.

If we compare the impact of the superplasticizers and calcite on the hydration kinetics of C_3S under paste and suspension conditions then we can see that at constant dosage (like in the pure dissolution experiments) PCE1 shows a stronger retardation as compared to PCE2 and PNFS. Calcite significantly accelerates the C_3S hydration. However, the C_3S dissolution rate is reduced in all cases (addition of either SPs or calcite). By the experimental data it can therefore not be ruled out/proven that the retarding and accelerating effect of SPs and calcite, respectively, on C_3S hydration is solely related to their impact on pure dissolution rate of C_3S and/or that the dissolution is the rate determining step during hydration. In particular it must be questioned if either the used experimental setup and/or the with respect to paste experiments very high dosage of SPs (paste: max. 0.0015 g_{SP}/g_{C3S}, dissolution experiments: max. 4 g_{SP}/g_{C3S}) leads to reasonable results. However, latter was necessary to observe any effects of SPs on C_3S dissolution rate. All in all it is concluded that further research is needed to cleary identify the impact of superplasticizers on dissolution rate of C_3S.

4.2.4.3 Concluding remarks

Experimental data reveal that the Ca ion concentration in the aqueous phase mainly influences the unconstrained dissolution rate of C_3S. Thereby, unconstrained dissolution rate decreases with increasing Ca ion concentration (Fig. 4-22 right hand). Maximum rates measure 97±26 and 0.73±0.25 $\mu mol/(sm^2)$ in water and saturated $Ca(OH)_2$ solution as

starting solutions at l/s=1000, respectively. It was claimed that Ca complexation of dissolved ions by functional groups of polymers in conditions strongly undersaturated with respect to C-S-H phases (unconstrained dissolution) leads to an increase in dissolution rate. Further, in presence of naphthalene sulfonate based superplasticizer (PNFS) the dissolution rate is slightly increased in both water (Fig. 4-24) and saturated $Ca(OH)_2$ solution as starting solution (Fig. 4-25). This can be attributed to the increased Ca ion complexation capability of PNFS compared to other SPs (Fig. 4-11). Finally, based on the gathered experimental data it is still unclear to indentify whether or not dissolution rate is significantly changed during conditions close to C_3S paste hydration and thus to account for the retarding effect. This point is discussed in combination with precipitation reactions in section 4.3.3.

4.2.5 Pure precipitation of C-S-H phases and portlandite

In the present section the kinetics of pure C-S-H and portlandite precipitation influenced by superplasticizer is studied. Therefore, polymers given in Table 3-1 are utilized. Crystallization was induced by mixing of homogeneous solutions, and the crystallization kinetics was followed by electrical conductivity. After that kinetic parameters (induction time, maximum growth rate) were related to the degree of supersaturation (eq. (41) and (42)). Special attention is paid on the importance of the aforementioned complexation and cluster formation on nucleation and growth of hydrate phases.

The present chapter commences with the nucleation of C-S-H phases and portlandite in accordance to classical nucleation theory as described in chapter 2.1.3.1. Finally, crystal growth is presented as well as the illustrations on the influences of superplasticizers on crystal morphology. Different to the other chapters in the present work the results are discussed in a separate section.

4.2.5.1 Experimental setup

The impact of superplasticizer on nucleation of both C-S-H phases and portlandite was investigated by adding superplasticizer (Table 3-1) prior the mixing in either $Ca(OH)_2$ or NaOH solution for C-S-H and portlandite experiments, respectively.

Electric conductivity was recorded in order to investigate the precipitation kinetics of both C-S-H phases and portlandite. Fig. 4-27 shows exemplary the time dependent development of the electrical conductivity during pure crystallization of portlandite.

In the beginning after mixing the solutions the electrical conductivity remains constant. Subsequently, a characteristic drop of the electrical conductivity is observed. In accordance to the classical nucleation theory (cf. chapter 2.1.3), these characteristics are referred to as induction time and crystal growth period, respectively. The maximum slope of the drop was referred to as the maximum growth rate. All precipitation experiments were performed under continuous stirring at constant rotational speed at 25 °C. In order to minimize carbonatization the experiments were conducted under N_2 atmosphere (glove box).

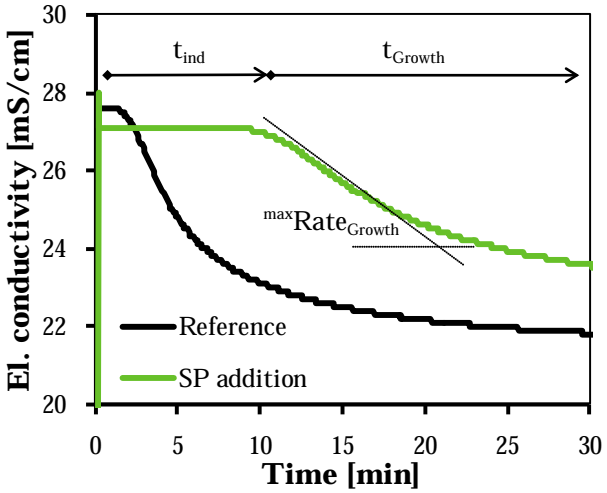

Fig. 4-27: Example of electrical conductivity over time for portlandite precipitation. The graph shows the hallmarks of the curve for the SP containing sample.

Calibration of the electrode permits the determination of Ca ion concentration in the aqueous phase. Based on this and the knowledge of the calcium content of the precipitating phase (in case of C-S-H phases determined by EDX) the growth rate was calculated and expressed as mmol/(l s).

It should be noted that degree of supersaturation refers to the initial state. Although ions are consumed by nucleation the degree of supersaturation until the crystal growth period varies not significantly. Both C-S-H phases and portlandite were visualized after the precipitation process by means of Electron Microscopy (section 3.2.4, p.69).

4.2.5.1.1 Portlandite precipitation experiments

For precipitation of portlandite, NaOH - and $CaCl_2$ -solutions with different ion strengths were used. The precipitation of portlandite from these solutions can be written as:

$$CaCl_2 + 2NaOH \Leftrightarrow Ca(OH)_2 \downarrow + 2Na^+(aq) + 2Cl^-(aq) \qquad (41)$$

For calculations on degree of supersaturation a solubility product for portlandite[10] of log K_{SP}=-5.19 was used.

From sodium hydroxide (Merck, pure) and calcium chloride (Merck, pure) stock solutions were prepared. These were filtered (0.45 µm pore size) in order to exclude the presence of particles in solution (potential nucleation centres). From these stock solutions different dilutions were used for the experiments.

50 ml $CaCl_2$ solution was filled in a beaker (PTFE), which was prepared with 50 ml of NaOH-solution with or without superplasticizer, under continuous stirring.

4.2.5.1.2 C-S-H precipitation experiments

Homogeneous precipitation of C-S-H was studied in solutions prepared by dissolving C_3S, which was continuously stirred at liquid/solid ratio (l/s) of 50 for 30 s. Then the aqueous phase was separated by filtration (0.1 µm pore size). Previous studies[14, 43] have shown that

under these conditions the maximum silicon concentration obtainable is 1.4 mmol/l. In a total volume of 200 ml of a glass or PTFE beaker, the filtered solution was mixed or not with solution containing Ca^{2+} and OH^- in various concentrations. When the action of superplasticizers was investigated, the SPs were added to the Ca^{2+} and OH^- containing solution before.

The degree of supersaturation with respect to tobermorite as model C-S-H phase was calculated based on following equation[118].

$$(Ca)_{0.83}(SiO_2)_1(OH)_{1.66}(H_2O)_{0.5} \leftrightarrow 0.83Ca^{2+} + HSiO_3^- + 0.66OH^- + 0.5H_2O \qquad (42)$$

For this equation, the solubility product of log K_{SP}=-8.0 was taken[118].

4.2.5.2 Results

4.2.5.2.1 Nucleation

A Reference without superplasticizers

The first step in crystallization is the formation of stable nuclei as described in chapter 2.1.3. As it is also mentioned in this section, often a time lag before the detection of nuclei is observed, i.e. the induction time. Note that this time is different from the induction period in cement hydration, c.f. chapter 2.2.3, because of the absence of solid phases. The influence of the degree of supersaturation (calculated from measured ion concentration) on the duration of the induction time (measured by electrical conductivity) is shown in Fig. 4-28 for C-S-H (left hand) and portlandite precipitation experiments (right hand). All data related to pure crystallization experiments are listed in Table A-11 to Table A-14 (appendix).

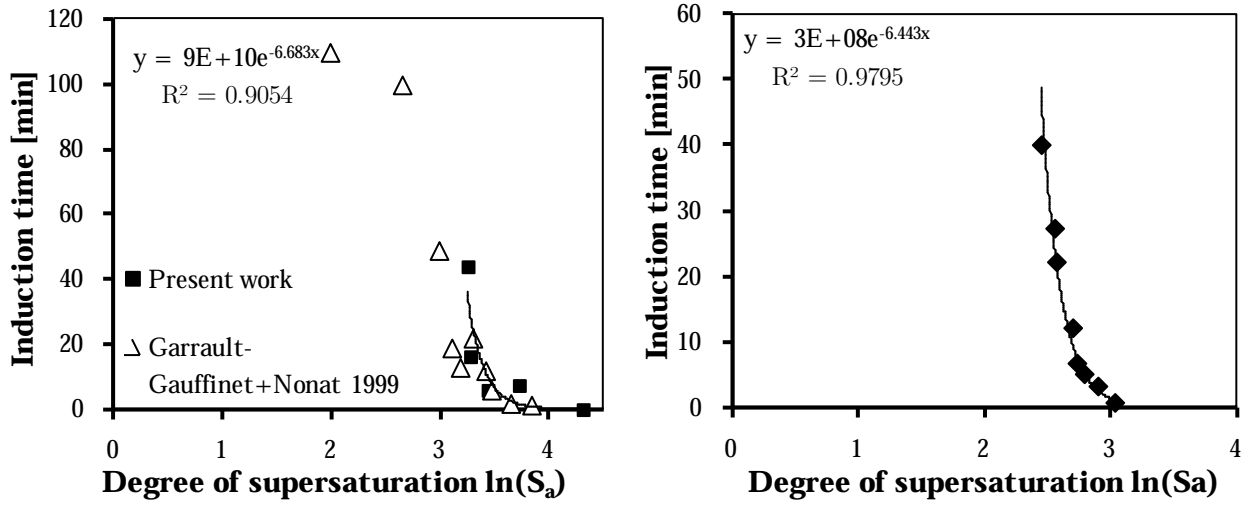

Fig. 4-28: Induction time as function of degree of supersaturation for (left hand) C-S-H and (right hand) portlandite. Points and red line represent data and fit, respectively. Data from Garrault-Gauffinet and Nonat[63] is also shown. In both cases the duration of the induction period decreases with increasing degree of supersaturation as known from literature[46, 128, 135].

As stated in chapter 2.1.3, the driving force for nucleation is the degree of supersaturation. In both systems the induction time decreases with increasing degree of supersaturation. C-S-H and portlandite are different in both ion composition and solubility which alters the absolute values of supersaturation. Consequently, the two curves in Fig. 4-28 are not

superposable. Comparison with literature data on C-S-H precipitation[63] shows good consistency.

According to chapter 2.1.3.1 the logarithmic plot of the induction time versus the inverse of the double logarithm of the degree of supersaturation gives straight lines. Slopes and intercepts of curves with ordinates correspond to interfacial energy and diffusion coefficient, respectively. These plots are presented in Fig. 4-29 for C-S-H (left hand) and portlandite (right hand) precipitation, respectively.

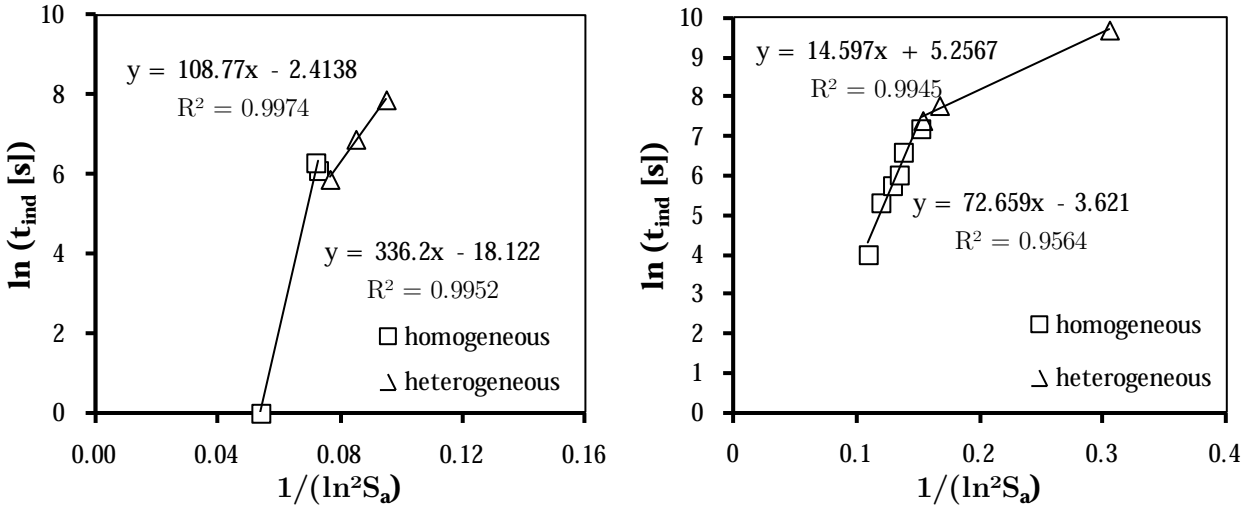

Fig. 4-29: Logarithmic vs. inverse double-logarithmic plot of induction time over degree of supersaturation for C-S-H (left hand) and portlandite (right hand) precipitation. Points and red line represent data and fit, respectively. These plots permit the distinction between homogeneous (high degree of supersaturation) and heterogeneous (low degree of supersaturation) nucleation processes.

Fig. 4-29 demonstrates the two modes of nucleation, namely homogeneous and heterogeneous. As shown in chapter 2.1.3, at high supersaturation nuclei may precipitate homogeneously, predominantly. On the contrary, at decreasing degree of supersaturation nucleation events becomes rare and mainly heterogeneous nucleation occurs. This behavior can be associated with two different linear slopes in graphs of Fig. 4-29. Using eq. (23), the interfacial energy between crystal and surrounding solution was estimated to 15.1(10.3) and 45.5(26.7) mJ/m^2 in case of homogeneous (heterogeneous) nucleation of C-S-H phases and portlandite, respectively. The diameter of critical spherical nuclei in accordance with classical nucleation theory was computed after eq. (14) and is given in Fig. 4-30 in dependence on the degree of supersaturation. Furthermore Fig. 4-30 shows the number of atoms/molecules present in the critical cluster calculated after eq. (16).

In Fig. 4-30 it is demonstrated that with increasing supersaturation the critical diameter of spherical nuclei decreases and thus the number of atoms/molecules in the cluster. Furthermore, in case of heterogeneous nucleation the critical diameters decrease. Because of the lower supersaturation in C-S-H precipitation experiments, their critical nuclei with diameters between 2.3(1.9) and 2.7(2.6) nm are large compared to those in portlandite nucleation experiments measuring between 0.8(0.6) and 1.0(0.8) nm for homogeneous (heterogeneous) nucleation, cf. Fig. 4-30. Those cluster contain between 10(6) and 16(14) molecules in case of C-S-H and between 5(2) and 9(5) in case of portlandite for

homogeneous (heterogeneous) nucleation, respectively. Because C-S-H phase precipitation follows the rules of crystallization, the present work prove further their crystallinity[166].

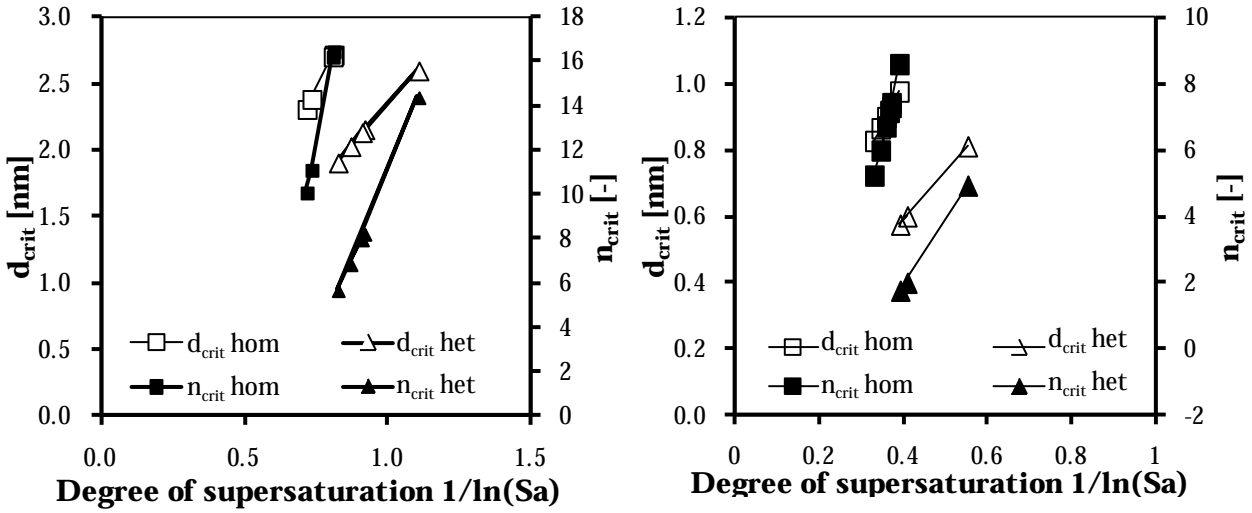

Fig. 4-30: Critical nuclei diameter (d_{crit}) of hypothetic spherical shape and corresponding number of molecules (n_{crit}) as function of degree of supersaturation for C-S-H (left hand) and portlandite (right hand). Points and red line represent data and fit, respectively.

In general, findings of the present study with respect to pure C-S-H precipitation are in accordance to results of Garrault-Gauffinet and Nonat[63]. This includes an interfacial energy of 12 mJ/m^2 and diameter of critical spherical nuclei for homogeneous nucleation of C-S-H at degree of supersaturation of 4 of 1.8 nm. For portlandite interfacial energy values ranging between 52[21], 65[102] and 86[21] mJ/m^2 are reported in literature for experiments conducted by double decomposition. Thus, interfacial energies for homogeneous and heterogeneous nucleation determined in the present work (45.5 and 26,7 mJ/m^2, respectively) are below the lower limit of reported values. This may be caused by the fact that data treatment (e.g. shape of the nuclei assumed, determination of homogenous nucleation domain) and experimental procedures are different. Furthermore, a discussion of interfacial energy is only possible when the values are computed within the same range of supersaturation. In consideration of these arguments it is nevertheless shown that values of the present work are in good agreement with literature data.

The results of double decomposition experiments shown in the present chapter can be used in order to relate paste hydration experiments to nucleation regimes. As shown in section 2.2.3.2 (p.52) and later (section 4.3.3, p.141), the aqueous phase during C_3S hydration is governed by ion concentrations reported as kinetic path[12-13, 40] and solubility of C-S-H(m)[70, 86]. As point Q in the Ca-Si diagram (Fig. 2-14, p.54) is reached (Ca approx. 4.5 mmol/l, Si=1350 µmol/l) the induction period during C_3S hydration starts until at point C portlandite precipitates (Ca approx. 36 mmol/l, Si=30 µmol/l). These values can be used to determine the degree of saturation with respect to tobermorite and portlandite. As calculated from data published by Barret and Bertrandie[14] at portlandite precipitation under C_3S paste hydration (Ca=37 mmol/l, Si=30 µmol/l), a degree of supersaturation of approx. S_a=4.05 must me established to induce fast precipitation of portlandite. In order to characterize the crystallization mode under C_3S paste hydration the maximum degree of

supersaturation with respect to tobermorite and portlandite is computed, respectively. The results are plotted in Fig. 4-31 as green vertical lines.

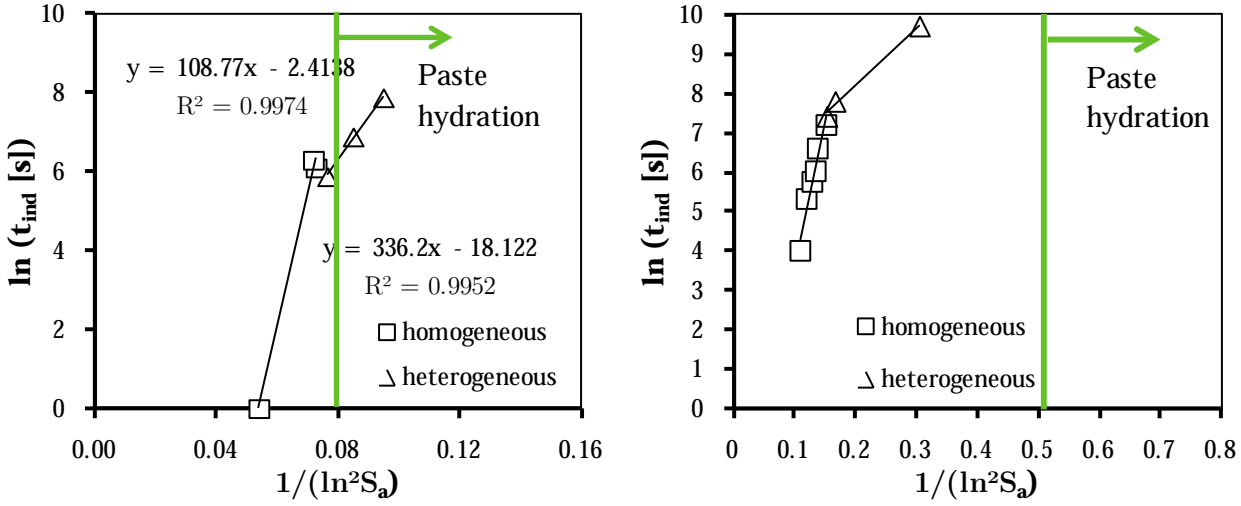

Fig. 4-31: Induction time as function of degree of supersaturation for (left hand) C-S-H and (right hand) portlandite. The region of paste hydration is indicated by a vertical line and follows degree of saturation in direction of the arrow.

As illustrated in Fig. 4-31 the nucleation mode of C-S-H phases and portlandite during C_3S hydration is predominantly heterogeneous. For homogeneous nucleation increased degrees of supersaturation with respect to these phases are required. Those are restricted by ion concentrations mentioned as kinetic path[12-13, 40] and solubility of C-S-H(m)[70, 86]. Therefore C-S-H and portlandite preferentially nucleate on C_3S surfaces. Also calcite and other silicate phases can serve as substrate for nucleation of C-S-H phases[63, 95, 156, 169-170, 179]. In literature it is speculated if portlandite precipitation is poisoned by the presence of silicate ions[192] inducing high degree of supersaturation with respect to portlandite. But compared to precipitation from solution, C_3S paste hydration induces relative low degree of supersaturation with respect to portlandite, i.e. portlandite grows heterogeneously.

B Impact of superplasticizer on homogeneous nucleation

Overview

Fig. 4-32 illustrates the impact of superplasticizer addition on the induction time for both C-S-H phases and portlandite nucleation.

As shown in Fig. 4-32 the presence of superplasticizers retards C-S-H and portlandite nucleation. This retardation is linearly related to SP dosage with different magnitude in both systems. PCE2 induces highest retardation in both C-S-H and portlandite crystallization with stronger impact on C-S-H as indicated by the higher slope (m~90 for C-S-H and m~54 for portlandite). In comparison, the addition of PCE1 induces lower retardation, but here portlandite precipitation is stronger influenced by this SP (m~12 for portlandite and m~9 for C-S-H). Interestingly, PNFS based superplasticizer induces strong retardation at low dosages which is reduced with increasing dosage. This effect is also observed during portlandite precipitation (induction time at dosages of 1.7 and 6.7 ml/l is 61 and 47 min, respectively). Additionally it is shown in portlandite experiments that

retardation increases again with further PNFS addition (which causes a lower correlation coefficient with respect to other SPs).

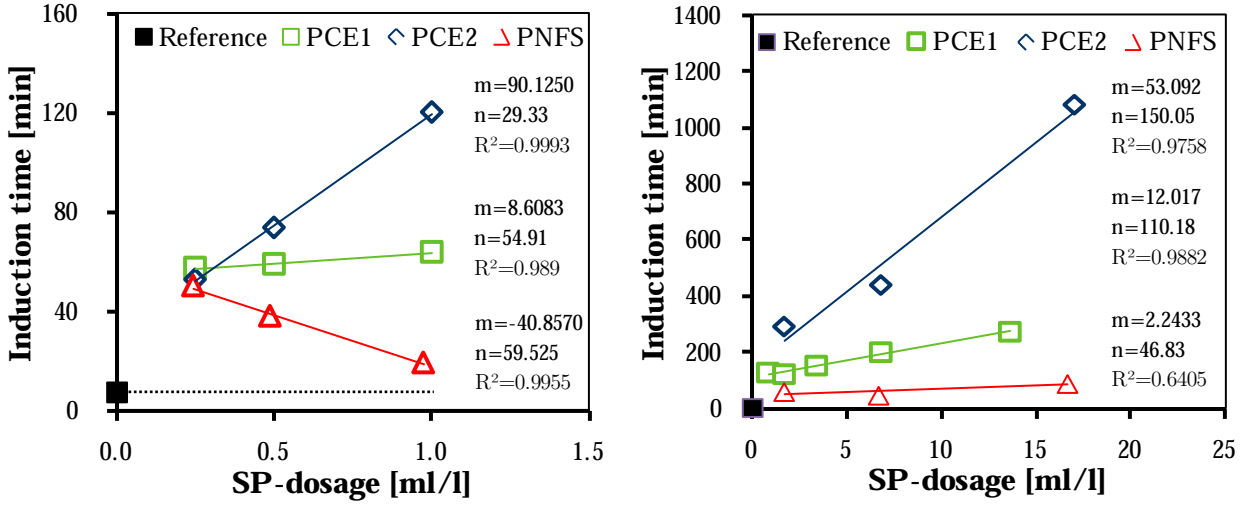

Fig. 4-32: Impact of superplasticizers on induction time for C-S-H (left hand) and portlandite (right hand) precipitation. Data (points) was fitted (lines) linearly (parameters from top to bottom: PCE1, PCE2, PNFS). Dotted line showing reference serves as guide for the eye.

According to classical nucleation theory the induction time is directly proportional to the interfacial energy and inversely proportional to the degree of supersaturation (see eq. (23)). In the following it is tested if the observed retardation of C-S-H and portlandite nucleation (indicated by prolonged induction time) can be related to a variation of these parameters. Considering the principal modes of action of superplasticizers as documented in chapter 4.1 (p.75) it is assumed that variations of interfacial energy and degree of supersaturation is induced by the interaction of the functional groups of the polymers with ions on surfaces and in solution, respectively. In order to test this hypothesis in a first step the dosage given in Fig. 4-32 is recalculated to the number of functional groups by means of Table 4-2 and related to the induction time. Fig. 4-33 presents the results of these calculations.

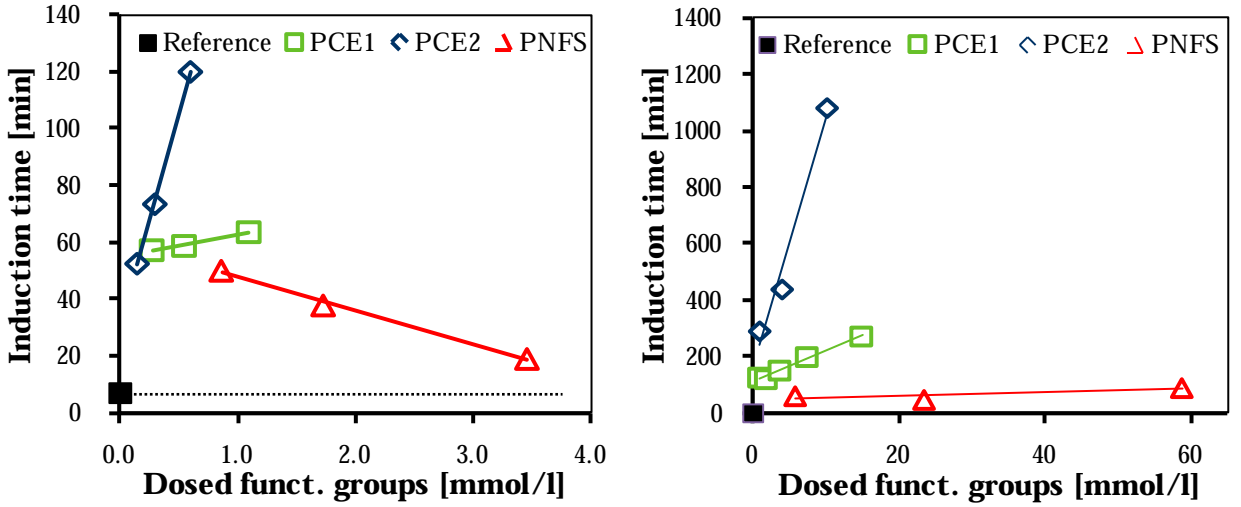

Fig. 4-33: Impact of dosed functional groups of polymers on induction time for C-S-H (left hand) and portlandite (right hand) precipitation. Dotted line showing reference serves as guide for the eye.

Fig. 4-33 suggests that the retarding effect of SPs on nucleation can be related to the number of functional groups. But because data of PCE1 and PCE2 describes two different functions (for carboxy groups) in both C-S-H and portlandite precipitation experiments also a further parameter is involved. From literature[33] it is known that crystallization comprises aggregation processes of nuclei. Accordingly and based on data presented in Fig. 4-33 it is therefore most likely that superplasticizers grafted with side chains hinder this aggregation due to their steric performance. Following that increasing length of side chains may increase the dispersion power of macromolecules in systems with low fractions of solid phases, i.e. in homogeneous crystallization experiments. Data of naphthalene sulfonate based superplasticizer, however, leads to conclude that in certain range of dosage a promoting effect on nucleation exists. Thus, this SP can serve as template for crystallization (cf. section 4.3.3) of both C-S-H phases and portlandite.

In the next steps the second possible mechanism for prolonging the induction time is investigated, i.e. the variation of the degree of supersaturation. This parameter can be altered as a result of complexation of ions in solution by the functional groups of polymers (according to section 4.1.3 (p.84)). It is assumed that this complexation reduces the degree of supersaturation with respect to the precipitating crystal. Because supersaturation is the driving force for the process (resume chapters 2.1.1 and 2.1.3) lower induction times are expected.

Role of complexation of Ca in aqueous solution for the nucleation

In order to investigate solely the impact of complexation of dissolved Ca ions on induction time, the following procedure was conducted.

(1) Determination of the amount of complexed Ca ions by superplasticizers in dependency of SP-dosage by utilizing equations given in Table 4-4 (p.88).

(2) Calculation of the degree of supersaturation at lower Ca ion concentration.

(3) Calculation of theoretical induction times at lowered degree of supersaturation (determined in step 2) by fits given in Fig. 4-28.

The theoretical induction times induced by Ca complexation of superplasticizers are compared with measured induction times. Fig. 4-34 draws these induction times for C-S-H and portlandite precipitation in presence of PCE1.

The Ca complexation capability of PCE1 reduces the supersaturation with respect to both C-S-H phases and portlandite. In both cases the measured induction time exceeds the theoretical induction time purely induced by a reduced supersaturation due to Ca complexation, cf. Fig. 4-34. The impact of solely sodium on the calculated induction time is because low variations in ion activity of minor importance (e.g. portlandite: only Na addition (t_{ind}=1.2 min), with Na addition and Ca complexation (t_{ind}=15.1 min), measured (t_{ind}=199 min)).

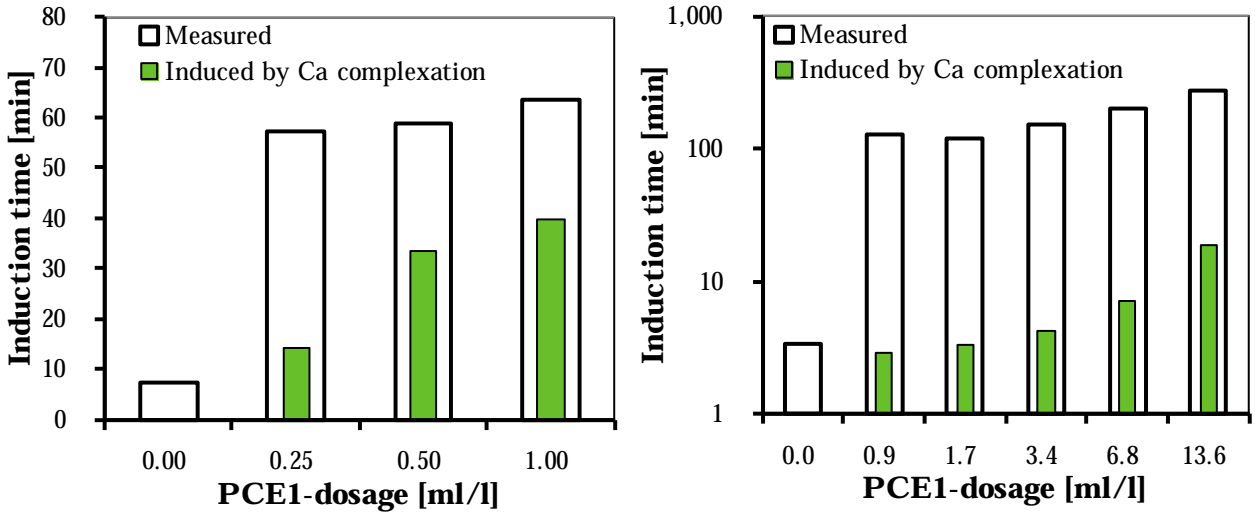

Fig. 4-34: Measured induction time (open bars) and theoretical induction time solely induced by Ca complexation (filled bars) of PCE1 for C-S-H (left hand) and portlandite (right hand) precipitation, respectively. It can be seen that measured induction times are not caused solely by complexation of dissolved Ca ions in aqueous solution.

Fig. 4-35 shows the theoretical induction time induced by complexation of Ca ion in solution in comparison to the measured induction time for the crystallization of C-S-H and portlandite in presence of PCE2.

Similarly to PCE1, the induction times in presence of PCE2 are not solely induced by the capability of the functional groups of PCE2 to complex calcium ions in solution. Again, the solely impact of sodium addition by superplasticizer PCE2 is of minor importance since the ion activity product is only marginally varied (e.g. portlandite: only Na addition (t_{ind}=1.3 min), with Na addition and Ca complexation (t_{ind}=32.1 min), measured (t_{ind}=443 min)). Therefore it is concluded that retardation is not only the result of a lowered degree of supersaturation induced either by Ca complexation or sodium content of PCE polymers.

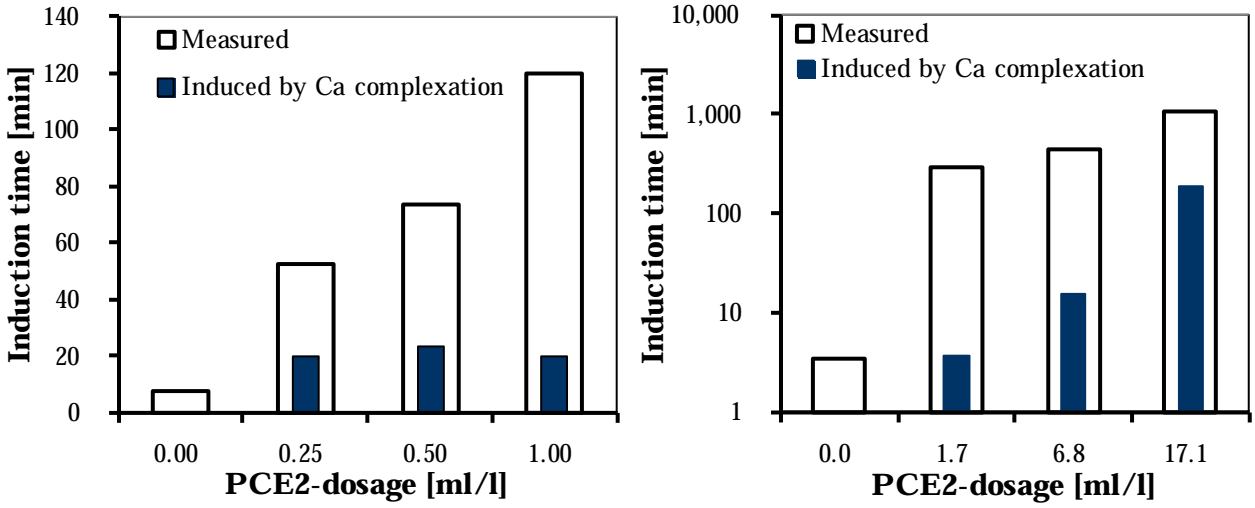

Fig. 4-35: Measured induction time (open bars) and theoretical induction time solely induced by Ca complexation (filled bars) of PCE2 for C-S-H (left hand) and portlandite (right hand) precipitation, respectively. Complexation of Ca ions dissolved in aqueous solution is not solely responsible for the measured induction time.

Finally, Fig. 4-36 presents the results for the induction time consideration for naphthalene sulfonate based superplasticizer PNFS.

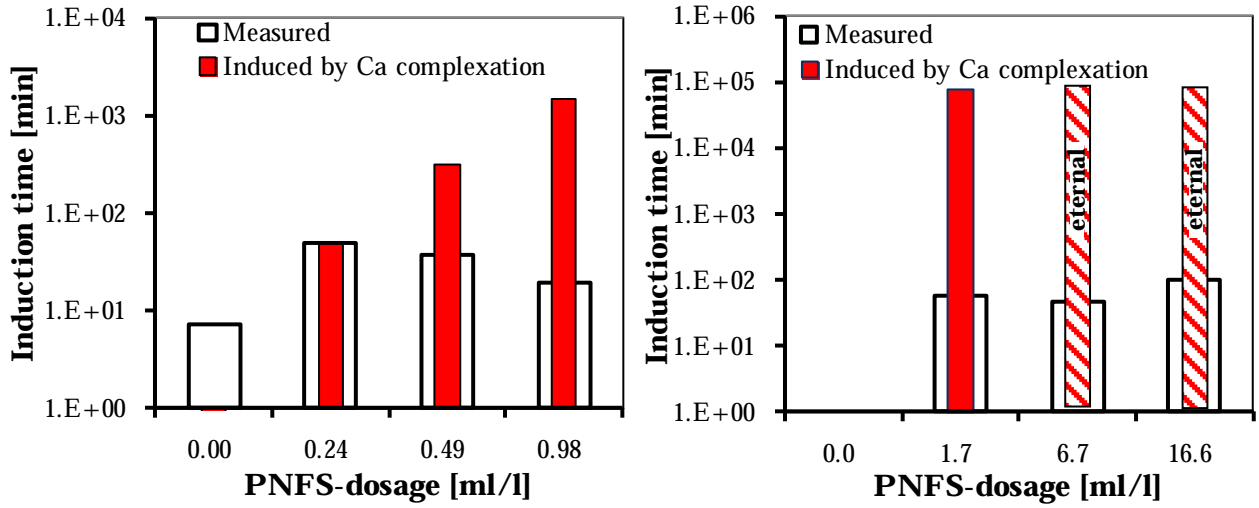

Fig. 4-36: Measured induction time (open bars) and theoretical induction time induced solely by Ca complexation (filled bars) of PNFS for C-S-H (left hand) and portlandite (right hand) precipitation, respectively. The measured induction time is significantly shorter than expected by solely complexation of dissolved Ca ions in aqueous solution. This effect is related to the pronounced template performance of this superplasticizer.

Results of the Ca complexation capability of PNFS showed a strong interaction of Ca and naphthalene sulfonate, cf. chapter 4.3.3. In Fig. 4-36 the impact of the Ca complexation capability of naphthalene sulfonate is shown for both C-S-H and portlandite precipitation. In case of C-S-H, the Ca complexation of superplasticizer at lowest dosage can be solely associated with the induction time, cf. right hand graph in Fig. 4-36. Similar to portlandite, increased PNFS dosages lead to decreasing measured induction times although increasing induction times induced by Ca complexation are expected.

For portlandite similar results are gathered as for the PCE based superplasticizer at high dosages. But calculations show that at higher PNFS dosage undersaturation (saturation index <0) with respect to portlandite is to be expected. Therefore the theoretical induction time induced by complexation of Ca ions in aqueous solution is only visualized by a dashed bar in Fig. 4-36. But the observation of relative low induction time despite the high Ca ion complexation capability in presence of highest PNFS dosage leads to further conclusion on the performance of superplasticizer as template for the crystallization of both C-S-H and portlandite. Similarly to the impact of PCE on nucleation of C-S-H and portlandite the addition of sodium by PNFS induces only minor variations in activity product. Thus, sodium addition alone is not able to account for the experimental data (e.g. portlandite: only Na addition (t_{ind}=1.6 min), with Na addition and Ca complexation (t_{ind}=74500 min), measured (t_{ind}=58 min)).

4.2.5.2.2 Crystal growth

A Reference without superplasticizers

Subsequently to nucleation, crystal growth processes occur. Similar to nucleation, crystal growth rate (measured by electrical conductivity (slope after the induction time) and

recalculation into ion concentrations) is a function of the degree of supersaturation. For both C-S-H and portlandite crystallization this relationship is given in Fig. 4-37.

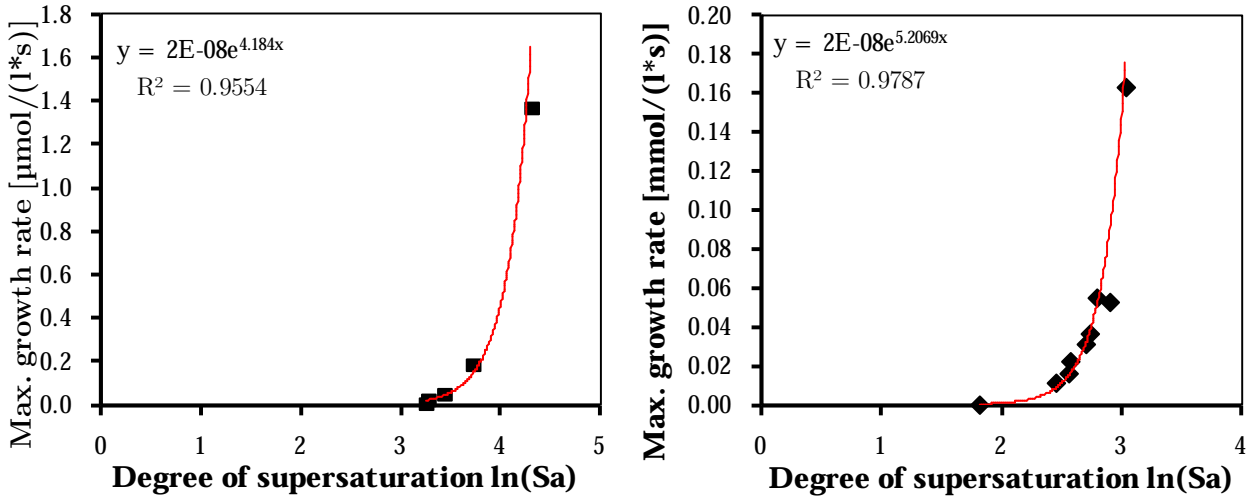

Fig. 4-37: Crystal growth rate as function of degree of supersaturation for (left hand) C-S-H and (right hand) portlandite. As expected from theory[46, 128, 135], at increasing supersaturation the growth rate increases.

For both C-S-H and portlandite also a strong correlation between growth rate and degree of supersaturation as stated in chapter 2.1.3 was found. This relationship is more pronounced for C-S-H than for portlandite precipitation. Furthermore, the growth rate of C-S-H phases exceeds that of portlandite at similar degrees of supersaturation, cf. left hand and right hand graphic of Fig. 4-37.

B Impact of superplasticizer on maximum crystal growth rate

Overview

From literature[97, 103, 122] it is known that besides degree of supersaturation crystal growth rate depends on the number of nuclei formed. Because the superplasticizers were added in the starting solution before mixing effects on crystal growth rate may also be induced by differences in the number of nuclei. Fig. 4-38 shows analogously to induction time the impact of superplasticizers on the growth rate of C-S-H phases and portlandite.

Both graphs of Fig. 4-38 demonstrate that the impact of the used SPs is different in both systems even if the doubled dosage of superplasticizers in portlandite crystallization experiments is taken into account. Interestingly, lowest dosages of superplasticizer promote crystal growth in case of portlandite. During C-S-H precipitation experiments this effect is only observed for PCE2. Contrary, the presence of PCE1 induces lowest growth rates of examined superplasticizers in both systems. Especially at highest dosage, the naphthalene sulfonate based superplasticizer (PNFS) induces smallest reduction of both C-S-H and portlandite growth rates. In case of C-S-H the reduction in growth rate is independent on the PNFS dosage. Comparing the maximum growth rates at highest SP dosage it is obvious that portlandite growth is hindered in more extent as compared to C-S-H growth.

Accordingly to nucleation experiments it is investigated in the following if the reduction in crystal growth rate is mainly dependent on the functional groups of the added polymers. Therefore, in Fig. 4-39 growth rates are plotted against dosed number of functional groups.

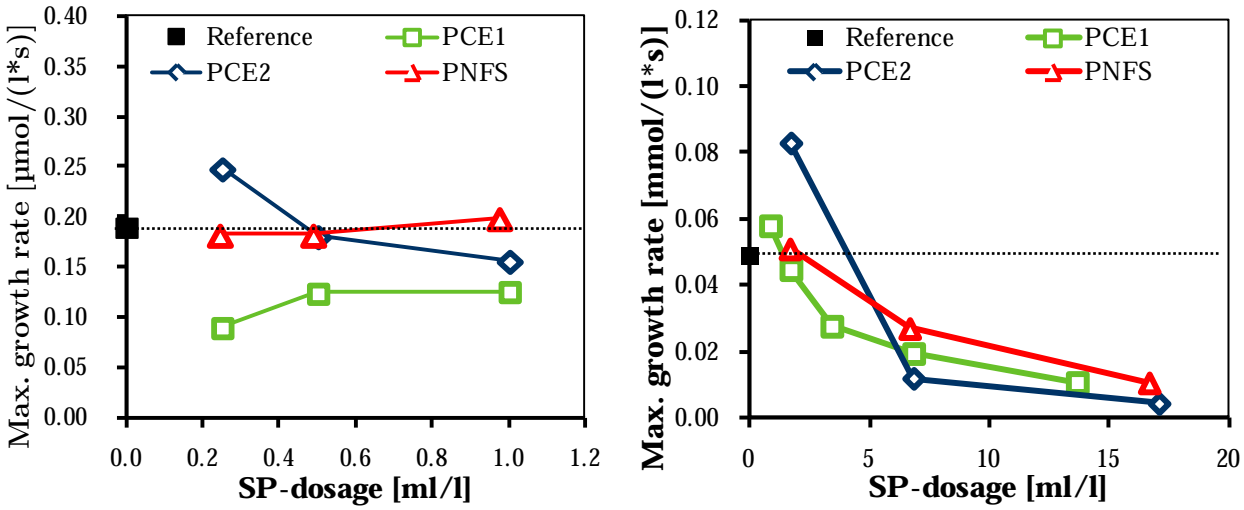

Fig. 4-38: Maximum growth rate during the crystallization of both C-S-H phases (left hand) and portlandite (right hand) in the presence of superplasticizers. Results demonstrate that superplasticizer reduce the crystal growth rate with similar impact on C-S-H phases and portlandite.

Results in Fig. 4-39 reveal the impact of dosed functional groups on crystallization rate. In case of C-S-H phases lowest amounts of PCE1 are sufficient to alter the growth rate markedly. Also the addition of PNFS shows reduction in C-S-H growth rate independently on the dosed number of sulfonic groups. Only for PCE2 a strong decrease in growth rate is observed when this polymer is added in small dosages. From these results it is concluded that reduction of C-S-H crystal growth rate is not only dependent on the number of dosed functional groups as both PCE1 and PCE2 do not fall on the same curve. Despite of that, portlandite crystal growth is mainly retarded by the dosed number of functional groups. Therefore, carboxy groups interact stronger with portlandite crystals compared to sulfonic groups. Because at increased PCE dosages both carboxy group bearing polymers show different behavior it is concluded that not only the number of functional groups but also a further polymer parameter becomes more important at a certain dosage.

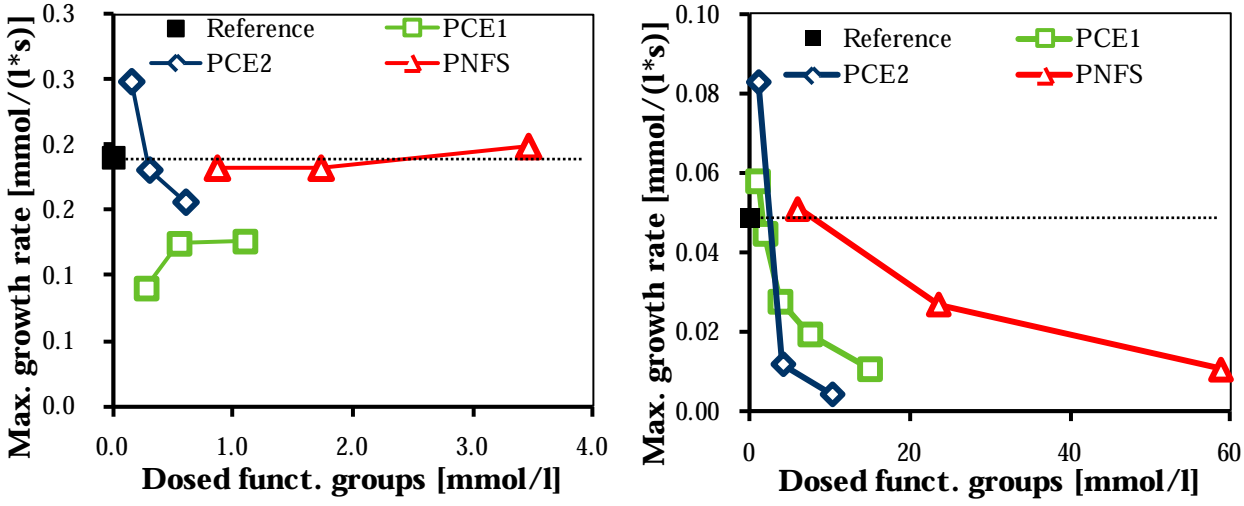

Fig. 4-39: Maximum growth rate during the crystallization of both C-S-H phases (left hand) and portlandite (right hand) in the presence of superplasticizers. Results demonstrate that superplasticizer reduce the crystal growth rate of C-S-H phases and portlandite differently.

Role of complexation of Ca ions dissolved in aqueous solution for crystal growth

Analog to the approach for the induction time, the impact of complexation of dissolved Ca ions by functional groups of polymers on the maximum growth rate was investigated according to the following procedure.

(1) Determination of the total amount of complexed ions by the polymers in dependency of SP-dosage by utilizing equations given in Table 4-4 (p.88).

(2) Calculation of the degree of supersaturation at lower Ca ion concentration determined in step 1.

(3) Calculation of crystal growth rates (induced by superplasticizers) by their dependency on degree of supersaturation (determined in step 2) by fits given in Fig. 4-37.

For PCE1 the impact of Ca complexation on the growth rate is shown in Fig. 4-40.

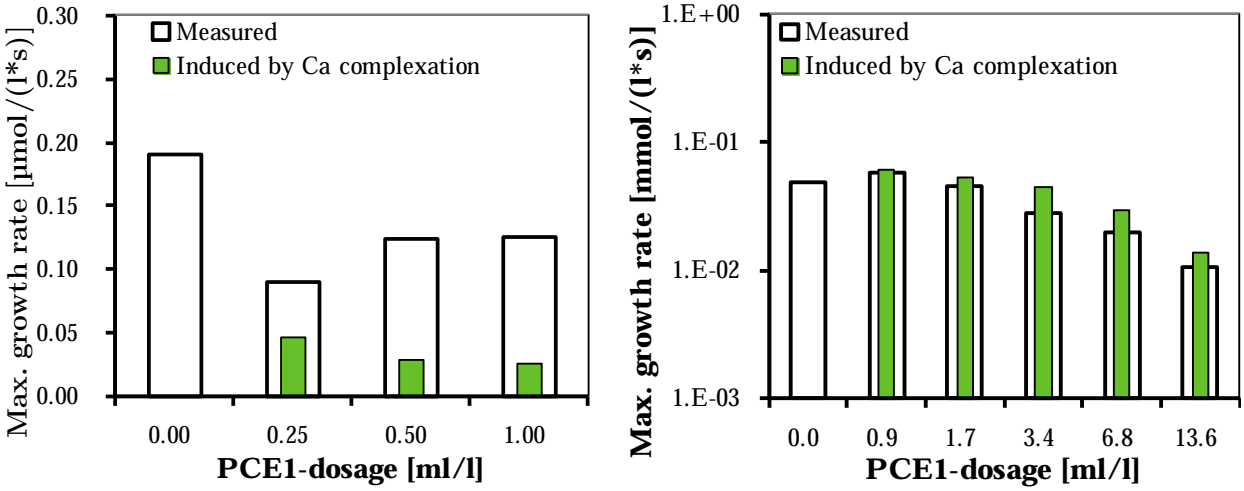

Fig. 4-40: Measured maximum growth rate (open bars) and theoretical rate induced solely by complexation of Ca ions in the aqueous phase (filled bars) during the crystallization of (left hand) C-S-H phases and (right hand) portlandite in presence of different dosages of PCE1. Note the logarithmic scale of the ordinate in the right hand graph. Results indicate that complexation of Ca ions in the aqueous phase should induce lower and higher growth rates for C-S-H phases and portlandite, respectively, as measured.

Fig. 4-40 shows that the measured maximum growth rate is reduced in presence of PCE1 for both C-S-H and portlandite crystallization as also shown in Fig. 4-38. In case of C-S-H crystallization the growth rate is nearly independent on increasing PCE1 dosage, Fig. 4-40 left hand. Contrary, the maximum growth rate of portlandite decreases with increasing PCE1 dosage, see Fig. 4-40 right hand. The maximum growth rate induced by complexation of Ca ions in aqueous solution is lower than the measured rate during C-S-H crystallization. Thus, in addition to induction time a promoting effect of PCE1 during crystal growth period is observed. But, if Ca ion complexation is considered as the only performance of PCE1, the maximum growth rate of portlandite should be higher than measured. This implies that not only complexation of ions in solution are responsible for the observed retarding effect on crystal growth rate but also additional interactions. Based

on sections 2.2.3.4 (p.58) and 4.1.2 (p.75) most likely to induce this effect is the adsorption of polymers on growth centers of portlandite crystals. The impact of PCE2 on maximum growth rate is shown in Fig. 4-41 during (left hand) C-S-H and (right hand) portlandite crystallization.

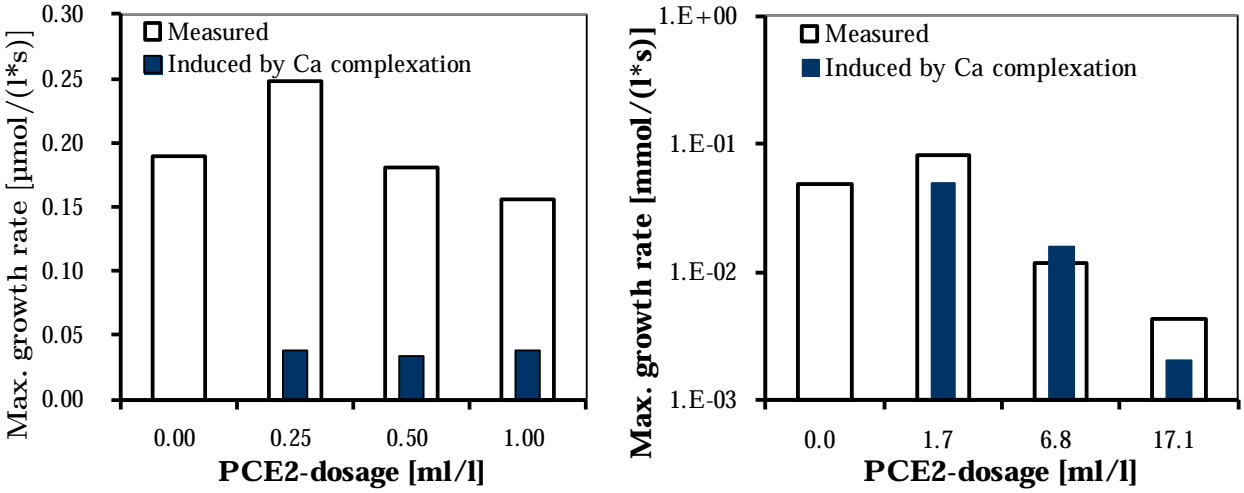

Fig. 4-41: Measured maximum growth rate (open bars) and theoretical rate induced solely by complexation of Ca ions in the aqueous phase (filled bars) during the crystallization of (left hand) C-S-H phases and (right hand) portlandite in presence of different dosages of superplasticizer PCE2. Note the logarithmic scale of the ordinate in the right hand graph. It is illustrated that complexation of Ca ions in the aqueous phase should induce lower growth rates as measured for both C-S-H phases and (except of interim dosage) portlandite.

In principle, PCE2 shows similar behaviour compared to PCE1. Also the solely impact of Ca complexation should result in lower growth rates than observed for C-S-H phases and portlandite. Only during portlandite precipitation with middle PCE2 dosage an increase in max. growth rate is calculated. But generally, this superplasticizer promotes the crystal growth for both C-S-H and portlandite overcoming the effect of complexation Ca ions from solution.

Fig. 4-42 depicts the impact of naphthalene sulfonate based superplasticizer (PNFS) on the crystal growth rate of C-S-H and portlandite.

The presence of PNFS causes no change in maximum C-S-H and portlandite growth rate, see Fig. 4-42. But again, solely impact of Ca complexation on the growth rate should result in a reduced growth rate in both systems. In case of portlandite no growth should accur if only complexation of Ca ion in solution accounts for the retarding effect. The fact that the C-S-H growth rate is nearly unaffected by the presence of PNFS shows again the template effect of this superplasticizer on crystallization. This is underlined by the observation that despite calculated undersaturation with respect to portlandite (saturation index <0) at highest PNFS dosage, growth of this phase occurs.

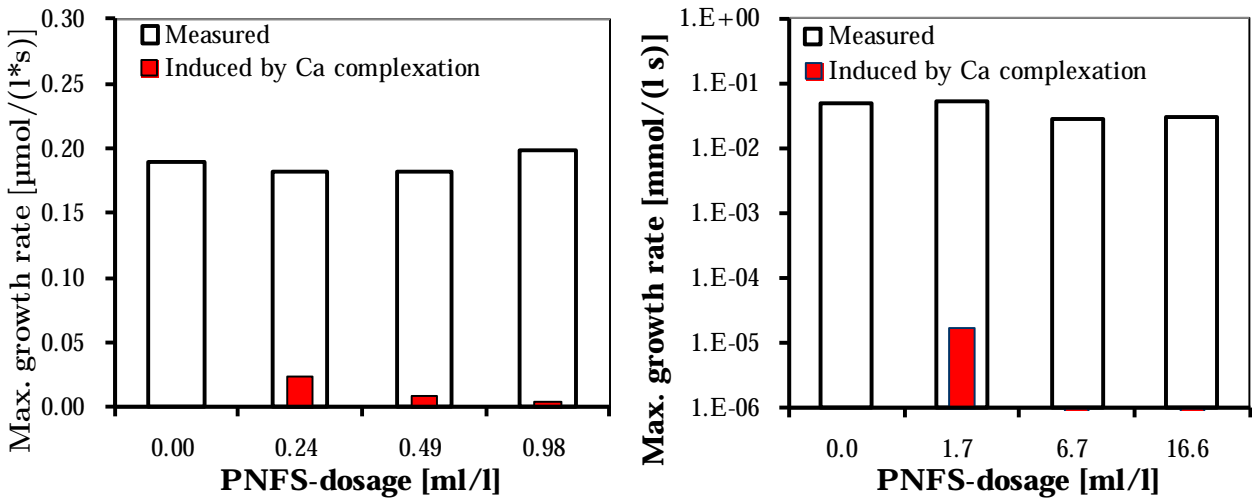

Fig. 4-42: Measured maximum growth rate (open bars) and theoretical rate induced solely by complexation of Ca ions in the aqueous phase (filled bars) during the crystallization of (left hand) C-S-H phases and (right hand) portlandite in presence of different dosages of superplasticizer PNFS. Again, complexation of Ca ions in the aq. phase should induce lower growth rates than measured. Middle and high dosages of PNFS should hinder crystallization.

As a consequence of hindered nucleation and growth of C-S-H phases and portlandite in the presence of superplasticizers and according to the principle of detailed balancing (section 2.1.1, p.23) an increase in solubility of both phases may be expected. This is proven by findings on tests of C-S-H and portlandite solubility shown in section 4.2.3 (p.94).

4.2.5.2.3 Crystal morphology

As a result of growth, crystals form a specific shape. As demonstrated before, both nucleation and crystal growth are influenced by the presence of superplasticizer. The present chapter shows SEM images. Combined with the kinetic study shown in the paragraphs before, the understanding of interaction between superplasticizer and both C-S-H and portlandite can be improved. Firstly, the impact of superplasticizers on C-S-H precipitates is shown followed by the experiments on portlandite.

A Impact of superplasticizers on C-S-H morphology

Compared to portlandite, the testings concerning kinetics and SEM are more difficult in case of C-S-H phases. As shown in Fig. 4-43 during homogeneous nucleation without superplasticizer nanoscaled C-S-H phases form spherical agglomerates with diameters between 1.39 and 1.49 µm, see Fig. 4-43 left hand. Increased magnification reveals that these agglomerates are composed of foils. Because of their nanoscaled size it was nearly impossible to resolve individual C-S-H crystals, cf. Fig. 4-43 right hand. But the foil like shape of C-S-H phases can be seen.

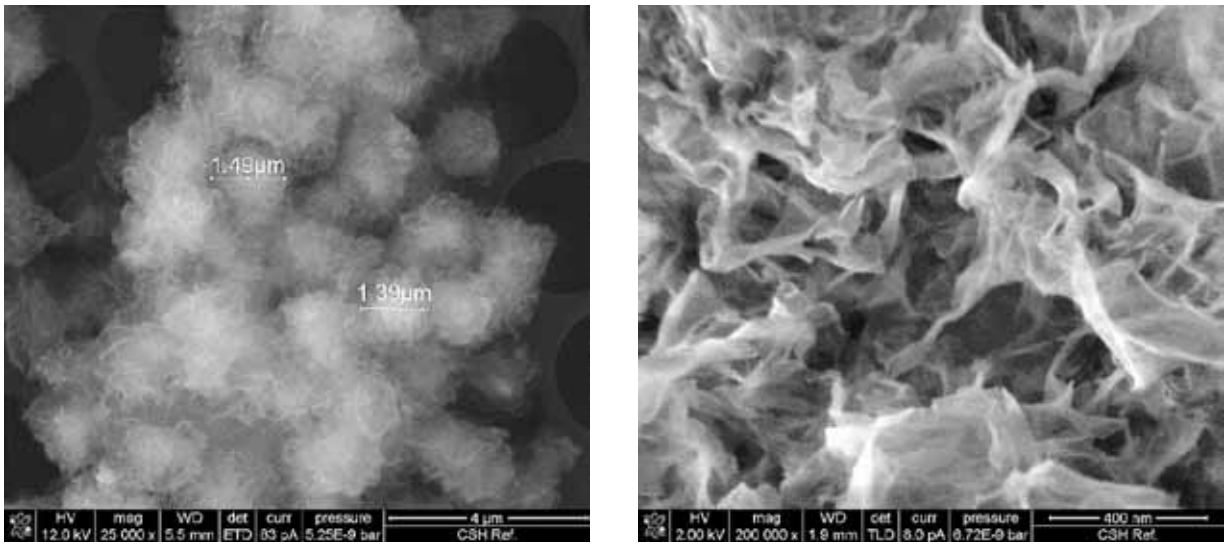

Fig. 4-43: C-S-H phases precipitated without superplasticizer. Picture on the right hand shows that agglomerates visible in the left hand picture are composed of single C-S-H particles.

The presence of PCE1 causes formation of agglomerates smaller in diameter compared to the reference, cf. Fig. 4-44. It is noticeable that those agglomerates are very uniform in sizes, i.e. between 200 and 400 nm in diameter.

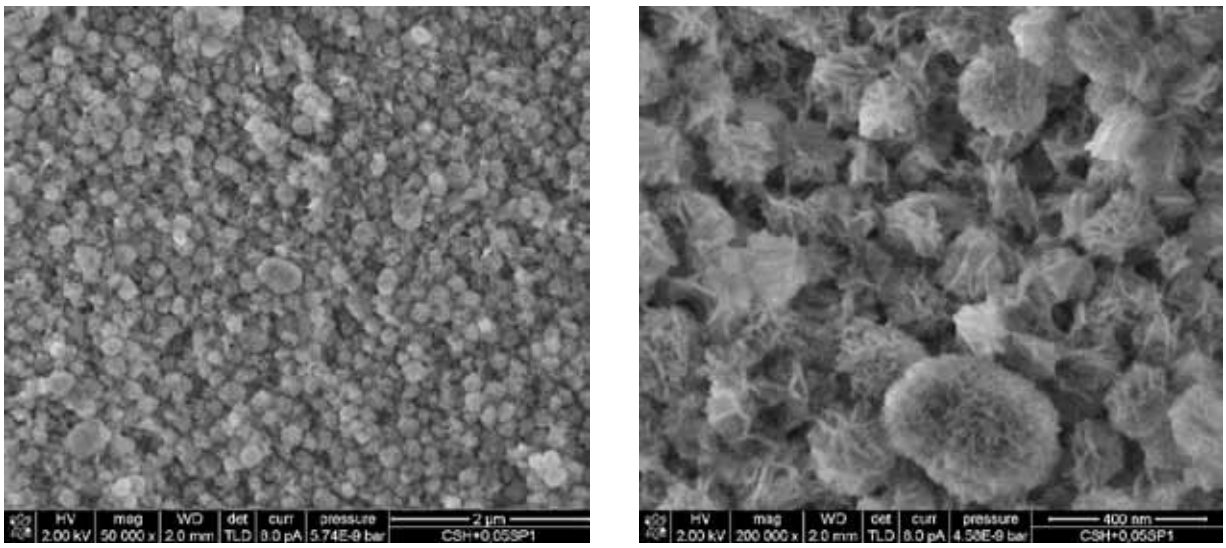

Fig. 4-44: C-S-H phases precipitated in presence of 0.25 ml/l PCE1 (as received). Again as the reference, C-S-H phases are composed of agglomerates which are on the right hand graph shown in higher magnification.

At higher PCE1 dosage the agglomerates observed become smaller. Diameters measure between 140 and 170 nm, cf. Fig. 4-45 left hand (the different magnification in the left hand picture as compared to the low dosage of PCE1 in Fig. 4-44 should be noted). The same sample at increased magnification shows that the single particles within these agglomerates are more dispersed due to higher dosage of PCE1, see Fig. 4-45 right hand.

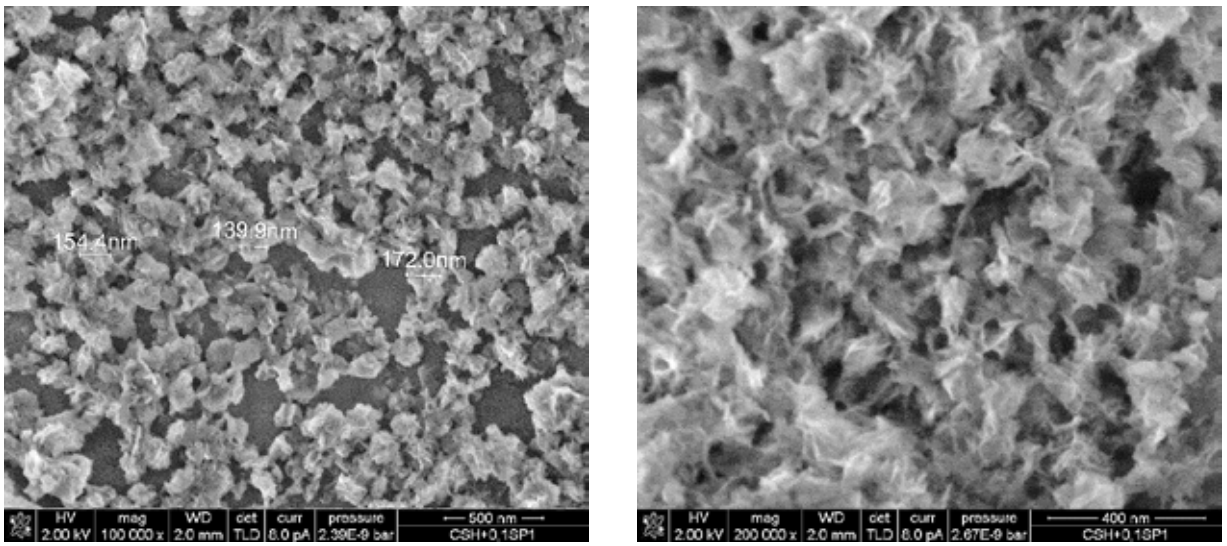

Fig. 4-45: C-S-H phases precipitated in presence of 0.5 ml/l PCE1 (as received). Agglomerates of C-S-H phases which are on the right hand graph shown in higher magnification become smaller in diameter compared to lower PCE1 dosage in Fig. 4-44.

Changing polymer conformation from flexible backbone worm (FBW, PCE1) to flexible backbone star (FBS, PCE2) leads to higher dispersion of the agglomerates which are not spherical in shape as in the reference and PCE1 containing samples, cf. Fig. 4-46 left hand. Higher magnification reveals that the foil structure of C-S-H agglomerates becomes more compact, see Fig. 4-46 right hand.

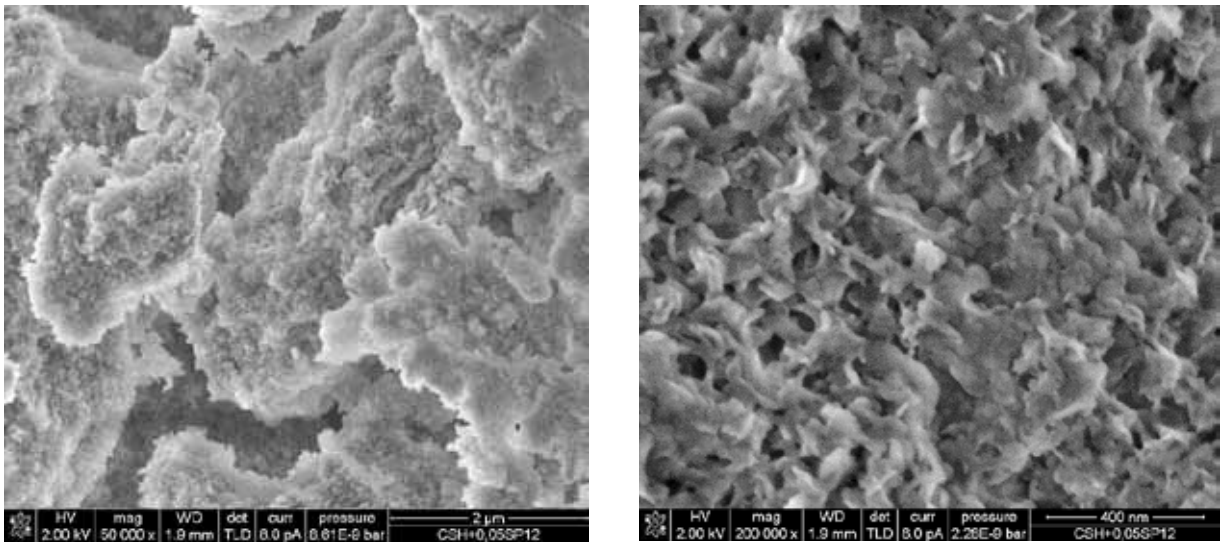

Fig. 4-46: C-S-H phases precipitated in presence of 0.25 ml/l PCE2 (as received). Agglomerates of C-S-H phases are not spherical. Right hand graph shows in higher magnification that C-S-H foils become more tightly packed.

When superplasticizer based on naphthalene sulfonate (PNFS) is present, single C-S-H precipitates are more compact and not arranged in spherical agglomerates, see Fig. 4-47. Higher PNFS dosage causes insignificant changes in the structure of C-S-H agglomerates, cf. Fig. 4-47 right hand.

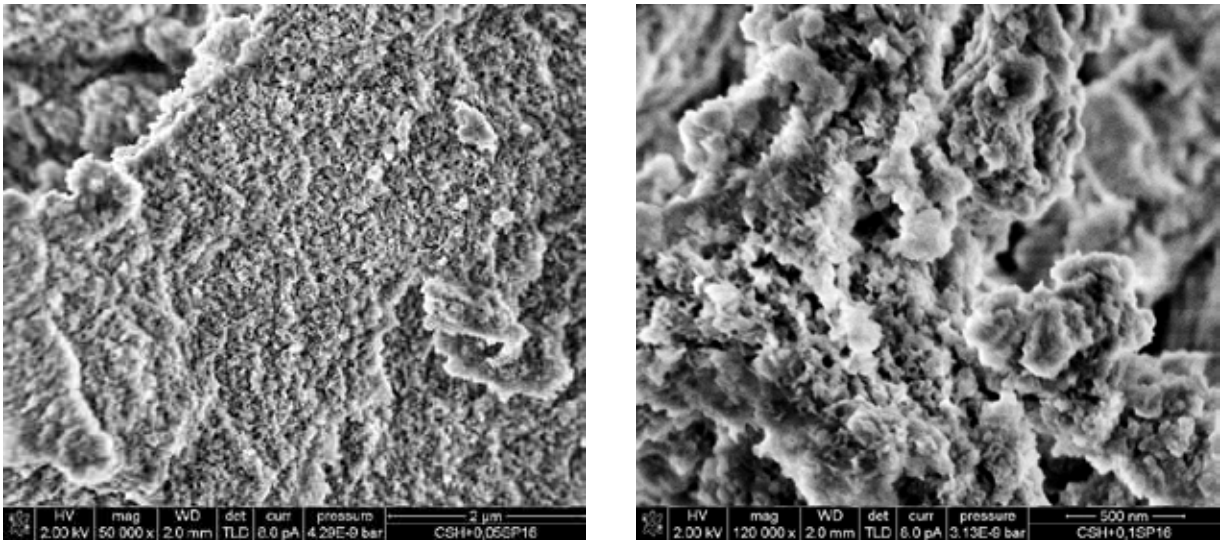

Fig. 4-47: C-S-H phases precipitated in presence of 0.25 ml/l (left hand) and 0.50 ml/l (right hand) PNFS (as received). Agglomerates of C-S-H phases are no longer spherical. Right hand graph shows in higher magnification that C-S-H foils become more compact.

During pure precipitation of C-S-H only formation of agglomerates of those particles is observed. Because of their scale within nanometre range and their weakness against both vacuum conditions and electron dose[166], single C-S-H phases are nearly impossible to detect by means of SEM in the present work. In order to characterize the impact of different superplasticizers on the chemical composition of C-S-H phases EDX analysis with respect to the calcium and silicon content in C-S-H phases was performed. Results are given in Table 4-10.

Table 4-10: Molar Ca/Si ratio of C-S-H phases precipitated in presence of different SPs and SP dosages determined on given number of spots by means of EDX

Sample	SP-dosage [ml/l]	Number of EDX spots	Mean Ca/Si ratio
Reference	0	8	1.22±0.05
PCE1	0.25	13	1.18±0.19
PCE1	0.50	3	1.05±0.03
PCE2	0.25	7	1.19±0.17
NFS	0.24	4	1.18±0.15
NFS	0.49	5	1.22±0.27

When standard deviation is considered no clear change in the molar Ca/Si ratio of C-S-H phases can be found despite high dosage of PCE1 and the reference. Here the present of high dosage of PCE1 decreases the molar Ca/Si ratio in C-S-H phases (i.e. from 1.22 to 1.05). All in all, results indicate that superplasticizers have a minor effect on the chemical composition of C-S-H phases.

B Influence of superplasticizers on portlandite crystal morphology

As stated before, the testings of portlandite crystallization was simpler compared to that of C-S-H phases. Commencing with the reference without addition of superplasticizer in Fig.

4-48 the impact of superplasticizers on the crystal morphology of portlandite is demonstrated in Fig. 4-49 to Fig. 4-54.

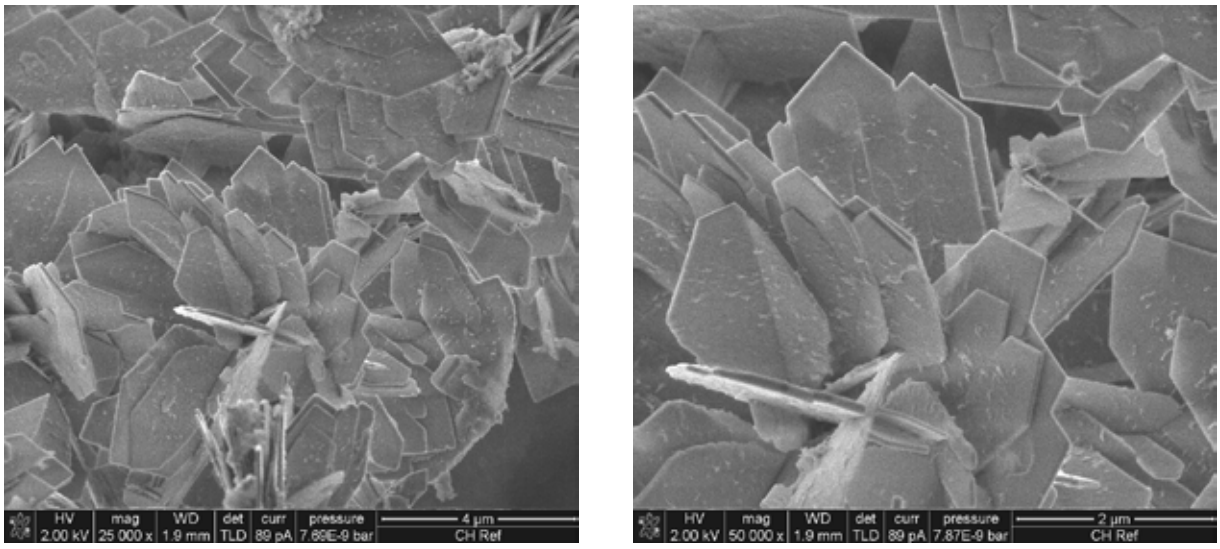

Fig. 4-48: Portlandite crystals at saturation index of 1.26 (left hand: overview, right hand: detail) in the absence of superplasticizer. Platy crystals covered with small precipitates indicate surface nucleation at high degree of supersaturation.

Precipitation of portlandite at a supersaturation index of 1.26 reveals that crystals appear as pseudo-hexagonal plates with dominant occurance of the {100} crystal face. As stated in chapter 2.1.3.2 crystal *habitus* and *tracht* are dependent on supersaturation. Accordingly, growth of crystal faces with highest energy is to be expected in particular at low degrees of supersaturation. In contrast, at high degree of supersaturation also nucleation is possible as indicated by small crystal covering large portlandite particles in Fig. 4-48. Thus, the degree of supersaturation chosen in the present experiments is too high to produce smooth surfaces.

At same degree of supersaturation with respect to portlandite the presence of low dosage of PCE1 causes crystals to grow generally smaller in dimension and more isometric, see Fig. 4-49. Moreover, the images suggest that the {101} face becomes more pronounced. A reduction in crystal size compared to the reference may be the result of promoting nucleation, inhibition of crystal growth, or both. A variation of crystal *tracht* is the result of adsorption of polymers not uniformly at different crystal faces. Thus, Fig. 4-49 shows that PCE1 reduces the growth rate of the {101} crystal face. Besides of the common portlandite morphology also fan-shaped crystals are formed (center of right hand picture of Fig. 4-49) which may be the consequence of variable stacking of individual crystal platelets.

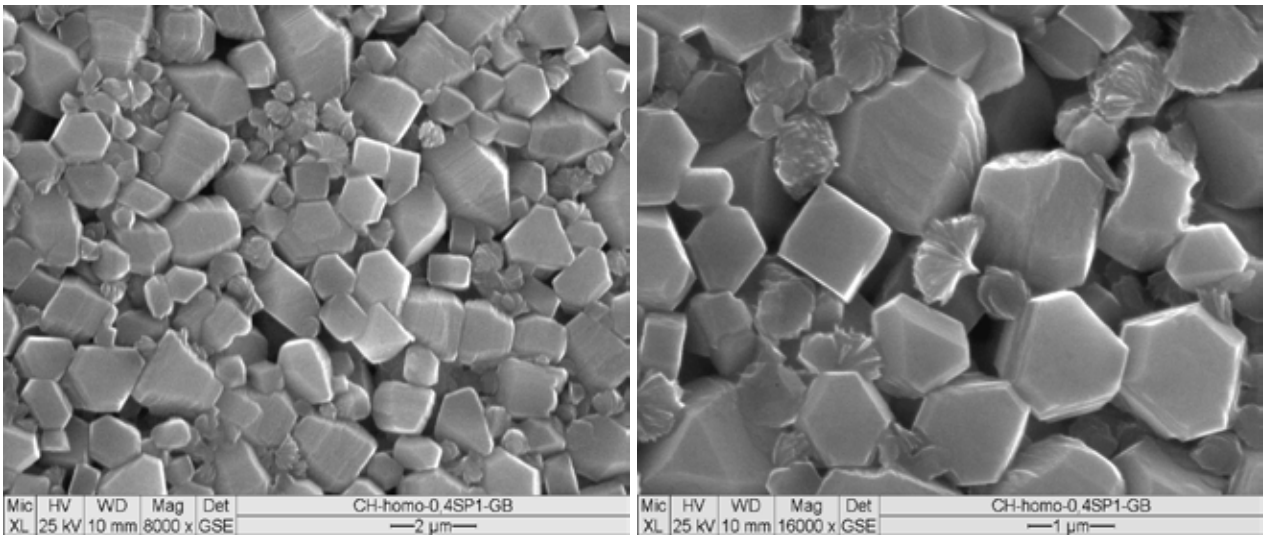

Fig. 4-49: Portlandite crystals at saturation index of 1.26 in presence of PCE1 at 3.4 ml/l. The crystal morphology is more isometric.

Increasing dosage of PCE1 further improves the isometric crystal morphology and the formation of fan-shaped portlandite crystals, see Fig. 4-50.

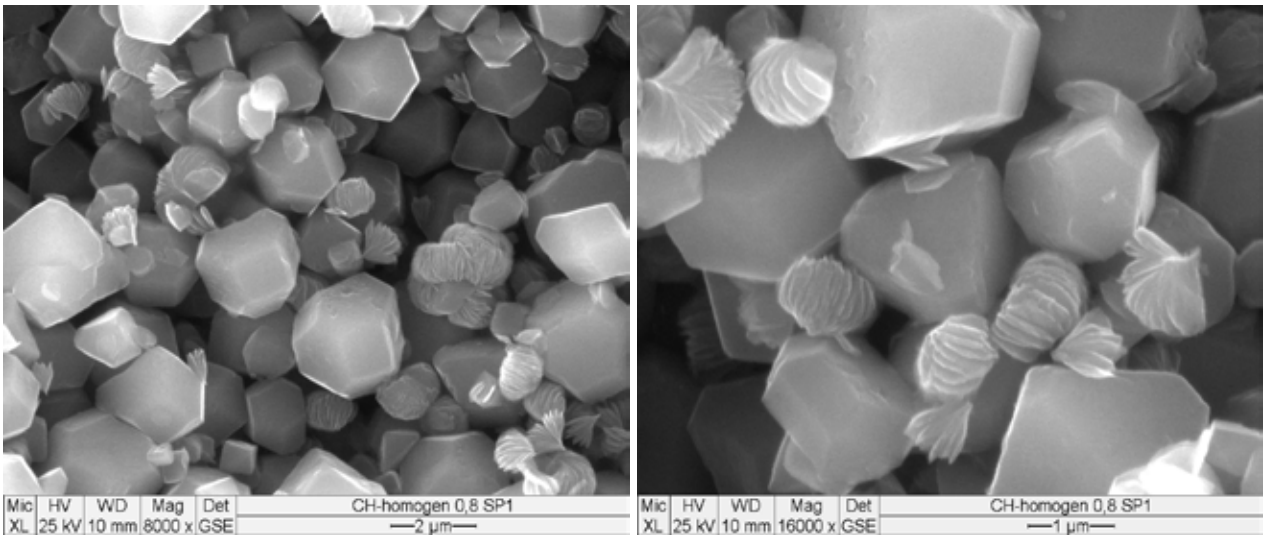

Fig. 4-50: Portlandite crystals precipitated at saturation index of 1.26 in presence of 6.8 ml/l PCE1. Isometric and fan shaped crystals (divergent crystal growth).

In accordance to findings with PCE1 the presence of low dosages of PCE2 reduces crystal sizes of portlandite compared to the reference. With respect to PCE1 some crystals show an even more development of the {101} face.

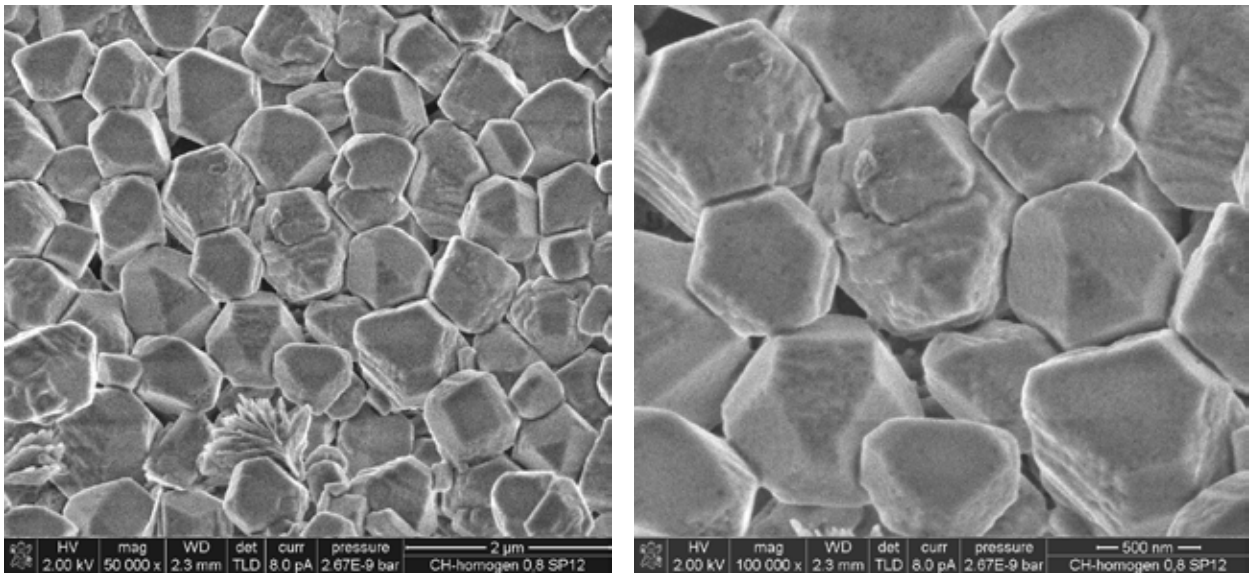

Fig. 4-51: Portlandite crystals revealed at saturation index of 1.26 in presence of PCE2 at 6.8 ml/l. Again crystals are more isometric and euhedral compared to the reference (Fig. 4-48).

The portlandite crystals in Fig. 4-51 are even more euhedral as compared to those in Fig. 4-49 and Fig. 4-50 An euhedral shape of crystals leads to a good packing density of crystals indicated by 120° angles of adjacent grains (triple junctions). By atomistic modeling the euhedral shape of crystals in Fig. 4-51 is predicted for portlandite precipitation in lime solution[62].

Higher dosage of PCE2 seems to have no effect on crystal size. But besides of fan-shaped crystals also the occurance of twinned crystals is observed, see Fig. 4-52.

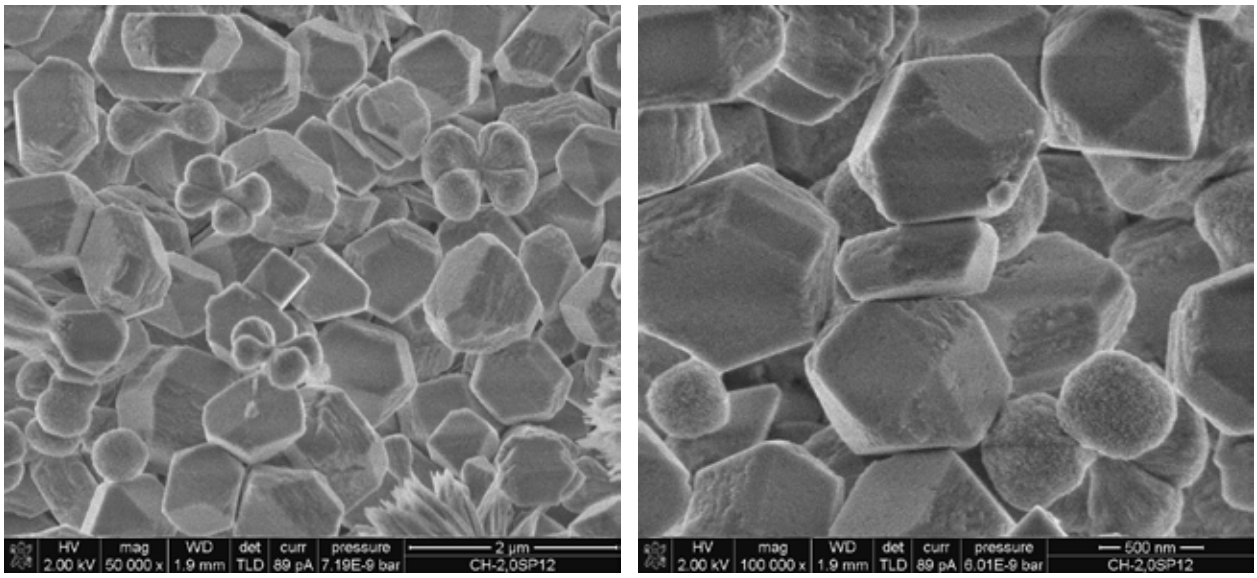

Fig. 4-52: Portlandite crystals precipitated at saturation index of 1.26 in presence of 17.1 ml/l PCE2. Additional to isometric crystals also twinned crystals are formed.

Similar to the addition of PCEs the presence of naphthalene sulfonate based superplasticizer (PNFS) leads to formation of isometric portlandite crystals (Fig. 4-53). Higher magnification reveals that the surfaces are not as well developed as in the cases of the two other superplasticizers (right hand picture of Fig. 4-53). This may be caused by

blowing up of crystal platelets which are covered by PNFS and overgrown by further crystal platelets. This effect may cause artifacts under high vacuum conditions during examination of the samples in the SEM.

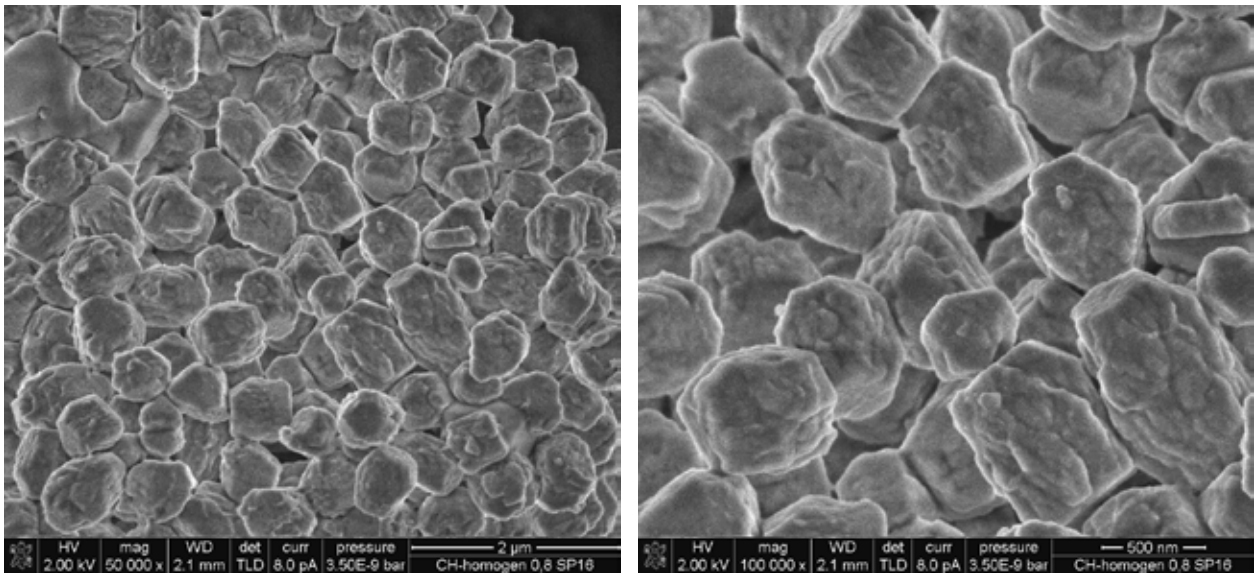

Fig. 4-53: Portlandite crystals obtained at saturation index of 1.26 in presence of PNFS at 6.7 ml/l. Again as for PCEs the crystals are more isometric compared to the reference and faces are rough.

Increased PNFS dosage leads to a broadening of crystal size distribution (with a higher fraction of small crystals), cf. Fig. 4-54. During nucleation and growth investigations it was claimed that PNFS may act as a template for crystallization especially at increased dosage. Hence it is postulated that this template performance leads to additional formation of crystals which have a smaller particle size. Furthermore, the pictures suggest an ongoing surface roughening in the presence of higher dosages of PNFS.

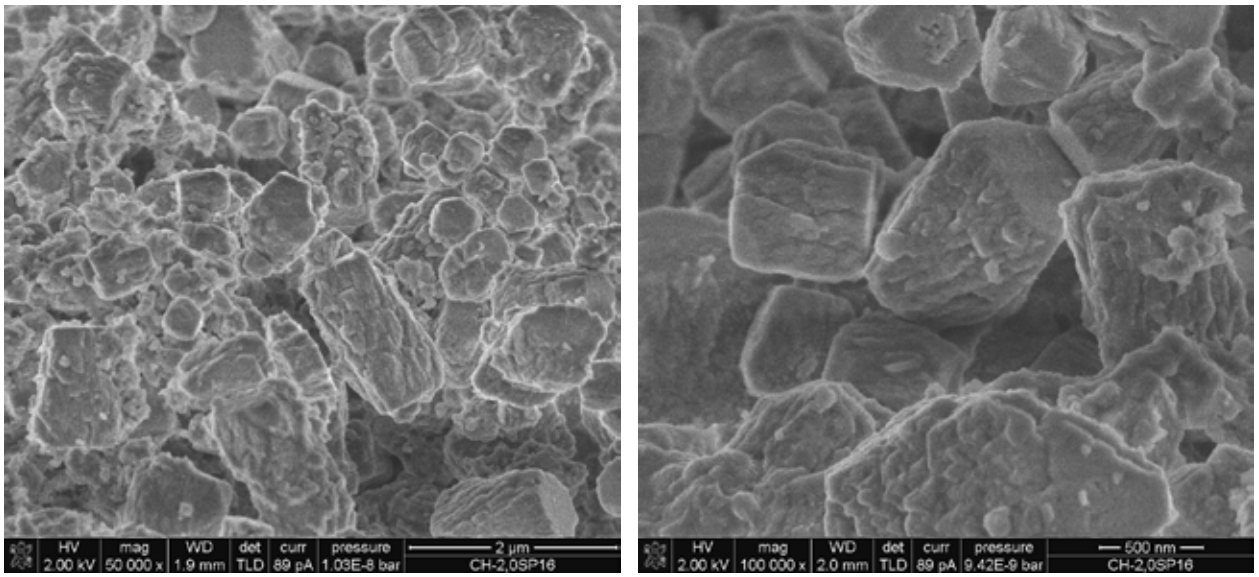

Fig. 4-54: Portlandite crystals precipitated at saturation index of 1.26 in presence of 16.6 ml/l PNFS. The fraction of smaller crystals increases which may be the result of template effects.

It is concluded that SEM investigations reveal a strong impact of superplasticizers on the crystal morphology (*habitus* and *tracht*) of portlandite. In accordance to Wulff's theorem on

crystal growth (section 2.1.3.2), this behavior is related to a decrease in interfacial energy which leads to a reduction of growth rates of individual crystal faces. Based on this principle it is revealed that superplasticizers adsorb in different amounts on individual crystal faces. Finally, SEM investigations support the observation that superplasticizer influence crystallization kinetics (nucleation and growth) as shown in sections 4.2.5.2.1 and 4.2.5.2.2.

4.2.5.3 Discussion

Based on crystallization theory the observed retarding effect of superplasticizers on pure crystallization of C-S-H phases and portlandite are discussed in the present section. Basically as deduced from classical nucleation theory, an increase in induction time may be related to a decrease in interfacial energy and/or a decrease of the degree of supersaturation (see eq. (23)). Both possibilities are discussed in the following.

Although variations in interfacial energy are not directly investigated in the present work, changes in crystal morphology permits a discussion of the impact of varied interfacial energies by adsorbed polymers. In particular, changes in crystal *tracht* of portlandite in the presence of superplasticizers (section 4.2.5.2.3 (p.125)) leads to conclude that based on crystallization theory (Wulff's theorem, section 2.1.3.2) both global crystal growth rates and growth of individual crystal faces are decreased as a result of polymer adsorption (complexation of calcium ions on surfaces). This was demonstrated for portlandite with a strong impact on the {101} crystal face. At the same degree of supersaturation the superplasticizer reduced growth of portlandite leads to the precipitation of euhedrical portlandite crystals. This crystal *habitus* is predicted by Galmarini[62] for portlandite precipitation from pure lime solution. C-S-H phases, however, appear in agglomerates instead of individual crystals. But it was also shown that superplasicizers impacts theses C-S-H agglomerates mainly by decreasing their size. It was furthermore revealed that the molar Ca/Si ratio of C-S-H phases was not strongly influenced by the presence of superplasticizers. Thus, the complexation of calcium ions on surfaces (adsorption) by the functional groups of polymers is to a major part responsible for the reduction in crystal growth rate.

On the other hand the degree of supersaturation may be reduced as a result of ion complexation by polymer's functional groups in solution. This effect causes both an increase of the induction time and a decrease of the maximum crystal growth rate. By using correlation shown in Fig. 4-11 which enable the determination of the amount of complexed calcium ions in solution at a given polymer dosage this effect was analyzed (calculations of theoretical induction times and theoretical maximum crystal growth rates). For both C-S-H phases and portlandite it was shown that complexation of dissolved Ca ions can not solely account for the prolonged induction time (Fig. 4-34, Fig. 4-35 and Fig. 4-36) and reduced maximum crystal growth rate (Fig. 4-40, Fig. 4-41 and Fig. 4-42). Nevertheless, complexation of Ca ions is able to alter both kinetic parameters by their impact on supersaturation during pure crystallization experiments. It is claimed that this effect is of minor importance in cement systems[108], since the complexation can be easily compensated by additional dissolution of solid material. This was demonstrated on C-S-H

and portlandite solubility (section 4.2.3 (p.94)). Hence, a further mechanism must hinder crystallization.

An indication for this additional mechanism can be found in the surprising behavior of the PCEs during nucleation. Because contrary to findings during C_3S hydration in the presence of SPs (section 4.3.4.2.6, p.162) it is observed that changing polymer conformation from flexible backbone worm (PCE1, shorter side chains, longer backbone) to flexible backbone star (PCE2, longer side chains, shorter backbone) increases retardation. This effect may imply that particle assembly, i.e. nuclei agglomeration, which occurs during induction time plays a pivotal role in crystallization and this effect is related to polymer structure. Moreover, this may lead to conclude that the pure nucleation is not strongly retarded by polymers. In order to interpret the data it is hypothesized in analogy to colloids[193] that superplasticizers may adsorb on nuclei and hinder their agglomeration due to their dispersing performance, see section 2.1.4 (p.42). This effect seems to be directly related to conformation of the polymers (side chain length, see sketch in Fig. 4-55) and accounts for the observed effects.

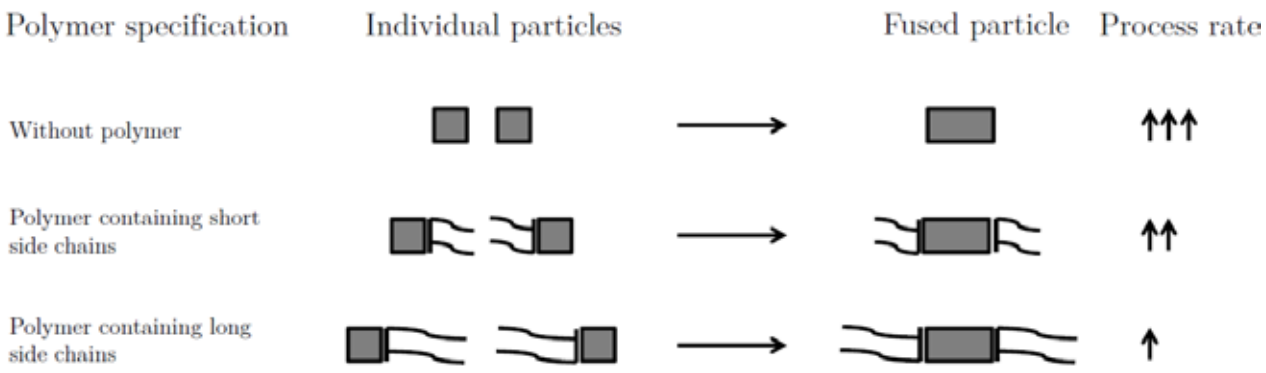

Fig. 4-55: Scheme of the dependency of particle fusion rate on polymer specification in adaption of the particle mediated crystallization approach by Cölfen and Antonietti[33].

In Fig. 4-55 the principles of particle mediated crystallization is schemed. This model is adapted from approaches in biomineralization[33] and extended to the kinetic dependency of crystal fusion and polymer specification. Therefore single particles are formed from ions in supersaturated solutions. This stage is not much affected by the presence of superplasticizers. After a critical size of the particles is reached then the further growth of these particles is affected by adsorbed polymers with dispersing performance, i.e. particles are stabilized. As a consequence, after nucleation the crystal ripening process as following step during crystallization is hindered when surfaces of individual particles are occupied by polymers. Furthermore, the steric performance caused by grafted side chains has a major contribution in hindering particle fusion. This effect strongly impacts crystallization (increase of induction time and reduction of maximum growth rate) *via* particle fusion and is directly related to the conformation of polymers (grafting degree, length of side chains).

This model is in accordance to results on principal modes of action of polymers gathered by means of Analytical Ultracentrifugation (AUC). There it was shown that C-S-H clusters are formed in the aqueous phase of C_3S pastes, see section 4.1.4 (p.88). In this respect it

was demonstrated that superplasticizers can induce cluster formation and thus act as template. An earlier clue for particle formation was given by Garrault *et al.*[64]. By means of AFM they showed that C-S-H builds up particles with sizes of 60x30x5 nm. Furthermore, the model is consistent to the data interpretation regarding the solubility experiments of C-S-H phases and portlandite, see section 4.2.3.2.2 (p.100). There it was claimed that superplasticizer are partly adsorbed on surfaces. As a result both solubility and pure crystallization are affected.

In terms of materials structure it is known that polymers may act as templates for crystallization. This effect is well studied in biomineralization[1-2, 6, 33]. Analogously, results demonstrate that superplasticizers may act as templates during pure crystallization of both C-S-H and portlandite. The observation of decreased length of induction period at increased dosage of SPs leads to conclude that template effects promote the crystallization process in terms of kinetics. The ability to complex dissolved calcium ions by the polymer's functional groups can thus be associated with the first step in the performance as template. In a second step anionic species may adsorb on the Ca layer and successively nuclei/cluster are formed[6]. This is supported by AUC experiments where it was shown that polymer-C-S-H complexes present in the aqueous phase of C_3S pastes are larger than simple Ca-polymer complexes (chapter 4.1.4, p.88).

Fig. 4-56 summarizes schematically the several contributions to the induction time during crystallization in presence of superplasticizers.

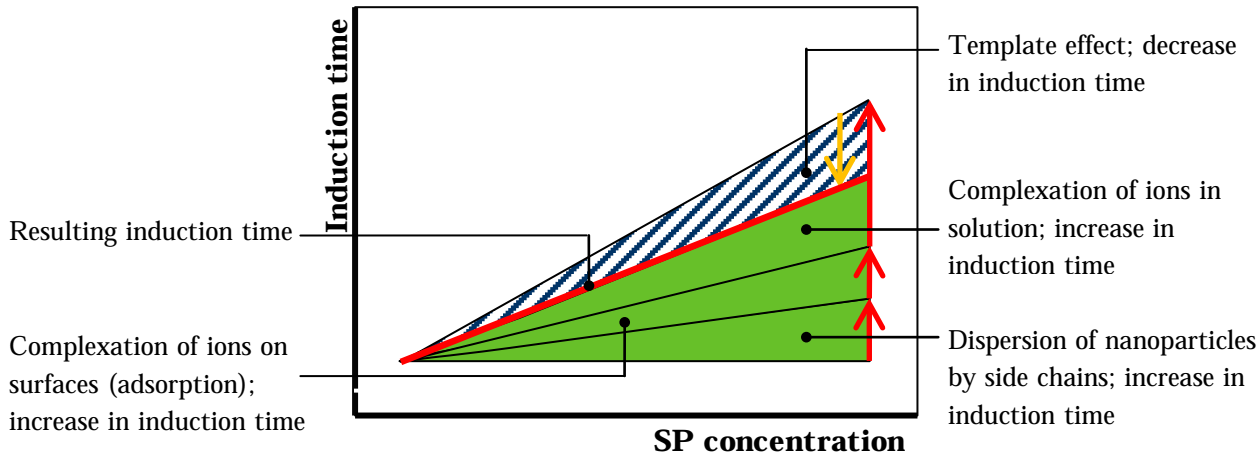

Fig. 4-56: Schematic illustration of the influences of superplasticizer induced effects on the resulting induction time (red line) in crystallization. Retardation is induced by complexation of ions (in solution and on surfaces) and dispersion of nanoparticles. Template effect of superplasticizers induces acceleration of the crystallization process. All effects are dependent on the SP-dosage.

4.2.5.4 Summary

In the present section the pure precipitation of the products of C_3S hydration namely C-S-H phases and portlandite was investigated. Thereby dissolution reactions of solid educt phases were omitted by double decomposition of appropriate ions during mixing of solutions resulting in crystallization. Classical nucleation theory (chapter 2.1.3) was applied

in order to determine kinetic parameters, i.e. induction time and crystal growth rate. These parameters were measured by means of electrical conductivity and correlated with the degree of supersaturation (eqs. (41) and (42)). In accordance to classical nucleation theory (chapter 2.1.3) it was shown that with increasing degree of supersaturation induction time decreases whereas the maximum growth rate increases. By use of eq. (23) interfacial energy between crystal and surrounding solution was estimated to 15.1(10.3) and 45.5(26.7) mJ/m^2 for homogeneous (heterogeneous) nucleation of C-S-H phases and portlandite, respectively. Critical diameters for stable nuclei were determined to 2.3(1.9) and 2.7(2.6) nm for C-S-H phases and 0.8(0.6) and 1.0(0.8) nm for portlandite homogeneous (heterogeneous) nucleation, respectively. These values range within reported ones[21, 63, 102] showing that the used approach is reasonable.

As demonstrated in chapter 4.2.5 and claimed by others[91, 125] superplasticizers retard the pure crystallization of C-S-H and portlandite. During pure precipitation experiments (double decomposition), this behaviour is characterized by both prolonged induction time (Fig. 4-32) and reduced crystal growth rates (Fig. 4-38). Based on classical crystallization theory variations in interfacial energy and degree of supersaturation by the polymers was discussed. It is concluded that both mechanism retard crystallization. But based on the comparison of PCE1 (flexible backbone worm) and PCE2 (fexible backbone star) it is shown that particle fusion during the period of particle mediated crystallization (i.e. after nucleation) is crucial for the overall crystallization kinetics. Therefore it is proposed that particle fusion is hindered by polymers grafted with side chains. This effect increases with increasing side chain length.

Exemplarily on PNFS it was further demonstrated that crystallization can be promoted by the presence of polymers *via* template effects.

4.2.6 Concluding remarks

The present chapter was dedicated to investigate the impact of the principal modes of action of superplasticizers (chapter 4.1, p.75) on the solubility of hydrates (C-S-H phases, portlandite, section 4.2.3), pure dissolution kinetics of C_3S (section 4.2.4) and the pure precipitation kinetics of both C-S-H phases and portlandite (section 4.2.5). Thus, dissolution and precipitation reactions occurring during C_3S hydration are investigated separately.

The experimental part of chapter 4.2 started with the **synthesis of C-S-H phases**. It was found that the used method (mixing CaO with nanosized SiO_2 in water) leads to C-S-H phases with a molar Ca/Si ratio of 1.4.

In section 4.2.3 it is concluded that the ability of functional groups of the polymers to complex Ca ions in solution leads to an increase of the **solubility of C-S-H phases and portlandite**. Moreover, data are used to compute complexation constants. Comparison of these constants with those determined in $CaCl_2$ solution (section 4.1.3) revealed that superplasticizers are partly adsorbed on C-S-H phases and portlandite. Thereby, polymers complex calcium ions from solution prior to the adsorption on C-S-H phases leading to reduced calcium ion concentrations in the aqueous phase. Compared to portlandite the

adsorption is stronger on C-S-H phases. In the case of portlandite calcium ions are accumulated in the aqueous phase, i.e. an increase in calcium ion concentration is observed.

Experiments on the **pure dissolution of C_3S** illustrated in section 4.2.4 proved findings from other studies[47, 106, 110] that dissolution rate is dependent on the degree of undersaturation with respect to the dissolving phase (C_3S). Increased dissolution rates are measured in the presence of PCE1 if ion activities in aqueous solution are very low. This was attributed to the complexation of Ca ions (released by C_3S) in solution. If this complexation is considered in the calculations of IAP then it was shown that all investigated superplasticizers reduce the C_3S dissolution rate at a broad range of IAP. But the ranking within the different superplasticizers with respect to the retarding efficiency at constant dosage is different from the results of the C_3S hydration experiments. If calcite is added then also a reduced unconstrained C_3S dissolution rate was determined. Because from the hydration kinetics of C_3S it is expected that an accelerated C_3S dissolution rate in the presence of calcite should be detected it is questioned if either the dissolution is the global rate determining step, the experimental setup is appropriate and/or a futher parameter in dissolution theory needs to be included. All in all it is concluded that the role of dissolution reactions on retarding and accelerating effects induced by superplasticizers and calcite, respectively, during C_3S hydration remains unclear.

In contrast, results on **pure crystallization of C-S-H phases and portlandite** presented in section 4.2.5 reveal a strong impact of superplasticizers on crystallization kinetics, i.e. induction time and crystal growth rate. Also the crystal morphology is varied in the presence of superplasticizers. It is shown in this section that complexation of Ca ions (dissolved in solution and constituted on surfaces (adsorption)) induces retardation of the crystallization process. Results show a hindered crystal growth of certain faces. This hindered growth is mostly responsible for the retarding effect in pure crystallization experiments. A further retarding effect is attributed to the dispersion of nanoparticles by grafted side chains, which is claimed to be based on particle mediated crystallization processes. In contrast it was shown that under certain conditions (polymer structure, aqueous phase composition) superplasticizers can act as template for crystallization. By this effect the crystallization kinetics can be promoted.

4.3 Influence of superplasticizers on the parallel dissolution-precipitation process of tricalcium silicate hydration

4.3.1 Aim

Findings of tests on separate dissolution and precipitation kinetics are utilized in order to investigate the hydration of tricalcium silicate. Thereby, effects which were found for the separate consideration of dissolution and precipitation in presence of superplasticizers (chapter 4.2, p.93) are now analysed in parallel.

The tests address thermodynamics (activation energy, ion concentrations), kinetics (isothermal calorimetry) and microstructure (SEM, SDT). By means of the principle modes of action of polymers (complexation of Ca ions (in solution and on surfaces), cluster formation) defined in chapter 4.1, observed effects are discussed in the light of the polymer structure. Furthermore, the role of the side chain length on the magnitude of retardation is focused in more detail. In a first step, the retarding effect of superplasticizers is investigated with respect to their temperature dependency.

4.3.2 Influence of superplasticizers on the activation energy

As commonly known, kinetics of most reactions is dependent on temperature. In the following it is investigated whether or not superplasticizer causes a variation in this general rule. Moreover, these tests are able to characterize the performance of superplasticizers on hydration kinetics from a more general point of view.

4.3.2.1 Experimental setup

Isothermal conduction calorimetry (section 3.2.2, p.69) was performed on C_3S pastes with or without additions of superplasticizer PCE1 (0.1 m.-% bwoC_3S) at temperatures in the range between 5°C, 20°C, 30°C and 40°C. From the heat release rate the end of the induction period was determined as point of onset of the acceleration period. The total heat released during the hydration at this point was used to determine the degree of hydration. From that the amount of reacted C_3S was calculated and subsequently related to the length of the induction period. This value corresponds to a reaction rate surpassing the induction period.

Arrhenius parameters (activation energy, frequency factor) were determined by plotting the natural logarithm of the reaction rate against the inverse temperature in Kelvin. The slope and the intercept with the ordinate correspond to the activation energy and the frequency factor, respectively.

4.3.2.2 Results and discussion

Fig. 4-57 shows the heat release rate obtained at different temperatures for the reference samples (dotted lines) and the corresponding superplasticizer blended samples (solid lines).

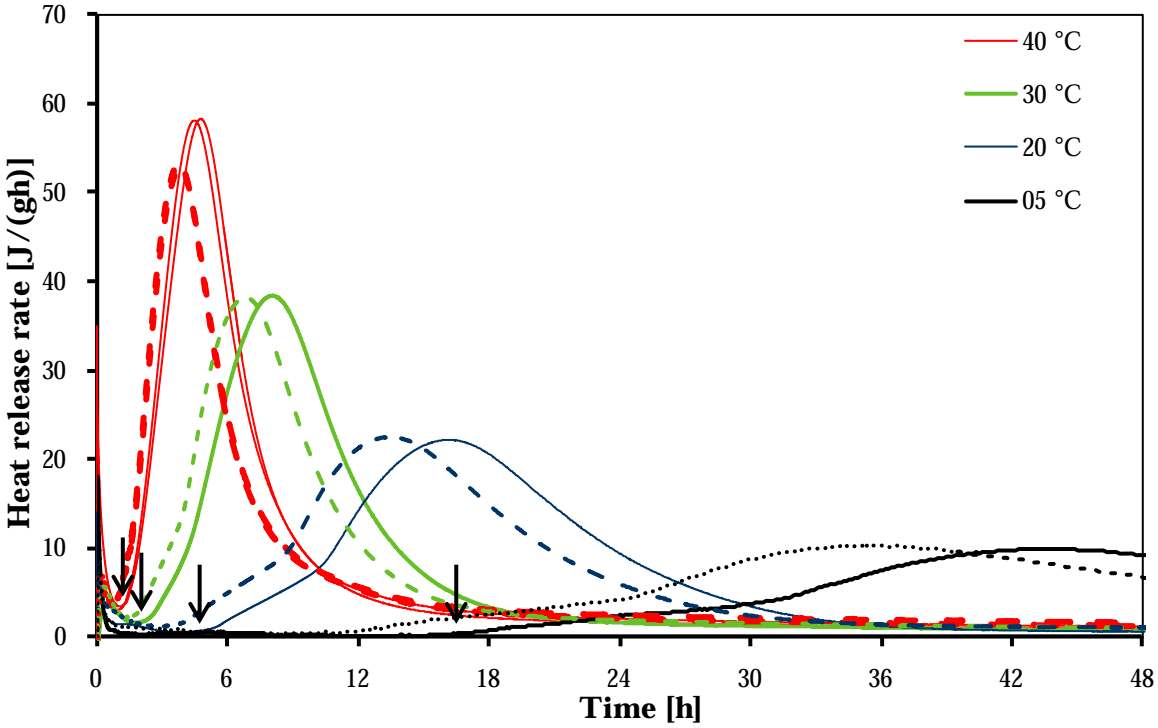

Fig. 4-57: Heat release rate during C_3S hydration influenced by PCE1 (0.1 m-% bwoC_3S) at given temperatures and l/s ratio of 0.37. Dotted lines represent the reference samples without superplasticizer and arrows the end of the induction period of the superplasticizer containing samples. Increasing temperature leads to increased reaction rates and shortened duration of the induction period. Only at increased temperature, PCE1 leads to increased heat release rate during main hydration period with respect to the control sample.

As expected the hydration kinetics is strongly affected by temperature. Thereby with increasing temperature heat release rate increases and the onset of hydration stages is shifted to earlier periods. Furthermore, the addition of superplasticizer causes increased duration of the induction period (arrows in Fig. 4-57) at all investigated temperatures.

From the calorimetric data the degree of hydration and subsequently the amount of reacted C_3S was determined according to 3.2.2 (p.69). Related to the length of the induction period, a reaction rate was calculated. The natural logarithm of these values plotted against inversed temperature gives the so called Arrhenius plot, see Fig. 4-58 (left hand).

Fig. 4-58 (left hand) shows furthermore that the reaction rate is temperature dependent. With increasing temperature the rate increases. From the slopes and the ordinate intercepts in Fig. 4-58 (left hand) the activation energy and the frequency factor were computed and given in Fig. 4-58 (left hand).

It can be seen that the prolonged induction period with respect to the reference in presence of PCE1 is associated with a slight increase in activation energy from 53.43 kJ/mol (reference) to 54.48 kJ/mol, i.e. very low and most probably not significant considering the experimental errors. In contrast the difference in the frequency factor is much more notable and beyond the scope of experimental error. For the frequency factor values of 4.70 10^5 mol/h and 3.56 10^5 mol/h are determined for the reference and the PCE1 containing sample, respectively. Thus, because activation energy being characteristic of a chemical process and that differences are so small, we conclude that the same mechanism is

controlling hydration. However, this occurs at a lower rate as revealed by the significant differences in the frequency factors.

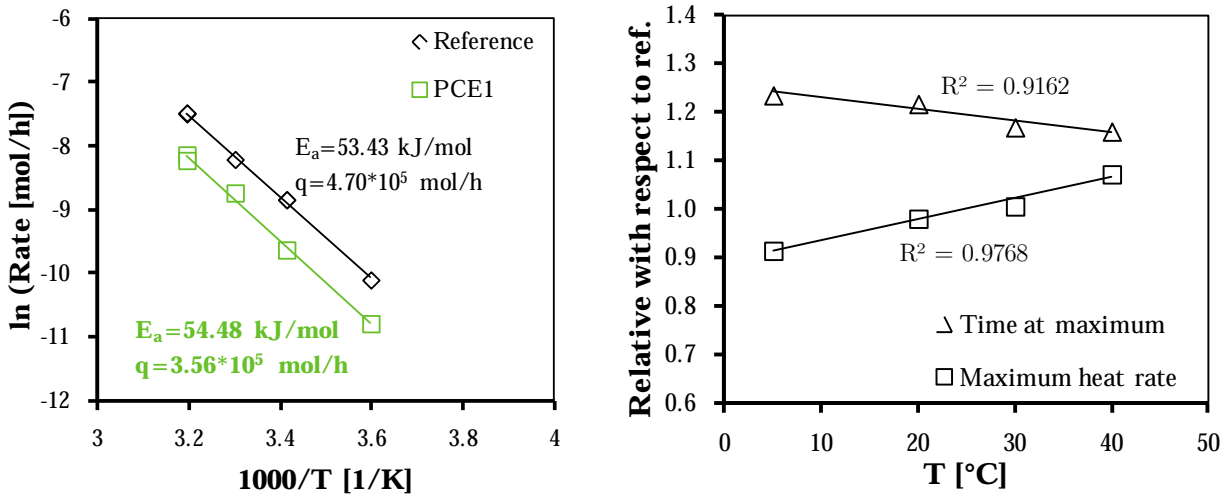

Fig. 4-58: Arrhenius plot (left hand) with corresponding Arrhenius parameters (E_a, q) for the end of induction period and (right hand) value and time of the heat release maximum with respect to the reference during C_3S hydration influenced by PCE1. Addition of PCE1 increases both activation energy and frequency factor. As a result of retardation, with increasing temperature both time at maximum and corresponding heat release rate occur at earlier and later periods, respectively.

With respect to the reference the main hydration peak is also influenced by PCE1, cf. Fig. 4-57. Examination of the maximum in Fig. 4-57 shown in right hand graph of Fig. 4-58 reveals that related to the reference the onset time of the maximum occurs earlier (linear dependency) with increasing temperature. But due to prolonged induction period the maximum is observed at later periods with respect to the reference. In contrast, the relative of maximum heat release rate with respect to the reference increases linearly with increasing temperature.

4.3.2.3 Summary

Experiments on variable temperatures indicate that with increasing temperatures the end of the induction period is reached at earlier time periods. This effect is utilized for decades in technical application to increase the strength development of cement mortars and concretes. Results shown here claim that superplasticizers act chemically as inhibitors to the onset time of the acceleration period in C_3S hydration. This is concluded on the basis of unchanged activation energy but decreased frequency factor with respect to the reference which confirms results by others[161]. Thus the retardation is mostly caused by reducing the reaction rates and not by changing reaction mechanisms. As a consequence of prolonged induction period also the maximum of the main hydration peak occurs at later periods. Thereby the maximum heat release rate increases with increasing temperature. This indicates that temperature increases the rate during the acceleration period. At increased temperature PCE1 shows a promoting effect by increasing the maximum heat release rates with respect to the reference sample without superplasticizer. But compared to the duration of the induction period this effect is less pronounced.

4.3.3 Influence of superplasticizers on aqueous ion composition of hydrating tricalcium silicate

Because the reaction of C_3S with water is a hydration process, i.e. it occurs through solution, measurements of the ion composition of the aqueous phase provide deep insights in C_3S hydration. The present chapter focuses on the ion composition in the aqueous phase of C_3S suspensions and pastes. Special attention is laid on the impact of superplasticizers on the ion concentration in the light of their principal modes of action outlined in chapter 4.1 (p.75).

4.3.3.1 Experimental setup

For suspension experiments, an appropriate amount of C_3S (to adjust different l/s ratios) was added to solutions by keeping constant the amount of liquid (100 ml). In cases with superplasticizers, those were added prior to C_3S into solution. Experiments were carried out in sealed beaker in N_2 atmosphere (glove box) under continuous stirring of the suspension at constant rate. Electrical conductivity was measured in parallel using InLab 731 (Mettler-Toledo) electrode; see section 3.2.5.1 (p.69).

The aqueous phase was withdrawn by filtering (0.2 µm) the suspension, if not otherwise stated, and additionally acidified with 5M HNO_3 in order to prevent precipitation of product phases before ICP-OES measurements were conducted (section 3.2.5.2, p.69). The exact dilution induced by acid addition was taken into account (dilution was between approx. 2 and 5 %). Microstructure was investigated by means of SEM (section 3.2.4, p.69).

4.3.3.2 Results and discussion

4.3.3.2.1 The pure C_3S system

As mentioned in chapter 2.2.3.2 (p.52), Ca and Si ion concentrations follow a well defined relationship. This is known as kinetic path[12-13, 40] and solubility of C-S-H(m)[70, 86]. In order to investigate the impact of superplasticizers on the ion composition of the aqueous phase, the pure C_3S-H_2O system was analyzed, precedingly. Results are given in Fig. 4-59. Additionally, data presented by Gartner and Jennings[70] is also shown. As mentioned in chapter 2.2.3.2 these authors examined a large dataset on published Ca and Si concentrations.

Experiments shown here confirm that the measured silicon and calcium concentrations describe a function. Moreover, the addition of calcite to C_3S suspensions leads to the same relationship. Thus it is concluded that the Ca-Si ion concentrations correlation is of general importance for C_3S hydration.

The Ca-Si relationship is mathematically modeled by the following expression:

$$\mathrm{Si}\,[\mu\mathrm{mol/l}] = 13.46755 \cdot \mathrm{Ca}\,[\mathrm{mmol/l}]^{20.69148 \cdot \mathrm{Ca}\,[\mathrm{mmol/l}]^{1.26031}} \qquad 5\ \mathrm{mmol/l} \le \mathrm{Ca} \le 39\ \mathrm{mmol/l} \qquad (43)$$

It should be emphasized that the hydration follows the function in direction of increasing Ca concentrations until at its maximum portlandite precipitates. During hydration the ion concentration follows that pathway.

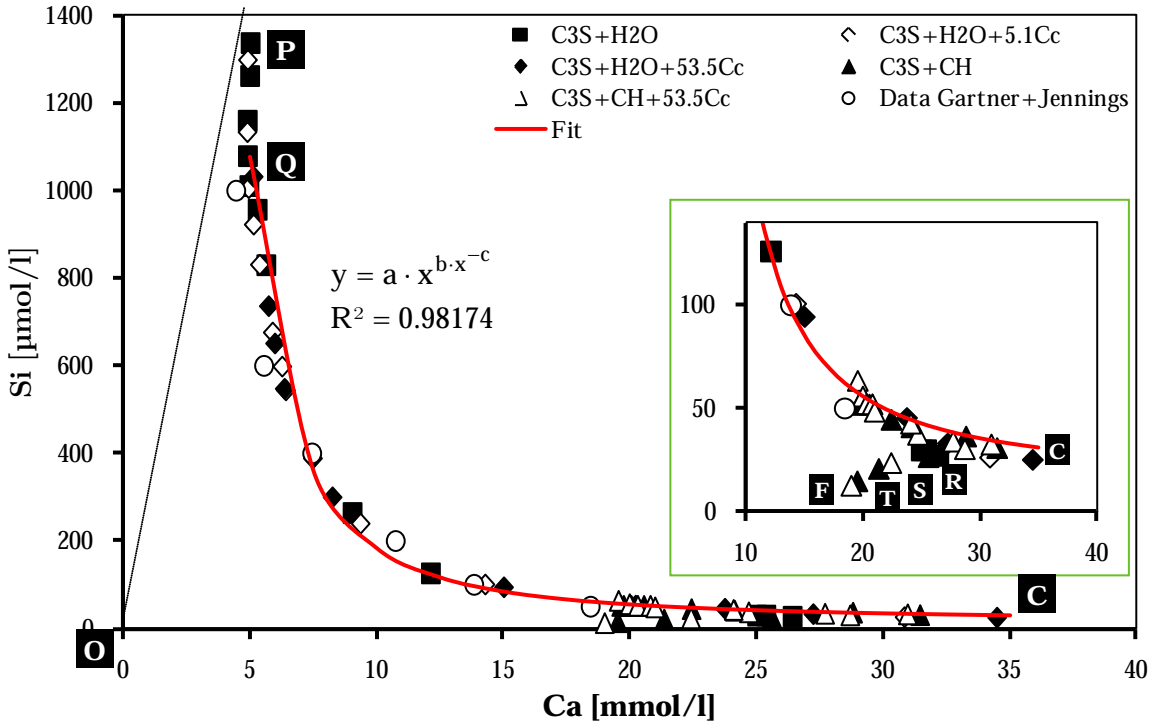

Fig. 4-59: Si concentration in the aqueous solution of C_3S suspensions (l/s=50) in different starting solutions with and without the addition of 5.1 and 53.5 m^2 calcite (Cc)/g C_3S as function of Ca concentration. Line represents computed Si concentrations derived from mathematical fit (eq. (43). All symbols refer to measured concentrations by means of ICP-OES. Literature data was taken from Gartner and Jennings[70]. Letters (O, P, Q, C, R) show points during C_3S hydration published by Damidot and Nonat[40] and additional points (S, T, F). The inset shows ranges of high Ca and low Si in more detail. It is demonstrated that during hydration ion concentrations are restricted (known as kinetic path[12-13, 40] and solubility of C-S-H(m)[70, 86]).

4.3.3.2.2 Influence of superplasticizers on the ion composition in the aqueous phase

The impact of superplasticizers (Table 3-1) on the ion concentration during C_3S hydration is shown in detail in Fig. 4-60 and in overview in Fig. 4-61. SP-dosage was adjusted to 0.1 m.-% with respect to C_3S at l/s of 50. Furthermore, in Fig. 4-60 and Fig. 4-61 the solubility of C-S-H phases and maximum concentration obtained during C_3S hydration[40] (solid lines) are shown.

In accordance to previous findings[13, 40], the precipitation of C-S-H phases starts in point P and ends in point Q after the congruent dissolution of C_3S (dotted line), see Fig. 4-60. This path is associated with decreasing silicate concentrations at constant calcium concentration and measured as plateau in the electrical conductivity (Fig. 4-64, p.149) and (Fig. 4-71, p.158). As shown by Fig. 4-60, the onset of C-S-H precipitation is affected by superplasticizer addition. In the case of both PCE1 and PNFS, in the beginning of the experiment ($P_{1,16}$) calcium and silicate ion concentrations exceeds the maximum supersaturation curve with respect to C-S-H phases. Based on results presented in chapter 4.1 (p.75), the complexation capability of calcium by the functional groups of the polymers

may account for this observation. But in this region the Ca/Si molar ratio equals 3. Thus this result more reasonable indicates that the precipitation of C-S-H phases is hindered (section 4.2.5, p.111) leading to an increase in C_3S solubility.

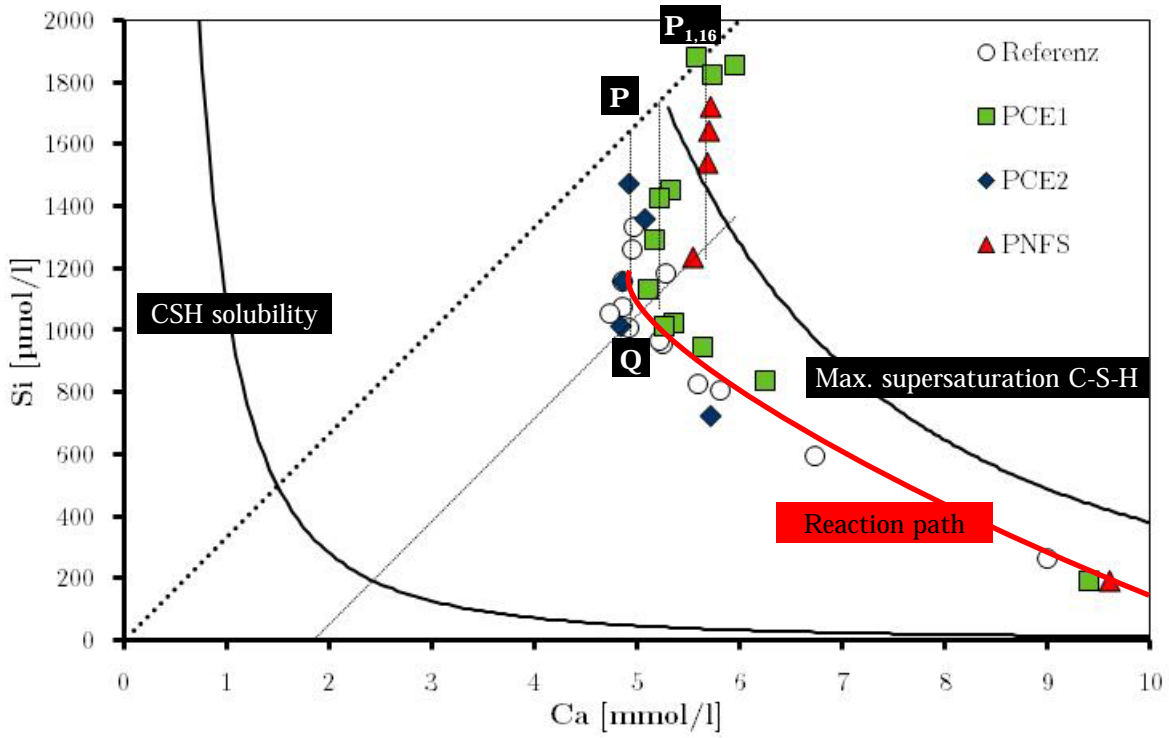

Fig. 4-60: Detail of Fig. 4-61. Dotted lines serve as guides for the eye and represent congruent C_3S dissolution (bold line) and the drop in silicate due to C-S-H precipitation for different superplasticizers. In the beginning (point P) polymers grafted with short side chains and PNFS based polymers induces increased ion concentrations which fall onto the reference curve in the further course of hydration.

During the silicate concentration drop from point P to point Q also calcium ions are consumed in presence of PCE1. This behavior is not observed in presence of other superplasticizers.

At increased calcium concentrations differences with respect to the reference are observed in the presence of all investigated superplasticizers. This effect remains until portlandite precipitates and is indicated with an increased Ca ion concentration in the aqueous phase which is in accordance to findings that electrical conductivity is increased when superplasticizers were added (electrical conductivity induced solely by SPs is substracted, Fig. 4-71, p.158). Also in the presence of PCE based superplasticizers increased silicate ion concentrations reaching maximum supersaturation with respect to C-S-H phases are measured. Moreover, also even higher concentrations are measured. These experimental data leads to the central question when C_3S hydration kinetics is considered: are the ion concentrations in the aqueous phase (known as kinetic path[12-13, 40] and solubility of C-S-H(m)[70, 86], termed reaction path in the present work) affected by the presence of superplasticizers or not? Because increased ion concentration with respect to the reference can be a result of the principal modes of action of superplasticizers (chapter 4.1 (p.75) and section 4.2.5 (p.111)) these effects are taken in particular into account to clearify this point.

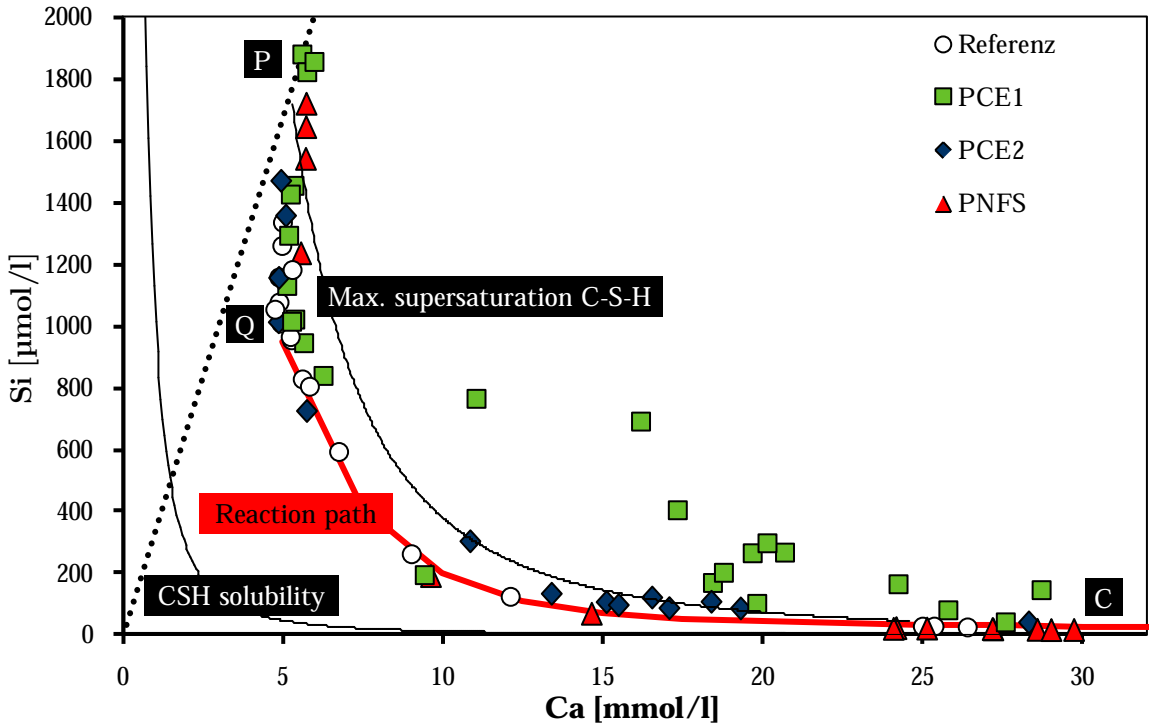

Fig. 4-61: Ca-Si concentration diagram of C_3S hydrated under suspension condition (l/s=50) in presence of PCE1, PCE2 and PNFS. Dotted line represents congruent dissolution of C_3S starting in water. At increased Ca ion concentrations in the presence of superplasticizer increased Si ion concentrations are measured.

From a practical point of view, difficulties in sampling were observed when PCE based superplasticizers were utilized during the experiments especially at increased Ca concentrations (>7 mmol/l). Analogously to experiments shown in section 4.1.2.1 (p.75), the separation of particles from the aqueous phase was found to be crucial in both duration of filtration and pore size of the used filter. In contrast, these difficulties were not observed when naphthalene sulfonate based superplasticizers were present. Thus, the enhanced dispersing performance of PCE compared to PNFS is responsible for this effect.

Discussed phenomenons with respect to principal modes of action are the complexation of ions in solution and the particle formation by cluster aggregation. In fact complexation of calcium ions by the functional groups of polymers leads to a shift of the reaction path to higher calcium ion concentrations maintaining silicium concentration. By this effect the curve representing the maximum supersaturation with respect to C-S-H phases can be reached. Because the PCEs are added to the starting solution this effect works only if complexation and release of calcium ions by the functional groups proceed on similar rates. If the rate of complexation is much higher than the corresponding calcium ion release rate then this effect is only expected in the beginning of the experiment. But this effect alone is not sufficient to account for the increased ion concentrations in particular in case of PCE1. Hence, particle formation may play an additional role for increased ion concentrations by causing artifacts.

In order to analyse if particles are formed in the aqueous phase, different modes of sample preparation were utilized, i.e. filtering and centrifuging. In Fig. 4-62 the influence of the

pore size on the determined calcium and silicate ion concentrations is shown. Additionally, filtered samples (0.7 µm) were centrifuged at 11,000g for 10 min prior to the ICP-OES measurements. It should be noted that principally all samples are acidified before ICP-OES is utilized which prevents precipitation of phases, but also causes dissolution of existing particles. In Fig. 4-62 direct comparison between different samples is not permitted because of different hydration progresses at sampling time. Only sample groups (e.g. PCE1) can be compared.

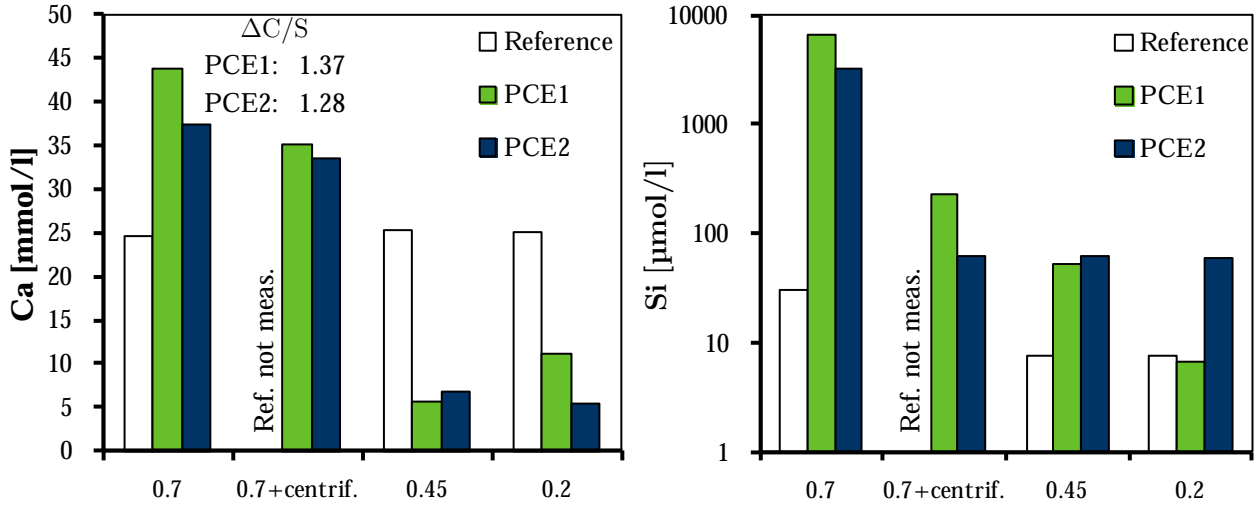

Fig. 4-62: Ca (left hand) and silicate (right hand) ion concentrations of the aqueous phase of C_3S suspensions (l/s=50) in dependence on the filter size (numbers refer to µm). Samples 0.7 µm were additionally centrifuged. Samples were taken at electrical conductivity [mS/cm] of 9.57 (Reference), 11.75 (PCE1) and 11.18 (PCE2). It is shown that due to the particles present in the sample, preparation plays a crucial role for the determination of ion concentrations.

In case of the reference without superplasticizer shown in Fig. 4-62 it can be seen that calcium ion concentrations are similar for all sample preparations. Also silicate ion concentrations are in the same order of magnitude for the reference sample. This shows that filtering at 0.7 µm pore size (in this particular case) is sufficient to separate C_3S particles from the surrounding solution in the absence of superplasticizers. In contrast, the presence of both superplasticizers causes variations in calcium and silicate concentrations in dependence on the sample preparation. The large difference in ion concentration between samples solely filtered through 0.7 µm pore size and those which were additionally centrifuged is obvious.

As shown by SEM experiments, particles are still present in the aqueous phase in case of 0.7 µm filtering, see Fig. 4-63. These particles appear as spherical clusters and lead to a turbitity of the aqueous solution. Because the aqueous phase is removed by filtering prior to the SEM imaging, these particles agglomerate as a residual layer (C_3S hydration products) on filter paper. Based on findings by AUC (section 4.1.4, p.88), it is reasonable to assume that these particles are dispersed in the aqueous phase prior to sampling. Analyses by means of ICP-OES showed that centrifuging causes sedimentation of these particles and thus to a decrease in ion concentration. Taking the differences in ion concentrations before and after centrifugation into account, the molar Ca/Si of the

sedimented particles is calculated to 1.37 and 1.28 in case of PCE1 and PCE2, respectively, and therefore increased to the measured values obtained by pure precipitation experiments (section 4.2.5, p.111). Thus, the formation of C-S-H phases in the aqueous phase of C_3S suspensions is furthermore proven when superplasticizers are present, cf. chapter 4.1.4 (p.88). As mentioned before, the polymer must excert a dispersing performance to induce particle formation in the aqueous phase.

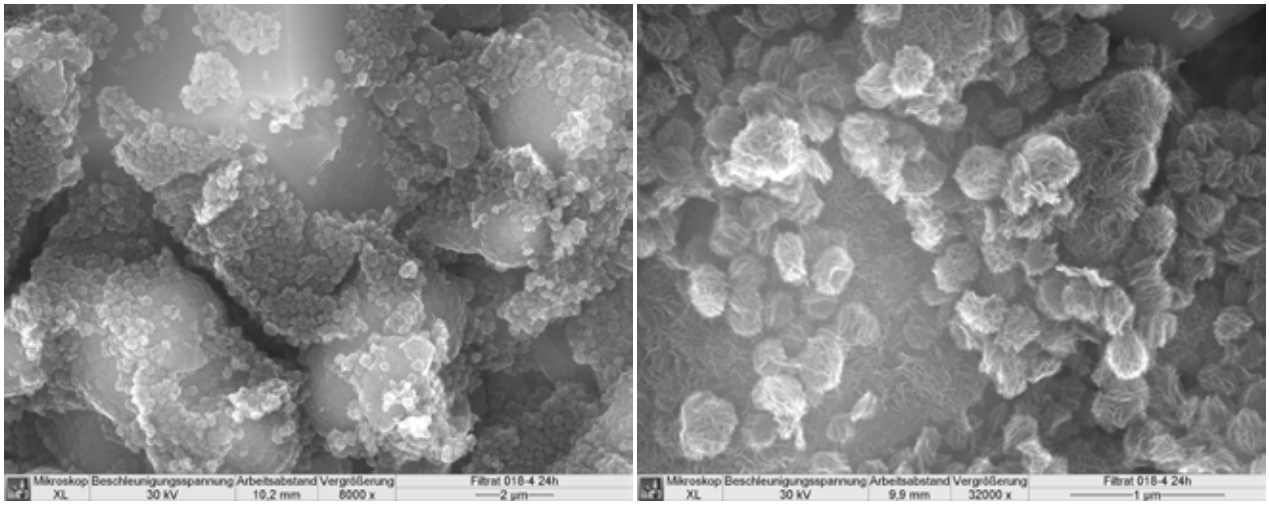

Fig. 4-63: ESEM image of the supernatant on 0.1 µm filter of PCE1 containing C_3S suspension (l/s=50, 24h) showing formation of spherical C-S-H clusters. These clusters are dispersed in solution. Right hand graph provides insights at the microstructure in higher magnification.

During hydration the size of these C-S-H particles increases. This effect may be responsible for the observation that intermediate ion concentrations (7≤Ca [mmol/l]≤25) are measured in case of PCE1 since filtering with different pore size was performed at later hydration periods, i.e. when C-S-H agglomerates are larger.

In summary it can be concluded that in the presence of PCEs the Ca-SiO_2 relationship (reaction path) is slightly surpassed reaching the supersaturation curve with respect to C-S-H phases. A clear statement on the impact of PCEs on the reaction path is complicated by the occurance of C-S-H particles surpassing the filter and, by that, causing artifacts (Fig. 4-61, Fig. 4-60). This effect is also discussed in section 4.2.3 (p.94) where the impact of SPs on the solubility of C-S-H phases were examined. Artifacts are not observed when PNFS is present. Furthermore, complexation of Ca ions in solution leads to increased ion concentrations analogously to findings on C-S-H phases and portlandite (section 4.2.3, p.94). Consequently, the electrical conductivity at portlandite precipitation is increased (section 4.3.4, p.147).

Apart from possible artifacts due to particles that may surpass the filter, increased ion concentrations can be interpreted by models regarding the cause of the induction period in tricalcium silicate hydration (section 2.2.3.2, p.52). Taken the kinetic model according to Barret and Bertrandie into account (which can be associated with the principle of detailed balancing (section 2.1.1, p.23)) then increased silicate ion concentrations indicate stronger impact on crystallization rates of C-S-H phases compared to the dissolution rate of C_3S although both rates may be altered. Whereas a strong impact on crystallization of both C-

S-H phases and portlandite by SPs was found, the influence of superplasticizers on dissolution in conditions close to C_3S hydration remains unclear. If the dissolution rate of C_3S is clearly not affected then measured ion concentrations should surpass strongly the reaction path. Thus, hindered dissolution of C_3S is possibly a further mechanism for the overall retardation. But it is unknown if this is the cause or the consequence of the overall retarding effect.

When the protective layer theory is considered then increased silicate ion concentrations suggest increased solubility of the protecting layer. This would be in accordance to the data on C-S-H and portlandite solubility in the presence of superplasticizers shown in section 4.2.3 (p.94). Thus, based on the experimental data of the present work arguments for and against the different theories on the cause of the induction period can be found. Therefore, a discussion on the cause of the induction period in C_3S hydration remains speculative at this point.

4.3.3.1 Summary

In the present section it was shown that ion concentrations in the aqueous phase are restricted by a relationship between calcium and silicate ions. Thus, results published as kinetic path[12-13, 40] and solubility of C-S-H(m)[70, 86] are proven.

Based on the complexation capability of dissolved Ca ions, it was demonstrated that superplasticizers induce increased ion concentrations (especially at portlandite precipitation). Analogously to experiments on C-S-H phases and portlandite solubility (section 4.2.3, p.94), increased Ca concentration leads to conclude that complexation of Ca ions by the functional groups of polymers causes increased solubility of C_3S and /or C-S-H phases since these complexes are additionally measured in the aqueous phase by means of ICP-OES.

Furthermore, it was found that superplasticizers cause particle formation (mainly constituted of C-S-H phases) in the aqueous phase which may induce artifacts when ion concentrations are determined. All in all it is claimed that the reaction path is not strongly affected by the presence of superplasticizers. This is in accordance to findings shown on activation energy in the previous section that superplasticizers cause decreased reaction rates while reaction mechanisms are unchanged.

4.3.4 Time dependent development of aq. ion concentrations during tricalcium silicate hydration

After in the previous section the impact of superplasticizers on ion concentrations of the aqueous phase of hydrating C_3S was investigated, the present section is aimed to monitor the time dependent development of ion concentrations during C_3S hydration. Generally, both ion concentration and ion mobility in aqueous solutions are accessable by means of electrical conductivity. Therefore, this method is utilized in the following considering findings from section 4.3.3 (p.141), i.e. restrictions in ion concentrations by kinetic path[12-13, 40] or solubility of C-S-H(m)[70, 86].

First an overview on measurements of electrical conductivity is given, and second the impact of liquid/solid (l/s) ratio is shown. In this respect, the correlation between ion

concentration and heat release rate is focused in detail. Moreover, an *in-situ* method for the determination of ion concentrations in C_3S pastes is established. Afterwards it is investigated, if superplasticizers cause a variation in the time dependent development of the electrical conductivity both in C_3S suspensions and C_3S pastes.

4.3.4.1 Experimental setup

Suspensions were prepared according to section 4.3.3.1 (p.141).

C_3S pastes were prepared by mixing either water or solution containing superplasticizers with powdered C_3S at l/s ratio of 0.5. Superplasticizer dosage was 0.1 m.-% by C_3S. Electrical conductivity (section 3.2.5.1, p.69) and heat release (isothermal conduction calorimetry, see section 3.2.2, p.69) were recorded on hydrating C_3S pastes on separate samples within the calorimeter. Calcium ion concentrations are computed from electrical conductivity according to eq. (44) in case of water as starting solution. With respect to SP containing samples Ca ion concentrations can not be calculated by the simple approach given in eq. (44) because ion mobility (activity) is varied by superplasticizers. For SEM (section 3.2.4, p.69) and STD (section 3.2.3, p.69) samples were mixed with 2-propanol and subsequently filtered (0.45 μm). The residue was dried at 100 mbar for 5 min.

4.3.4.2 Results and discussion

4.3.4.2.1 Overview

Fig. 4-64 shows the evolution of the electrical conductivity measured in C_3S suspension at l/s ratio of 50. Based on literature[14, 40-42, 65], the main characteristics can be summarized to:

(1) Conductivity plateau.

C_3S hydration commences with dissolution and consequently the electrical conductivity increases sharply. After this, a period with nearly constant value of the electrical conductivity is observed, the so called electrical conductivity plateau, during which mainly precipitation of C-S-H phases is observed.

(2) Inflection.

After the conductivity plateau, C-S-H phases grow and the amount of consumed Ca ions is lower than the released quantity. As a result, the electrical conductivity rises. In a range between 4 and 7 mS/cm at l/s=50 the curve shows an inflection which is associated with a change in growth mode of C-S-H phases (one interpretation being a change from parallel to perpendicular to the C_3S surface).

(3) Onset of portlandite precipitation.

The maximum value coincides with the maximum supersaturation with respect to portlandite, the precipitation of which is signalled by a sharp drop in electrical conductivity.

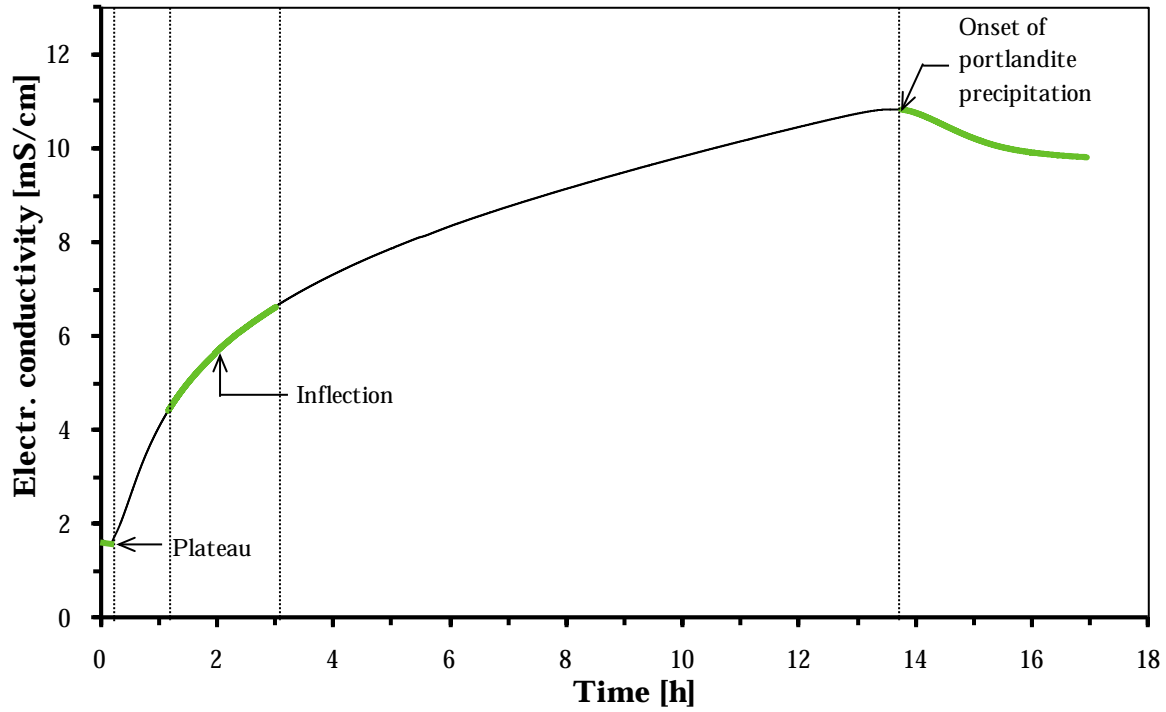

Fig. 4-64: Typical time dependent evolution of the electrical conductivity in a C_3S suspension at water/C_3S ratio of 50. Plateau, inflection and portlandite precipitation are sketched in the figure.

4.3.4.2.2 Liquid / solid ratio

Fig. 4-65 (left hand) shows the time dependent development of the electrical conductivity impacted by the l/s ratio of the starting mixture and the examination of the conductivity plateau (right hand side).

Generally, increased l/s ratio leads to increased duration of the plateau, increased magnitude of the inflection as well as delayed onset of portlandite precipitation, cf. left hand graph of Fig. 4-65.

In the present study water as starting solution was used to investigate the impact of superplasticizers on C_3S hydration kinetics. The experiments were performed under both suspension and paste conditions, i.e. l/s ratio of 50 and 0.5. Suspensions were chosen in order to increase the C-S-H precipitation on the C_3S surface provoking the effect of superplasticizers on the growth of C-S-H phases as demonstrated in section 4.2.5 (p.111).

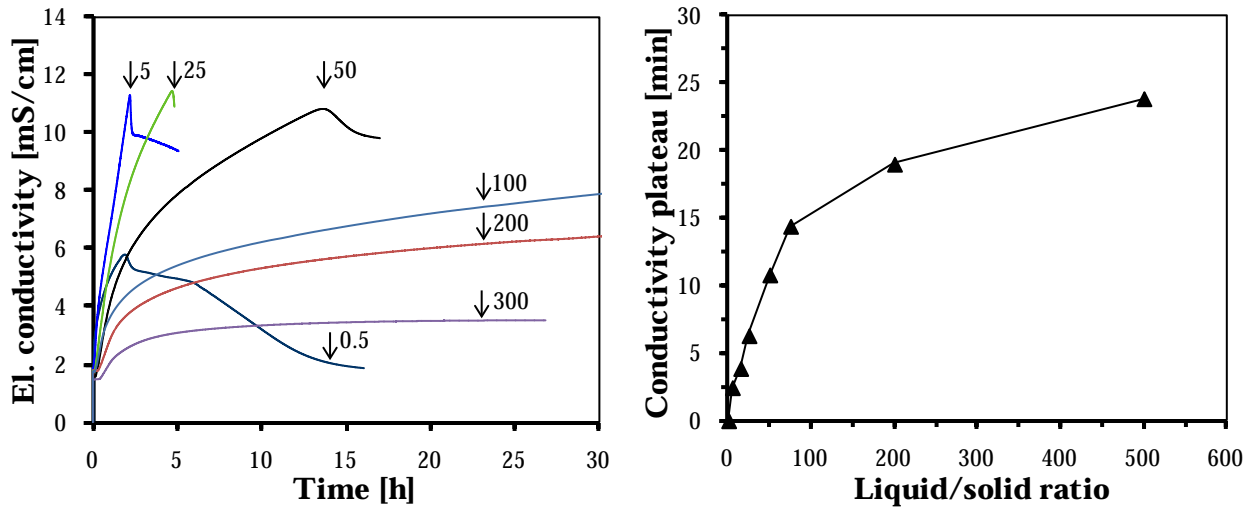

Fig. 4-65: Time dependent development of electrical conductivity during C_3S hydration with given water/C_3S ratios (left hand) and length of the electrical conductivity plateau as function of liquid/solid ratio in the starting mix of C_3S and water (right hand). It can be deduced that l/s ratio impacts both value of electrical conductivity and duration of characteristic periods, e.g. length of the plateau (right hand), observed during measurement.

In accordance to literature[14, 40-42, 65], results of the present study showed that a strong impact on duration of individual hydration periods stems from the l/s ratio. This variation can be explained by two effects, namely relation between thermodynamics and kinetics and number of precipitated C-S-H phases.

At first, the occurance of individual hydration periods is originated in the dependency of reaction kinetics on thermodynamics, see section 2.1.1, p.23. Ion concentrations in aqueous phase as driving force (thermodynamics) are dependent on solubility of educts and products. In C_3S hydration this issue is well studied (although also a kinetic origin is postulated, see section 2.2.3.2 (p.52)). Because ion concentrations and thus thermodynamics are restricted by concentrations published as kinetic path[12-13, 40] and solubility of C-S-H(m)[70, 86], the time (but not the rate) which is needed to reach certain concentrations varies when the l/s ratio is altered.

On the other hand, the dissolved fraction of C_3S increases with increasing l/s ratio. As a result, a larger amount of C-S-H phases is produced that precipitate on the surface of C_3S. Also this effect may contribute to the observation that the duration of the electrical conductivity plateau increases (right hand graph of Fig. 4-65) and the inflection is more pronounced if l/s ratio is increased (left hand graph of Fig. 4-65). It is therefore reasonable to account both scenarios (thermodynamics and precipitation of C-S-H phases on C_3S surfaces) when the duration of individual hydration periods are considered.

As shown in Fig. 4-65, with increasing l/s ratio the duration of the electrical conductivity plateau is prolonged. It should be noted that the electrical conductivity plateau at low l/s ratio (pastes) is not observed and consequently doesn't correspond to the classic induction period, see Fig. 4-68.

During the conductivity plateau the formation of first C-S-H phases occurs[13, 40]. Portlandite precipitates at later periods when the l/s ratio is increased. At l/s ratios of 0.5 and 5 portlandite precipitates equally after 3.8 hours, i.e. no difference can be found. The only

difference is the value of the electrical conductivity, which increases with increasing l/s ratio. Because no related literature can be found, it is claimed that this effect is an artifact caused by ion mobility (activity) which decreases with decreasing l/s ratio due to strong interaction of ions with surfaces.

4.3.4.2.3 *In-situ* determination of ion concentrations in the aqueous phase of hydrating C_3S

In section 4.3.3 (p.141) it was shown that the measurement of electrical conductivity in C_3S suspensions is a very suitable method to determine both ion composition (as integral) and variations of ion compositions over time. In combination with ion concentration relationship (kinetic path[12-13, 40], solubility of C-S-H(m)[70, 86]), this is utilized in order to determine ion concentrations *in-situ* during C_3S paste hydration.

According to chapter 3.2.5, electrical conductivity is related to both ion concentrations and ion mobility. In order to measure ion concentration with electrical conductivity both parameters must be known. Therefore, phase separation *via* extraction must be performed establishing *ex-situ* measurements. This is a very intensive task in C_3S pastes. In order to ease this process, in literature[64-65] and in the previous sections diluted suspensions were investigated. Direct relation of ion concentrations from electrical conductivity provides a promising analytical tool. This is also reported in other experiments[36], but the present study attempts a further approach.

A Methodology

Ca ion concentration and electrical conductivity were measured in C_3S suspensions, pastes and extracted aqueous solution of pastes (filtration, 0.1 μm), cf. Fig. 4-66. As shown by results in Fig. 4-66, electrical conductivity can be correlated with calcium ion concentration (measured by ICP-OES) with linear expression. This correlation is mainly dependent on the l/s of the mixture originated by the mobility of charge carring ions. Therefore, the sensitivity (slope) increases with decreasing l/s. However, results from suspension conditions (l/s≥50) show similar dependency, i.e. fitting was performed for l/s=50, 75, and 100. Moreover, the extracted aqueous phase of the C_3S paste (l/s=0.5) (filled spheres in Fig. 4-66) shows similar trend to C_3S suspensions. Thus, the correlation between electrical conductivity (κ) and Ca ion concentration in the aqueous phase can be written as:

$$\mathrm{Ca}\left[\frac{\mathrm{mmol}}{\mathrm{l}}\right] = \mathrm{m}\cdot\kappa\left[\frac{\mathrm{mS}}{\mathrm{cm}}\right]. \qquad (44)$$

Slope m (see Fig. 4-66) includes the ion mobility and thus expresses differences stemed from variations in l/s. It should be noted that any additional ion than released during C_3S hydration impacts the value of the electrical conductivity and thus may affect the calculated Ca concentrations. Determined slopes in Fig. 4-66 are thus only valid for tests on pure C_3S hydration with minor concentrations of foreign ions.

In the next step the silicon concentration can be calculated from calcium concentration obeying the aforementioned relationship in eq. (43).

For complete computation of ion concentrations during C_3S hydration, the hydroxide ion concentration can be assessed by following expression:

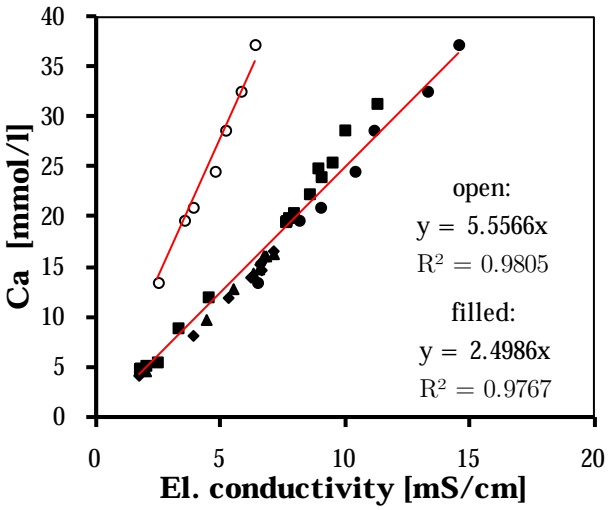

Fig. 4-66: Dependency of Ca concentration on electrical conductivity for C_3S hydrated at l/s of 0.5 (open spheres), 50 (squares), 75 (diamonds) and 100 (triangles). Filled spheres represents the measurements at l/s=0.5 after filtration. Electrical conductivity can be utilized to determined Ca ion concentrations in the aqueous phase of both C_3S pastes and suspensions.

$$Ca(OH)_2 \leftrightarrow Ca^{2+} + 2OH^- . \qquad (45)$$

B Method validation and discussion

Evaluation of the method was performed in two ways. Firstly, computed values were compared with measured ones. In this context also calcite was added to the mixture.

Fig. 4-67 shows measured (symbols) and computed (lines, eq. (44)) Ca concentrations in the aqueous phase of C_3S hydrated at l/s of 50 in dependence of different starting solutions and calcite additions. It can be seen that the computed and measured Ca concentrations for the different samples fit very well.

The method was secondly proved by independent measurements reported in literature[14]. There, the maximum Ca concentration is associated with the onset of portlandite formation (Barret and Bertrandie[14]). Comparing the Ca concentrations obtained in the present study by fitting (eq. (44), maximum Ca between 30.2 and 34.2 mmol/l) to reported value of 30.5 mmol/l (by Barret and Bertrandie[14]) shows good consistency. This is even achieved for the addition of calcite and also for different starting solutions. Thus, the present approach leads to reasonable values.

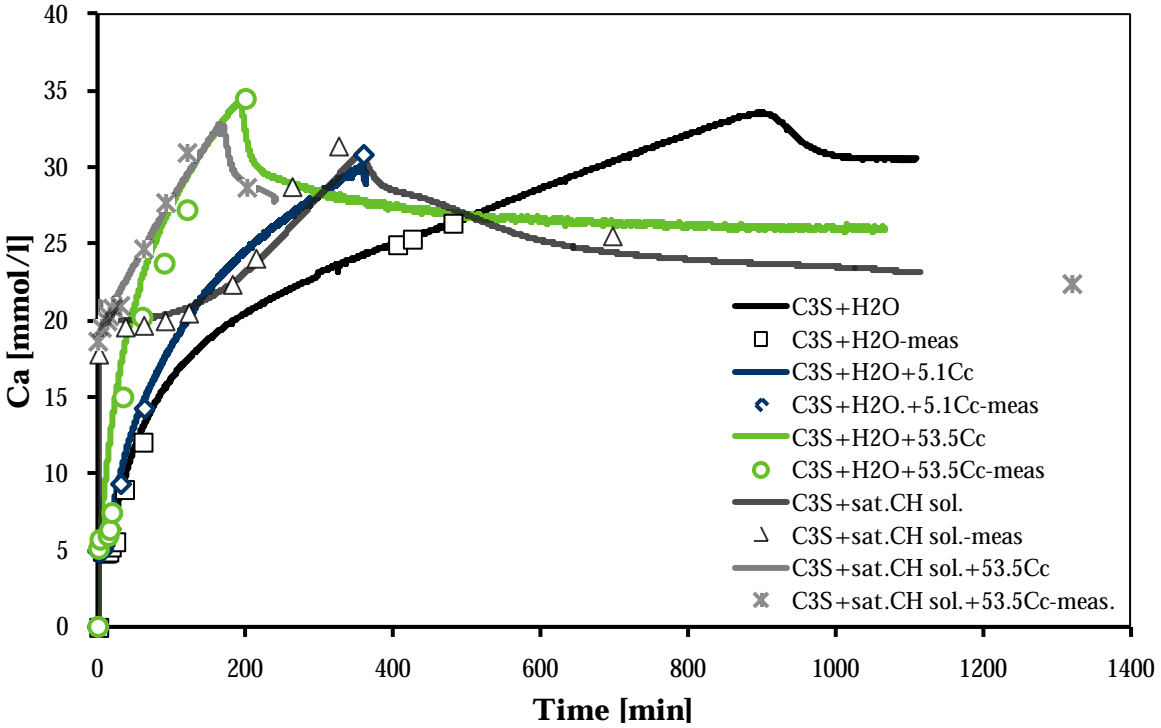

Fig. 4-67: Ca ion concentration in the aqueous phase of C_3S suspensions (l/s=50) in dependence of time. Starting solutions are either water (H_2O) or saturated $Ca(OH)_2$ solution (CH). Numbers in the legend represent the addition of 5.1 and 53.5 m^2 calcite (Cc)/g C_3S. Lines show computed (eq. (44)) and symbols measured Ca ion concentrations (ICP-OES). Measured and fitted (by electr. conductivity) Ca ion concentrations show consistency, i.e. the electrical conductivity can be utilized in order to determine Ca ion concentrations.

4.3.4.2.4 Paste hydration of C_3S followed by electrical conductivity and isothermal conduction calorimetry

The hydration of C_3S under paste conditions is investigated in parallel by means of electrical conductivity and isothermal conduction calorimetry. Therefore, both tests are putted in relation. From electrical conductivity Ca ion concentration is calculated by eq. (44). Commencing with ion concentrations and heat release, Fig. 4-68 illustrates their dependency during C_3S hydration.

Whilst conduction calorimetry allows distinguishing different stages of hydration as known from literature, see Fig. 2-13, electrical conductivity and thus Ca ion concentration provides a more differentiated view on early hydration stages that are symbolized by roman numbers in Fig. 4-68. These stages are defined by specific points in the Ca-Si diagram for the C_3S hydration, cf. Fig. 2-14 (p.54)[40] and Fig. 4-59 (p.142). Besides published points O, P, Q, C, R additional points during main hydration period entitled S, T and F are defined in the graph of Fig. 4-68. Thus seven stages of hydration can be identified. In the following, relations between ion concentrations (cf. Fig. 4-59, p.142) and heat release rate during C_3S paste hydration are outlined.

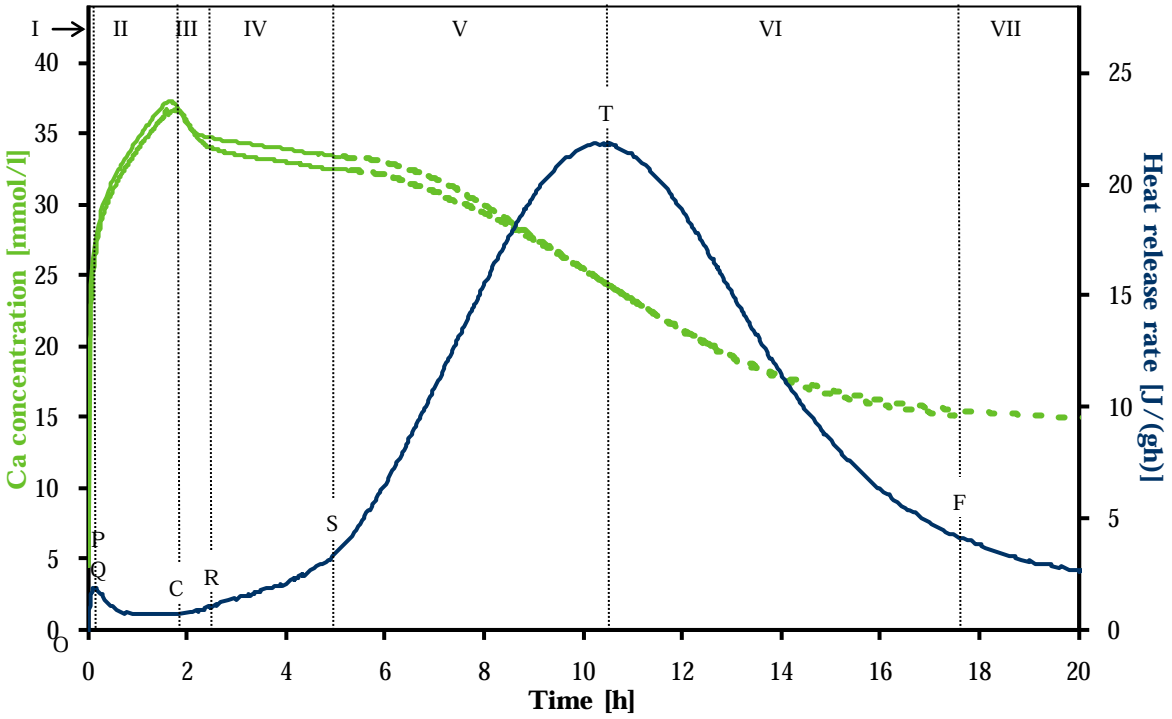

Fig. 4-68: Time dependent evolution of calculated Ca ion concentration from electrical conductivity (eq. (44), left hand axis) and corresponding heat release rate (right hand axis) during C_3S hydration (l/s=0.5). Different stages (roman numbers) of C_3S hydration are separated by dotted vertical lines. Dashed curves indicate Ca concentrations that may deviate from actual concentrations due to water incorporation into hydration products. Letters (O, P, Q, C, R) on heat release curve show points during the hydration of C_3S according to Damidot and Nonat[40] and additional points defined in the present work (S, T, F). It can be seen that the end of the induction period coincides with the drop in Ca ion concentration which is caused by portlandite precipitation. The main hydration period is separated into different stages (stages III-VI) by the rate of Ca consumption and heat release rate.

Stage I, defined by points O and P, represents the pure congruent C_3S dissolution period and induces the first maximum in the heat release rate curve. The increase of Ca ion concentrations during stage II (period Q-C) is associated with decreasing heat release rate. After unconstrained dissolution of C_3S during stage I the following hydration is characterised by a dissolution-precipitation process in accordance to general consideration by others[13, 71, 195]. This change in reaction mechanism is often not clearly separated in recent literature[94, 133, 174]. It is underlined by findings in section 4.3.3 and by others[12-13, 40, 68] that this transition is characterised by approaching ion concentrations published as kinetic path[12-13, 40] and solubility of C-S-H(m)[70, 86]. This curve is reached in C_3S hydration starting in water at point Q (Fig. 2-14, Fig. 4-68) and corresponds to the beginning of the induction period in C_3S paste hydration. During this stage the unconstrained dissolution of C_3S is not observed anymore (incongruent dissolution, drop in silicate concentration). The ion concentration follows the reaction path in direction to point C (Fig. 4-68), which is in accordance to conclusions drawn in literature[12-14, 40-41, 44, 69, 88].

In general stage II can be considered as induction period during C_3S hydration under paste conditions. The end of the induction period is marked by a sharp drop in electrical

conductivity (Ca ion concentration), which is caused by fast portlandite precipitation[40, 43] during stage III (period C-R), cf. Fig. 4-59 (p.142) and Fig. 4-68. The formation of portlandite is reflected in Fig. 4-69 and Table 4-11 (p.166).

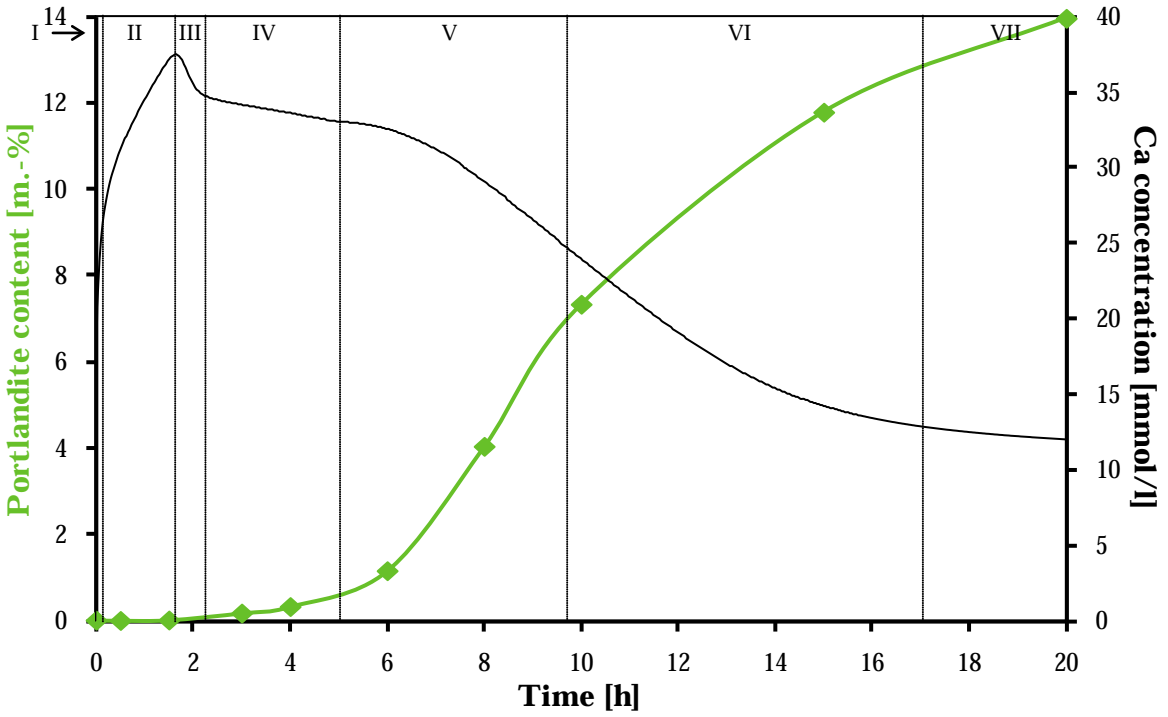

Fig. 4-69: Portlandite content measured by means of STD (mass loss) associated with different hydration stages shown in Fig. 4-68 during hydration of C_3S. Significant formation of portlandite is observed not before stage III.

The acceleration starts with stage III during which portlandite precipitates. The importance of portlandite precipitation for the end of the induction period is, however, discussed controversely, cf. chapter 2.2.3.3 (p.58) and Table 2-3. Under paste conditions (i.e. l/s ratio of e.g. 0.5) the end of the induction period coincidences with the onset of the portlandite precipitation as second hydration product, see Fig. 4-68. This can be clearly seen by slightly increased heat release rate during stage III, i.e. during portlandite precipitation. Thus, the consumption of calcium ions promotes the C_3S hydration. If C_3S is hydrated under suspension conditions (e.g. l/s=50), portlandite precipitation occurs at later hydration stages during the main hydration peak[40, 43] or is suppressed[136] (very high l/s ratio). Thus it was concluded[40, 43] that the formation of portlandite does not govern the termination of the induction period. As demonstrated by others[14, 65], the number of C-S-H nuclei increases with increasing l/s ratio, which leads to decreasing length of induction period. Thus, according to that theory, the end of induction period may be governed by nucleation and growth of C-S-H phases. In accordance to previous assumptions[195] it is therefore postulated here that growth of either one or both hydration products (C-S-H phases, portlandite) causes the onset of the acceleration period (Fig. 4-68). Thereby, the growth of portlandite plays a crucial role only under paste conditions, since thereby ions accumulated in the aqueous phase are consumed and subsequently renewed by dissolution of C_3S as mentioned before. This is obvious by formation of etch pits. Makar *et al.*[115] reported the formation of etch pits at the end of the induction period and in another study

of the same authors[113] it is shown that the first derivative of the heat release rate curve provides a peak at the end of the induction period. Both results are in accordance with the conclusions drawn in the present work that the end of the induction period is correlated to the formation of portlandite in pastes. Moreover, Bullard and Flatt[27] emphasized the importance of portlandite precipitation for the onset of the acceleration period. Therefore, etch pit formation indicates the end of the induction period (stage II) during C_3S paste hydration.

The acceleration period as known from literature[71] can be subdivided into three parts by the utilized approach. Because portlandite precipitation induces a slight increase in the heat release rate, in the present work stage III is associated with the beginning of the acceleration period. The slight increase in heat release is mainly caused by higher enthalpy of dissolution of C_3S (strongly exothermic) compared to the enthalpy of precipitation of C-S-H phases (endothermic) and portlandite (marginally exothermic), see section 2.2.2 (p.48). Thus, the net heat release is exothermic at this and during the following stages. In stage IV as second part of the acceleration period (period R-S) growth of both C-S-H phases and portlandite is further accelerated and consequently the C_3S dissolution. The third part of the acceleration period (stage V) starts in point S. Here, electrical conductivity (and thus Ca ion concentration) shows a further sharp drop. This is mainly caused by increasing precipitation rates of C-S-H phases and portlandite which is associated with the consumption of water and an increase of the density of the matrix. Thus, the ion mobility is affected and consequently the electrical conductivity, see eq. (44). Therefore, actual Ca ion concentrations may deviate from calculations and thus drawn in dashed lines in Fig. 4-68. The curve during stages IV and V has similarities to those measured during pure precipitation of C-S-H phases (and portlandite) with respect to conductivity plateau and drop in electrical conductivity, cf. Fig. 4-27 (p.112). Because the degree of hydration is significantly increased during stage V, this period is referred in the following to as main acceleration period. The maximum of this period is obtained in point T. This point coincides with the inflexion point of the electrical conductivity (Ca ion concentration). During stage VI and VII the system slowly approaches equilibrium, which is established by formation of hydration products (C-S-H phases and portlandite) in point F.

The shape of the electrical conductivity (and Ca concentration) curve after stage III has similarities to the corresponding curves recorded during homogeneous nucleation experiments, see Fig. 4-70. This implies that similar mechanisms control the end of the induction period/time, i.e. nucleation and growth of hydration products.

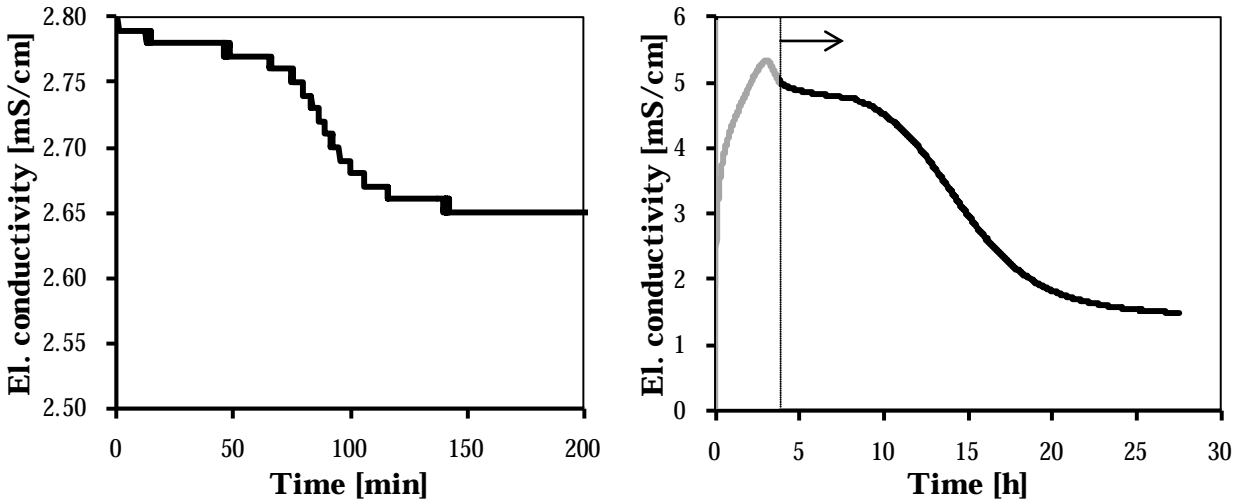

Fig. 4-70: Development of the electrical conductivity during (left hand) homogeneous precipitation of C-S-H phases in presence of 0.05 Vol.-% PCE1 and (right hand) C_3S paste hydration (l/s=0.5) in presence of 0.05 m.-% PCE1. Similar shape of the curve in left hand graph is indicated by an arrow.

4.3.4.2.5 Impact of superplasticizers on electrical conductivity in C_3S suspensions

The impact of superplasticizers on the hydration kinetics of C_3S under suspension conditions is presented in the following. Results of the electrical conductivity measurements as well as their examination with respect to characteristic periods (Fig. 4-64) are given in Fig. 4-71, Fig. 4-72 and Fig. 4-73, respectively.

As demonstrated in Fig. 4-71 and Fig. 4-72 (top row), the duration of the electrical conductivity plateau is increased with increasing dosage of PCE based superplasticizers, which is not solely related to the number of functional groups (Fig. 4-72 (top, right hand). The absolute plateau value of electrical conductivity slightly decreases with increasing PCE-dosage. This effect can be associated with the number of functional groups (Fig. 4-72, bottom, right hand). In case of naphthalene sulfonate addition, both value and duration of the electrical conductivity plateau are changed with increasing dosage. This can be related to the number of sulfonic groups in the system (compare left and right hand graph of Fig. 4-72). Surprisingly, the duration of the plateau firstly increases, and with further addition of PNSF the plateau duration decreases. Similar results are gathered during pure precipitation experiments given in chapter 4.2.5 (p.111). Therefore, the template performance of this superplasticizer is demonstrated here for C_3S hydration. The increased value of the plateau at increasing PNFS-dosage indicates that solubility of C_3S is increased similar to results of portlandite dissolution (section 4.2.3, p.94).

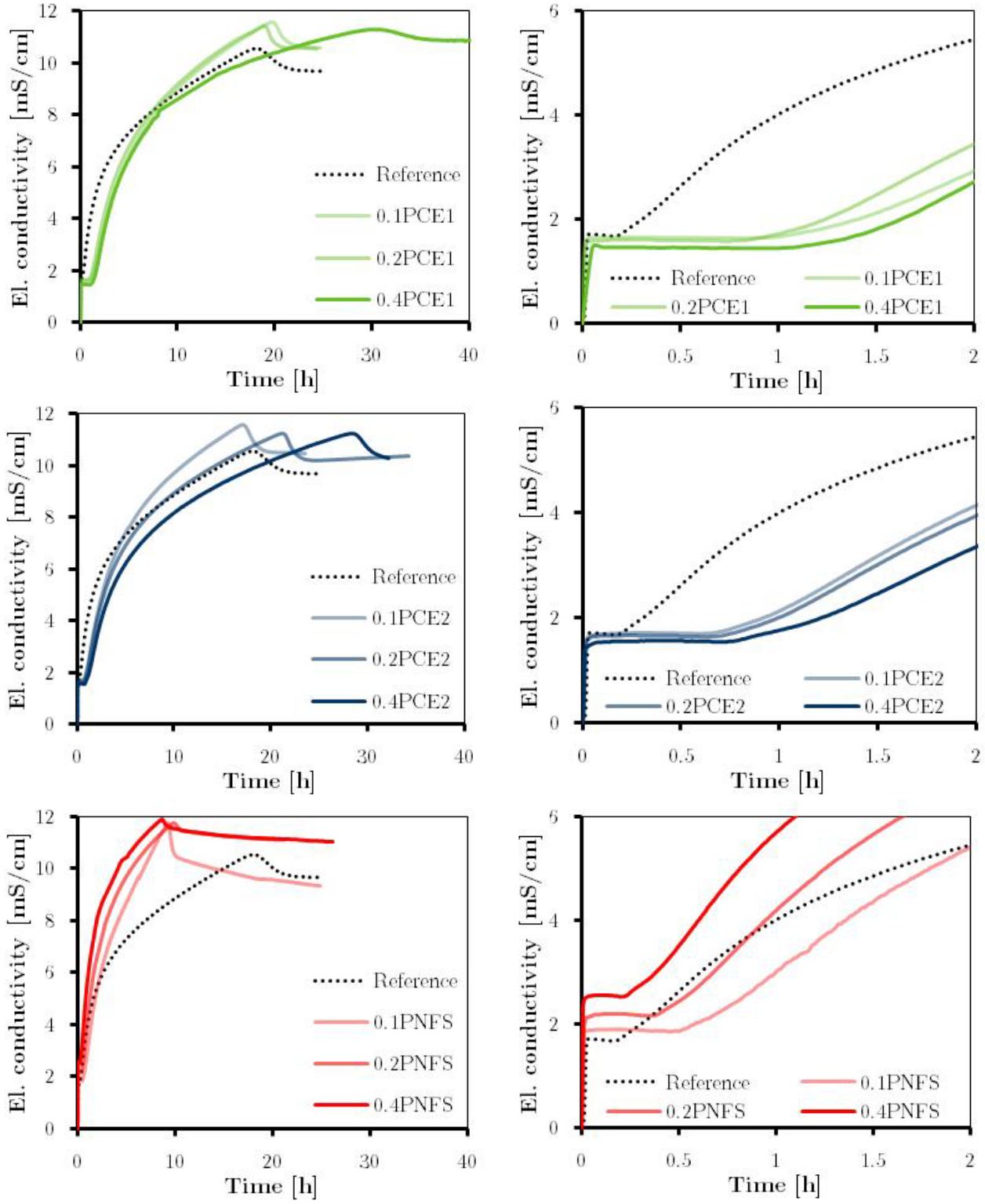

Fig. 4-71: Time dependent evolution of the electrical conductivity during C_3S hydration in presence of PCE1 (top), PCE2 (middle) and PNFS (bottom) at given dosages in m.-% at l/s ratio of 50. Right hand graph shows the conductivity plateau in more detail. PCEs increases the duration of the plateau and at highest dosage delay portlandite precipitation. PNFS, however, shortens the plateau and portlandite precipitates earlier compared to the reference.

Following the electrical conductivity in the presence of superplasticizers after the plateau, it is observed that the slope of the curve, in particular the inflection, is varied. Generally, an increased slope of the electrical conductivity curve indicates increased reaction rates during

C_3S hydration. The presence of low PCE-dosages reduces the magnitude of the inflection. But with increasing dosage the inflection becomes more pronounced. In contrast to PCEs, superplasticizer based on naphthalene sulfonate (PNFS) reduces the magnitude of inflection with increasing dosage.

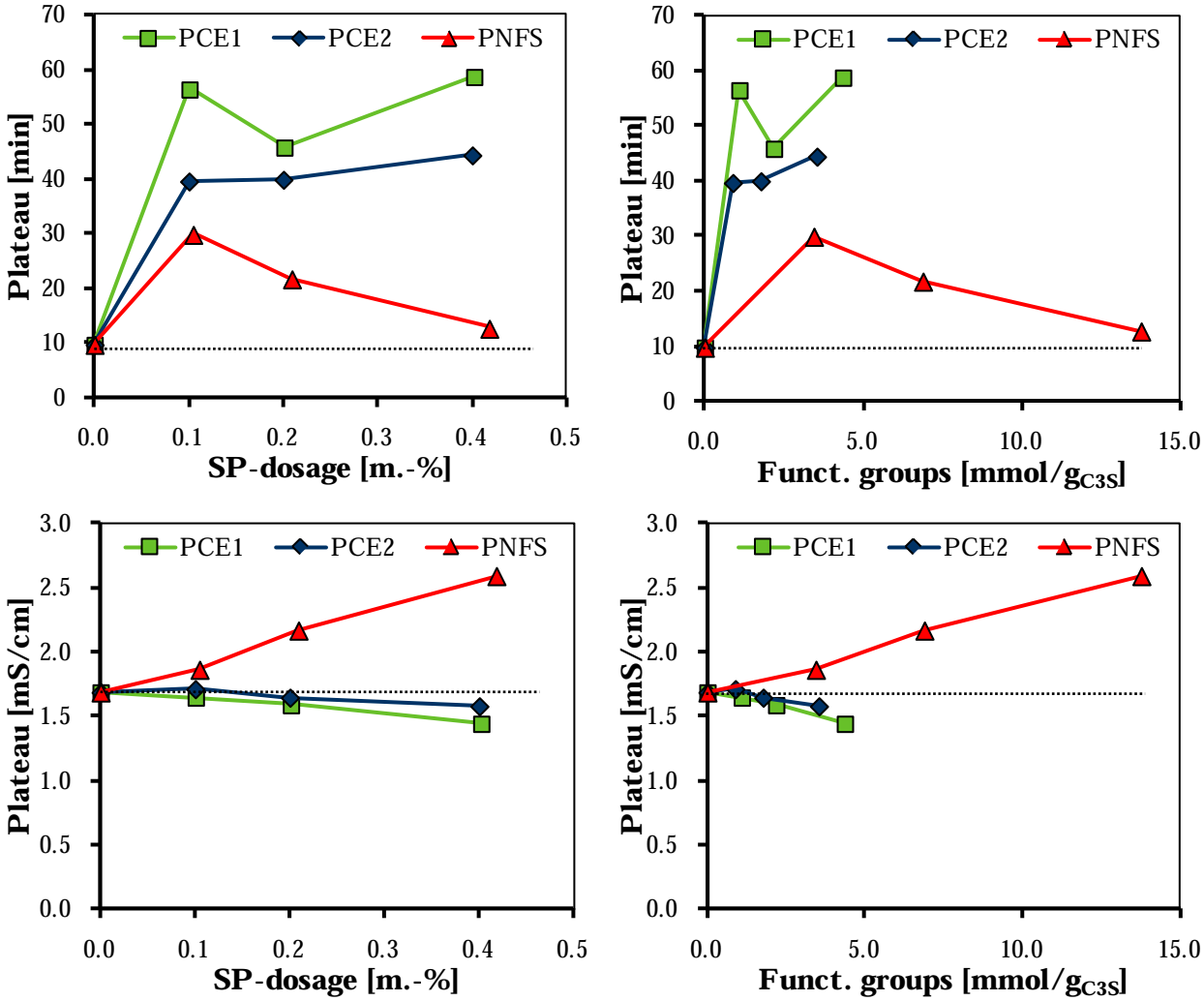

Fig. 4-72: Conductivity plateau length (top row) and value (bottom row) in dependence on (left hand) SP-dosage (in m.-% with respect to C_3S) and (right hand) number of added functional groups during C_3S hydration at l/s ratio of 50. Lines indicate reference values and serves as guides for the eyes. The value of the electrical conductivity plateau is mostly affected by the number of functional groups, but not the plateau length.

Compared to the reference portlandite precipitation occurs at increased electrical conductivity, cf. Fig. 4-73 (top row) which can not be clearly related to the number of functional groups (Fig. 4-73, top, right hand). As a result of decreased reaction rates (indicated by decreased slopes), the onset of portlandite precipitation is delayed, cf. Fig. 4-73 (bottom row) which is mainly dependent on the number of functional groups (Fig. 4-73, bottom, left hand). However, in presence of naphthalene sulfonate based superplasticizer portlandite precipitation occurs earlier. This effect is independent on the dosage and again attributed with the template performace.

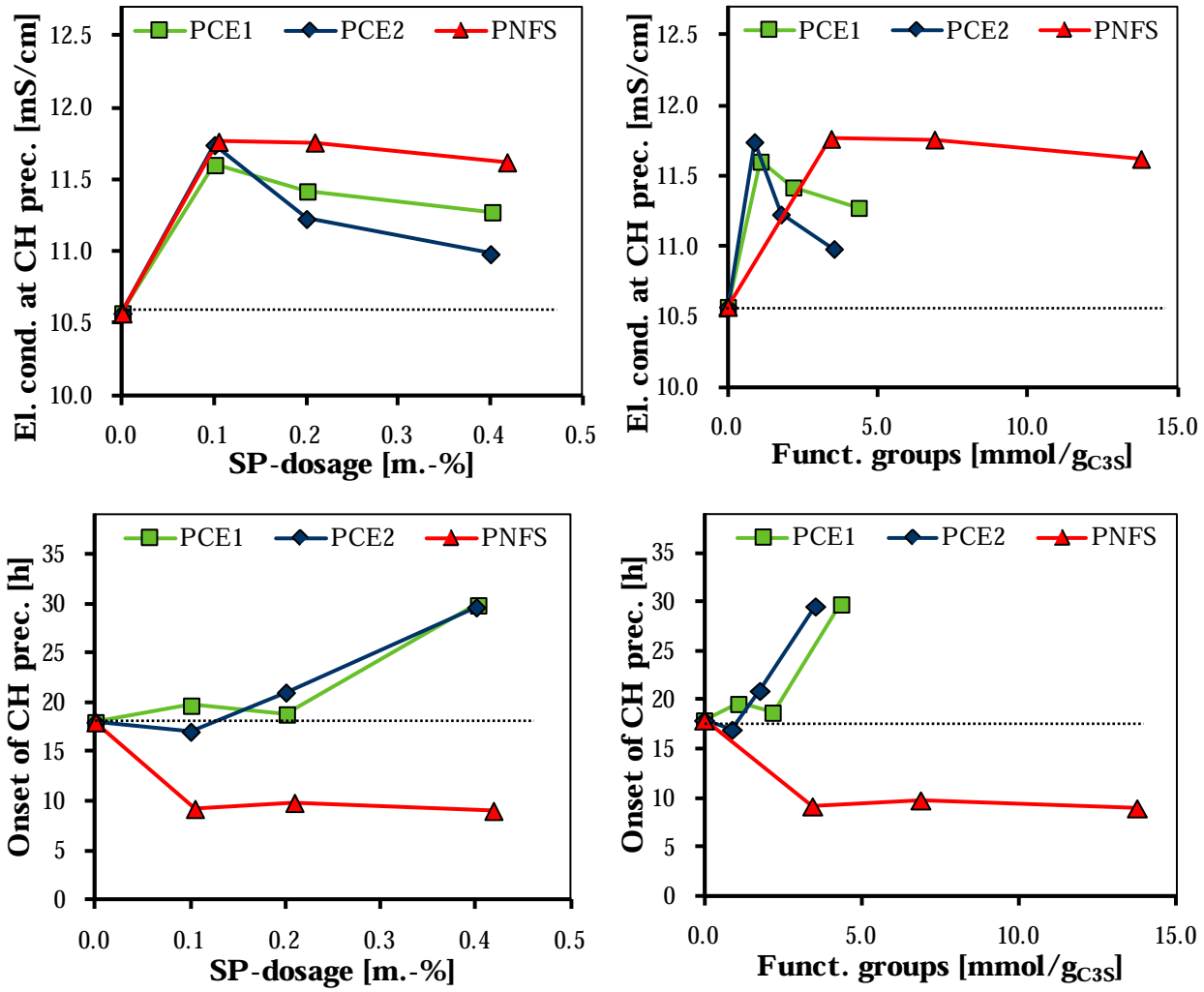

Fig. 4-73: Electrical conductivity at portlandite precipitation (top row) and corresponding onset (bottom row) in dependence of SP-dosage (left hand) and number of functional groups (right hand) during C_3S hydration at l/s ratio of 50. Lines indicate reference values and serves as guides for the eyes. The onset of CH precipitation may be related to the number of functional groups, in general CH precipitation is delayed and promoted by PCE and PNFS, respectively.

With respect to principal mode of action of superplasticizers outlined in chapter 4.1 (p.75), the impact of superplasticizers on the electrical conductivity is discussed in the following and schematically summarized in Fig. 4-74.

It was shown that the presence of PCE based superplasticizers causes a prolonged duration of the electrical conductivity plateau. In accordance to findings gathered in pure systems (section 4.2.5, p.111) the prolonged duration of the electrical conductivity plateau indicates that the precipitation of C-S-H phases during C_3S hydration is strongly affected by superplasticizers. This effect can on the one hand be attributed to complexation of Ca ions on surfaces (adsorption) by functional groups which decrease the rate of C-S-H precipitation. On the other hand particle mediated crystallization reduces the crystal growth rate. However, PNFS based superplasticizers cause decreased duration of the electrical conductivity plateau. This effect is attributed to the template performance of naphthalene sulfonates which promotes the precipitation of C-S-H phases and explains the

finding by Ridi *et al.*[162] that superplasticizers lower the energy threshold which is needed for nucleation.

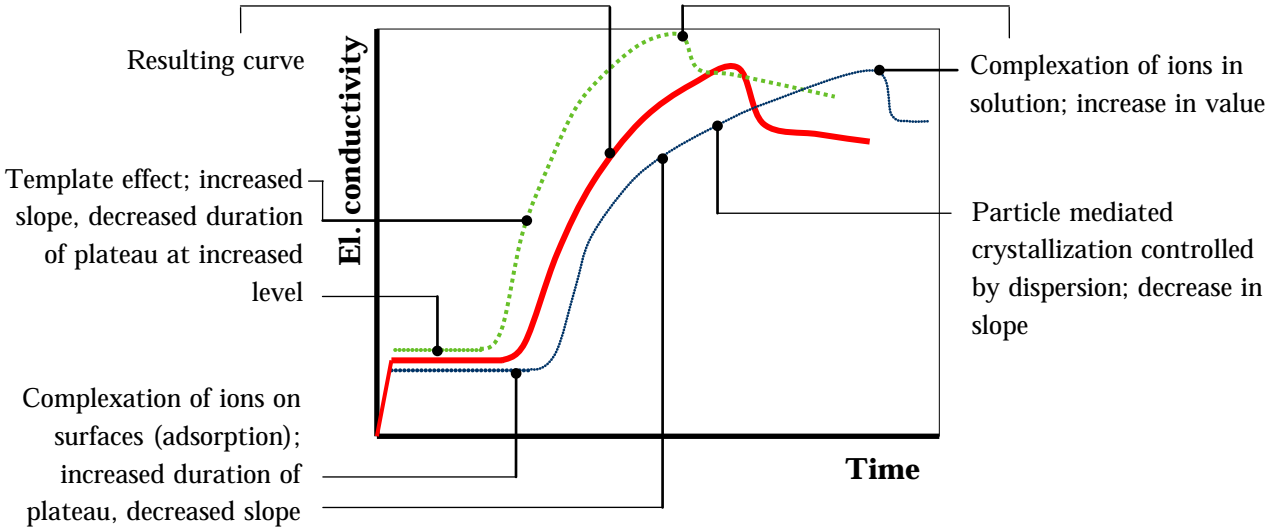

Fig. 4-74: Schematic of the influences of superplasticizer induced effects on the resulting electrical conductivity (red line) during C_3S hydration. The magnitude of all effects is dependent on the SP-dosage.

Whereas the conductivity plateau is prolonged by PCE based superplasticizers, the value of the plateau is unaffected by those SPs. Experiments on the impact of superplasticizers on the aqueous phase (section 4.3.3, p.141) revealed that PCE1 induce increased Ca and silicate ion concentrations with respect to the reference without SP (Fig. 4-60), but simultaneously no variation in electrical conductivity. Thus, the unaffected value of the electrical conductivity plateau shown in Fig. 4-72 (right hand, top) proves the formation of C-S-H-polymer clusters in the aqueous phase of C_3S suspensions (section 4.3.3.2.2, p.142). These clusters, which are not able to carry electrical currents, are dispersed in the aqueous phase and may cause artifacts during ICP-OES measurements. As a result, the development of the ion concentrations in the aqueous phase continuous reaching the same level as without superplasticizers. By that mechanism the electrical conductivity remains unchanged.

In case of PNFS the increased value of the electrical conductivity at the plateau is caused by with respect to the reference increased Ca and silicate concentrations in the aqueous phase (compare Fig. 4-60 and Fig. 4-72 right hand, top). Therefore it is concluded that either simple ion-polymer complexes or small C-S-H-polymer clusters which are able to carry electrical currents are formed in presence of PNFS. In contrast to PCEs in both cases a correct determination of ion concentrations by means of ICP-OES (without artifacts) is possible due to the low dispersing ability of PNFS based superplasticizers as discussed in section 4.3.3.2.2 (p.142).

It is shown in previous studies that the inflection in electrical conductivity at approx. 4-7 mS/cm (Ca approx. 12-18 mmol/l) is associated with a change in the growth mode of C-S-H phases (from parallel to perpendicular to the C_3S surface[65]). Superplasticizers alter the inflection of the electrical conductivity curve. Thus it can be concluded that superplasticizers change the growth mechanism of C-S-H phases. Furthermore, the

magnitude of the inflection (differences in slope before and after the inflection of the curve) is reduced when PCE and PNFS based superplasticizers are added in low and both low and increased dosages, respectively. This observation may be explained by different principal modes of action on superplasticizers, i.e. template effect, complexation of ions in solution and particle mediated crystallization. Common to all sceneries is that C_3S surface is to a lower extent covered by hydration products and the amount of C-S-H phases is increased.

Finally, the onset of portlandite precipitation and the value of the electrical conductivity at portlandite precipitation are influenced by superplasticizers. Based on findings on solubility (section 4.2.3 (p.94)) and crystallization (section 4.2.5, p.111), these observations can be attributed, respectively, to template effects, the complexation of Ca ions in solution as well as to particle mediated crystallization.

4.3.4.2.6 Impact of superplasticizers on tricalcium silicate paste hydration

A Hydration kinetics

The impact of superplasticizers on the hydration of C_3S under paste conditions is presented in the following. Here Ca ion concentrations from electrical conductivity were not computed because also mobility of ions (activity) is varied by polymers. Nonetheless, electrical conductivity provides valuable insights on the impact of superplasticizers on C_3S hydration under paste conditions. Fig. 4-75 presents results of experiments on time dependent evolution of the electrical conductivity and corresponding heat release rate recorded during C_3S hydration at l/s ratio of 0.5.

It can be seen that in presence of superplasticizers C_3S hydration can be separated into stages as mentioned before (section 4.3.4.2.4). However, with respect to the reference sample without superplasticizers the slopes (i.e. rates) of individual hydration stages are modified. Whereas during stage I no significant difference in reaction rate (slope) is detected, in stage II lower rates compared to the reference are observed. Following to point C, with increasing SP-dosage the slope of the electrical conductivity curve is decreased compared to the reference, cf. Fig. 4-75 (right hand). This effect is more pronounced for PCE based superplasticizers. Analogously to findings shown in section 4.2.5 (p.111) this can be attributed to lower precipitation rates of portlandite in presence of superplasticizers. Because results on hydration stages show that their duration is prolonged, the retardation of C_3S hydration induced by superplasticizers is not limited only to stage II and III (Q-C, C-R). Moreover, the retarding effect manifests in lower reaction rates during stage IV (R-S). Taken into account that superplasticizers impact strongly precipitation rates (chapter 4.2.5, p.111) then the results suggest that stages II-IV are originated by precipitation reactions (C-S-H phases, portlandite). At the onset of stage V (point S) the slope of the electrical conductivity curve is similar with respect to the reference sample which leads to conclude that the retarding effect of superplasticizers vanishes. This leads further to conclude that during the main acceleration stage the C-S-H precipitation is too robust to be influenced by superplasticizer.

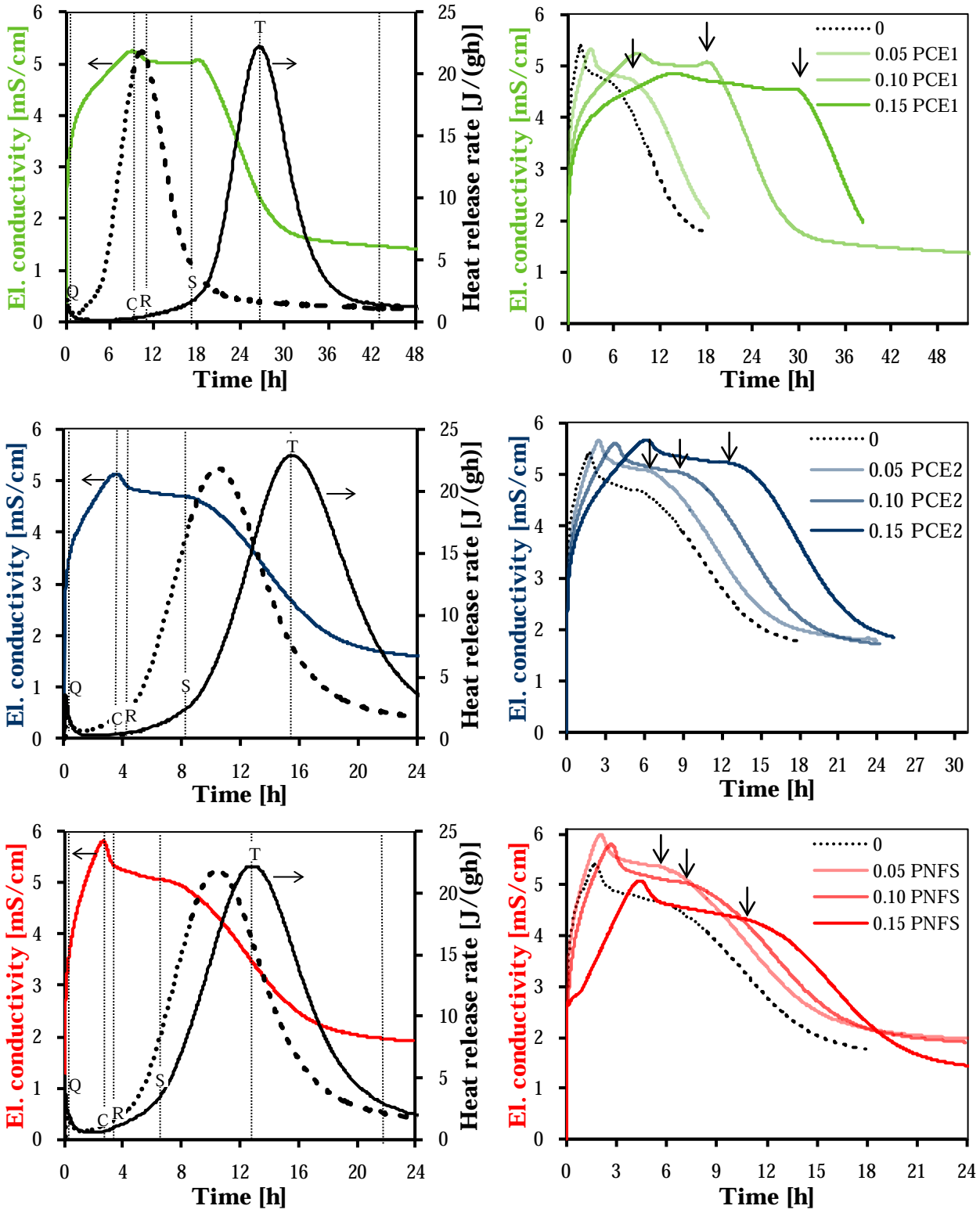

Fig. 4-75: El. conductivity of C_3S pastes (l/s=0.5) in presence of PCE1 (top row), PCE2 (middle row) and PNFS (bottom row) at given dosages (m.-% with respect to C_3S). Arrows indicate onset of main acceleration period (point S). Left hand graph additionally shows corresponding heat release rate at dosage of 0.1 m.-% (dotted line: reference). It can be seen that hydration stages are consistent in all samples. Retardation is associated with decrease in slope of the electrical conductivity and delayed precipitation of C-S-H and portlandite.

In Fig. 4-76 the onset of portlandite precipitation (which is associated with the end of the induction period during the performed paste experiments) is plotted as a function of SP-

dosage. It can be seen that the length of the induction period increases monotonically with SP-dosage. Thereby, PCE2 induces a lower retardation of the C_3S hydration as compared to PCE1. This leads to the earlier occurrence of characteristic points of hydration if PCE2 is compared with PCE1. But with respect to reference without superplasticizer, PCE2 still retards hydration (Fig. 4-75, middle). The presence of PNFS (Fig. 4-75, bottom) shows similar behavior as PCE2.

As indicated in Fig. 4-76 the molecular architecture of superplasticizers polymers plays an important role regarding retardation. In literature[202, 204, 213] as a main influence on the duration of the induction period, the lenght of grafted side chains to the polymers backbone is frequently discussed. Thereby, grafting of shorter side chains to the polymers backbone compared to longer side chains induces stronger retardation of both cement and C_3S hydration. For C_3S this situation is reflected in Fig. 4-76. Contrary, in pure crystallization systems (section 4.2.5, p.111) polymers grafted with longer side chains induce stronger retardation compared to short side chain grafted polymers. In the following these apparently contradictory results are investigated in more detail.

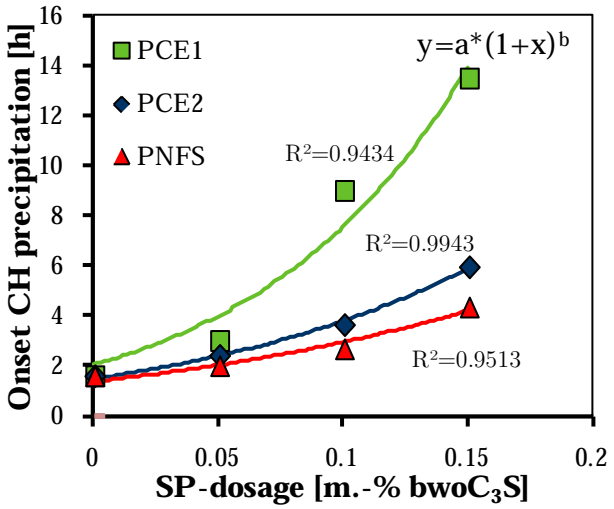

Fig. 4-76: Onset of portlandite precipitation as a function of SP-dosage during C_3S paste hydration (l/s=0.5). Fit parameters: a=2.04(PCE1), 1.48 (PCE2), 1.37 (PNFS); b=13.76 (PCE1), 9.89 (PCE2), 8.02 (PNFS).

The examination of the data of electrical conductivity and heat release rate is used in the following in order to investigate the role of the functional groups on C_3S paste hydration. For this Fig. 4-77 shows the increase in the onset of portlandite precipitation during C_3S paste hydration (l/s=0.5) in dependence on the number of functional groups added by the polymers.

If the delay of the portlandite precipitation is plotted against the dosed number of functional groups added by the polymer then the effect of the used PCEs can be described solely by the number of carboxy groups introduced in the system, cf. Fig. 4-77. Thus, the data may suggest that differences in polymer architecture as length of grafted side chains and molecular weight (changing polymer conformation from flexible backbone worm to flexible backbone star) are of neglible importance for the duration of the induction period in C_3S paste hydration. Moreover it gets clear that sulfonic groups induce lower retardation as compared to carboxy groups although an increased complexation of calcium ions on surfaces (adsorption) is determined. These effects show that an explanation of the behavior of superplasticizers containing polymers with different chemical structures is not easily possible.

Because the complexity of the system renders a direct interpretation nearly to impossible, in the following we attempt to interpret the data by comparison with findings from ealier

sections on pure precipitation of C-S-H phases and portlandite. However, this implicates that we compare two systems with different fraction of water and thus different distributions of species between interface and the aqueous phase which makes them inherently different. Also the polymer dosage with respect to solids and the adsorption behavior are different. Under consideration of these restraints the model of the fusion of nanoparticles during crystallization as sketched in Fig. 4-55 is most reliable to explain the similar behavior of PCEs with different chemical structure (backbone length, side chain length). Based on this model we may conclude that in pastes the available space for stabilization of nanoparticles is insufficient for PCEs grafted with long side chains to induce stronger retardation as compared to those polymers which are grafted with shorter side chains. Thus, the comparison of homogeneous crystallization experiments and C_3S paste hydration experiments may indicate that the ability for maximum stretching the polymer structure is dependent on the l/s ratio.

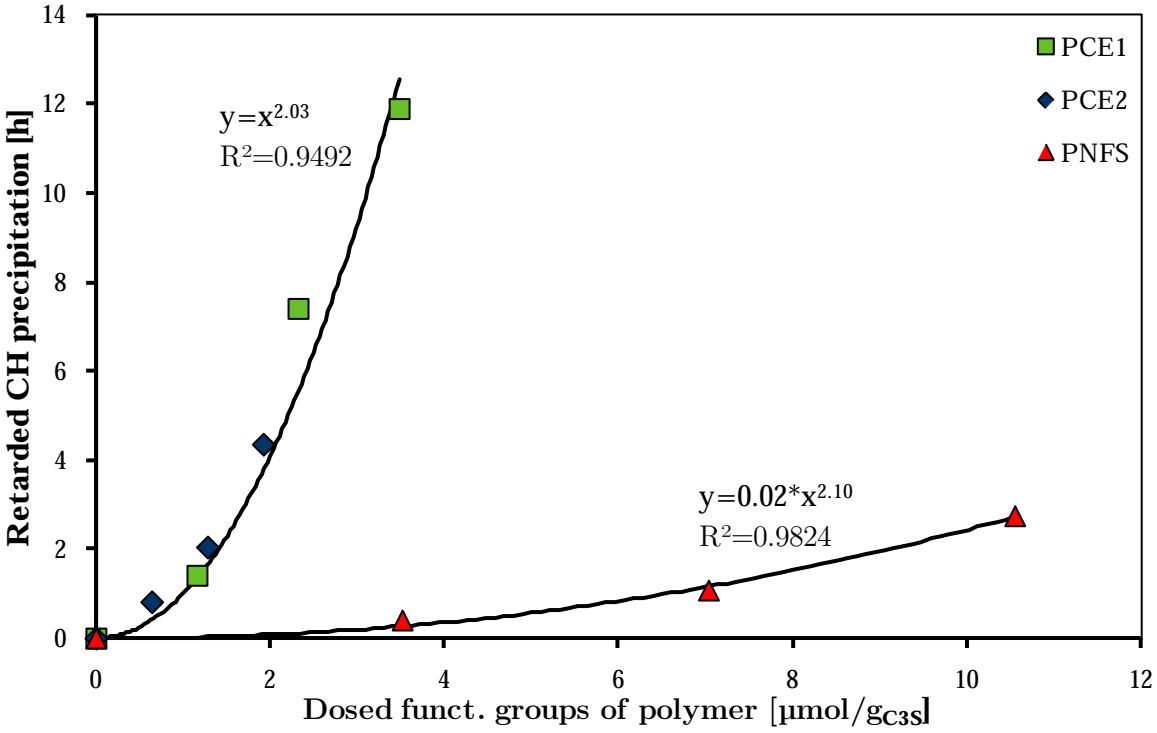

Fig. 4-77: Onset of the portlandite precipitation (reference value without superplasticizer is substracted) as a function of dosed number of functional groups by the polymers. The retardation of C_3S hydration can be related to the type and number of functional groups.

B Portlandite content

Besides time of portlandite precipitation it is further investigated if superplasticizers influence the also the amount of precipitated portlandite under paste conditions. For this, the total content of portlandite was analysed by means of STD (mass loss in the range of 380 to 480 °C assuming that the number of C-S-H phases is roughly constant). Results of these experiments are shown in Table 4-11.

Taking standard deviation into account, no portlandite is detected during stage II. This is in accordance to electrical conductivity measurements shown in Fig. 4-68 and Fig. 4-75.

Table 4-11 documents an increase of portlandite content during stage IV which proves that portlandite precipitation starts with the drop in electrical conductivity during stage III.

Table 4-11: Portlandite content [m.-%] of C_3S pastes determined by mass loss (STD) during different hydration stages.

Sample	Stage II		Stage IV		Stage V	Stage VI
	Start	End	Start	End		
Reference	0.1±0.1	0.2±0.1	0.4±0.1	1.4±0.1	4.4±0.1	15.0±0.1
PCE1	0.1±0.1	0.1±0.1	0.2±0.1	0.2±0.1	3.5±0.1	13.6±0.1
PCE2	0.0±0.1	0.1±0.1	0.3±0.1	1.0±0.1	3.8±0.1	11.9±0.1
PNFS	0.1±0.1	0.1±0.1	0.2±0.1	0.5±0.1	2.0±0.1	12.2±0.1

Portlandite content increases until the end of stage IV. The presence of superplasticizers (except of PCE2) reduces the portlandite content. During stages V and VI a progress in portlandite formation is detected. Thereby the presence of all SPs reduces the portlandite content with respect to the control sample which can be related to the increased solubility of portlandite in the presence of superplasticizers; see section 4.2.3 (p.94).

C Microstructure

SEM micrographs of the surface of C_3S show the phase development during different hydration stages, cf. Fig. 4-78 to Fig. 4-80. After 30 min of hydration (stage II, induction period) the C_3S surface becomes roughened and first C-S-H phases are visible. But the majority of the C_3S surface remains uncovered by those products. Only the mixture of C_3S with naphthalene sulfonate based superplasticizer (PNFS) shows a pronounced rhoughening of the C_3S surface (Fig. 4-78, bottom). Until the end of this stage the number of first C-S-H phases increases slowly (right hand column of Fig. 4-78). After point C and during stage IV (left hand column of Fig. 4-79) etch pits on the surface of C_3S are visible [94, 114], those are predominantly observed in mixtures containing water and PNFS. Moreover, etch pits are not homogeneously distributed on the surface. Similar to minerals[187] and drugs[146] this effect may be attributed to different reactivity of single crystal faces of C_3S against water[124]. At the end of stage IV (right hand column in Fig. 4-79) C-S-H phases increases in length but the sample of C_3S blended with PCE1 shows only minor progress in C-S-H growth. At further hydration, etch pits grow in diameter (right hand column of Fig. 4-80), and C-S-H phases appear to grow on etch pit boundaries. With the growth of C-S-H phases also the number and size of etch pits on the C_3S surface increases. The main hydration period (stages V and VI) is characterized by fast growth of both C-S-H phases (Fig. 4-80) and portlandite (Table 4-11). Because during main acceleration period C-S-H phases grow very dense on the C_3S surface, etch pits become hardly visible in SEM. C-S-H phases and portlandite are most abundant in the microstructure at stages V and the following (Fig. 4-80). In spite of the fact that sampling for SEM is performed at similar hydration stages, the presence of PCE1 leads to smaller/shorter C-S-H phases compared to all other samples. This may be attributed to the strong retarding effect of this superplasticizer. Similar to homogeneous precipitation experiments of C-S-H outlined in section 4.2.5 (Fig. 4-44, p.126), spherical agglomerates of C-S-H phases are found in C_3S pastes when PCE1 is utilized.

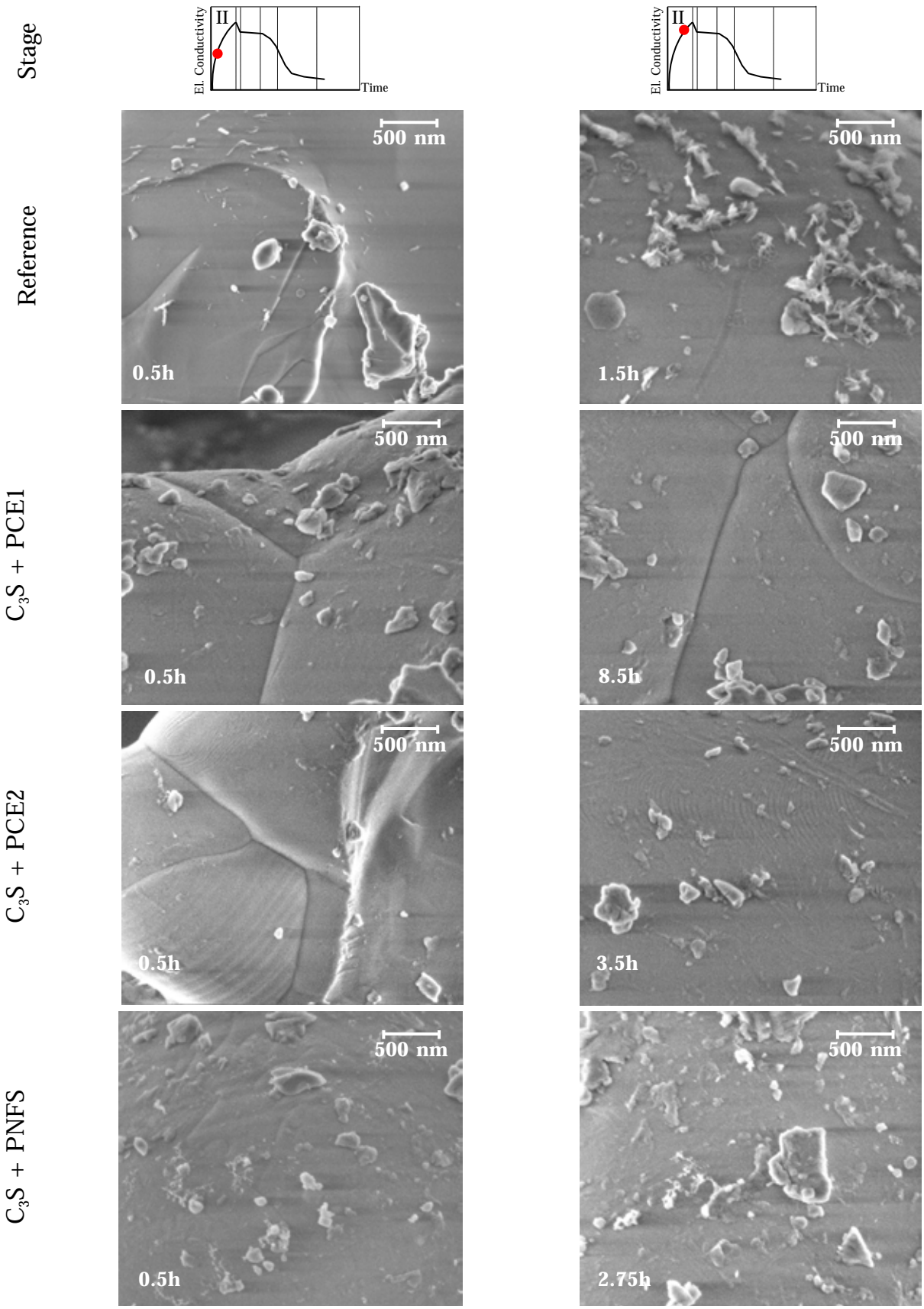

Fig. 4-78: SEM micrographs of C_3S surface during stage II. Hydration started in water (2nd row), in presence of PCE1 (3rd row), PCE2 (4th row) and PNFS (bottom row) (all: 0.1m.-%). During stage II first C-S-H phases appear and the C_3S surface becomes slightly roughened.

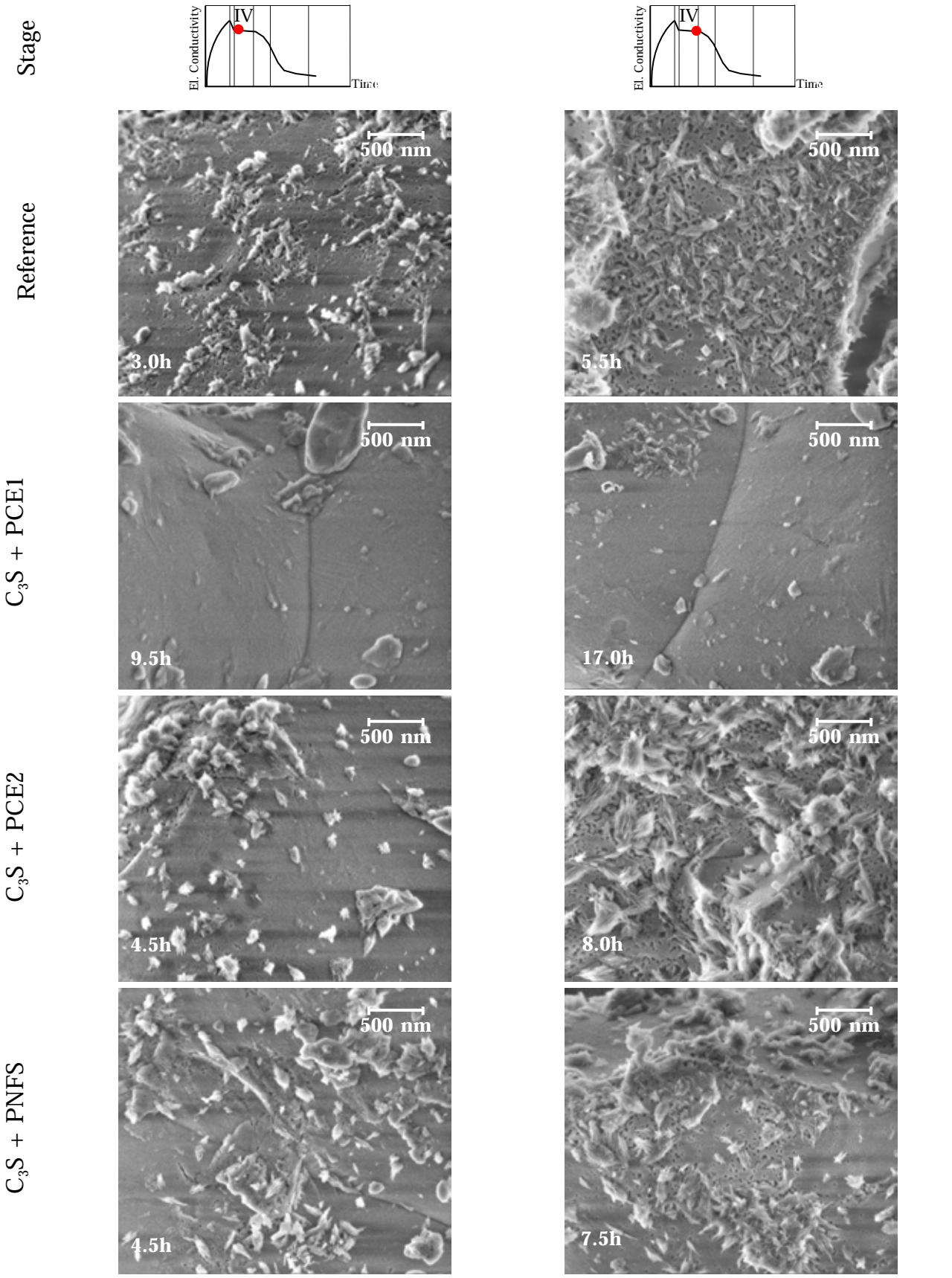

Fig. 4-79: SEM micrographs of C_3S surface during stage IV. Hydration started in water (2nd row), in presence of PCE1 (3rd row), PCE2 (4th row) and PNFS (bottom row) (all: 0.1m.-%). After portlandite precipitation (stage III), etch pits are formed. C-S-H phases grow further.

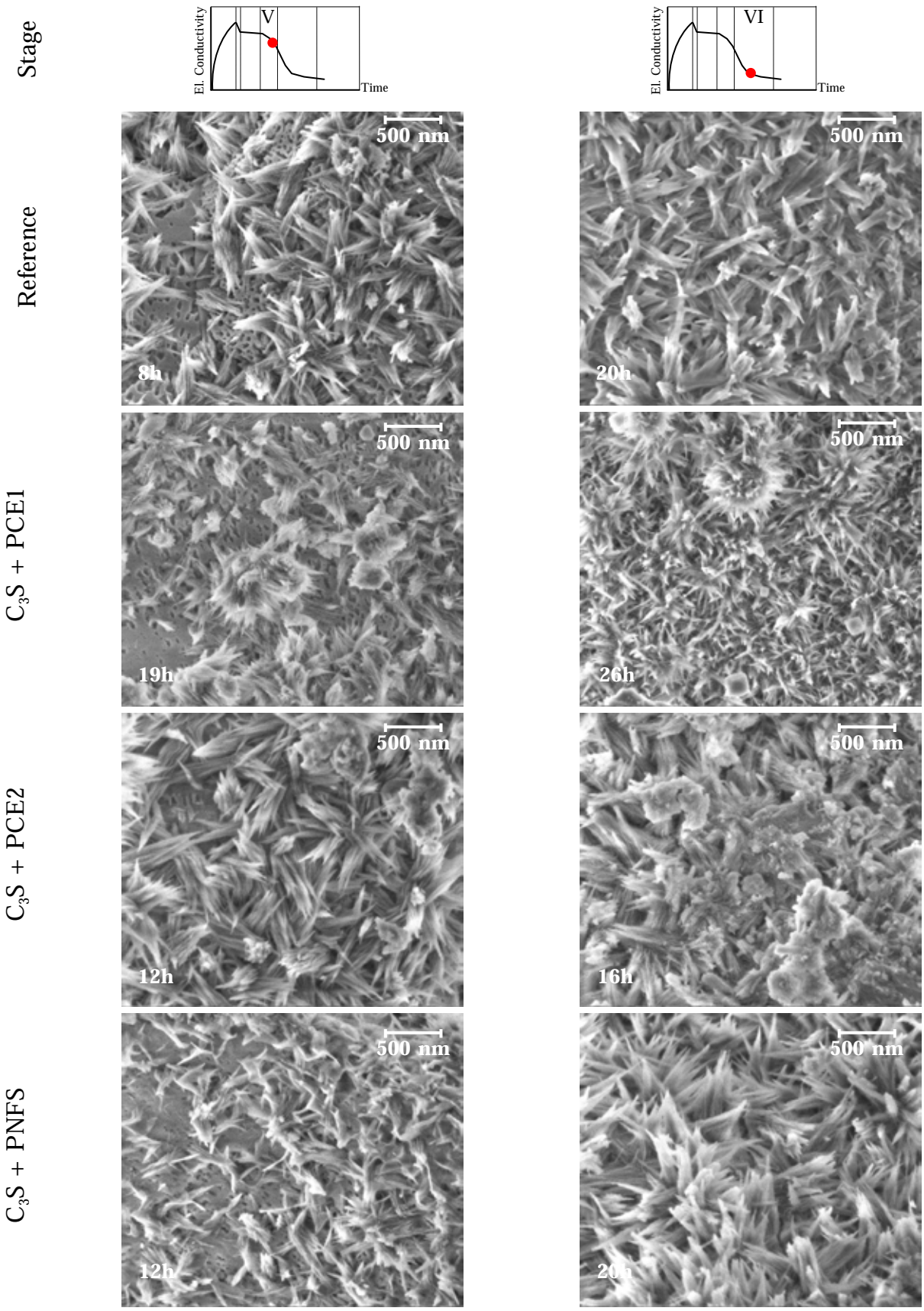

Fig. 4-80: SEM micrographs of C_3S surface during stages V and VI. Hydration started in water (2nd row), in presence of PCE1 (3rd row), PCE2 (4th row) and PNFS (bottom row) (all: 0.1 m.-%). During stage V-VI only for PCE1 the retarding effect is visible on the slow growth of C-S-H phases.

4.3.4.3 Summary

In the present section the time dependent development of the ion concentration of the aqueous phase during C_3S hydration was investigated. Thereby, both suspensions and pastes were produced and analysed by means of electrical conductivity. Results reveal that the most important influence on the hydration kinetics stems from the l/s ratio and the presence of superplasticizers. The utilization of both the electrical conductivity and isothermal conduction calorimetry in C_3S pastes permits the differentiation of the main hydration period in four stages. Therefore, the induction period ends with the precipitation of portlandite which is associated with a slight increase of the heat release rate. Afterwards, a stage is observed during which both C-S-H phases and portlandite grow on low rate. Then this rate sharply increases in the following stage, namely the main acceleration stage. Finally, the rate reduces and the diffusion controlled slow period is established.

Electrical current is transported by ions, as a result ion concentrations and their mobility are parameters which control electrical conductivity. Thus, the computation of ion concentrations based on data related to the Ca-Si relationship is permitted *in-situ* by measuring electrical conductivity. Results of this method are also shown in the present section.

The impact of superplasticizers on the time dependent development of ion concentration was fathomed in more detail by means of both electrical conductivity and isothermal conduction calorimetry. Similar to the SP free samples both suspensions and pastes were investigated. The measured effects are discussed with respect to principal performance of superplasticizers, i.e. complexation of Ca ions (in solution and on surfaces), template effects (section 4.1, p.75) and particle mediated crystallization (4.2.5, p.111). It was concluded that the aforementioned differentiation of the main hydration period is again observed when superplasticizers are present. Only the rates of individual hydration stages differ with respect to the reference sample without superplasticizer.

Under suspension conditions (l/s=50) PCE based superplasticizers prolong the duration of the first conductivity plateau independently on the SP-dosage and thus hinder C-S-H precipitation. But this effect is not associated with an increase in electrical conductivity value at the plateau. It was concluded that increased ion concentrations measured in section 4.3.3 (p.141) are due to formation of C-S-H-polymer clusters. However, PNFS based superplasticizers causes a decreased duration of the conductivity plateau with increasing dosage, but simultaneously increase both ion concentrations and electrical conductivity. Therefore it is concluded that PNFS based superplasticizers induce formation of ion-polymer complexes or small C-S-H-polymer complexes.

Following the hydration to later periods these effects changes the electrical conductivity curve (magnitude of inflection, onset of portlandite precipitation). In case of PCE based superplasticizer portlandite precipitation occurs earlier with respect to the reference. But at increased PCE-dosage portlandite precipitation is observed at later periods compared to the reference. Thereby, no differences between polymers grafted with short and long side chains were found. In spite of that, portlandite precipitates earlier than in the reference sample when naphthalene sulfonate based superplasticizers are present. This behavior is

independent on the PNFS-dosage and can be attributed to template performance of PNFS-based superplasticizer (including Ca complexation). Furthermore, the value of electrical conductivity at portlandite precipitation was increased in all superplasticizer containing samples. In accordance to findings presented in section 4.2.3 (p.94), this effect may be the result of increased solubility of portlandite in presence of either superplasticizer.

Analogously to suspension experiments, the impact of superplasticizers on the hydration kinetics (electrical conductivity and isothermal conduction calorimetry) was tested under paste conditions (l/s=0.5). It was pointed out that under paste conditions no plateau of the electrical conductivity was observed before portlandite is precipitated. Similar to paste experiments without superplasticizers, the end of the induction period coincidences with the formation of portlandite. In contrast to the findings on suspension experiments, where portlandite precipitates after similar time periods independently on the length of grafted side chains, in pastes portlandite is precipitated earlier in presence of polymers grafted with long side chains. However, this effect can be related to the type and number of functional groups of the polymer. It is observed that carboxy groups induce stronger reatardation as compared to sulfonic groups. Compared to homogeneous nucleation experiments it gets obvious that retardation of C_3S hydration under paste conditions is more complex and data may interpreted in terms of conformation of polymers on surfaces. This effect is proposed to be a function of the solids content of the mixture (l/s ratio).

4.3.5 Concluding remarks

In the present chapter the influence of superplasticizers on parallel occurring dissolution-precipitation processes during hydration is investigated. These experiments are conducted on C_3S as appropriate model for cement.

First, the **temperature dependency** of the impact of superplasticizers on the hydration kinetics of C_3S was tested. It was demonstrated that superplasticizers act chemically as inhibitors showing no effect on activation energy but decreasing the frequency factor to overcome the induction period. Thus only the reaction rates are changed not the reaction mechanisms when SPs are present.

The impact of superplasticizers on the **ion composition of the aqueous phase of hydrating C_3S** was analysed in order to test if polymers excert differences in ion concentrations. These experiments are discussed in parallel with findings on the time dependent development of the electrical conductivity. Thereby, the contribution of polymer structure parameters on the magnitude of retardation is discussed in the present chapter with general findings outlined in previous chapters. It was found that the impact of superplasticizers is based on the affinity of the functional groups to interact with calcium. This is schematically illustrated in Fig. 5-1. From these two constitutions of calcium ions during hydration are important for the polymers: 1) free (dissolved) calcium ions and 2) calcium ions on surfaces. It was shown that superplasticizers can complex free Ca ions which lead to increased solubility of Ca containing solids. These Ca-polymer complexes may further act as templates for crystallization. The template effect includes the formation of additional hydration products (e.g. C-S-H phases) in the aqueous phase.

Following that an ***in-situ*** **method for the determination of ion concentrations in the aqueous phase of C_3S pastes** based on electrical conductivity was propoesed. This approach permits the examination of C_3S hydration by combining classical isothermal conduction calorimetry to development of Ca ion concentration in the aqueous phase of hydrating C_3S. Based on the proposed approach, the acceleration period can be subdivided into three parts: portlandite precipitation stage (III), slow acceleration stage (IV), fast acceleration stage (V). Under paste conditions the induction period (stage II) ends with onset of the portlandite precipitation stage. The superplasticizers induced retardation is limited to stages II-IV.

Finally the **retarding effect of superplasticizers on C_3S hydration** is discussed. Based on complexation of calcium ions on surfaces (adsorption), the blocking of crystal faces and the reduction of crystal growth rates is concluded. Grafting of side chains to the polymers backbone induces steric stability against agglomeration of particles. It is underlined that PCE based superplasticizers induce formation of C-S-H-polymer clusters in the aqueous phase of hydrating C_3S both under suspension and paste conditions. Thus, the particle mediated crystallization discussed in the field of biomineralization (non-classical nucleation theory) can be adapted to C_3S/cement hydration. Moreover, in the present work it is proposed that the particle mediated crystallization may affect not only bulk properties of crystals, but also the kinetics of product formation. In other words, it is claimed that due to impact of superplasticizers on the particle mediated crystallization of C-S-H phases and portlandite the kinetics of precipitation is decreased and thus hydration is retarded. This behavior is seen to be dependent on the conformation of polymers on surfaces. The polymer conformation is, however, dependent on the solids content of the mixture. Based on this assumption, the contradicted behavior of superplasticizers grafted with long and short side chains during pure crystallization of C-S-H phases and during C_3S paste hydration can be explained. In summary, the retarding effect of superplasticizers on the hydration of cement/C_3S is caused by reduced crystal growth either by blocking of crystal faces (adsorption) or by stabilization of C-S-H particles against agglomeration (particle mediated crystallization). It was not possible to point out the importance of dissolution reactions on the global hydration kinetics of C_3S.

Based on the particle mediated crystallization, the interpretation of results obtained by the examination of the compostition of the aqueous phase during C_3S hydration is permitted. The aforementioned template performance of superplasticizers induces increased concentrations of ions in the aqueous phase of hydrating C_3S as a result of artifacts. This effect is enhanced by grafting of side chains with the polymers backbone. It is postulated that the ion composition follows the general relationship (kinetic path[12-13, 40] and solubility of C-S-H(m)[70, 86]).

5 CONCLUSIONS AND OUTLOOK

The present work was aimed at gaining insights on the causes of the retarding effect of superplasticizers on the hydration kinetics of tricalcium silicate. To address the retarding effect the work was divided into three major parts: 4.1. Calcium complexation and cluster formation as principal modes of action of superplasticizers, 4.2. Influence of superplasticizers on separate dissolution and precipitation processes occurring during C_3S hydration and 4.3. Influence of superplasticizers on the parallel dissolution-precipitation process of tricalcium silicate hydration.

Polymers contain functional groups that interact with ions. In case of cement paste's aqueous phase the most important ion for these interactions is calcium. For the superplasticizers considered, these are further influenced by side chains that can be grafted on the polymer's backbone. **Chapter 4.1** of the thesis deals with the **principal modes of action of superplasticizers in cementitious systems**. In this respect it was differentiated between interaction of functional groups with calcium and the steric performance of superplasticizers. The principal modes of action of superplasticizers are: complexation of Ca ions both in solution (aqueous phase) and on surfaces (generally known as adsorption) and cluster formation / aggregation in the aqueous phase. The latter is caused by steric hindrance (dispersion) of superplasticizers that leads to a shift of crystallization events more into the aqueous phase than solely on surfaces. Adsorption data on C_3S was used to calculate complexation constants for the different polymers. As a result the interaction of sulfonic groups with calcium is shown to be dependent on the polymer dosage. At very low dosage sulfonic groups interact stronger with calcium as compared with carboxy groups. But at increased dosage this ranking is turned over.

In **chapter 4.2** the effects of the principal modes of action of superplasticzers on basic reactions occurring during cement hydration were analysed. In particular the **solubility, pure dissolution rate and pure crystallization kinetics in dependence of superplasticizer presence** were addressed in detail. Reactions were carried out with different model systems relevant for the cement system, i.e. C-S-H phases, portlandite and C_3S. Based on the principal modes of action it was demonstrated that complexation of calcium ions in solution leads to a change in ion concentration during dissolution of C-S-H phases and portlandite. In C-S-H solubility experiments a characteristic decrease in calcium ion concentration was detected that was proportional to the number of functional groups of the polymer. At the same time a strong increase in silicate ion concentration was detected which was not related to polymer structural parameters. However, a characteristic increase in calcium ion concentration with respect to the added number of functional groups by the polymers was detected in portlandite experiments. Examination of the data with respect to complexation constants and comparison to the corresponding constants determined in $CaCl_2$ solution presented in chapter 4.1 shows that adsorption of polymers on both C-S-H phases and portlandite has occured. From the data it is concluded that the polymers are stronger adsorbed on C-S-H phases as compared to portlandite. Furthermore, in C-S-H solubility experiments it is proposed that polymers needs to complex calcium ions from solution in order to adsorb on C-S-H. It is concluded that the complexation of ions on surfaces (adsorption) is too weak to compensate the dissolution promoting effect of Ca complexation in solution. In the next step the impact of superplasticizers on the dissolution

rate of C_3S was addressed in more detail. The gathered experimental results suggest that in the presence of SP the dissolution rate of C_3S is either increased or decreased in aqueous solution with very low ion activity product for C_3S dissolution. This behavior is dependent on the polymer's chemical structure, and the increase in C_3S unconstrained dissolution rate was attributed to the complexation of released calcium ions by the functional groups of polymers. Analogous results were shown before for the solubiltiy of C-S-H phases and portlandite. If the complexation capability of superplasticizers is considered in the calculation of the ion activity product then it was shown that all investigated superplasticizers reduce the unconstrained dissolution rate of C_3S. But also the addition of calcite leads to a reduction of this rate. Because it is known that superplasticizers and calcite show a different impact on C_3S hydration kinetics (retardation, acceleration) it is concluded that this experimental data permits no clear relation to C_3S paste hydration kinetics. Therefore, hindered dissolution as possible cause of retardation is still open for discussion. In spite of that, a strong impact on pure crystallization by the polymers was found. Thereby, the crystallization kinetics was differentiated in induction time and crystal growth rate. The obtained experimental results clearly suggest that polymers strongly retard crystallization kinetics with respect to both kinetic parameters (induction time, crystal growth rate). This behavior is mainly attributed to complexation of calcium ions on surfaces (adsorption) and hindered agglomeration of clusters. In these experiments grafting of longer side chains with the polymers backbone induces stronger retardation compared to short side chain containing polymers. With respect to dissolution reactions it is concluded that the crystallization rate is predominantly retarded by superplasticizers.

Because hydration comprises both **dissolution and precipitation** reactions, the findings of the separate consideration handled in chapter 4.2 are investigated **in parallel in chapter 4.3**. In the first two sections of this chapter, special attention was laid on the impact of superplasticizers on the temperature dependency of the C_3S paste hydration kinetics and ion concentrations in the aqueous phase of hydrating C_3S. It was shown that superplasticizers can be associated chemically with inhibitors until the main hydration period is established. A strong impact of superplasticizers on the ion concentrations in the aqueous phase of hydrating C_3S was not found. Measured unusually high ion concentrations were associated with artifacts that are caused by filtering. Again this is consistent to previous findings on the principal modes of action of superplasticizers (chapter 4.1) and can be related to the formation of C-S-H phases that are dispersed by superplasticizers. The size of these particles is smaller then the filter used to separate the solids from the aqueous phase. As a result these particles surpass the filter with the consequence that increased ion concentrations are measured. In this respect the particle mediated crystallization *via* cluster formation and agglomeration/fusion of C-S-H phases in the presence of superplasticizers was again proven by measuring ion concentrations. In the last two sections of chapter 4.3 the impact of superplasticizers on the hydration kinetics of C_3S was addressed in more detail. The experimental results were discussed in the light of previous findings. Therefore, the individual importance of complexation of ions both in solution and on surfaces and the particle mediated C-S-H crystallization for the magnitude of retardation induced by superplasticizers was emphasized. Moreover, the utilization of electrical conductivity during

C_3S paste hydration provided more details on the hydration stages known from literature. In combination with isothermal heat release rate the acceleration period was divided into three different stages. 1. under paste conditions the induction period ends with the onset of portlandite precipitation which is signaled by a sharp drop in electrical conductivity and slight increase in heat release of C_3S. 2. afterwards growth of both C-S-H phases and portlandite leads to slow increase in the dissolution rate of C_3S. The last acceleration stage is characterised by increased reaction rates, thus called main hydration period. This sequence of hydration periods is observed in all paste experiments without and with superplasticizers and may thus be of general importance for C_3S / cement hydration kinetics.

In view of the purpose of the present work, the retarding effect of superplasticizers on C_3S paste hydration is the consequence of:

- Blocking of growth sites of crystals by polymers
- Hindered C-S-H nanoparticle aggregation during the particle mediated crystallization by the steric performance of polymers.

It should be emphasized that the impact of superplasticizers on pure dissolution rate of C_3S remains open for investigation. Thus, hindered pure dissolution of C_3S is possibly a further cause for the overall retardation.

These results are based on the fact that the induction period during C_3S hydration ends with the growth of hydration products, i.e. C-S-H phases and portlandite.In Fig. 5-1 all mentioned interactions of superplasticizers are summarized schematically.

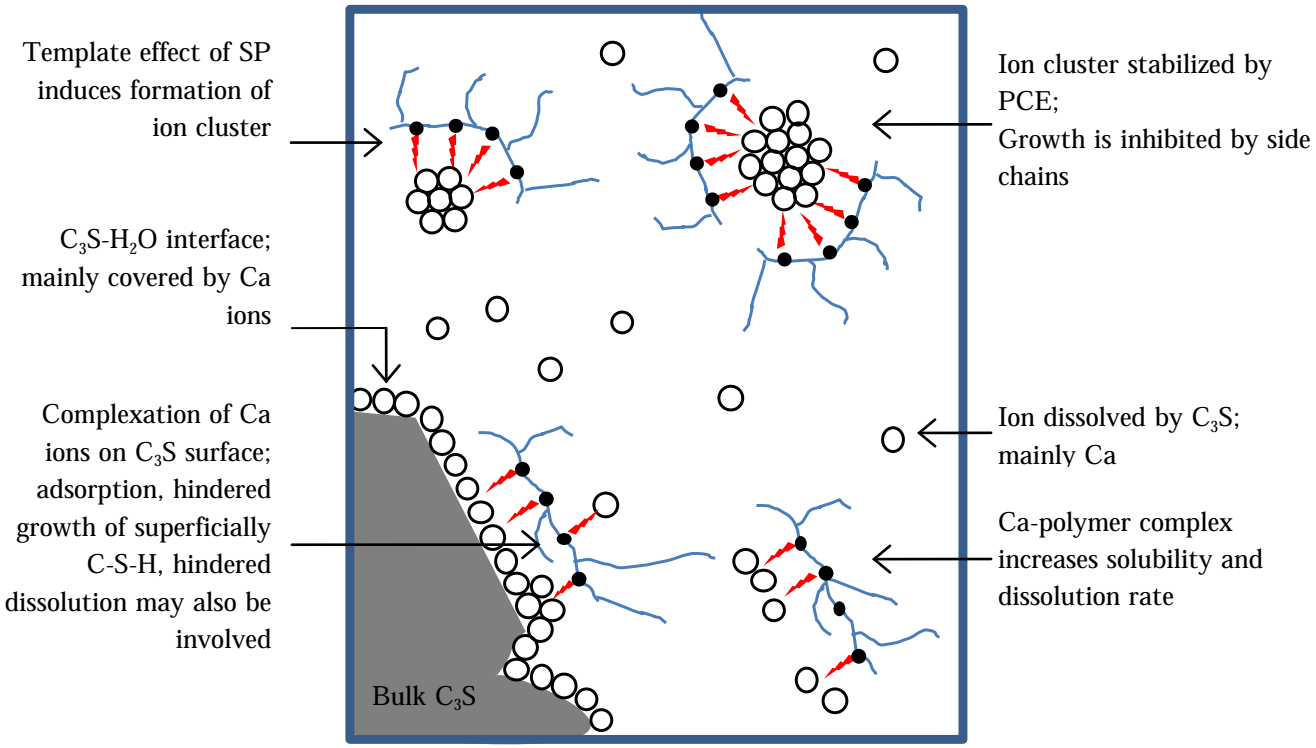

Fig. 5-1: Schematic illustration summarizing principal interactions of superplasticizers (with side chains) and C_3S during hydration with impact on retardation.

Further work should address the particle mediated crystallization of C-S-H phases in the presence of polymers in more detail. In this respect the advantages of promoted dissolution and increase in solubility can be utilized in order to stimulate C_3S /cement hydration. Moreover, the interaction of organic polymers with inorganic crystals provides a promising field of bioinspired materials for constructions.

Besides these possibilities a further field of research is the origin of the induction period during C_3S / cement hydration. In this respect it would be advantageous to utilize new techniques in combination with findings on the interaction of polymers and other admixtures with C_3S in order to test hypothesis on the cause of the induction period.

As indicated by results in section 4.2.4 it was found that superplasticizers induce increased dissolution rate of C_3S at very low ion concentrations in the aqueous phase. Thereby, the rate equalizes with the reference sample when ion concentration increases. A clear experimental argument on the impact of superplasticizers on pure dissolution of C_3S was not found. This aspect is embedded in the discussion on the causes of the induction period in tricalcium silicate hydration and should be investigated in more detail.

The role of functional groups of polymers in particular on adsorption and C_3S hydration kinetics should be investigated in more detail. The utilization of a broader set of defined structured polymers can help to identify if the data gathered in the present work are of general importance.

LIST OF FIGURES

LIST OF TABLES

APPENDIX

Table A- 1: Chemical analysis of tricalcium silicate.

Parameter	Content [mass.-%]
Loss on drying	0
Loss on ignition	0.1
CaO	72.4
SiO_2	26.0
Al_2O_3	0.1
Fe_2O_3	0
SO_3	0.7
K_2O	0.01
Na_2O	0
TiO_2	0
MnO	0
MgO	0
CaO_{free}	0.2
Total	99.5

Table A- 2: Chemical composition of cement CEMI 42.5R.

Parameter	Content [mass.-%]
Loss on drying	0.2
Loss on ignition	2.9
CaO	63.2
SiO_2	20.1
Al_2O_3	4.8
Fe_2O_3	2.2
SO_3	3.2
K_2O	1.13
Na_2O	0.20
K_2O (water soluble)	0.81
Na_2O (water soluble)	0.07
TiO_2	0.18
MnO	0.03
MgO	1.4
Cl	
CaO_{free}	0.2
total	100.6

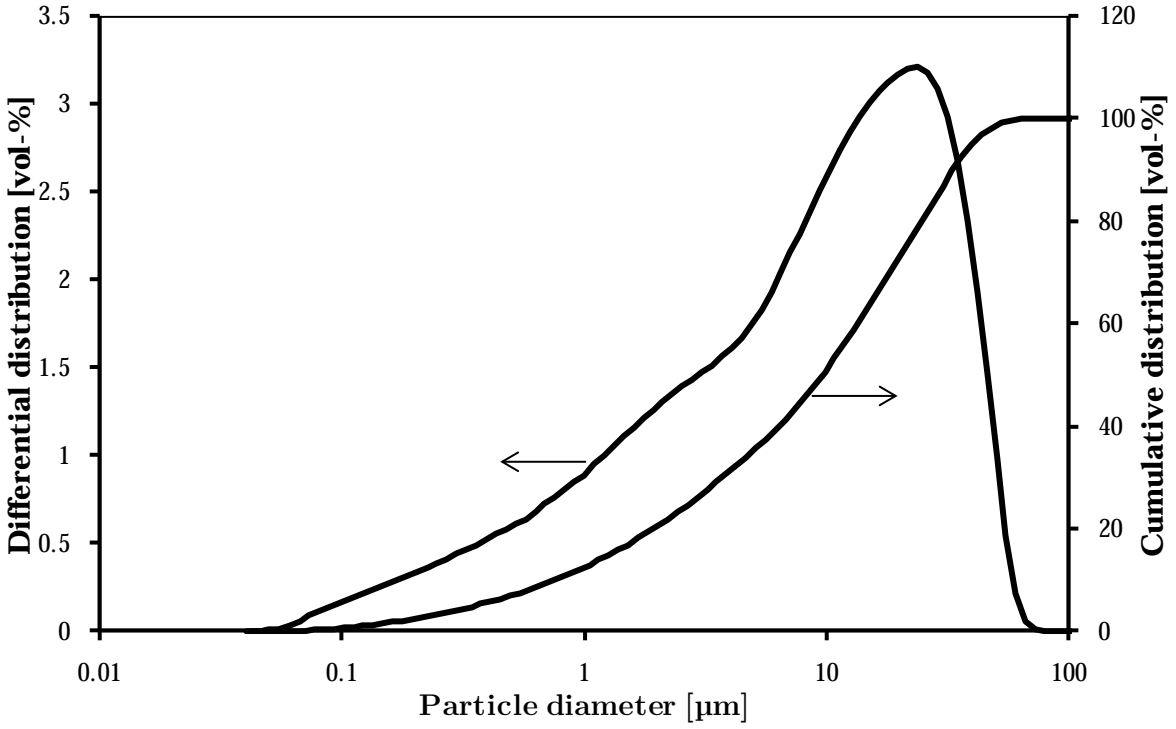

Fig. A- 1: Particle size distribution of cement CEMI 42.5R.

Table A- 3: Phase content of the cement CEMI 42.5R determined by QXRD.

Phase	Content [%]
a-C_2SMueller	8.1
Alite mcl (DeLaTorre)	50.1
Amorphous content	3.3
Anhydrite	0.5
Brownmillerite(Si,Mg)	5.9
C_2S beta (MUMME)	16.3
C_3A cubic	1.6
C_3A Na orthorhombic	5.4
Calcite	8.5
Quartz	0.4
Total	100.0

Table A- 4: Adsorption data of superplasticizers on tricalcium silicate (l/s=0.5). Standard deviation determined on three different samples was 5%.

Sample	Dosage		TOC initial [mg/l]	TOC aqueous phase [mg/l]	TOC adsorption [mg/l]	Adsorption [mg/g]
	m.-% bwoC_3S	[mg/g]				
Starting water	0	0	24	-	-	-
C_3S+H_2O	0	0	72	-	-	-
C_3S+PCE1	0.1	1	1070	340	802	0.75
	0.25	2.5	2730	1136	1666	1.53
	0.54	5.4	5540	3013	2599	2.53
	1.5	15	15910	8117	7865	7.42
C_3S+PCE2	0.1	1	973	329	716	0.74
	0.25	2.5	2690	1025	1737	1.61
	0.54	5.4	5730	3975	1827	1.72
	1.5	15	15660	8864	6868	6.58
C_3S+PCE3	0.1	1	942	232	782	0.83
	0.25	2.5	2580	1009	1643	1.59
	0.54	5.4	5570	3534	2109	2.04
	1.5	15	15200	7049	8223	8.11
C_3S+PCE4	0.1	1	1010	169	913	0.90
	0.25	2.5	2500	1099	1474	1.47
	0.54	5.4	5510	3921	1661	1.63
	1.5	15	15400	7465	8007	7.80
C_3S+PCE5	0.1	1	950.4	229	794	0.84
	0.25	2.5	2560	978	1654	1.62
	0.54	5.4	5350	3890	1532	1.55
	1.5	15	15320	1860	13532	13.25

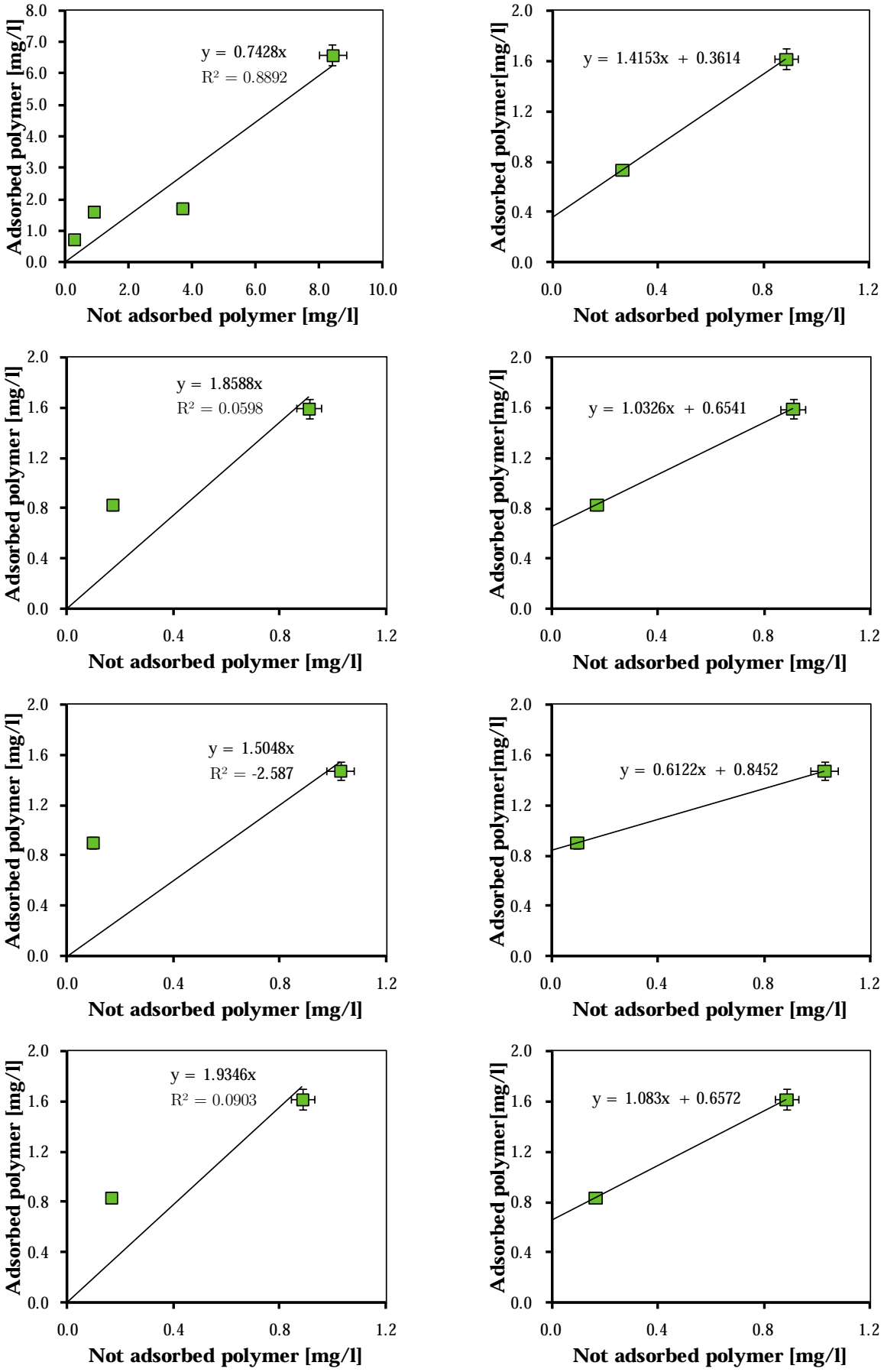

Fig. A- 2: Linear fits according to scenario A (left hand) and B (right hand) for the adsorption of (from top to bottom) PCE2, PCE3, PCE4 and PCE5 on C_3S.

Table A- 5: Ion concentrations in the aqueous phase of C-S-H phases in different starting solutions (l/s=70) and in presence of superplasticizers.

Series	Comment	SP dosage [g/gCSH]	Number funct. groups per gram C-S-H [mmol/g]	Ca [mmol/l]	Si [µmol/l]	Na [mmol/l]	pH
1s	Starting solution	0.00		0.0	2.6	0.0	-
1r	Reference	0.00	0.00	3.8	56.5	0.0	12.09
1a	PCE1	0.03	0.08	3.9	190.4	0.3	12.09
1b	PCE1	0.11	0.29	3.8	329.3	1.2	12.07
1c	PCE1	0.20	0.54	3.7	336.4	2.1	12.04
1d	PCE2	0.03	0.07	3.6	118.1	0.2	12.10
1e	PCE2	0.10	0.22	3.8	459.8	0.7	12.07
1f	PCE2	0.23	0.52	3.6	340.4	1.6	12.06
1g	PNFS	0.08	0.62	3.1	64.8	1.7	12.08
1h	PNFS	0.13	0.99	3.0	71.4	2.8	12.09
1i	PNFS	0.20	1.60	3.0	123.3	4.5	12.08
2s	Starting solution	0.00		5.6	12.2	0.0	-
2r	Reference	0.00	0.00	7.2	16.3	0.0	12.37
2a	PCE1	0.04	0.10	7.2	106.3	0.4	12.36
2b	PCE1	0.11	0.30	7.2	165.5	1.2	12.35
2c	PCE1	0.20	0.55	7.0	85.4	2.1	12.34
2d	PCE2	0.04	0.09	7.2	164.4	0.3	12.37
2e	PCE2	0.10	0.23	7.2	246.2	0.7	12.38
2f	PCE2	0.23	0.52	6.9	120.9	1.6	12.36
2g	PNFS	0.02	0.16	7.0	21.7	0.4	12.38
2h	PNFS	0.11	0.86	6.5	23.9	2.5	12.36
2i	PNFS	0.20	1.54	6.4	32.3	4.4	12.36

Table A-5: (continued)

Series	Comment	SP dosage [g/gCSH]	Number funct. groups per gram C-S-H [mmol/g]	Ca [mmol/l]	Si [µmol/l]	Na [mmol/l]	pH
3s	Starting solution	0.00		11.9	13.0	0.0	-
3r	Reference	0.00	0.00	12.7	6.9	0.0	12.60
3a	PCE1	0.02	0.06	12.5	58.7	0.3	12.59
3b	PCE1	0.13	0.34	12.2	101.8	1.3	12.57
3c	PCE1	0.21	0.55	12.1	92.7	2.2	12.57
3d	PCE2	0.03	0.06	12.8	155.1	0.2	12.60
3e	PCE2	0.11	0.25	12.4	199.4	0.8	12.59
3f	PCE2	0.22	0.49	12.1	117.1	1.6	12.57
3g	PNFS	0.03	0.24	13.2	9.4	0.7	12.58
3h	PNFS	0.10	0.82	12.4	9.8	2.5	12.58
3i	PNFS	0.20	1.58	12.2	14.5	4.6	12.56
4s	Starting solution	0.00		16.7	31.2	0.0	-
4r	Reference	0.00	0.00	18.8	4.7	0.0	12.72
4a	PCE1	0.03	0.09	16.4	37.7	0.4	12.71
4b	PCE1	0.10	0.28	15.8	122.7	1.1	12.69
4c	PCE1	0.22	0.60	15.6	98.7	2.4	12.67
4d	PCE2	0.04	0.10	16.6	231.3	0.3	12.71
4e	PCE2	0.11	0.25	16.2	109.6	0.7	12.71
4f	PCE2	0.21	0.46	15.9	109.7	1.5	12.69
4g	PNFS	0.05	0.41	15.9	6.2	1.2	12.69
4h	PNFS	0.13	1.01	15.4	5.8	2.9	12.67
4i	PNFS	0.20	1.57	15.0	6.9	4.5	12.68

Table A-5: (continued)

Series	Comment	SP dosage [g/gCSH]	Number funct. groups per gram C-S-H [mmol/g]	Ca [mmol/l]	Si [µmol/l]	Na [mmol/l]	pH
5s	Starting solution	0.00	0.00	23.1	5.5	0.0	-
5r	Reference	0.00	0.00	22.7	3.3	0.0	12.83
5a	PCE1	0.32	0.86	22.4	66.6	0.4	12.83
5b	PCE1	0.13	0.35	21.7	156.0	1.4	12.81
5c	PCE1	0.21	0.57	22.5	103.7	2.3	12.80
5d	PCE2	0.04	0.08	22.3	208.5	0.3	12.84
5e	PCE2	0.15	0.34	23.4	137.3	1.1	12.82
5f	PCE2	0.21	0.47	24.7	153.0	1.5	12.82
5g	PNFS	0.03	0.25	22.4	3.6	0.7	12.83
5h	PNFS	0.11	0.84	22.4	3.6	2.5	12.83
5i	PNFS	0.27	2.11	22.4	9.8	6.0	12.79

Table A- 6: Development of ion concentrations during pure dissolution of tricalcium silicate (BET 0.8772 m^2/g) starting in water and determined on three different samples (a-c).

l/s				500					
Ref		a			b			c	
Time	Ca	Si	Rate	Ca	Si	Rate	Ca	Si	Rate
s	mmol/l	µmol/l	µmol/(sm²)	mmol/l	µmol/l	µmol/(sm²)	mmol/l	µmol/l	µmol/(sm²)
0	0.0	21.8	48.0	0.0	10.9	96.0	0.0	10.9	84.1
15	2.1	717.9	14.0	2.4	838.7	9.5	2.5	862.7	10.6
30	2.7	934.9	5.7	2.9	1000.3	4.8	2.9	1014.4	4.2
45	3.0	1045.0	3.3	3.1	1083.4	3.1	3.2	1102.5	2.8
60	3.3	1104.3	2.3	3.4	1161.6	1.8	3.4	1157.2	2.0
75	3.4	1153.3	1.6	3.4	1179.2	1.0	3.5	1194.8	1.4
90	3.5	1185.2	1.2	3.5	1198.7	0.7	3.6	1219.7	0.9
105	3.5	1211.2	0.8	3.6	1222.8	0.7	3.7	1248.1	0.6
120	3.8	1224.7	0.6	3.6	1242.5	0.6	3.7	1252.0	0.5
l/s				1000					
Ref		a			b			c	
Time	Ca	Si	Rate	Ca	Si	Rate	Ca	Si	Rate
s	mmol/l	µmol/l	µmol/(sm²)	mmol/l	µmol/l	µmol/(sm²)	mmol/l	µmol/l	µmol/(sm²)
0	0.0	14.6	126.4	0.0	14.5	83.3	0.0	22.5	80.7
15	1.9	641.1	18.8	1.8	610.2	24.1	1.4	472.7	13.7
30	2.3	780.7	11.6	2.3	788.3	8.8	1.7	582.7	6.6
45	2.6	886.2	7.8	2.4	851.3	5.2	1.9	650.4	5.1
60	2.7	963.1	5.2	2.6	918.4	4.4	2.0	706.5	4.2
75	2.9	1010.4	3.5	2.8	960.0	4.0	2.2	755.2	3.4
90	3.0	1043.7	3.0	2.9	999.8	3.7	2.2	776.4	2.7
105	3.0	1078.1	2.9	3.0	1040.8	3.2	2.3	818.9	2.0
120	3.5	1129.0	2.5	3.1	1070.5	2.4	2.4	831.1	1.5
l/s				2000					
Ref		a			b			c	
Time	Ca	Si	Rate	Ca	Si	Rate	Ca	Si	Rate
s	mmol/l	µmol/l	µmol/(sm²)	mmol/l	µmol/l	µmol/(sm²)	mmol/l	µmol/l	µmol/(sm²)
0	0.0	14.5	88.0	0.0	14.5	88.6	0.0	14.6	79.9
15	0.9	312.9	27.8	1.1	354.9	32.5	1.1	371.0	40.3
30	1.3	443.4	19.1	1.4	489.5	17.8	1.6	548.2	19.9
45	1.6	540.3	15.3	1.7	573.2	13.6	1.8	611.3	12.1
60	1.8	613.4	12.3	1.9	642.8	11.8	2.0	677.2	10.5
75	1.9	668.5	10.0	2.0	698.9	10.5	2.1	738.6	10.4
90	2.1	723.1	8.6	2.2	745.6	9.2	2.3	787.0	10.3
105	2.2	758.4	8.0	2.3	794.6	7.9	2.4	829.5	7.3
120	2.3	801.1	7.8	2.4	825.6	6.5	2.5	855.5	0.8

Table A- 7: Development of ion concentrations during pure dissolution of tricalcium silicate (BET 1.0575 m^2/g) starting in saturated $Ca(OH)_2$ (l/s=1000) determined on four different samples (a-d).

Ref-CH		a			b			c	
Time	Ca	Si	Rate	Ca	Si	Rate	Ca	Si	Rate
s	mmol/l	µmol/l	µmol/(sm²)	mmol/l	µmol/l	µmol/(sm²)	mmol/l	µmol/l	µmol/(sm²)
0	21.8	10.6	0.5	22.2	4.0	1.1	22.3	11.8	0.5
15	22.2	18.9	0.4			0.7	23.6	20.7	0.4
30	22.3	22.8	0.4	22.5	27.3	0.4	23.8	29.1	0.3
45	22.2	29.9	0.2	22.2	31.2	0.3	23.8	30.3	0.3
60	22.6	33.0	0.2	22.1	33.4	0.2	24.0	36.9	0.2
75	22.4	36.1	0.2	22.4	36.0	0.1	24.0	35.5	0.2
90	22.2	39.8	0.1	22.2	50.3	0.1	23.8	38.8	0.1
105	22.5	46.6	0.1	22.4	39.8	0.0	23.8	41.1	0.1

Ref-CH		d	
Time	Ca	Si	Rate
s	mmol/l	µmol/l	µmol/(sm²)
0	22.0	4.0	0.8
15	23.8	16.8	0.5
30	23.9	39.2	0.4
45	23.9	26.0	0.3
60	23.8	30.0	0.2
75	23.9	34.6	0.1
90	23.9	32.2	0.1
105	24.0	36.1	0.1

Table A- 8: Development of ion concentrations during pure dissolution of tricalcium silicate (BET 0.7228 m^2/g) starting in water (l/s=2000) and in presence of calcite ($17.8 m^2/g_{C3S}$).

	a			b			c		
time	Ca	Si	Rate	Ca	Si	Rate	Ca	Si	Rate
s	mmol/l	µmol/l	[µmol/(sm²)]	mmol/l	µmol/l	[µmol/(sm²)]	mmol/l	µmol/l	[µmol/(sm²)]
0	0.0	14.6	82.6	0.0	14.7	69.4	0.0	14.6	37.1
15	1.1	330.8	31.4	1.0	311.2	31.5	0.8	233.9	26.4
30	1.4	469.5	19.0	1.4	452.9	16.4	1.1	341.2	18.4
45	1.8	619.2	13.7	1.6	513.5	11.0	1.3	445.5	12.9
60	1.6	553.2	10.4	1.7	571.1	9.2	1.5	504.5	9.6
75	2.0	669.6	8.2	1.9	629.4	8.4	1.6	543.8	8.0
90	2.1	712.0	7.1	2.0	661.0	7.4	1.6	559.2	7.8
120	2.2	743.5	7.2	2.0	694.6	5.9	1.9	636.9	8.3
150	2.3	785.2	7.3	2.1	724.0	3.8	2.0	678.9	9.3

Table A- 9: Development of ion concentrations during pure dissolution of tricalcium silicate (BET 0.8772 m^2/g) starting in water and in presence of PCE1 determined on three different samples (a-c) and three dosages ($g_{SP}/g_{C3S,}$ given in the top left of each data set).

1.0 PCE1		a			b			c	
time	Ca	Si	Rate	Ca	Si	Rate	Ca	Si	Rate
s	mmol/l	µmol/l	µmol/ sm^2	mmol/l	µmol/l	µmol/sm^2	mmol/l	µmol/l	µmol/sm^2
0	0.0	14.7	134.0	0.0	14.7	192.9	0.0	14.9	165.9
15	1.2	404.2	27.1	1.2	412.8	23.6	1.4	473.5	26.8
30	1.7	512.7	14.0	1.5	525.6	17.6	1.6	568.3	11.0
45	1.7	570.7	11.1	1.8	609.4	14.9	1.8	613.2	10.0
60	1.9	632.5	9.4	2.0	678.8	12.5	2.0	672.9	9.8
75	2.1	685.9	7.8	2.2	752.4	10.6	2.1	728.3	9.7
90	2.1	703.3	6.5	2.3	786.6	9.2			8.6
105	2.2	746.3	5.3	2.4	830.2	8.2	2.3	802.9	6.9
120	2.2	766.2	4.2	2.5	872.4	7.9	2.4	836.9	4.4
2.0 PCE1		a			b			c	
time	Ca	Si	Rate	Ca	Si	Rate	Ca	Si	Rate
s	mmol/l	µmol/l	µmol/sm^2	mmol/l	µmol/l	µmol/sm^2	mmol/l	µmol/l	µmol/sm^2
0	0.0	29.7	146.7	0.0	14.5	191.2	0.0	14,6	188.6
15	1.4	451.8	29.2	1.5	506.5	29.9	1.4	472,3	24.7
30	1.7	561.1	15.1	1.8	615.1	15.5	1.6	565,3	13.5
45	1.9	639.1	12.1	2.0	691.5	12.6	1.9	636,2	12.5
60	2.1	689.8	10.2	2.2	744.4	10.7	2.0	690,4	11.7
75	2.2	739.5	8.6	2.4	797.9	9.3	2.2	762,9	10.4
90	2.3	783.6	7.1	2.5	840.0	8.3	2.3	797,2	8.7
105	2.4	810.8	5.8	2.4	818.3	7.8	2.5	837,6	6.4
120	2.5	838.2	4.8	2.7	913.6	7.7	2.5	862,8	3.6
4.0 PCE1		a			b			c	
time	Ca	Si	Rate	Ca	Si	Rate	Ca	Si	Rate
s	mmol/l	µmol/l	µmol/sm^2	mmol/l	µmol/l	µmol/sm^2	mmol/l	µmol/l	µmol/sm^2
0	0.0	7.3	237.9	0.0	7.3	40.0	0.0	0.0	199.9
15	1.5	509.9	31.8	1.6	555.7	34.1	1.1	404.0	16.5
30	1.9	645.1	21.2	1.4	473.1	28.8	1.3	468.3	9.8
45	2.2	742.1	15.3	1.7	571.5	24.2	1.5	525.9	8.6
60			10.8	2.0	681.2	20.1	1.6	561.7	7.4
75	2.4	809.8	8.0	2.3	782.3	16.6	1.7	596.4	5.8
90	2.6	876.3	7.1	2.5	861.9	13.6	1.8	630.6	3.9
105	2.7	925.3	7.0	2.7	923.8	11.0	1.8	639.4	1.8
120	2.8	959.9	6.7	2.9	976.0	8.9	1.9	666.4	1.6

Table A- 10: Development of ion concentrations during pure dissolution of tricalcium silicate (BET 0.7228 m^2/g) starting in water (l/s=2000) and in presence of SPs (dosage: 4.0 g_{SP}/g_{C3S}).

4.0 SP	PCE2			PNFS		
time	Ca	Si	Rate	Ca	Si	Rate
s	mmol/l	µmol/l	[µmol/(sm²)]	mmol/l	µmol/l	[µmol/(sm²)]
0	0.2	12.4	80.4	0.5	8.8	81.9
15	1.2	320.6	49.7	1.5	352.1	60.3
30	1.7	534.1	30.5	2.3	646.2	43.7
45	2.0	648.4	19.3	2.6	773.0	31.6
60	2.2	693.5	12.9	2.8	854.0	22.6
75	2.3	722.9	9.3	3.0	901.1	16.5
90	2.4	774.8	7.5	3.2	996.4	12.4
120	2.5	803.1	6.5	3.4	1063.8	9.6
150	2.6	852.8	5.6	3.5	1091.9	5.9
240	3.1	999.6	5.2	3.9	1208.6	4.9

Table A- 11: Development of ion concentrations during pure dissolution of tricalcium silicate (BET 0.7228 m^2/g) in saturated $Ca(OH)_2$ solution and in presence of SPs (dosage: 4.0 g_{SP}/g_{C3S}).

	PCE1			PCE2			PNFS		
time	Ca	Si	Rate	Ca	Si	Rate	Ca	Si	Rate
s	mmol/l	µmol/l	[µmol/(sm²)]	mmol/l	µmol/l	[µmol/(sm²)]	mmol/l	µmol/l	[µmol/(sm²)]
0	20.9	12.4	0.3	20.3	16.8	0.2	15.2	29.2	0.9
15	20.5	11.9	0.3	20.7	21.9	0.2	15.4	32.9	0.8
30	20.5	15.1	0.3	20.5	41.9	0.2	15.7	41.7	0.8
45	20.7	16.7	0.3	20.6	46.4	0.2	17.4	44.4	0.7
60	21.0	19.9	0.3	20.8	22.3	0.2	15.7	46.2	0.7
75	20.6	19.4	0.3	20.8	21.6	0.2	15.9	47.6	0.6
90	20.8	20.9	0.3	20.4	23.7	0.2	15.7	50.8	0.6
120	20.8	22.3	0.3	20.9	25.0	0.2	15.8	61.3	0.5
150	20.8	25.2	0.3			0.2	15.9	64.1	0.5
240	20.8	50.3	0.3	20.4	32.3	0.2	15.9	73.1	0.2

Table A- 12: Pure precipiation of C-S-H phases (eq. (42)) with degree of supersaturation (S_a), saturation index (SI) and kinetic parameter induction time (t_{ind}) and maximum growth rate.

Calcium [mmol/l]	Silicon [µmol/l]	OH^- [mmol/l]	S_a	SI	t_{ind} [min]	Max. growth rate [µmol/(l*s)]
13.5	721.2	27.5	74.1	1.87	0.0	1.375
8.3	734.6	15.5	41.7	1.62	9.0	0.16
8.2	706.3	16.5	40.7	1.61	5.8	0.21
7.2	705.6	16.7	37.2	1.57	6.0	n.d.
6.7	689.2	13.1	30.9	1.49	16.3	0.05
5.9	673.6	12.0	26.3	1.42	n.d.	0.03
5.4	705.7	11.7	25.7	1.41	44.0	0.11
3.7	697.7	7.7	15.8	1.20	45.0	0.07

Table A- 13: Pure precipiation of C-S-H phases (eq. (42)) in presence of SPs and different dosages with degree of supersaturation (S_a), saturation index (SI) (calculated before and after complexation of Ca ions by superplasticizers) and kinetic parameter induction time (t_{ind}) and maximum growth rate.

SP	SP-dosage [ml/l]	Calcium [mmol/l]	Silicon [µmol/l]	OH^- [mmol/l]	S_a before	SI before	S_a after	SI after	t_{ind} [min]	Max. growth rate [µmol/(l*s)]
PCE1	0.25	8.2	610.7	14.1	33.1	1.52	33.1	1.52	57.3	0.09
	0.50	8.2	606.5	12.1	30.2	1.48	29.5	1.47	58.8	0.12
	1.00	8.2	591.1	12.4	30.2	1.48	28.8	1.46	63.7	0.13
PCE2	0.25	8.3	592.2	13.8	31.6	1.50	31.6	1.50	52.6	0.25
	0.50	8.2	592.8	13.5	31.6	1.50	30.9	1.49	73.5	0.18
	1.00	8.3	607.6	13.7	32.4	1.51	31.6	1.50	120.0	0.16
PNFS	0.24	8.5	628.3	11.9	31.6	1.50	28.2	1.45	50.1	0.18
	0.49	8.4	629.3	9.8	28.2	1.45	21.9	1.34	37.9	0.18
	0.97	8.5	639.8	12.7	32.4	1.51	17.8	1.25	19.1	0.20

Table A- 14: Pure precipiation of portlandite by double decomposition with degree of supersaturation (S_a), saturation index (SI) and kinetic parameter induction time (t_{ind}) and maximum growth rate determined on up to four different samples (a-d).

Starting solutions [mol/l]						t_{ind} [min]				t_{ind} [min]		Max. growth rate [mmol/(l*s)]	
Ca	Cl	Na	OH	S_a	SI					Mean	Standard deviation	Mean	Standard deviation
						a	b	c	d				
0.12	0.24	0.17	0.17	20.72	1.32	1.1	0.8	-	-	0.9	0.2	0.16	0.013
0.10	0.20	0.16	0.16	18.13	1.26	2.6	4.3	9.4	-	5.4	3.6	0.05	0.006
0.07	0.14	0.09	0.09	6.11	0.79	272.0	-	-	-	272.0	-	0.02	-
0.10	0.19	0.16	0.16	16.26	1.21	5.3	4.7	5.8	8.3	6.0	1.6	0.002	-
0.08	0.17	0.16	0.16	15.35	1.19	6.9	-	-	-	6.9	-	0.06	-
0.08	0.16	0.16	0.16	14.85	1.17	12.3	13.5	11.1	-	12.3	1.2	0.04	-
0.06	0.12	0.16	0.16	13.05	1.12	21.4	22.8	20.8	-	21.7	1.0	0.023	-
0.06	0.12	0.16	0.16	12.87	1.11	26.3	27.5	28.6	-	27.4	1.2	0.016	-
0.05	0.10	0.16	0.16	11.57	1.06	36.5	41.0	43.0	-	40.2	3.3	0.011	-

Table A- 15: Pure precipiation of portlandite by double decomposition (starting solutions: 0.1M $CaCl_2$, 0.16M NaOH) with degree of supersaturation (Sa), saturation index (SI) (calculated before and after complexation of Ca ions by superplasticizers) and kinetic parameter induction time (tind) and maximum growth rate.

SP	SP-dosage [ml/l]	S_a before	SI before	S_a after	SI after	Induction time [min] a	b	c	Mean	Max. growth rate [mmol/(l*s)]
PCE1	0.9	18.13	1.26	17.56	1.25	126.3	-	-	-	0.058
	1.7	18.13	1.26	17.14	1.23	120.7	-	-	-	0.045
	3.4	18.13	1.26	16.54	1.22	151.0	-	-	-	0.028
	6.8	18.13	1.26	15.29	1.18	198.9	-	-	-	0.019
	13.6	18.13	1.26	13.16	1.12	271.6	-	-	-	0.011
PCE2	1.7	18.13	1.26	16.88	1.23	290	-	-	-	0.083
	6.8	18.13	1.26	13.55	1.13	438	448	-	443	0.012
	17.1	18.13	1.26	9.18	0.96	1080	-	-	-	0.004
PNFS	1.7	18.13	1.26	3.63	0.56	60.3	56.6	-	58.4	0.051
	6.7	18.13	1.26	0.23	-0.65	47.2	48.1	43.5	46.3	0.027
	16.6	18.13	1.26	0.14	-0.84	89	116	-	102.5	0.011

REFERENCES

1. L. Addadi and S. Weiner, *Interactions between acidic proteins and crystals: stereochemical requirements in biomineralization.* Proceedings of the National Academy of Sciences of the United States of America, 1985. **82**(12): p. 4110-4114.
2. L. Addadi, S. Weiner and M. Geva, *On how proteins interact with crystals and their effect on crystal formation.* Zeitschrift für Kardiologie, 2001. **90**(15): p. III92-III98.
3. P.-C. Aitcin, *Binders for durable and sustainable concrete*. Modern concrete technology series, ed. A. Bentur and S. Mindess. 2008, New York: Taylor & Francis.
4. P.-C. Aïtcin, *Cements of yesterday and today: Concrete of tomorrow.* Cement and Concrete Research, 2000. **30**(9): p. 1349-1359.
5. P.-C. Aïtcin and W. Wilson, *Cements of today, concretes of tomorrow.* Cement Wapno Beton, 2014(6): p. 349-358.
6. J. Aizenberg, A. J. Black and G. M. Whitesides, *Oriented Growth of Calcite Controlled by Self-Assembled Monolayers of Functionalized Alkanethiols Supported on Gold and Silver.* Journal of the American Chemical Society, 1999. **121**(18): p. 4500-4509.
7. A. J. Allen, J. J. Thomas and H. M. Jennings, *Composition and density of nanoscale calcium-silicate-hydrate in cement.* Nature Materials, 2007. **6**: p. 311-316.
8. G. M. Anderson and D. A. Crerar, *Thermodynamics in geochemistry: the equilibrium model*. 1993: Oxford University Press.
9. P. W. Atkins, J. D. Paula, A. Höpfner and M. Baer, *Physikalische Chemie*. 2006: Wiley-VCH.
10. V. I. Babuskin, G. M. Matveev and O. P. Mcedlov-Petrosjan, *Termodinamika silikatov, Stroiisdat*. 1986, Moscow.
11. M. M. Barak, J. D. Currey, S. Weiner and R. Shahar, *Are tensile and compressive Young's moduli of compact bone different?* Journal of the Mechanical Behavior of Biomedical Materials, 2009. **2**(1): p. 51-60.
12. P. Barret and D. Bertrandie, *Comment on "Aqueous Solubility Relationships for Two Types of Calcium Silicate Hydrate".* Journal of the American Ceramic Society, 1988. **71**(2): p. C-113-C-115.
13. P. Barret and D. Bertrandie, *Fundamental hydration kinetic features of the major cement constituents: Ca[3]SiO[5] and beta Ca[2]SiO[4].* Journal de chimie physique, 1986. **83**(11-12).
14. P. Barret and D. Bertrandie, *Importance of the liquid to solid weight ratio in the powdered solid-liquid reactions : Example drawn from cement constituent hydration.* Solid State Ionics, 1997. **101-103**(Part 1): p. 359-365.
15. P. Barret and D. Bertrandie, *Saturated Solutions of Anhydrous Phases in the System Lime-Silica-Water: Example of beta-C2S.* Journal of the American Ceramic Society, 1990. **73**(11): p. 3486-3492.

16. P. Barret and D. Ménétrier, *Filter dissolution of C3S as a function of the lime concentration in a limited amount of lime water.* Cement and Concrete Research, 1980. **10**(4): p. 521-534.
17. F. Begarin, S. Garrault, A. Nonat and L. Nicoleau, *Hydration of alite containing aluminum.* Advances in Applied Ceramics, 2011. **110**(3): p. 127-130.
18. F. Bellmann, D. Damidot, B. Möser and J. Skibsted, *Improved evidence for the existence of an intermediate phase during hydration of tricalcium silicate.* Cement and Concrete Research, 2010. **40**(6): p. 875-884.
19. M. Bellotto, *Particle aggregation phenomena during the early hydration stages, studied by small amplitude rheological measurements.* XIII ICCC International Conference on the Chemistry of Cements, 2011
20. M. Bellotto and F. Faini, *The use of phosphonates as dispersants and rheology modifiers in mortar and concrete.* 9th CANMET/ACI International Conference on Superplasticizers and Other Chemical Admixtures in Concrete, 2009
21. S. Bhandarkar, R. Brown and J. Estrin, *Studies in rapid precipitation of hydroxides of calcium and magnesium.* Journal of Crystal Growth, 1989. **97**(2): p. 406-414.
22. A. Blum and A. C. Lasaga, *Role of surface speciation in the low-temperature dissolution of minerals.* Nature, 1988. **331**(4): p. 431-433.
23. A. E. Blum, R. A. Yund and A. C. Lasaga, *The effect of dislocation density on the dissolution rate of quartz.* Geochimica et Cosmochimica Acta, 1990. **54**(2): p. 283-297.
24. E. Bonaccorsi, S. Merlino and H. F. W. Taylor, *The crystal structure of jennite, Ca9Si6O18(OH)6 · 8H2O.* Cement and Concrete Research, 2004. **34**(9): p. 1481-1488.
25. S. L. Brantley, S. R. Crane, D. A. Crerar, R. Hellmann and R. Stallard, *Dissolution at dislocation etch pits in quartz.* Geochimica et Cosmochimica Acta, 1986. **50**(10): p. 2349-2361.
26. P. W. Brown, E. Franz, G. Frohnsdorff and H. F. W. Taylor, *Analyses of the aqueous phase during early C3S hydration.* Cement and Concrete Research, 1984. **14**(2): p. 257-262.
27. J. W. Bullard and R. J. Flatt, *New Insights Into the Effect of Calcium Hydroxide Precipitation on the Kinetics of Tricalcium Silicate Hydration.* Journal of the American Ceramic Society, 2010. **93**(7): p. 1894-1903.
28. J. W. Bullard, H. M. Jennings, R. A. Livingston, A. Nonat, G. W. Scherer, J. S. Schweitzer, K. L. Scrivener and J. J. Thomas, *Mechanisms of cement hydration.* Cement and Concrete Research, 2011. **41**(12): p. 1208-1223.
29. O. Burgos-Montes, M. Palacios, P. Rivilla and F. Puertas, *Compatibility between superplasticizer admixtures and cements with mineral additions.* Construction and Building Materials, 2012. **31**(0): p. 300-309.
30. H. M. Burt and A. G. Mitchell, *Crystal defects and dissolution.* International Journal of Pharmaceutics, 1981. **9**(2): p. 137-152.
31. J. Chen, J., L. Sorelli, M. Van Damme, F.-J. Ulm and G. Chanvillard, *A Coupled Nanoindentation/SEM-EDS Study on Low Water/Cement Ratio Portland Cement*

Paste: Evidence for C-S-H/Ca(OH)2 Nanocomposites. Journal of the American Ceramic Society, 2010. **93**(5): p. 1484-1493.

32. J. J. Chen, J. J. Thomas, H. F. W. Taylor and H. M. Jennings, *Solubility and structure of calcium silicate hydrate.* Cement and Concrete Research, 2004. **34**(9): p. 1499-1519.
33. H. Cölfen and M. Antonietti, eds. *Mesocrystals and Nonclassical Crystallization*. in. Vol. 1. 2008, John Wiley & Sons Ltd.: West Sussex (England).
34. H. Cölfen and T. Pauck, *Determination of particle size distributions with angström resolution.* Colloid & Polymer Science, 1997. **275**(2): p. 175-180.
35. S. Cordes and I. Odler, *Initial hydration of tricalcium silicate as studied by secondary neutrals mass spectrometry: I. Sample preparation and calibration.* Cement and Concrete Research, 2002. **32**(7): p. 1071-1075.
36. D. Damidot. *Etude de l'hydratation du silicate tricalcique en suspensions diluées par microcalorimétrie isotherme*. Universite De Bourgogne. 1990.
37. D. Damidot, F. Bellmann, B. Möser and T. Sowoidnich, *Calculation of the dissolution rate of tricalcium silicate in several electrolyte compositions.* Cement Wapno Beton, 2007(2): p. 57-67.
38. D. Damidot, F. Bellmann, B. Möser and T. Sowoidnich, *Investigation of the early dissolution behavior of C3S.* 12th International Conference on the Chemistry of Cement, 2007
39. D. Damidot, F. Bellmann, B. Möser and T. Sowoidnich, *Measurement and simulation of the dissolution rate of minerals in conditions close to cement paste: from gypsum to tricalcium silicate.* 17. ibausil, 2009
40. D. Damidot and A. Nonat, *C3S hydration in diluted and stirred suspensions: (I) study of the two kinetic steps.* Advances in Cement Research, 1994. **6**(21): p. 27-35.
41. D. Damidot and A. Nonat, *C3S hydration in diluted and stirred suspensions: (II) properties of C-S-H precipitated during the two kinetic steps.* Advances in Cement Research, 1994. **6**(22): p. 83-91.
42. D. Damidot and A. Nonat. *Investigation of the C3S hydration process during the first hours of hydration*. in *International RILEM Workshop on Hydration and Setting*. 1992. Université de Bourgogne, France.
43. D. Damidot, A. Nonat and P. Barret, *Kinetics of Tricalcium Silicate Hydration in Diluted Suspensions by Microcalorimetric Measurements.* Journal of the American Ceramic Society, 1990. **73**(11): p. 3319-3322.
44. D. Damidot, A. Nonat, P. Barret, D. Bertrandie, Z. H. and R. Rassem, *C3S hydration in diluted and stirred suspensions: (III) NMR study of C-S-H precipitated during the two kinetic steps.* Advances in Cement Research, 1995. **7**(25): p. 1-8.
45. L. De Windt and P. Devillers, *Modeling the degradation of Portland cement pastes by biogenic organic acids.* Cement and Concrete Research, 2010. **40**(8): p. 1165-1174.
46. J. A. Dirksen and T. A. Ring, *Fundamentals of crystallization: Kinetic effects on particle size distributions and morphology.* Chemical Engineering Science, 1991. **46**(10): p. 2389-2427.

47. P. M. Dove and N. Han, *Kinetics of Mineral Dissolution and Growth as Reciprocal Microscopic Surface Processes Across Chemical Driving Force.* AIP Conference Proceedings, 2007. **916**(1): p. 215-234.
48. J. I. Drever and L. L. Stillings, *The role of organic acids in mineral weathering.* Colloids and Surfaces A: Physicochemical and Engineering Aspects, 1997. **120**(1-3): p. 167-181.
49. L. Ferrari, J. Kaufmann, F. Winnefeld and J. Plank, *Interaction of cement model systems with superplasticizers investigated by atomic force microscopy, zeta potential, and adsorption measurements.* Journal of Colloid and Interface Science, 2010. **347**(1): p. 15-24.
50. P. Fierens and J. P. Verhaegen, *Hydration of tricalcium silicate in paste — Kinetics of calcium ions dissolution in the aqueous phase.* Cement and Concrete Research, 1976. **6**(3): p. 337-342.
51. P. Fierens and J. P. Verhaegen, *Induction period of hydration of tricalcium silicate.* Cement and Concrete Research, 1976. **6**(2): p. 287-292.
52. R. Flatt and I. Schober, *Superplasticizers and the rheology of concrete.* Understanding the Rheology of Concrete, 2012
53. R. J. Flatt, *Dispersion forces in cement suspensions.* Cement and Concrete Research, 2004. **34**(3): p. 399-408.
54. R. J. Flatt and Y. F. Houst, *A simplified view on chemical effects perturbing the action of superplasticizers.* Cement and Concrete Research, 2001. **31**(8): p. 1169-1176.
55. R. J. Flatt, I. Schober, E. Raphael, C. d. Plassard and E. Lesniewska, *Conformation of Adsorbed Comb Copolymer Dispersants.* Langmuir, 2009. **25**(2): p. 845-855.
56. R. J. Flatt, I. Schober, E. Raphael, C. d. Plassard and E. Lesniewska, *Conformation of Adsorbed Comb Copolymer Dispersants.* Langmuir, 2008. **25**(2): p. 845-855.
57. R. J. Flatt, J. Zimmermann, C. Hampel, C. Kurz, I. Schober, L. Frunz, C. Plassard and E. Lesniewska. *The role of adsorption energy in the sulfate-polycarboxylate competition*. in *Ninth ACI International Conference on Superplasticizers and other chemical admixures*. 2009. Sevilla (Spain): American Concrete Institute.
58. E. P. Flint and L. S. Wells, *Study of the system CaO-SiO2-H2O at 30 C and of the reaction of water on the anhydrous calcium silicates.* Bureau of Standards Journal of Research, 1934. **12**(6): p. 751-783.
59. E. Fratini, S.-H. Chen, P. Baglioni and M.-C. Bellissent-Funel, *Quasi-Elastic Neutron Scattering Study of Translational Dynamics of Hydration Water in Tricalcium Silicate.* The Journal of Physical Chemistry B, 2001. **106**(1): p. 158-166.
60. K. Fujii and W. Kondo, *Communications of the American Ceramic Society Estimation of Thermochemical Data for Calcium Silicate Hydrate (C-S-H).* Journal of the American Ceramic Society, 1983. **66**(12): p. C-220-C-221.
61. K. Fujii and W. Kondo, *Heterogeneous equilibrium of calcium silicate hydrate in water at 30°C.* Journal of the Chemical Society, Dalton Transactions, 1981(2): p. 645-651.

62. S. C. Galmarini. *Atomistic Simulation of Cementitious Systems*. École Polytechnique Fédérale De Lausanne. 2013.
63. S. Garrault-Gauffinet and A. Nonat, *Experimental investigation of calcium silicate hydrate (C-S-H) nucleation.* Journal of Crystal Growth, 1999. **200**(3-4): p. 565-574.
64. S. Garrault, E. Finot, E. Lesniewska and A. Nonat, *Study of C-S-H growth on C3S surface during its early hydration.* Materials and Structures, 2005. **38**(4): p. 435-442.
65. S. Garrault and A. Nonat, *Hydrated Layer Formation on Tricalcium and Dicalcium Silicate Surfaces: Experimental Study and Numerical Simulations.* Langmuir, 2001. **17**(26): p. 8131-8138.
66. S. Garrault, A. Nonat, Y. Sallier and L. Nicoleau, *On the Origin of the Dormant Period of Cement Hydration.* XIII ICCC International Congress on the Chemistry of Cement, 2011
67. E. Gartner, *Are There Any Practical Alternatives to the Manufacture of Portland Cement Clinker?* Journal of The Chinese Ceramic Society, 2012. **40**(1): p. 61-68.
68. E. Gartner, *Discussion of the paper "Dissolution theory applied to the induction period in alite hydration" by P. Juilland et al., Cem. Concr. Res. 40 (2010) 831-844.* Cement and Concrete Research, 2011. **41**(5): p. 560-562.
69. E. M. Gartner and J. M. Gaidis, *Hydration Mechanism, I.* Materials Science of Concrete, 1989
70. E. M. Gartner and H. M. Jennings, *Thermodynamics of Calcium Silicate Hydrates and Their Solutions.* Journal of the American Ceramic Society, 1987. **70**(10): p. 743-749.
71. E. M. Gartner, J. F. Young, D. A. Damidot and I. Jawed, eds. *Hydration of Portland Cement*. in Structure and Performance of Cements, ed. J. Bensted and P. Barnes. 2002. 57-113.
72. C. Gay and E. Raphael, *Comb-like polymers inside nanoscale pores.* Advances in Colloid and Interface Science, 2001. **94**(1-3): p. 229-236.
73. D. Gebauer and H. Cölfen, *Prenucleation clusters and non-classical nucleation.* Nano Today, 2011. **6**(6): p. 564-584.
74. D. Gebauer, A. Volkel and H. Colfen, *Stable Prenucleation Calcium Carbonate Clusters.* Science, 2008. **322**(5909): p. 1819-1822.
75. C. Giraudeau, J.-B. d. E. d. Lacaillerie, Z. Souguir, A. Nonat and R. Flatt, J., *Surface and Intercalation Chemistry of Polycarboxylate Copolymers in Cementitious Systems.* Journal of the American Ceramic Society, 2009. **92**(11): p. 2471-2488.
76. A. Glomme. *Biorelevante Löslichkeit schwerlöslicher Arzneistoffe*. Thesis. Johann Wolfgang Goethe-Universität. Göttingen. 2004.
77. J. Goodwin, *Colloids and Interfaces with Surfactants and Polymers: An Introduction*. 2004: Wiley.
78. S. A. Greenberg and T. N. Chang, *Investigation of the Colloidal Hydrated Calcium Silicates. II. Solubility Relationships in the Calcium Oxide-Silica-Water System at 25°.* The Journal of Physical Chemistry, 1965. **69**(1): p. 182-188.

79. S. A. Greenberg, T. N. Chang and E. Anderson, *Investigation of colloidal hydrated calcium silicates. I. Solubility products.* The Journal of Physical Chemistry, 1960. **64**(9): p. 1151-1157.
80. M. Gruber. *α-Allyl-ω-Methoxy-polyethylenglykol-comaleatbasierte Polycarboxylat-Fließmittel für ultra-hochfesten Beton (UHPC): Synthese, Eigenschaften, Wirkmechanismus und Funktionalisierung*. Thesis. Technische Universität München. München. 2010.
81. C. Han, C. B. Davis and W. Binghe, eds. *Evaluation of Drug Candidates for Preclinical Development. Pharmacokinetics, Metabolism, Pharmaceutics, and Toxicology.* in Wiley Series in Drug Discovery and Development, ed. W. Binghe. 2010, John Wiley & Sons, Inc.: Hoboken, New Jersey.
82. J. Hot, H. Bessaies-Bey, C. Brumaud, M. Duc, C. Castella and N. Roussel, *Adsorbing polymers and viscosity of cement pastes.* Cement and Concrete Research, 2014. **63**(0): p. 12-19.
83. Y. F. Houst, P. Bowen and F. Perche, *Adsorption of Superplasticizers on a Model Powder.* 12th International Conference on the Chemistry of Cement, 2007: p. T6-05.4
84. Y. F. Houst, P. Bowen, F. o. Perche, A. Kauppi, P. Borget, L. Galmiche, J.-F. o. Le Meins, F. o. Lafuma, R. J. Flatt, I. Schober, P. F. G. Banfill, D. S. Swift, B. O. Myrvold, B. G. Petersen and K. Reknes, *Design and function of novel superplasticizers for more durable high performance concrete (superplast project).* Cement and Concrete Research, 2008. **38**(10): p. 1197-1209.
85. D. Jansen, J. Neubauer, F. Goetz-Neunhoeffer, R. Haerzschel and W. D. Hergeth, *Change in reaction kinetics of a Portland cement caused by a superplasticizer - Calculation of heat flow curves from XRD data.* Cement and Concrete Research, 2012. **42**(2): p. 327-332.
86. H. M. Jennings, *Aqueous Solubility Relationships for Two Types of Calcium Silicate Hydrate.* Journal of the American Ceramic Society, 1986. **69**(8): p. 614-618.
87. H. M. Jennings, *Reply to the comment on "Aqueous Solubility Relationships for Two Types of Calcium Silicate Hydrate" by Barret and Bertrandie.* Journal of the American Ceramic Society, 1988. **71**(2): p. C-115-C-116.
88. H. M. Jennings, C. M. Neubauer, K. D. Breneman and B. J. Christensen, *Phase Diagrams Relevant to Hydration of C3S, Part I: A Case for Metastable Equilibrium.* 10th International Congress on the Chemistry of Cement, 1997. **II**
89. H. M. Jennings and P. L. Pratt, *An experimental argument for the existence of a protective membrane surrounding portland cement during the induction period.* Cement and Concrete Research, 1979. **9**(4): p. 501-506.
90. S. B. Johnson, G. V. Franks, P. J. Scales, D. V. Boger and T. W. Healy, *Surface chemistry-rheology relationships in concentrated mineral suspensions.* International Journal of Mineral Processing, 2000. **58**(1-4): p. 267-304.
91. C. Jolicoeur and M.-A. Simard, *Chemical admixture-cement interactions: Phenomenology and physico-chemical concepts.* Cement and Concrete Composites, 1998. **20**(2-3): p. 87-101.

92. B. Jönsson, A. Nonat, C. Labbez, B. Cabane and H. Wennerström, *Controlling the Cohesion of Cement Paste.* Langmuir, 2005. **21**(20): p. 9211-9221.
93. B. Jonsson, H. Wennerstrom, A. Nonat and B. Cabane, *Onset of Cohesion in Cement Paste.* Langmuir, 2004. **20**(16): p. 6702-6709.
94. P. Juilland, E. Gallucci, R. Flatt and K. Scrivener, *Dissolution theory applied to the induction period in alite hydration.* Cement and Concrete Research, 2010. **40**(6): p. 831-844.
95. E. H. Kadri and R. Duval, *Effect of Ultrafine Particles on Heat of Hydration of Cement Mortars.* ACI Materials Journal, 2002. **99**(2): p. 138-142.
96. D. L. Kantro, S. Brunauer and C. H. Weise, *Development of Surface in the Hydration of Calcium Silicates. II. Extension of Investigation to early and later Stages of Hydration.* The Journal of Physical Chemistry, 1962. **66**(10): p. 1804-1809.
97. D. Kashchiev, *Nucleation: Basic Theory With Applications*. 2000: Butterworth Heinemann.
98. A. K. Katz, J. P. Glusker, S. A. Beebe and C. W. Bock, *Calcium Ion Coordination: A Comparison with That of Beryllium, Magnesium, and Zinc.* Journal of the American Chemical Society, 1996. **118**(24): p. 5752-5763.
99. G. H. Kirby and J. A. Lewis, *Comb Polymer Architecture Effects on the Rheological Property Evolution of Concentrated Cement Suspensions.* Journal of the American Ceramic Society, 2004. **87**(9): p. 1643-1652.
100. W. Kleber, ed. *Einführung in die Kristallographie*. in 17. Auflage ed. 1990, Verlag Technik GmbH Berlin.
101. A. Kleidon, *Life, hierarchy, and the thermodynamic machinery of planet Earth.* Physics of Life Reviews, 2010. **7**(4): p. 424-460.
102. D. H. Klein and M. D. Smith, *Homogeneous nucleation of calcium hydroxide.* Talanta, 1968. **15**(2): p. 229-231.
103. M. Kucher and M. Kind, *Experimentelle Untersuchungen zur Partikelbildung bei der Fällung von Barium- und Strontiumsulfat.* Chemie Ingenieur Technik, 2007. **79**(3): p. 266-271.
104. C. Labbez, B. Jönsson, I. Pochard, A. Nonat and B. Cabane, *Surface Charge Density and Electrokinetic Potential of Highly Charged Minerals: Experiments and Monte Carlo Simulations on Calcium Silicate Hydrate.* The Journal of Physical Chemistry B, 2006. **110**(18): p. 9219-9230.
105. D. Langmuir, *Aqueous environmental geochemistry*. 1997: Prentice Hall.
106. A. C. Lasaga, *Kinetic Theory in the Earth Sciences*. Princeton Series in Geochemistry, ed. H. D. Holland. 1998, Princeton: Princeton University Press.
107. H. M. Le Chatelier, *Recherches expérimentales sur la constitution des mortiers hydrauliques*. 1904, Paris: Dunod.
108. B. Lothenbach, F. Winnefeld and R. Figi, *The influence of superplasticizers on the hydration of Portland Cement.* 12th International Conference on the Chemistry of Cement, 2007: p. W1-05.3
109. J. E. Lovelock, *A Physical Basis for Life Detection Experiments.* Nature, 1965. **207**(4997): p. 568-570.

110. A. Lüttge, *Crystal dissolution kinetics and Gibbs free energy.* Journal of Electron Spectroscopy and Related Phenomena, 2006. **150**(2-3): p. 248-259.
111. J. Lyklema, H. P. van Leeuwen, M. Vliet and A. M. Cazabat, *Fundamentals of Interface and Colloid Science: Fundamentals*. 1991: Academic Press.
112. P. Macheras and A. Iliadis, *Modeling in biopharmaceutics, pharmacokinetics, and pharmacodynamics: homogeneous and heterogeneous approaches*. Interdisciplinary Applied Mathematics, ed. S. S. Antman, J. E. Marsden, L. Sirovich and S. Wiggins. 2006: Springer.
113. J. Makar, G. Chan and K. Esseghaier, *A peak in the hydration reaction at the end of the cement induction period.* Journal of Materials Science, 2007. **42**(4): p. 1388-1392.
114. J. Makar, M. and G. Chan, W., *End of the Induction Period in Ordinary Portland Cement as Examined by High-Resolution Scanning Electron Microscopy.* Journal of the American Ceramic Society, 2008. **91**(4): p. 1292-1299.
115. J. M. Makar, J. J. Beaudoin, T. Sato, R. Alizadeh and L. Raki, *Discussion of "Dissolution theory applied to the induction period in alite hydration".* Cement and Concrete Research, 2011. **41**(5): p. 565-567.
116. S. Mann, *Biomineralization: Principles and Concepts in Bioinorganic Materials Chemistry*. 2001: Oxford University Press on Demand.
117. D. Marchon, U. Sulser, A. Eberhardt and R. J. Flatt, *Molecular design of comb-shaped polycarboxylate dispersants for environmentally friendly concrete.* Soft Matter, 2013. **9**(45): p. 10719-10728.
118. T. Matschei, B. Lothenbach and F. P. Glasser, *Thermodynamic properties of Portland cement hydrates in the system CaO-Al2O3-SiO2-CaSO4-CaCO3-H2O.* Cement and Concrete Research, 2007. **37**(10): p. 1379-1410.
119. M. Medala, C. Labbez, I. Pochard and A. Nonat, *Ettringite surface chemistry: Interplay of electrostatic and ion specificity.* Journal of Colloid and Interface Science, 2011. **354**(2): p. 765-770.
120. F. C. Meldrum and R. P. Sear, *Now You See Them.* Science, 2008. **322**(5909): p. 1802-1803.
121. P. Meredith, A. M. Donald and K. Luke, *Pre-induction and induction hydration of tricalcium silicate: an environmental scanning electron microscopy study.* Journal of Materials Science, 1995. **30**(8): p. 1921-1930.
122. A. Mersmann, M. Kind and J. Stichlmair, *Thermische Verfahrenstechnik: Grundlagen Und Methoden*. 2005: Springer.
123. B. Middendorf and N. B. Singh, *Poly (methacrylic acid) Sodium Salt interaction with hydrating Portland Cement.* 12th International Congress on the Chemistry of Cement, 2007: p. T6-04.4
124. R. K. Mishra, R. J. Flatt and H. Heinz, *Force Field for Tricalcium Silicate and Insight into Nanoscale Properties: Cleavage, Initial Hydration, and Adsorption of Organic Molecules.* The Journal of Physical Chemistry C, 2013. **117**(20): p. 10417-10432.

125. M. Y. A. Mollah, W. J. Adams, R. Schenach and D. L. Cocke, *A review of cement-superplasticizer interactions and their models.* Advances in Cement Research, 2000. **12**(4): p. 153-161.
126. M. Y. A. Mollah, W. Yu, R. Schennach and D. L. Cocke, *A Fourier transform infrared spectroscopic investigation of the early hydration of Portland cement and the influence of sodium lignosulfonate.* Cement and Concrete Research, 2000. **30**(2): p. 267-273.
127. B. Möser and J. Stark, *A New Model Of Ordinary Portland Cement Hydration Derived By Means Of ESEM-FEG*. Materials Science of Concrete: Cement and Concrete - Trends and Challenges, ed. A. J. Boyd, S. Mindess and J. P. Skalny. 2002: Wiley.
128. J. W. Mullin, ed. *Crystallization*. in 4 ed. 2001, Reed Educational and Professional Publishing Ltd: Oxford.
129. L. Nachbaur. *Thèse de Doctorat*. Université de Bourgogne. 1997.
130. C. M. Neubauer, M. Yang and H. M. Jennings, *Interparticle Potential and Sedimentation Behavior of Cement Suspensions: Effects of Admixtures.* Advanced Cement Based Materials, 1998. **8**(1): p. 17-27.
131. A. M. Neville, *Properties of Concrete*. 2012: Prentice Hall.
132. B. Nickerson, *Properties That Impact Sample Preparation and Extraction of Pharmaceutical Dosage Forms*. Sample Preparation of Pharmaceutical Dosage Forms: Challenges and Strategies for Sample Preparation and Extraction, ed. B. Nickerson. 2011, New York, Dordrecht, Heidelberg, London: Springer.
133. L. Nicoleau. *Interactions physico-chimiques entre le latex et les phases minérales constituant le ciment au cours de l´hydratation*. Thesis. Universite de Bourgogne. Dijon. 2004.
134. L. Nicoleau, A. Nonat and D. Perrey, *The di- and tricalcium silicate dissolutions.* Cement and Concrete Research, 2013. **47**(0): p. 14-30.
135. A. E. Nielsen, *Kinetics of precipitation*. 1964: Pergamon Press.
136. A. Nonat, *Interactions between chemical evolution (hydration) and physical evolution (setting) in the case of tricalcium silicate.* Materials and Structures, 1994. **27**(4): p. 187-195.
137. A. Nonat, J. C. Mutin, X. Lecoq and S. P. Jiang, *Physico-chemical parameters determining hydration and particle interactions during the setting of silicate cements.* Solid State Ionics, 1997. **101-103, Part 2**(0): p. 923-930.
138. I. Odler and S. Cordes, *Initial hydration of tricalcium silicate as studied by secondary neutrals mass spectrometry: II. Results and discussion.* Cement and Concrete Research, 2002. **32**(7): p. 1077-1085.
139. I. Odler and J. Schüppstuhl, *Early hydration of tricalcium silicate III. Control of the induction period.* Cement and Concrete Research, 1981. **11**(5-6): p. 765-774.
140. A. Ohta, D. Sugiyama and T. Uomoto, *Study of dispersing effects of polycarboxylate-based dispersant on fine particles.* 6th CANMET/ACI International Conference on Superplasticizers and Other Chemical Admixtures in Concrete, 2000

141. R. J.-M. Pellenq and H. Van Damme, *Why Does Concrete Set?: The Nature of Cohesion Forces in Hardened Cement-Based Materials.* MRS Bulletin, 2004. **29**(05): p. 319-323.
142. F. Perche, Y. Houst, P. Bowen and G. Hofmann, *Adsorption of lignosulfonates and polycarboxylates depletion and electroacoustic methods.* 7th CANMET/ACI International Conference on Superplasticizers and Other Chemical Admixtures in Concrete, 2003
143. PHREEQC, *http://wwwbrr.cr.usgs.gov/projects/GWC_coupled/phreeqc/.*
144. A. Picker. *Influence of Polymers on Nucleation and Assembly of Calcium Silicate Hydrates*. Universität Konstanz. 2013.
145. G. A. Pilkington and W. H. Briscoe, *Nanofluids mediating surface forces.* Advances in Colloid and Interface Science, 2012. **179-182**(0): p. 68-84.
146. S. Pinnamaneni, N. G. Das and S. K. Das, *Formulation approaches for orally administered poorly soluble drugs.* Die Pharmazie: An international journal of pharmaceutical sciences, 2002. **57**(5): p. 291-300.
147. J. Plank, *Bauchemische Zusatzmittel.* Bauchemie Vorlesung TUM,
148. J. Plank, G. Bassioni, Z. Dai, H. Keller, B. Sachsenhauser and N. Zouaoui, *Neues zur Wechselwirkung zwischen Zementen und Polycarboxylat-Fließmitteln.* 16. ibausil, 2006. **1**: p. 0579-0598
149. J. Plank and C. Hirsch, *Impact of zeta potential of early cement hydration phases on superplasticizer adsorption.* Cement and Concrete Research, 2007. **37**(4): p. 537-542.
150. J. Plank, K. Pöllmann, N. Zouaoui, P. R. Andres and C. Schaefer, *Synthesis and performance of methacrylic ester based polycarboxylate superplasticizers possessing hydroxy terminated poly(ethylene glycol) side chains.* Cement and Concrete Research, 2008. **38**(10): p. 1210-1216.
151. J. Plank and B. Sachsenhauser, *Experimental determination of the effective anionic charge density of polycarboxylate superplasticizers in cement pore solution.* Cement and Concrete Research, 2009. **39**(1): p. 1-5.
152. J. Plank, B. Sachsenhauser and J. de Reese, *Experimental determination of the thermodynamic parameters affecting the adsorption behaviour and dispersion effectiveness of PCE superplasticizers.* Cement and Concrete Research, 2010. **40**(5): p. 699-709.
153. J. Plank, D. Stephan and C. Hirsch, *Bauchemie*. Chemische Technik: Prozesse und Produkte. Anorganische Grundstoffe, Zwischenprodukte, ed. K. Winnacker, R. Dittmeyer and L. Küchler. 2004: Wiley-VCH.
154. K. L. Planken and H. Colfen, *Analytical ultracentrifugation of colloids.* Nanoscale, 2010. **2**(10): p. 1849-1869.
155. S. Pourchet, C. Comparet, L. Nicoleau and A. Nonat, *Influence of PC superplasticizers on C3S hydration.* 12th International Conference on the Chemistry of Cements, 2007
156. V. S. Ramachandran, *Thermal analyses of cement components hydrated in the presence of calcium carbonate.* Thermochimica Acta, 1988. **127**(0): p. 385-394.

157. Q. Ran, P. Somasundaran, C. Miao, J. Liu, S. Wu and J. Shen, *Effect of the length of the side chains of comb-like copolymer dispersants on dispersion and rheological properties of concentrated cement suspensions.* Journal of Colloid and Interface Science, 2009. **336**(2): p. 624-633.
158. R. Rassem, H. Zanni-Theveneau, C. Vernet, D. Heidemann, A. R. Grimmer, P. Barret, A. Nonat, D. Bertrandie and D. Damidot. *An NMR investigation of C3S hydration in pastes and in stirred dilute suspensions*. in *International RILEM Workshop on Hydration and Setting*. 1992. Université de Bourgogne, France.
159. M. Regourd, J. H. Thomassin, P. Baillif and J. C. Touray, *Study of the early hydration of Ca3SiO5 by X-ray photoelectron spectrometry.* Cement and Concrete Research, 1980. **10**(2): p. 223-230.
160. I. G. Richardson, J. Skibsted, L. Black and R. J. Kirkpatrick, *Characterisation of cement hydrate phases by TEM, NMR and Raman spectroscopy.* Advances in Cement Research, 2010. **22**(4): p. 233-248.
161. F. Ridi, L. Dei, E. Fratini, S.-H. Chen and P. Baglioni, *Hydration Kinetics of Tri-calcium Silicate in the Presence of Superplasticizers.* The Journal of Physical Chemistry B, 2003. **107**(4): p. 1056-1061.
162. F. Ridi, E. Fratini, R. Alfani and P. Baglioni, *Influence of acrylic superplasticizer and cellulose-ether on the kinetics of tricalcium silicate hydration reaction.* Journal of Colloid and Interface Science, 2013. **395**(0): p. 68-74.
163. S. A. Rodger, G. W. Groves, N. J. Clayden and C. M. Dobson, *Hydration of Tricalcium Silicate Followed by 29Si NMR with Cross-Polarization.* Journal of the American Ceramic Society, 1988. **71**(2): p. 91-96.
164. P. S. Roller and G. Ervin, *The System Calcium Oxide-Silica-Water at 30°. The Association of Silicate* Ion in Dilute Alkaline Solution.* Journal of the American Chemical Society, 1940. **62**(3): p. 461-471.
165. C. Rößler. *Hydratation, Fließfähigkeit und Festigkeitsentwicklung von Portlandzement - Einfluss von Fließmitteln, Alkalisulfaten und des Abbindereglers*. Thesis. Bauhaus-University Weimar. Weimar. 2006.
166. C. Rößler, J. Stark, F. Steiniger and W. Tichelaar, *Limited-Dose Electron Microscopy Reveals the Crystallinity of Fibrous C-S-H Phases.* Journal of the American Ceramic Society, 2006. **89**(2): p. 627-632.
167. J. F. Roulet and S. Zimmer, *Prophylaxe und Präventivzahnmedizin*. 2003: Thieme.
168. E. Sakai, K. Yamada and A. Ohta, *Molecular Structure and Dispersion-Adsorption Mechanisms of Comb-Type Superplasticizers Used in Japan.* Journal of Advanced Concrete Technology, 2003. **1**(1): p. 16-25.
169. T. Sato and J. J. Beaudoin, *Effect of nano-CaCO3 on hydration of cement containing supplementary cementitious materials.* Advances in Cement Research, 2011. **23**(1): p. 33-43.
170. T. Sato and F. Diallo, *Seeding Effect of Nano-CaCO3 on the Hydration of Tricalcium Silicate.* Journal of the Transportation Research Board, 2010(2141): p. 61-67.

171. Scheffer and Schachtschabel, *Lehrbuch der Bodenkunde*. 16. ed. 2010, Heidelberg: Spektrum Akademischer Verlag Heidelberg.
172. P. Schuck, *Size-Distribution Analysis of Macromolecules by Sedimentation Velocity Ultracentrifugation and Lamm Equation Modeling.* Biophysical Journal, 2000. **78**(3): p. 1606-1619.
173. J. S. Schweitzer, R. A. Livingston, C. Rolfs, H. W. Becker and S. Kubsky, *Ion beam analysis of the hydration of tricalcium silicate.* Nuclear Instruments and Methods in Physics Research Section B: Beam Interactions with Materials and Atoms, 2003. **207**(1): p. 80-84.
174. K. L. Scrivener and A. Nonat, *Hydration of cementitious materials, present and future.* Cement and Concrete Research, 2011. **41**(7): p. 651-665.
175. J. Siepmann, F. Siepmann and A. T. Florence, *Factors influencing Oral Drug Absorption and Drug Availability*. Modern Pharmaceutics, Fifth Edition, Volume 1: Basic Principles and Systems, ed. A. T. Florence and J. Siepmann. Vol. 1. 2009, New York: Informa Healthcare.
176. F. Söllner, *Thermodynamik und Umweltökonomie*. Umwelt und Ökonomie, ed. W. Müller and P. Schuster. 1996, Heidelberg: Physica-Verlag Heidelberg.
177. J. Stark, B. Möser and F. Bellmann, *Hydratation von Portlandzement.* Lehrbrief des F.A. Finger-Instituts für Baustoffkunde, Bauhaus-Universität Weimar, 2004
178. J. Stark, B. Möser and F. Bellmann, *New approaches to Ordinary Portland Cement Hydration in the Early Hardening Stage.* 11th International Conference on the Chemistry of Cement, 2003
179. J. Stark, B. Möser, F. Bellmann and C. Rößler, *Quantitative Charakterisierung der Zementhydratation.* 16. Ibausil, 2006. **1**: p. 0047-0066
180. J. Stark and B. Wicht, *Geschichte der Baustoffe*. 1998, Wiesbaden und Berlin: Bauverlag GmbH.
181. J. Stark and B. Wicht, *Zement und Kalk: Der Baustoff Als Werkstoff*. 2000: Birkhäuser.
182. H. N. Stein, *Thermodynamic considerations on the hydration mechanisms of Ca3SiO5 and Ca3Al2O6.* Cement and Concrete Research, 1972. **2**(2): p. 167-177.
183. H. N. Stein and J. M. Stevels, *Influence of silica on the hydration of 3CaOSiO2.* Journal of Applied Chemistry, 1964. **14**(8): p. 338-346.
184. D. Stephan and S. Wistuba, *Influence of the inclusion of foreign ions on the structure, reactivity and hydration products of tricalcium silicate and tricalcium aluminate.* Cement International, 2005. **3**(4): p. 107-117.
185. W. Stumm, *Aquatic chemical kinetics: reaction rates of processes in natural waters*. 1990: John Wiley & Sons, Inc.
186. W. Stumm, *Chemistry of the Solid-Water Interface. Processes at the Mineral-Water and Particle-Water Interface in Natural Systems*. 1992: John Wiley & Sons, Inc.
187. W. Stumm, *Reactivity at the mineral-water interface: dissolution and inhibition.* Colloids and Surfaces A: Physicochemical and Engineering Aspects, 1997. **120**(1-3): p. 143-166.

188. I. Sunagawa, *Crystals. Growth, Morphology and Perfection* 2005: Cambridge University Press.
189. K. Suzuki, T. Nichikawa, K. Kato, H. Hayashi and S. Ito, *Approach by zeta-potential measurement on the surface change of hydrating C3S.* Cement and Concrete Research, 1981. **11**(5–6): p. 759-764.
190. T. Svedberg and H. Rinde, *The determination of the distribution of size of particles in dispersed systems.* Journal of the American Chemical Society, 1923. **45**(4): p. 943-954.
191. T. Svedberg and H. Rinde, *The Ultra-Centrifuge, a new instrument for the determination of size and distribution of size of particle in amicroscopic colloids.* Journal of the American Chemical Society, 1924. **46**(12): p. 2677-2693.
192. M. E. Tadros, J. A. N. Skalny and R. S. Kalyoncu, *Early Hydration of Tricalcium Silicate.* Journal of the American Ceramic Society, 1976. **59**(7-8): p. 344-347.
193. T. F. Tadros, *Dispersion of Powders in Liquids and Stabilization of Suspensions*. 2012: Wiley.
194. H. F. W. Taylor, *726. Hydrated calcium silicates. Part I. Compound formation at ordinary temperatures.* Journal of the Chemical Society (Resumed), 1950(0): p. 3682-3690.
195. H. F. W. Taylor, *Cement Chemistry*. 2nd ed. 1997: Thomas Telford, London.
196. B. Tomazic, R. Mohanty, M. Tadros and J. Estrin, *Crystallization of calcium hydroxide from aqueous solution: I. Preliminary study.* Journal of Crystal Growth, 1986. **75**(2): p. 329-338.
197. R. Trettin, *Reactivity and Mechanism of Hydration of Cement Phases.* Proceedings of the 10th International Congress on the Chemistry of Cement, 1997. **2ii050**: p. 8.
198. R. Trettin and W. Wieker, *Zur Hydratation von Trikalziumsilikat I. Ursachen der Induktionsperiode.* Silikattechnik, 1986. **37**(3): p. 75-78.
199. H. Uchikawa, S. Hanehara and D. Sawaki, *The role of steric repulsive force in the dispersion of cement particles in fresh paste prepared with organic admixture.* Cement and Concrete Research, 1997. **27**(1): p. 37-50.
200. S. Weiner, *Biomineralization. Progress in Biology, Molecular Biology and Application. Edited by Edmund Bäuerlein.* Angewandte Chemie International Edition, 2005. **44**(31): p. 4833-4834.
201. S. Weiner and P. M. Dove, *An overview of Biomineralization Processes and the Problem of the Vital Effect.* Reviews in Mineralogy and Geochemistry: Biomineralization, 2003. **54**
202. F. Winnefeld, S. Becker, J. Pakusch and T. Götz, *Effects of the molecular architecture of comb-shaped superplasticizers on their performance in cementitious systems.* Cement and Concrete Composites, 2007. **29**(4): p. 251-262.
203. K. Yamada, S. Ogawa and S. Hanehara, *Controlling of the adsorption and dispersing force of polycarboxylate-type superplasticizer by sulfate ion concentration in aqueous phase.* Cement and Concrete Research, 2001. **31**(3): p. 375-383.

204. K. Yamada, T. Takahashi, S. Hanehara and M. Matsuhisa, *Effects of the chemical structure on the properties of polycarboxylate-type superplasticizer.* Cement and Concrete Research, 2000. **30**(2): p. 197-207.
205. J. Yoreo and P. Vekilov, *Principles of Crystal Nucleation and Growth.* Reviews in Mineralogy and Geochemistry: Biomineralization, 2003. **54**
206. J. Yoshikawa, J. A. Lewis and B.-W. Chun, *Comb Polymer Architecture, Ionic Strength, and Particle Size Effects on the BaTiO3 Suspension Stability.* Journal of the American Ceramic Society, 2009. **92**: p. S42-S49.
207. K. Yoshioka, E. Sakai, M. Daimon and A. Kitahara, *Role of Steric Hindrance in the Performance of Superplasticizers for Concrete.* Journal of the American Ceramic Society, 1997. **80**(10): p. 2667-2671.
208. K. Yoshioka, E.-i. Tazawa, K. Kawai and T. Enohata, *Adsorption characteristics of superplasticizers on cement component minerals.* Cement and Concrete Research, 2002. **32**(10): p. 1507-1513.
209. J. F. Young, H. S. Tong and R. L. Berger, *Compositions of Solutions in Contact with Hydrating Tricalcium Silicate Pastes.* Journal of the American Ceramic Society, 1977. **60**(5-6): p. 193-198.
210. V. D. Zementwerke, *Tätigkeitsbericht des VDZ 2007-2009.* 2009.
211. J. Zimmermann, C. Hampel, C. Kurz, L. Frunz and R. J. Flatt. *Effect of polymer structure on the sulfate-polycarboxylate competition*. in *Ninth ACI International Conference on Superplasticizers and other chemical admixtures*. 2009. Sevilla (Spain): American Concrete Institute.
212. A. Zingg, L. Holzer, A. Kaech, F. Winnefeld, J. Pakusch, S. Becker and L. Gauckler, *The microstructure of dispersed and non-dispersed fresh cement pastes -- New insight by cryo-microscopy.* Cement and Concrete Research, 2008. **38**(4): p. 522-529.
213. A. Zingg, F. Winnefeld, L. Holzer, J. Pakusch, S. Becker, R. Figi and L. Gauckler, *Interaction of polycarboxylate-based superplasticizers with cements containing different C3A amounts.* Cement and Concrete Composites, 2009. **31**(3): p. 153-162.
214. A. Zingg, F. Winnefeld, L. Holzer, J. Pakusch, S. Becker and L. Gauckler, *Adsorption of polyelectrolytes and its influence on the rheology, zeta potential, and microstructure of various cement and hydrate phases.* Journal of Colloid and Interface Science, 2008. **323**(2): p. 301-312.

EHRENWÖRTLICHE ERKLÄRUNG

Ich erkläre hiermit ehrenwörtlich, dass ich die vorliegende Arbeit ohne unzulässige Hilfe Dritter und ohne Benutzung anderer als der angegebenen Hilfsmittel angefertigt habe. Die aus anderen Quellen direkt oder indirekt übernommenen Daten und Konzepte sind unter Angabe der Quelle gekennzeichnet.

Alle Proben wurden von mir selbst hergestellt und ausgewertet, die Rohdatenerhebung spezieller Analysen (z.B. ICP-OES, SEM, BET) wurde üblicherweise von den Mitarbeiterinnen und Mitarbeitern der jeweiligen Abteilung des Instituts durchgeführt.

Weitere Personen waren an der inhaltlich-materiellen Erstellung der vorliegenden Arbeit nicht beteiligt. Insbesondere habe ich hierfür nicht die entgeltliche Hilfe von Vermittlungs- bzw. Beratungsdiensten (Promotionsberater oder anderer Personen) in Anspruch genommen. Niemand hat von mir unmittelbar oder mittelbar geldwerte Leistungen für Arbeiten erhalten, die im Zusammenhang mit dem Inhalt der vorgelegten Dissertation stehen. Die Arbeit wurde bisher weder im In- noch im Ausland in gleicher oder ähnlicher Form einer anderen Prüfungsbehörde vorgelegt. Ich versichere ehrenwörtlich, dass ich nach bestem Wissen die reine Wahrheit gesagt und nichts verschwiegen habe.

Weimar, den 20.03.2014 Thomas Sowoidnich